ARMY RESEARCH LABORATORY

Enabling Technologies for Point and Remote Sensing of Chemical and Biological Agents Using Surface Enhanced Raman Scattering (SERS) Techniques

by Mikella E. Hankus, Dimitra N. Stratis-Cullum, and Paul M. Pellegrino

ARL-TR-4957 **September 2009**

NOTICES

Disclaimers

The findings in this report are not to be construed as an official Department of the Army position unless so designated by other authorized documents.

Citation of manufacturer's or trade names does not constitute an official endorsement or approval of the use thereof.

Destroy this report when it is no longer needed. Do not return it to the originator.

Army Research Laboratory
Adelphi, MD 20783-1197

ARL-TR-4957 **September 2009**

Enabling Technologies for Point and Remote Sensing of Chemical and Biological Agents Using Surface Enhanced Raman Scattering (SERS) Techniques

Mikella E. Hankus, Dimitra N. Stratis-Cullum, and Paul M. Pellegrino
Sensors and Electron Devices Directorate, ARL

REPORT DOCUMENTATION PAGE

Form Approved
OMB No. 0704-0188

1. REPORT DATE *(DD-MM-YYYY)*	2. REPORT TYPE	3. DATES COVERED (From - To)
September 2009	Summary	

4. TITLE AND SUBTITLE
Enabling Technologies for Point and Remote Sensing of Chemical and Biological Agents using Surface Enhanced Raman Scattering (SERS) Techniques

5a. CONTRACT NUMBER
W91CRB-04-D-0016

5b. GRANT NUMBER

5c. PROGRAM ELEMENT NUMBER

6. AUTHOR(S)
Mikella E. Hankus, Dimitra N. Stratis-Cullum, and Paul M. Pellegrino

5d. PROJECT NUMBER

5e. TASK NUMBER

5f. WORK UNIT NUMBER

7. PERFORMING ORGANIZATION NAME(S) AND ADDRESS(ES)
U.S. Army Research Laboratory
ATTN: RDRL-SEE-O
2800 Powder Mill Road
Adelphi, MD 20783-1197

8. PERFORMING ORGANIZATION REPORT NUMBER
ARL-TR-4957

9. SPONSORING/MONITORING AGENCY NAME(S) AND ADDRESS(ES)

10. SPONSOR/MONITOR'S ACRONYM(S)

11. SPONSOR/MONITOR'S REPORT NUMBER(S)

12. DISTRIBUTION/AVAILABILITY STATEMENT
Approved for public release; distribution unlimited.

13. SUPPLEMENTARY NOTES

14. ABSTRACT
First responders and military personnel are in need of a fast, reliable, and accurate method to identify and quantify defense-related hazardous materials. Raman spectroscopy is a form of vibrational spectroscopy that is rapidly becoming a valuable tool for homeland defense applications, as it is well suited to the molecular identification of a variety of compounds, including explosives, and chemical and biological hazards. To measure trace levels of these types of materials, surface enhanced Raman scattering (SERS), a specialized form of Raman scattering, can be employed. The SERS enhancements are produced on, or in close proximity to, a nanoscale roughened metal surface, and are normally associated with increased local electromagnetic field strengths. Due to the nature of the SERS substrate fabrication process, there are challenges in substrate reproducibility that often result in the presence of field "hot spots," making reliable sample quantification difficult. Using both a portable Raman system and an industry stand-alone, we have investigated commercially available and fabricated SERS substrates with a variety of samples (e.g., standard chemicals, explosives and bacterial endospores), and will report figures of merit for the analysis of substrates and system performance.

15. SUBJECT TERMS
SERS, raman, FON, endospore, chemical hazard, biological hazard

16. SECURITY CLASSIFICATION OF:			17. LIMITATION OF ABSTRACT	18. NUMBER OF PAGES	19a. NAME OF RESPONSIBLE PERSON
a. REPORT	b. ABSTRACT	c. THIS PAGE			Mikella E Hankus
Unclassified	Unclassified	Unclassified	UU	132	19b. TELEPHONE NUMBER (*Include area code*) (301) 394-0948

Contents

List of Figures

List of Tables

Acknowledgments

This work was supported by the U.S. Army Research Laboratory (contract #W91CRB-04-D-0016). Thank you to Dr. Brian M. Cullum (University of Maryland Baltimore County) for use of the Denton Explorer-14 evaporator, and to Dr. Jason Guicheteau at the Edgewood Chemical Biological Center (ECBC) for the generous gift of the silver colloid solution. This work was done in support of TPA EC-SE-2006-02.

Executive Summary

This report was produced to fulfill the requirements of the U.S. Army Research Laboratory's (ARL) Technology Program Annex (EC-SE-2006-02) in support of continuing ECBC efforts to investigate the utility of Surface Enhanced Raman Scattering (SERS). In particular, the goal of this research is to assess the ability of SERS as a possible enabling technology for water monitoring applications. The work contained within this annex will leverage current research, which suggests that it is possible to discriminate among structurally similar compounds, as well as categorize similar hazardous materials using SERS. The research will produce a substrate decision-point report and a final methodology report in FY06 and FY08, respectively. Along with written analysis, we will adapt and test a commercially available handheld Raman instrument for utility as a SERS-based biosensor (FY08). This work will be fully coordinated with our RDEC partner and has the potential to feed directly into the Joint Service Agent Water Monitoring (JSAWM) program.

Although the original intent was to use top-down engineering as a means to increase substrate reproducibility and, thus, enable improvements in quantitative and discriminatory ability, the goal was deemed beyond reach or scope of the effort. With substrate fabrication efforts deferred, the remainder of the studies concentrated on the discriminatory power of SERS for several biological materials (bacterial endospores and viruses) using commercially fabricated substrates, and the evaluation of combining SERS substrates with current compact Raman instrumentation. The early biological studies resulted in several open literature publication and have some credence to the analytic power of SERS, but cannot by any means be considered exhaustive. The final reporting of the combination of commercially available, commonly fabricated SERS substrates and portable Raman instrumentation is contained within this report.

Recommendations or insights contained in this report should be considered as starting points for continued ARL effort in the area of SERS and are meant to compliment the long-standing efforts at ECBC to use SERS as a multi-use hazardous material sensing platform. Finally, introductory material within this report is included for completeness. Experienced spectroscopists or SERS researchers could easily bypass front-matter and begin with the experimental section without loss of continuity.

1. Introduction

There are a variety of methods and techniques used for the identification and quantification of hazardous materials. Methods often used for explosive and chemical agent detection include high performance liquid chromatography/ mass spectrometry (HPLC/MS), gas chromatography/ mass spectrometry (GC/MS), ion mobility spectrometry (IMS), and vibration-based spectroscopies (*1–3*). Typically, these techniques require significant sample preparation that can be both time and labor intensive. For the identification of biological agents, time consuming culture-based methods are often used (*4, 5*). For military and first responders, there is a need for a technique that requires little to no sample preparation, is applicable to many types of hazardous materials, and can provide fast accurate identification and quantification. A vibrational-based spectroscopy like Raman scattering can potentially meet these requirements.

Raman spectroscopy is a form of vibrational spectroscopy that is rapidly becoming a valuable tool for defense applications, as it is well suited to the molecular identification of a variety of compounds, including biological, explosive and chemical hazards (*6–8*). Raman-based measurements rely on specific vibrations within the molecule to produce a fingerprint spectrum from which sample component identification and quantification are possible. Raman-based techniques are also advantageous as they do not suffer from interferences from water and are relatively insensitive to the excitation wavelength employed, making them applicable in a variety of environments. As many biological, explosive, and chemical simulant samples demonstrate low Raman cross-sections (*6*), often Raman signal enhancing techniques are employed for detection methods (*9*). Many research groups are exploring the use of Surface Enhanced Raman Scattering (SERS) as a Raman signal enhancing technique, as it combines all the advantages of Raman with the added advantage of higher sensitivity (single molecule in certain cases) (*10–15*). For example, SERS signal enhancements as compared to spontaneous Raman have been reported as much as 14 orders of magnitude greater (*10, 16*). The signal enhancement from SERS is achieved by depositing an analyte onto a roughened metal surface, irradiating the surface, and then taking advantage of chemical and electromagnetic enhancements that occur (*17, 18*).

Due to the many advantages offered by SERS, it is not surprising that many researchers are working to apply the technique to the identification of hazardous materials such as explosives and chemical and biological agents (*3, 6, 7, 19–35*). However, real-world applications of SERS still remain challenging due, in part, to difficulties in achieving reproducible and uniform substrates from which repeatable measurements can be obtained (*36–39*). The challenge in reproducibility often results from the difficulty in creating a substrate capable of batch fabrication that is uniformly roughened on the nanoscale (*40*). To meet the reproducibility and sensitivity challenge, several SERS platforms have been demonstrated (nanostructures, film over nanospheres, lithographically produced structures) (*11, 27, 40–55*), and, at best, generally

demonstrate 15% relative standard deviation (RSD)—the measure of the reproducibility of an analysis—from substrate-to-substrate and SERS signal enhancements of seven to eight orders of magnitude (*54*, *56*).

Some success fabricating and applying uniform SERS substrates has been demonstrated with the commercially available Klarite™ substrates (D3 Technologies Ltd.) (*23*, *57*, *58*). These substrates were developed using Si-based semiconductor fabrication techniques (*57*). The Klarite substrates demonstrate plasmon absorbance bands in both the visible and near-infrared (IR) regions, and, therefore, can be used with a range of laser excitation sources. Additionally, due to the fabrication process used, these substrates have demonstrated typical RSDs ranging from 10–15% (*57*).

Recent commercial product availability of both the Klarite SERS substrates and portable Raman instrumentation have prompted our investigations reported here. Using both a portable Raman system (B&WTek) and an industry stand-alone (Renishaw), we have investigated commercially available (Klarite) and fabricated (film over nanosphere [FON]) SERS substrates with a variety of samples (e.g., biological samples like endospores, explosives, and chemical simulants), and report results from the analysis of substrate and system performance. Additionally, a previously characterized silver nanoparticle colloid solution was also used for SERS measurements of endospore samples (*19*).

1.1 Background and Theory

1.1.1 Chemical and Biological Agents

Chemical and biological warfare (CBW) is defined as the use of harmful or deadly chemical or biological agents as weapons (*3*, *31*). Chemical and biological warfare agents date back thousands of years, as evidenced by the primitive use of poisoned arrows. Other examples of CBW use include the use of poisonous or irritating smokes by the Chinese in 1000 BC, the Russians catapulting diseased cadavers into enemy camps in Crimea in the 14th century, the dispersal of contaminated blankets to the American Indians by the English military in colonial America, and the widespread use of chlorine gas by the German military during WWI (*59*). More recently, a notable example of chemical warfare agent use includes the release of the nerve agent Sarin, in 1995, into the Tokyo subway, which affected nearly 1000 people. As recent as 2001, the biological agent anthrax was distributed to unsuspecting victims via the U.S. mail system, ultimately killing five people and infecting 17 others.

Modern chemical and biological warfare agents are often colorless, odorless, and tasteless, and can be widely dispersed, affecting unknowing victims. Since total protection from chemical and biological hazards is difficult, minimizing their effects has become a priority. One means by which this is accomplished is through early detection. Towards this end, efforts of both industry and government research have been directed toward the rapid identification and quantification of both chemical and biological hazards (*34*). However, despite research efforts, these goals have

remained somewhat elusive, partially because of the very complex nature of these chemicals, and the complex matrix in which many of these compounds are often found. Additionally, many of the agents are suspended in lofting type media for dispersal; these media often mask or interfere with ease of detection (*60*). In biological systems, spectroscopic measurements and interpretation can be affected by matrix effects like growth conditions, growth phase, and even media conditions.

Due to all of these complications, there is a focus on the research and development of rapid, accuracy-focused technologies/techniques for CBW hazard detection. Raman and Raman-based techniques are becoming more widely used, as they allow for fingerprint identification (in some cases) and quantification of samples, require little to no sample preparation, are often label-free, and can be used under a range of experimental conditions. Raman and Raman-based techniques also have the distinct potential advantage of application to both chemical and biological hazard detection applications within a single platform.

1.1.2 Raman Principles

In Raman scattering-based techniques, incident radiation strikes a molecule, the radiation interacts with that molecule, and most of the radiation is elastically scattered (Rayleigh scattering); however, a small number of photons are inelastically scattered to a frequency different than that of the incoming radiation. The difference in energy corresponds to the energy of the vibrations of the bonds in the molecule; see figure 1 for a partial Jablonski diagram. Therefore, characteristic vibrational fingerprint spectra are obtained from molecules and can be used for chemical identification.

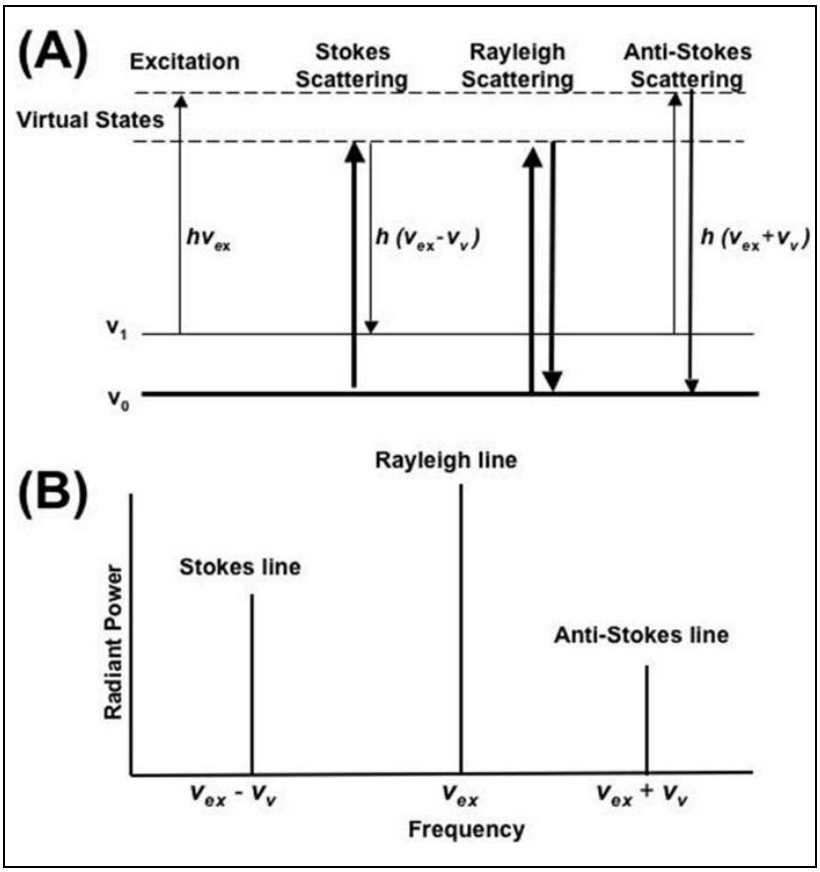

Figure 1. a) Energy level diagram demonstrating Raman scattering, b) resulting spectrum (not drawn to scale).

In figure 1a, a partial Jablonski diagram demonstrates Raman scattering. This figure shows a ground vibrational state molecule interacting with a photon of energy, causing the molecule to be vibrationally excited to the lowest level of a virtual state. This figure also shows an excited vibrational state molecule interacting with a photon, causing the molecule to be excited to a higher level virtual state. The energy of the incident photon then returns to the ground state via Rayleigh scattering (elastic), or inelastically, via Stokes and anti-Stokes Raman scattering. The lower frequency scattering is called Stokes scattering, and the higher frequency scattering is called anti-Stokes scattering. In figure 2b, the intensity and energy of the Stokes, Rayleigh, and anti-Stokes lines are shown.

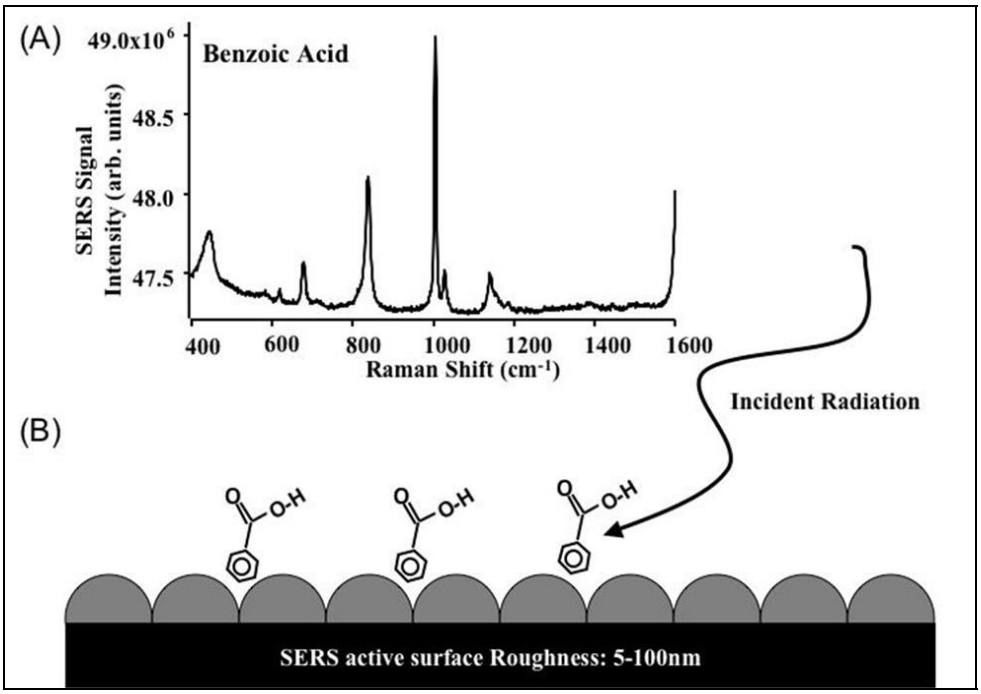

Figure 2. (a) Raman spectrum of benzoic acid. (b) SERS active substrate surface with benzoic acid adsorbed to surface. Nanoscale roughened features with metal overlay range in diameter from 5 nm to 100 nm (not drawn to scale).

1.1.3 Principles of SERS

SERS provides all of the advantages of Raman but with sensitivity potentially rivaling that of fluorescence spectroscopy (single molecule in some cases) (*10–15*). The increased sensitivity in signal observed in SERS, relative to spontaneous Raman, results from two enhancement mechanisms, chemical and electromagnetic. The electromagnetic enhancement is the dominant enhancement factor, adding to as much as 12 orders of magnitude in signal enhancement (*61*), while the chemical enhancement is reported to add to the overall signal enhancement by one to two orders of magnitude (*62*).

The electromagnetic enhancement is dependent on nanoscale roughened features or individual nanoparticles (5 nm to 100 nm) of metal on which a surface plasmon band can be propagated, shown in figure 2b. A surface plasmon band is a collective oscillation of electrons on some surface; for SERS work, it is located on the metalized substrate surface. The chemical enhancement is dependent on a sample adsorbing onto the sample substrate surface, resulting in either resonant processes occurring on the sample molecule or as the result of charge-transfer processes that occur between the molecule and the metal surface.

1.1.3.1 Electromagnetic Enhancement

SERS was first documented in the 1970s when it was observed that pyridine absorbed onto the surface of metallic surfaces (gold, silver, copper) demonstrated increased Raman signal intensities (*63, 64*). Since then, SERS has become known as a nanostructure effect, with surface

plasmons propagating across these metallic nanoscale features or particles, resulting in the large electromagnetic Raman signal enhancement. The SERS electromagnetic enhancement has been theoretically modeled by several research groups (*65–67*). To describe the model, two principle effects are considered: 1) that scattering takes place in the enhanced local optical field of the metallic nanostructures (electromagnetic enhancement), and 2) that the molecule adsorbed onto the metal surface has a cross-section more enhanced than the Raman cross-section of the free molecule (chemical enhancement). The term (σ^{R}_{ads}) describes the enhanced SERS cross-section due to adsorption of the molecule onto the metal, as compared to the normal spontaneous Raman cross-section (σ^{R}_{Free}). To describe the new effective SERS cross-section (σ_S^{SERS}), see equation 1. In equation 1, the term $A(\nu_L)$ is the field enhancement factor for the laser, and $A(\nu_S)$ is the field enhancement factor for Raman scattering (*65–67*)

$$\sigma_S^{SERS} = \sigma^{R}_{ads} |A(\nu_L)|^2 |A(\nu_S)|^2 \quad (1)$$

The terms and relationships to describe an estimation of the overall SERS Stokes signal ($P^{SERS}(\nu_S)$), as the result of an enhancement in the SERS cross-section are shown in equation 2.

$$P^{SERS}(\nu_S) = N \sigma_S^{SERS} I(\nu_L) \quad (2)$$

In equation 2, $P^{SERS}(\nu_S)$ is the SERS signal for a particular vibrational mode, N is the number of molecules involved in the SERS process, σ_S^{SERS} is the SERS enhanced cross-section of the adsorbed molecule for a particular mode, and $I(\nu_L)$ is the excitation laser intensity. This equation shows that electromagnetic SERS enhancement factor is influenced by the fourth power of the total field enhancement, when both laser and scattered frequencies are within the extent of the surface plasmon curve.

SERS measurements typically use visible excitation sources when coinage metals like gold, silver, or copper are employed as the choice metal to overcoat the roughened surface features. These metals are commonly used, as their plasmon absorbance bands fall within the wavelength range of visible and IR lasers. Silver-coated SERS active substrates produce the overall largest SERS signal enhancement; as they readily oxidize, however, their enhancement capabilities diminish with time. Gold is also a good choice as a SERS active metal surface, as it does not oxidize and is biologically compatible.

1.1.3.2 Chemical Enhancement

While the electromagnetic enhancement is often critical to enable SERS measurements, it is the chemical enhancement that often dictates what is observed in SERS spectra. SERS spectra provide information about the absorbate and its environment, specifically providing information regarding the absorbates interaction with the metalized surface of the roughened nanoparticle/nanofeatures, and even the spatial orientation of the absorbate onto the metalized nanosurface.

The chemical enhancement observed in SERS is commonly explained as a charge transfer (CT) mechanism. The chemical enhancement mechanism involves the incident radiation striking the roughened metallic surface, resulting in an electron being excited within the Fermi level of the metal to an unoccupied higher energy level molecular orbital of the absorbate or vice versa. From this excited state, a charge transfer process to a vibrational level of the same energy within the sample analyte takes place. After the transfer of a photon of different frequency being passed back to the metallic energy levels from the absorbate, it is returned to the ground state of the metal.

2. Experimental Methods

2.1 Chemicals and Reagents

The following chemicals: brilliant cresyl blue (BCB; Sigma), phenylalanine (PHE; Sigma), diisopropyl methylphosphonate (DIMP; Sigma), dimethyl methylphosphonate (DMMP), cyclotrimethylenetrinitramine (RDX; Cerilliant) and 2,4,6-trinitrotoluene (TNT; Cerilliant) were used as received. Chemical concentrations used will be discussed in the results section. Spore suspension samples were purchased from Raven Biological Laboratories. Spore suspensions include: *B. subtilis* (ATCC# 35021, designation 5230); *B. stearothermophilus* (ATCC# 10149); *B. atrophaeus* (ATCC# 9372); *B. pumilus* (ATCC# 27142); B. cereus (ATCC# 11778); *B. megaterium* (ATCC# 8245); *B. thuringiensis* (ATCC# 29730); *B. coagulans* (SUS-CG); *B. sphericus* (SUSCI). All sample spores were used as received, at a log 4 or 6 population per 0.1 ml of solution.

2.2 Substrates

Commercially available, slide-mounted Klarite SERS substrates were purchased from D3 Technologies Ltd. Slides were individually wrapped and vacuum sealed. The SERS active area on these slides is a 4 mm x 4 mm wafer attached to a gold surface. The Klarite slides were only used once and opened just prior to measurement to avoid any possible surface contamination.

Multilayer SERS FON substrates were fabricated following a previously documented scheme (*54, 56, 68*), with some modifications. Glass microscope slides were cleaned in a 1% nitric acid (HNO_3)solution. The silica sphere solution (Bangs laboratory) was suspended in an acetone and ethanol solution (90% acetone v/v). A 3 uL aliquot of the sphere solution was drop-coated onto each cut glass microscope slide and allowed to air-dry. Metal was then evaporated onto the slides, creating a 7-layer (7X) Au/Ag multilayer (100 nm Au separated by 2 nm of Ag, repeat 6X). The silver was allowed to oxidize for about 5 min of time between lifting the bell jar to switch deposition metals. These substrates were not optimized to reduce background from the underlying roughened surface.

2.3 Metal Deposition onto Fabricated SERS Substrates

Deposition of 99.99% pure silver and gold onto the glass substrates was performed using an Explorer-14 (Denton Vacuum) vacuum evaporator. During the metal deposition process, the slides are suspended 15 cm above a tungsten resistive heating boat (R. D. Mathis Co.) containing the evaporating silver. Metals are then deposited at a rate of 2.0 nm/s, under a pressure of 3.0×10^{-6} Torr. The amount of metal deposited is monitored with a quartz crystal microbalance (Inficon XTM/2 film thickness monitor) mounted beside the sample holder in the vacuum chamber. Slides rotate (counter clockwise) during deposition to ensure that a surface of uniform metal thickness is produced.

2.4 Silver Colloids

We used silver colloids as we received them from the Edgewood Chemical Biological Center (ECBC). Fabrication and characterization of these colloids has been previously documented (*19*). Briefly, the silver nanoparticles are fabricated using a modified Lee and Meisel procedure. The resulting nanoparticle suspension demonstrates a plasmon absorbance band located at 400 nm, and typically nanoparticles are 36 nm ± 10 nm in diameter (*19*).

2.5 Transmission Data

All transmission and reflectance data were obtained using either an Ocean Optics HR2000 system (001Base32 software) or an Avantes spectrometer (AvaSpec software). All data analysis were performed using Igor Pro 6.0 (WaveMetrics, Inc.). Unless otherwise indicated, data acquisition parameters were 500 ms exposure time, for 10 accumulations, and 3 spectral averages.

2.6 Scanning Electron Microscope

Scanning electron microscope (SEM) images were obtained using a FEI environmental SEM (Quanta 200 FEG).

2.7 Atomic Force Microscopy

All atomic force microscopy (AFM) measurements were performed using a Veeco NanoMan5 Scanning probe microscope in tapping mode, and Veeco NanoScope 7.0 image software.

2.8 Raman Measurement Systems

SERS and Raman spectra were collected using a Renishaw in Via Reflex Raman microscope. The Renishaw microscope has three lasers operating at 514 nm (25 mW), 632 nm (25 mW), and 785 nm (300 mW, 30 mW with the pinhole in). Spectra were collected using the NIR 785 nm laser unless otherwise indicated. The system uses an air-cooled charge coupled device (CCD) detector. The laser light was focused onto the sample using a 50X objective. Samples were moved into position using a motorized XY translational stage. Spectra were collected (typically 10 random spots/substrate unless otherwise stated), and the instrument was run using Wire 2.0

software operating on a dedicated computer. Data analysis was achieved using IgorPro 6.0 software (Wavemetrics, Inc.). Typically, results are reported showing a relative standard deviation (%RSD). The RSD is the measure of the reproducibility of an analysis and is determined by dividing the standard deviation (of a sample rather than the population) by the mean for the same set and then multiplying by 100%.

A portable (6.8 lbs) B&WTek MiniRam II Raman spectrometer (Newark, DE) system was used to collect Raman and SERS data. The portable system is equipped with a 785 nm laser (500 mW, 200–245 mW at sample position). A thermoelectric (TE)-cooled 2048 CCD array is the detector on the system. The system has a static response range from 175–3100 cm^{-1}. The system was coupled to a BAC100–785 fiber optic probe with an OD 8 elastic scattering filter in place. Spectra were collected using the B&WTek software. All files were exported to Excel, and data analysis was achieved using IgorPro 6.0 software (Wavemetrics, Inc.).

3. Results and Discussion

To fully evaluate commercial-off-the-shelf (COTS) SERS substrates and Raman detection systems, SERS substrates were characterized and evaluated for biological application. From these results, a study was conducted evaluating some figures of merit, and then viability of these technologies for other hazard sensing (explosives and simulants) was performed.

3.1 Substrate Characterization

One of the ongoing challenges associated with SERS is the difficulty in creating a reproducible nanoscale-structured surface from which reproducible uniform SERS signal enhancements can be measured (*39, 40, 42, 43, 54*). To evaluate substrates for potential SERS applications, the surfaces of commercially available Klarite substrates, FON, and well-characterized silver colloids were characterized. Characterization techniques typically included obtaining SEM images of the surfaces, collecting surface plasmon resonance data, and topographically analyzing the surface by AFM. Based on the characterization results from these measurements, FON substrates were fabricated that demonstrated a uniformly structured surface, and were able to be matched to an excitation source, and were topographically reproducible.

For the fabrication of SERS substrates, there are several techniques that are used commonly. In one of the more simple and inexpensive fabrication methods, nanoscale particles (e.g., silica spheres) are deposited onto glass slides, followed by controlled vapor deposition over-coating with the desired coinage metal. The plasmon absorption properties can be tuned through size and concentration of the nanoscale particles. Several sizes of silica nanospheres (510 nm, 600 nm, and 700 nm) were evaluated, over a range of concentrations (spheres, ratio of solvents), resuspended in several concentrations of solution and deposition techniques (drop coating, spin coating) to assure a uniformly covered surface. Figures 3a and 3b show photographs of two

different solvent concentrations used in FON fabrication. In figure 3a, the non-uniform nanoparticle distribution often referred to as the "coffee ring" effect is very clearly visible. By contrast in figure 3b, an optimized FON is observed with a fairly uniformly packed inner circle area is shown. Although some "coffee ring" effect is still observed in figure 3b, it is limited to only the outer edges substrate, defined outside the active substrate region used in subsequent studies.

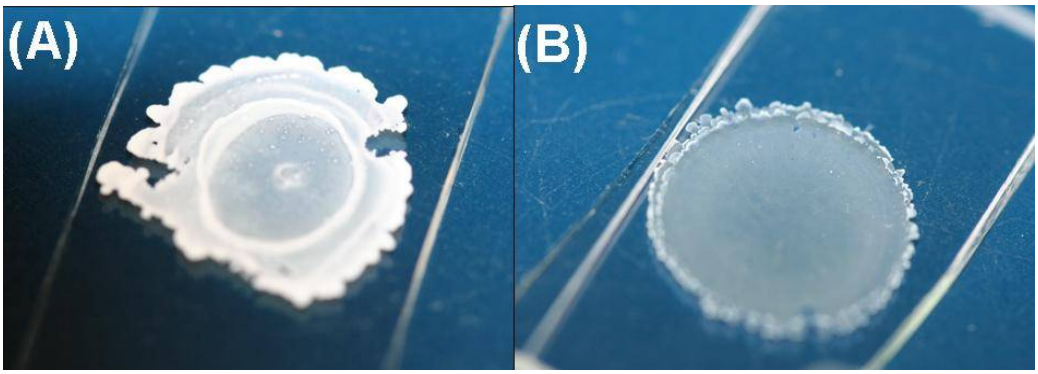

Figure 3. SERS substrates (a) FON non-optimized for surface steps and (b) optimized uniform FON.

As the different parameters were varied, SEM analysis was used to characterize the uniformity of the surface (see figure 4). From SEM analysis, it was shown that a 3 uL aliquot of 5% w/v of spheres in a solution of 90% acetone/10% ethanol, drop-wise applied to a microscope slide, produced the most uniform substrate structure with minimal "coffee ring" effects, having fewer steps, and showed fairly uniform packing. Figure 4b illustrates that the multi-layers of 700 nm silica spheres are tightly packed in a hexagonal honeycomb pattern. After the deposition of silica spheres, a 7X Au/Ag multi-layer was deposited onto the substrate surface, and the surface plasmon was measured across the substrates to determine which sphere size correlated best to available excitation wavelengths.

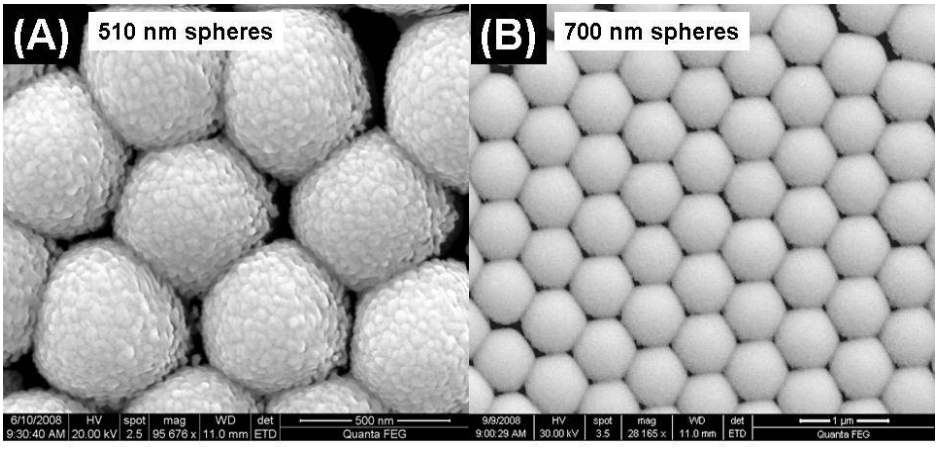

Figure 4. SEM images fabricated SERS substrates under different magnifications. (a) Individual 510 nm spheres shown, (B) overall substrate with 700 nm spheres demonstrating uniform hexagonal packing.

In order to achieve maximum SERS signal enhancement, the plasmon absorbance band needs to be located between the excitation wavelength and the wavelengths that are Raman-scattered by the analyte molecule (*16*). The SERS signal can be both enhanced and tuned for the plasmon absorbance band to match the laser excitation source by 1) changing the underlying nanoscale structure of the substrate, 2) using different metal over-coatings, or 3) changing the materials of the underlying structures. To evaluate the location of plasmon absorbance band of the various SERS substrates, reflectance measurements were collected. An example showing the locations of the plasmon absorbance bands for the silica spheres is shown in figure 5. From these results it was determined that the 510 nm silica spheres demonstrated a plasmon absorbance band located at 625 nm (figure 5a), the 600 nm silica spheres had a plasmon absorbance band located at 755 nm (figure 5b), and the 700 nm silica spheres had a plasmon absorbance band located at 866 nm (figure 5c). It was further determined that an increased SERS signal enhancement could be achieved by using 700 nm spheres in conjunction with a 785 nm laser.

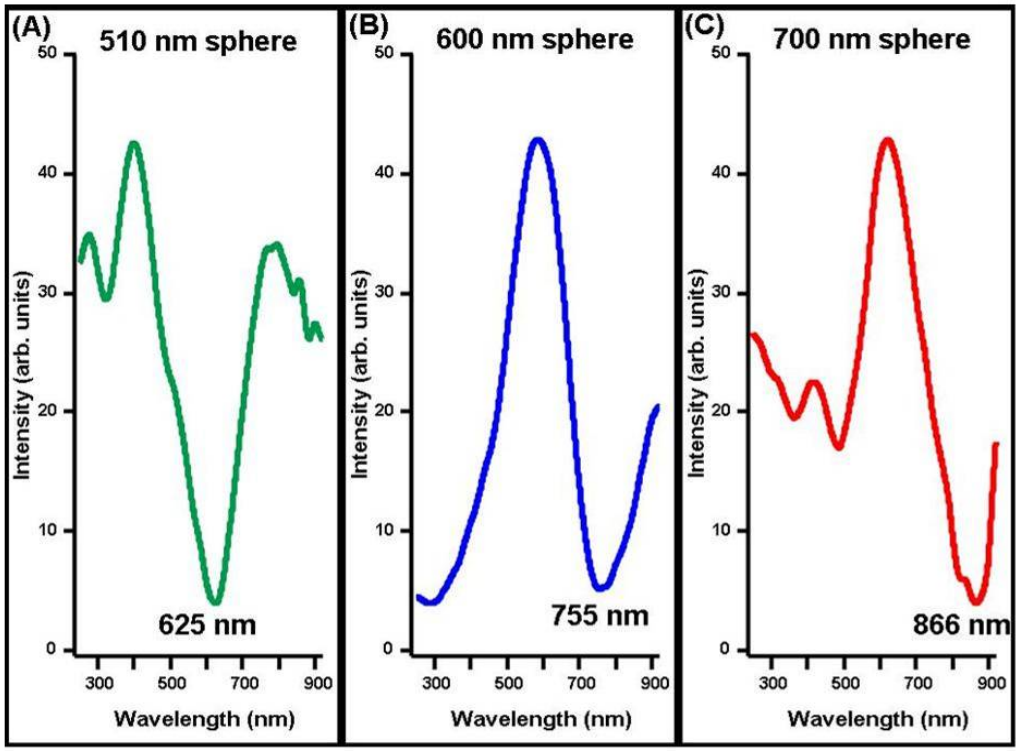

Figure 5. Reflectance curves for different sphere sizes (A) 510 nm, (B) 600 nm, and (C) 700 nm. Minima are indicated with wavelength values.

Some success producing uniform SERS signal enhancing substrates has been achieved with Klarite substrates (D3 Technologies Ltd.). The substrates are fabricated using a Silicon fabrication process (*23, 57*). Briefly, using optical lithography, a silicon diode mask is defined using optical lithography on a <100> oriented silicon wafer. Then potassium hydroxide (KOH) anistophic wet-etching is used to etch the <111> planes. This differential etching results in an array of inverted pyramids, demonstrating high reproducibility and uniformity. Following the

fabrication of the underlying silicon surface, approximately 100 nm of gold is deposited onto the surface. The structure of the Klarite substrates was characterized using a SEM, and some sample images are shown in figure 6. From the SEM images it can be seen that the substrate surface is composed of a lattice of inverted pyramidal structures.

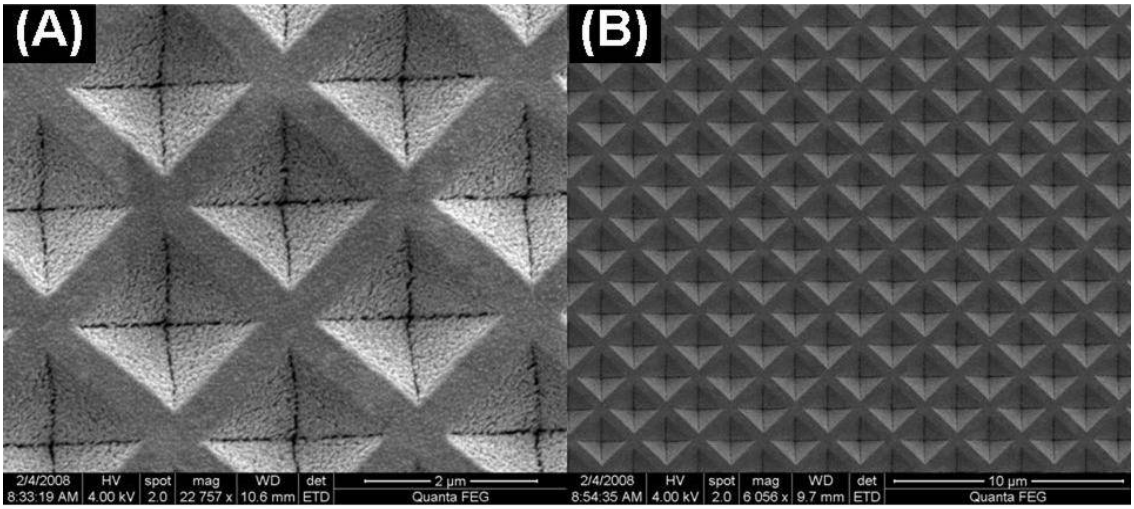

Figure 6. SEM images Klarite SERS substrates under different magnifications. (a) Individual inverted pyramids are clearly visible at a magnification of 22,757X, (b) overall substrate shown at a magnification of 6,056X.

AFM data were collected to characterize the depth profiles of the Klarite substrates (see figure 7). From the AFM data it can be seen that the surface of the substrate is highly uniform and defect-free. In the area of approximately nine pyramids shown in figures 7a and 7b, a line was snapped, and the depth profile shown in figure 7c demonstrates that the inverted pyramids are approximately 1.47 μm in width and 1 μm in depth. Reflectance data collected is shown in figure 7d and demonstrates plasmon absorbance bands located at 577 nm and 749 nm. Since these substrates have plasmon absorbance bands in the visible as well as near IR region, they can be used with a range of laser excitation sources.

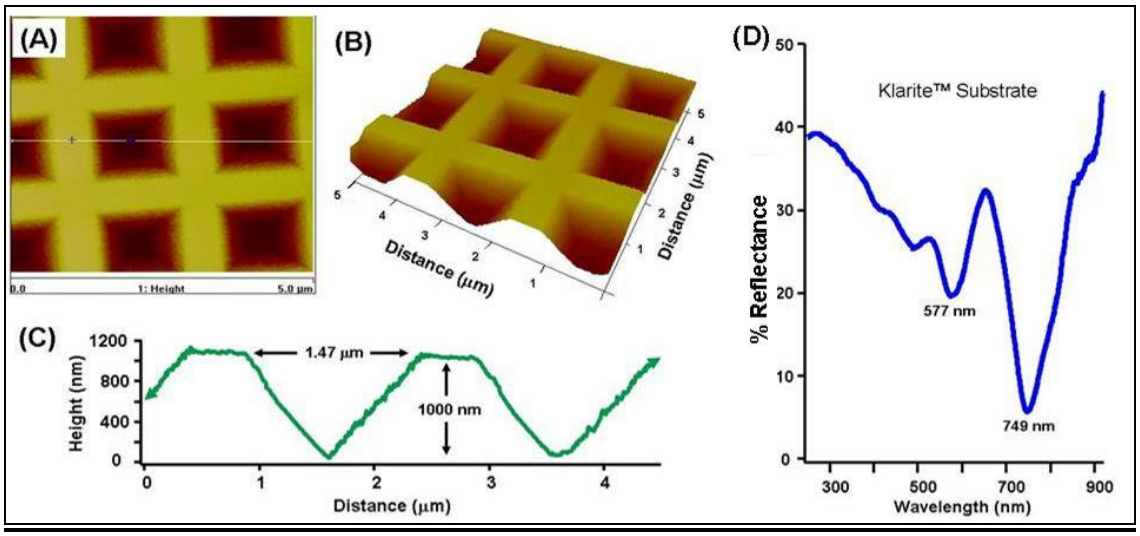

Figure 7. AFM data collected from Klarite substrate shown in (a) and (b). Analysis of surface heights shown in (c). Reflectance curve (d) of Klarite SERS substrates showing plasmon absorbance minima at 577 nm and 749 nm.

For biological experiments and for some characterization purposes, silver colloid solutions were used as received from the ECBC. These substrates were used as they had been previously characterized (*19*), and were able to serve as an example of a functional fabricated SERS substrate for comparison to the FON and Klarite substrates. These silver solutions were yellow-brown in color and demonstrated a slightly higher viscosity than water. For physical characterization experiments, a 5 uL aliquot of colloid solution was placed on a glass microscope slide and allowed to air-dry. An SEM image showing the silver colloids is provided in figure 8. From SEM analysis and previous characterization, the silver colloids were determined to be 36 nm ± 10 nm in diameter (*19*). Silver colloid solutions exhibit a strong plasmon absorbance band located at 400 nm (*19*).

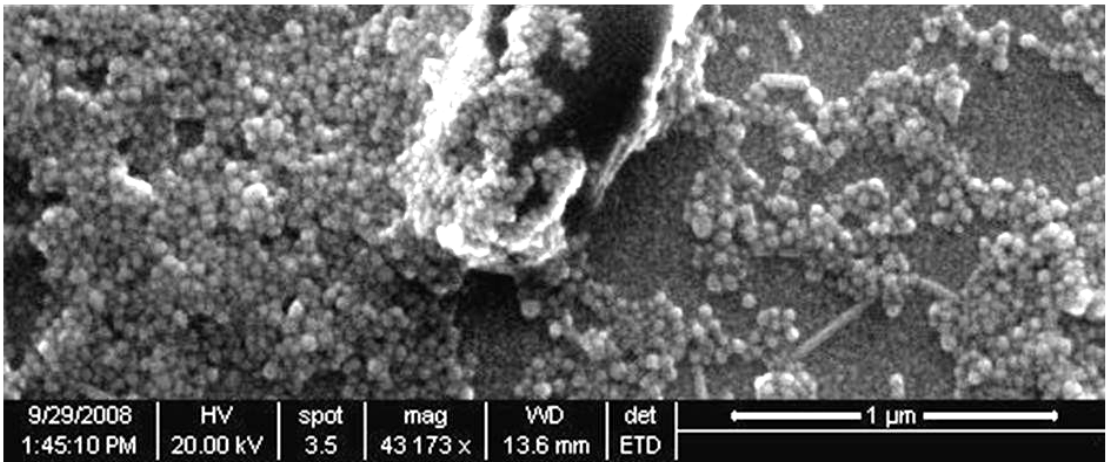

Figure 8. SEM image demonstrating silver colloid mixture dried across glass microscope slide.

For application to a range of both chemical and biological samples, the locations of the substrate background bands must be determined so that they can be distinguished from the analyte Raman bands. To evaluate the substrate background, a series of spectra were collected using the Renishaw microscope, and the average spectrum of five accumulations from five different slides is presented in figure 9. All of the data were collected under the same conditions (1% laser power, 10 s exposure time, 3 accumulations) and have been offset for visual clarity. In figure 9a, the background for the fabricated 510 nm sphere 7X Au/Ag substrate is shown. The fabricated substrate demonstrates Raman bands at 894 cm^{-1}, 1002 cm^{-1}, 1385 cm^{-1}, 1604 cm^{-1}, and 2130 cm^{-1}. Background reduction on the FON substrate could be possible through further optimization of material component composition (e.g., nanoparticle composition and glass substrate support), but was considered outside the scope of the current investigations. In figure 10b, the background of a newly opened Klarite substrate is shown. The Klarite substrate has Raman bands occurring at 895 cm^{-1}, 1018 cm^{-1}, 1132 cm^{-1}, 1442 cm^{-1}, and 2126 cm^{-1}. In figure 9c, the background for the silver colloid is shown. The silver colloid solution demonstrates Raman bands located at 608 cm^{-1}, 900 cm^{-1}, and 1057 cm^{-1}. Noting the scale differences in these results, we determined that when measuring samples without intense SERS bands, the Klarite substrates or the silver colloids with lower intensity background signature may be preferred.

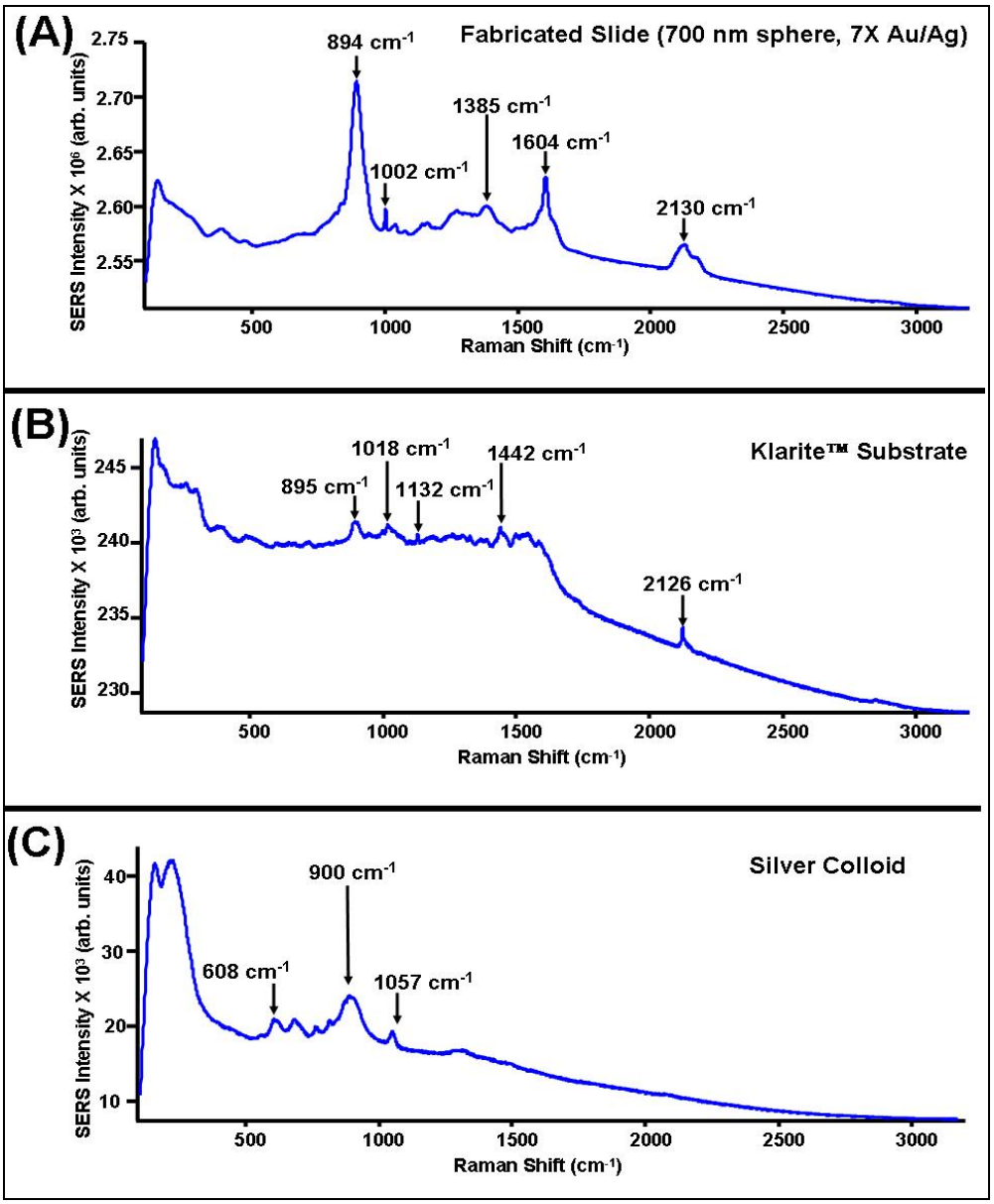

Figure 9. Spectra of backgrounds from (a) fabricated slide made with 510 nm sphere and 7X au/Ag multilayer, (b) newly opened Klarite substrate, and (c) silver colloid.

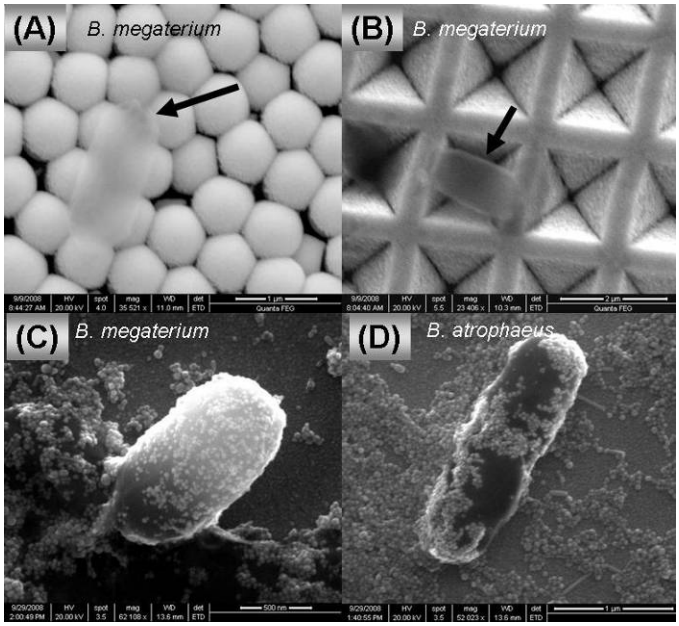

Figure 10. SEM images of various *Bacillus* spores on (a) fabricated substrate, (b) Klarite substrate, and (c) and (d) with the addition of silver colloid.

3.2 Biological Results

For Army-relevant detection and identification of biological hazards, there is a need to combine a COTS SERS substrate in a widely available and easily used Raman system. To determine the feasibility of this task, we evaluated commercially available Klarite substrates, commonly used FON SERS substrates, and well-characterized silver colloid solutions in combination with both a standard benchtop Renishaw Raman system, as well as a portable B&WTek Raman system with several different endospore samples. From these results, it is possible to determine a combination of SERS substrate and detection system that produces the most Army-relevant results, as well as to identify areas where further technology improvements need to occur.

SERS substrate performance was evaluated with the benchtop and portable Raman system spectra, using several common *bacillus* endospores. The endospore species investigated include *B. subtilis*, *B. stearothermophilus*, *B. atrophaeus*, *B. pumilus*, *B. cereus*, *B. megaterium*, *B. thuringiensis*, *B. coagulans* and *B. sphericus*. All sample spores were used as received, at a log 4 or 6 population per 0.1 ml of solution. For all SERS measurements, a 2 uL aliquot of endospores was applied directly to the substrate surface and allowed to air-dry. For SERS measurements using the silver colloid solution, a 3 uL aliquot of spheres was added to a 3 uL aliquot of spore solution, deposited onto a glass microscope slide, and then allowed to air-dry.

The instrument parameters used with the Renishaw are the same as was reported in the Experimental section. The instrumentation parameters used on the B&WTek system were as follows: 785 nm, laser, OD 8 probe head, 6000 ms acquisition times, 5 exposures. For each

spore/colloid sample, five measurements were made across the substrate surface and then averaged.

Several SEM images of the samples on the various substrates are shown in figure 10. In figure 10a, the SEM of *B. megaterium* on a fabricated substrate is shown. In this figure, the spore is seen to sit across the FON substrate surface. In figure 10b, the SEM of *B. megaterium* on a Klarite substrate is shown. In this figure, the spore sits across the inverted pyramidal structure; other images (not shown) of the spores show them "sitting inside" the inverted pyramids. In figure 10c, the SEM of *B. megaterium* with the application of the silver colloid is shown. In this image, it is possible to see how the colloids surround the spore. In figure 10d, the SEM of *B. atrophaeus* covered in silver colloid is shown. From these SEM images, it is possible to see how each of the SERS substrates interact with the some different samples, either sitting on top of a substrate platform or being "encapsulated."

Spectra from biological samples were initially collected using the Renishaw Raman system in combination with Klarite substrates. An example of data analysis (as performed with all subsequent biological results) is explained in figure 11, as different spectra were collected from different points across the same substrate surface. Once the spectral data for the set is collected, the spectra are averaged and presented as an average for the set. (see figure 11g). In figures 11a–f, the locations of the SERS bands remains the same, though the bands differ in intensity.

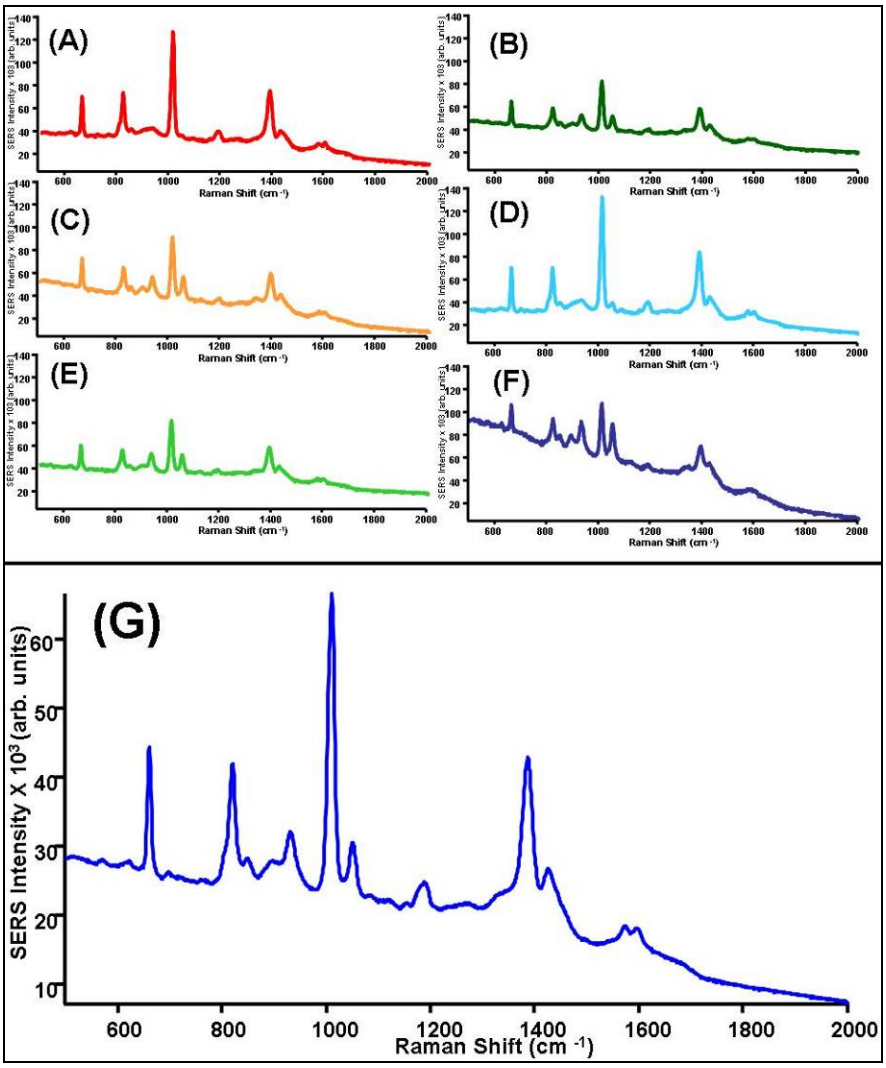

Figure 11. Example of data workup for biological sample *B. atrophaeus*. In (a–f) example single measurements are shown. In (g) the average of all measurements is displayed.

In figure 12, the average SERS spectra for each different spore set collected on a Klarite substrate using the Renishaw system is shown. From these results, it is possible to observe SERS bands (not assigned) specific to each spore. While the intensity of these SERS bands within a set did show some variation, the location of bands did not show great variation. An attempt was made to collect spectral signatures combining the Klarite substrates and the B&WTek system. Due to the poor detection capabilities of the system, however, no specific spore SERS bands could be distinguished from the substrate background.

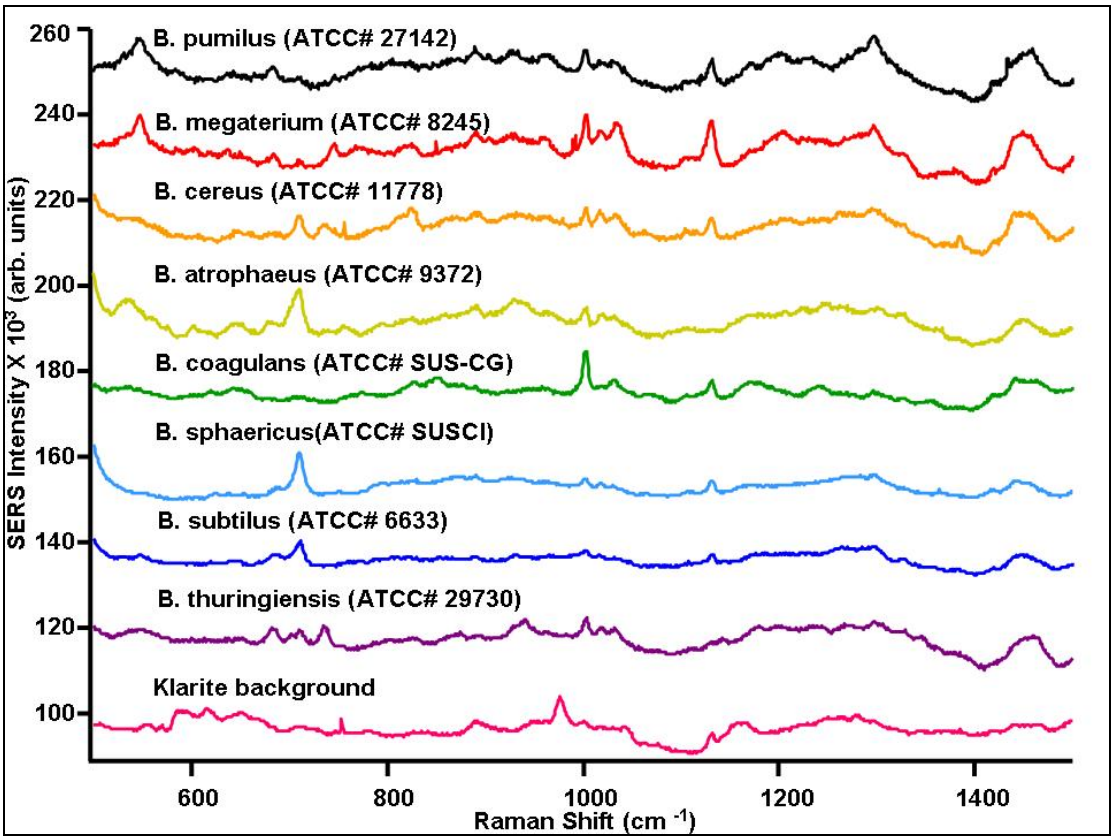

Figure 12. Comparison of SERS spectra from several Bacillus spore samples collected on Klarite substrates collected on Renishaw system.

Next, spore samples were measured using the FON substrates. In figure 13, the average for each spore set collected using the FON substrates is shown. On the FON substrate, while there are similar bands that appear in all spectra (primarily attributed to background 894 cm^{-1} band), there are still slight differences. However, it was very difficult to repeatedly measure the same subtle differences in spectra from the sample endospore samples (see figure 14 for an example with B. *subtilis*). In figure 14, replicate measurements (a–f) on the same sample are displayed and the spectral differences are clearly indicated with lines. These differences are believed to be due to 1) the SERS signal uniformity challenge associated with these types of substrates, 2) the nature of the biological samples varying widely from spore to spore and, finally, 3) the differences in how the surface of the substrate and the spore interact. Comparing observed bands with the literature reports, it was not possible to positively assign bands. We made an attempt to collect spectral SERS signatures combining the FON substrates and the B&WTek system. However, as with the Klarite substrates, the signal from the specific spore bands could not be distinguished from the background. Due to the general problems with the large slide background, spectral reproducibility challenges, and not being able to identify bands unique to the endospores, it was determined that the un-optimized FON substrates are not the ideal for biological applications.

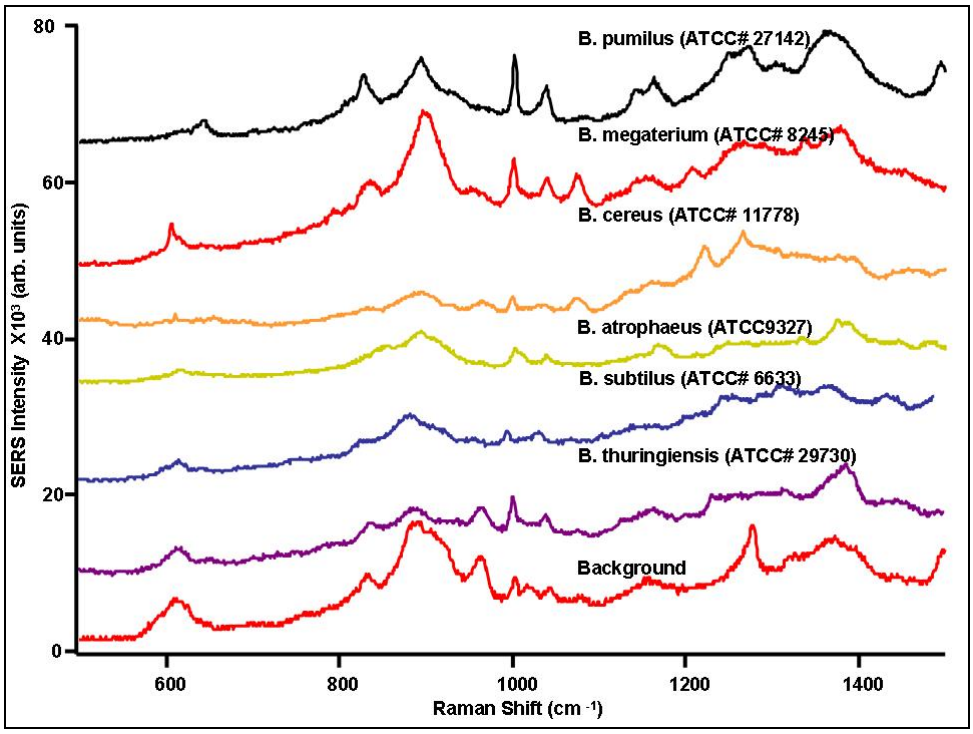

Figure 13. Comparison of SERS spectra from several Bacillus spore samples on FON substrates collected on Renishaw system.

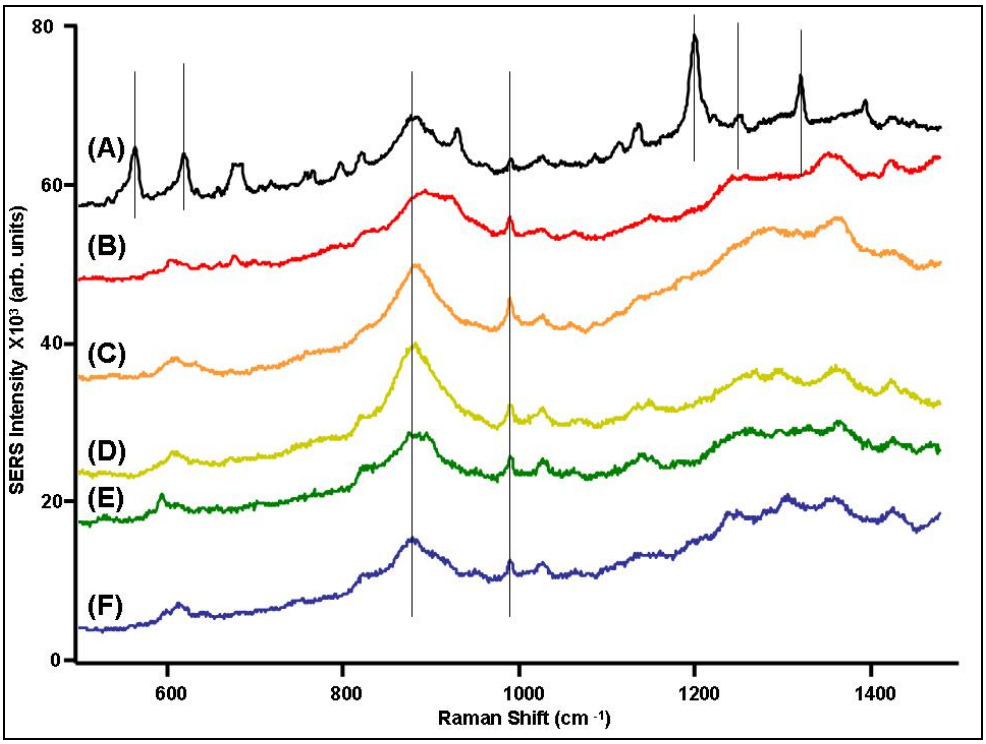

Figure 14. Comparison of several replicates (a–f) of SERS spectra from *Bacillus subtilis* spore samples on FON substrates collected on Renishaw system. Lines indicate bands common to most spectra, and some that are only seen in (a).

Next, the spectral SERS signatures of the endospores in combination with the silver colloid were collected. Taking SERS measurements of biological samples in colloidal suspensions is a fairly commonly used technique; obtaining reproducible results from these experiments, however, remains challenging. An example of an average data set for each spore sample is shown in figure 15. The SERS spectra for several of the spore samples appear distinguishable from each other. These data were compared to literature (*19*) and several common bands were able to be identified. From these results, we determined that the combination of the silver colloid and the Renishaw system worked well for SERS measurements of biological samples.

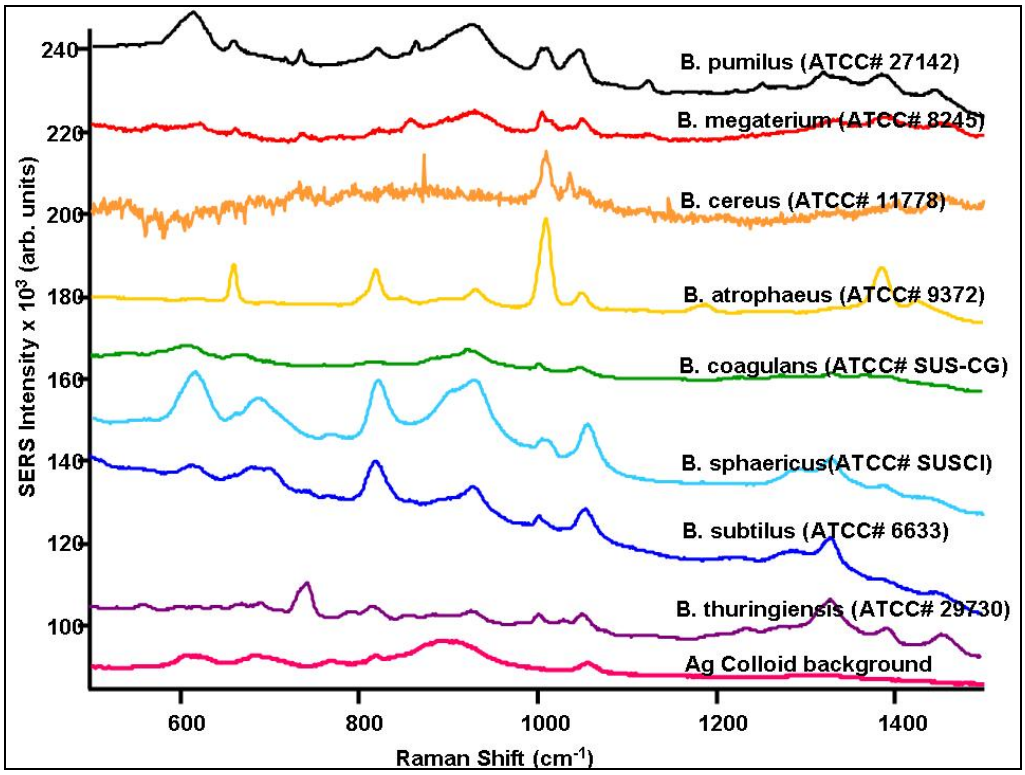

Figure 15. Comparison of SERS spectra from several Bacillus spore samples collected with silver colloids using the Renishaw system.

Next, SERS spectral signatures from the spore samples in combination with the silver colloid solution were collected using the B&WTek system. All spore samples were evaluated, but it was only possible to collect relevant spectral information (distinguishable form background) from *B. stearothermophilus, B. atrophaeus, B. megaterium, and B. thuringiensis* (see figure 16). Table 1 provides a summary of results from the Klarite and Ag colloid solutions and compares relevant SERS bands.

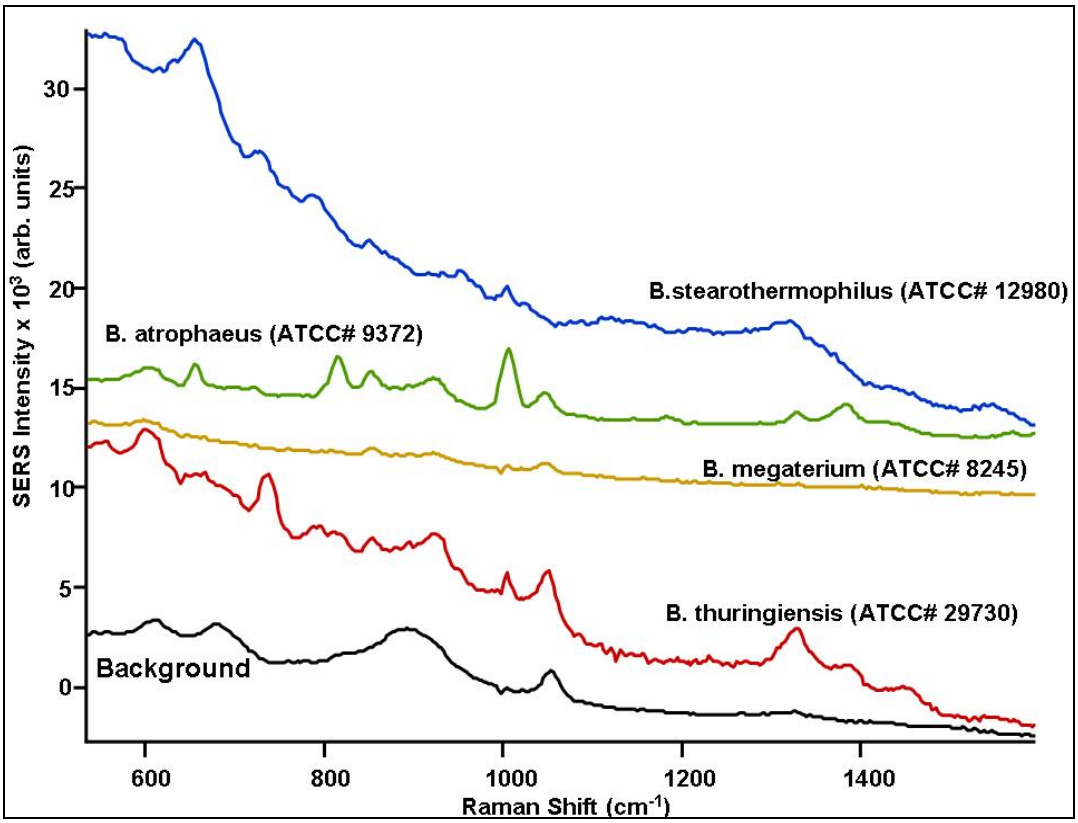

Figure 16. Comparison of SERS spectra from several Bacillus spore samples mixed with silver colloids measured using the B&WTek system. Listed top to bottom are *B. stearothermophilus*, *B. atrophaeus*, *B. megaterium*, *B. thuringiensis* and the background from the Ag colloid. Spectra have not been background subtracted. Unique bands to the samples are clearly visible.

Table 1. Summary of results measuring SERS of endospores.

Endospore	Renishaw+ Klarite Substrate Raman Band cm^{-1}	Renishaw + Silver Colloid Raman Band cm^{-1}	B&Wtek+ Silver Colloid Raman Band cm^{-1}
B. subtilis (ATCC# 35021, designation 5230)	892, 976, 1131	613, 692, 821, 929, 1002, 1055, 1330	NA
B. stearothermophilus (ATCC# 10149)	NA	658, 734, 793, 1006, 1047, 1327	654, 1004
B. Atrophaeus (ATCC# 9372)	492, 710, 1002, 1593	660, 819, 1011, 1051, 1386	658, 815, 850, 1006, 1045, 1327, 1381
B. pumilus (ATCC# 27142)	545, 684, 889, 927, 1002, 1131, 1449,	613, 658, 734, 821, 863, 925, 1006, 1045, 1124	NA
B. cereus (ATCC# 11778)	711, 735, 825, 1003, 1016, 1031, 1131, 1449	1010, 1037	NA
B. megaterium (ATCC# 8245)	548, 745, 1002, 1018, 1035, 1131, 1202, 1449	736, 857, 1004, 1052	853, 1045
B. thuringiensis (ATCC# 29730)	683, 711, 735, 940, 1532	744, 929, 1005, 1055, 1332	605, 734, 1004, 1048, 1327
B. Coagulans (SUS-CG)	1002, 1131	923, 1002, 1051	NA
B. sphericus (SUSCI)	710, 1002, 1131	613, 692, 821, 929, 1002, 1055, 1330	NA

Comparing results from figure 15 and 16, only SERS signatures from *B. atrophaeus* silver colloid, as measured between the two Raman systems, appear repeatable. As a summary of results from *B. atropheus*, the spectra from the endospore are plotted (i.e., Renishaw and colloid, B&WTek and colloid, and, finally, Renishaw and Klarite), shown in figure 17. It is clearly seen that the signature from the colloid has the same band location for the two colloid solutions. Comparing the colloid signature to that obtained from the Klarite substrate, a similar band is located at the 1000 cm^{-1} area; however, a new band is observed to grow in around 700 cm^{-1}. Additionally, the intensity of the Raman bands varies widely between the different substrates and systems, clearly demonstrating current challenges with using a portable Raman system and commercially available substrates. From these results, it can be concluded that discriminating among biological samples using the portable Raman system with a COTS substrate is not likely without continued optimization. Specifically, work still needs to be done toward the development of a SERS substrate with increased sensitivity and uniform SERS signal enhancement, in combination with a portable Raman system with increased detection capabilities.

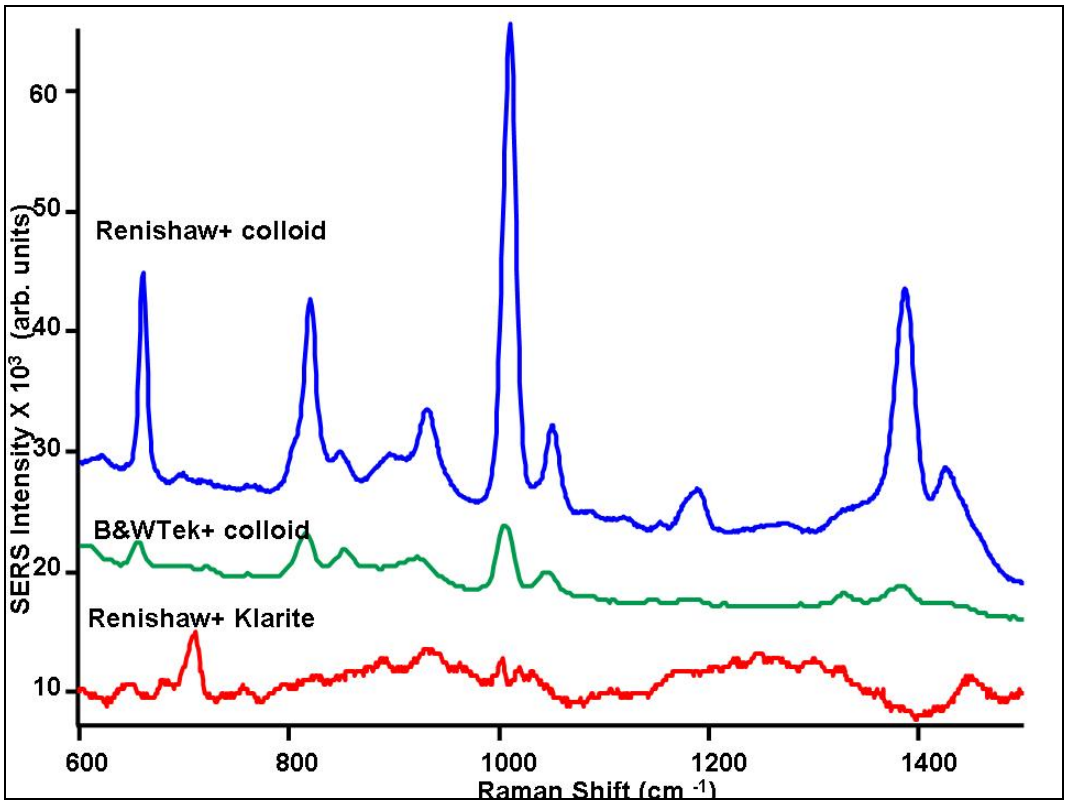

Figure 17. Comparison of *B. atropheus* with colloid on Renishaw (blue) and B&WTek system (green), and finally with Klarite SERS substrate measured with Renishaw (red).

3.3 Evaluation of Figures of Merit

Evaluation of the COTS substrates and Raman systems for biological sensing demonstrated that further optimization was necessary before these technologies are more widely Army applicable. Therefore, the utility of these systems for other types of hazard sensing was determined. The analytical figures of merit for these substrates (reproducibility of the measurements both within a substrate, across a fabricated batch of substrates, as well as batch-to-batch) were determined. Substrates under consideration were the COTS Klarite and the FON. The silver colloid solution was not evaluated, as the advantages and disadvantages of these types of systems have previously been well-documented.

For the evaluation of the figures of merit for the SERS substrates, the well-characterized SERS active chemical PHE was used. PHE was chosen as a model chemical for substrate evaluation, as it is a well-characterized Raman (*69*) and SERS standard chemical and exhibits main bands located at 621 cm^{-1}, 747 cm^{-1}, 1003.5 cm^{-1}, 1031 cm^{-1}, 1200 cm^{-1}, 1327 cm^{-1}, 1585 cm^{-1}, 1607 cm^{-1}, and 3064 cm^{-1} (see figure 18a). The lowest detectable concentration of analyte on the Klarite and fabricated multilayer slides was determined by depositing PHE over a range of concentrations (1 x 10^{-1} M to 1 x 10^{-8} M), and measuring the resulting SERS spectra. These concentrations were chosen as they ranged from being Raman to SERS active. For each set of measurements, three different substrates were used, and five random individual spots were

measured across each substrate. The concentration study results are shown in figure 18, where the average measurements for each concentration of PHE are plotted and offset for clarity. For comparison, this concentration study was performed on both Klarite substrates (figure 18b) and FON substrates (figure 18c) under the same experimental conditions.

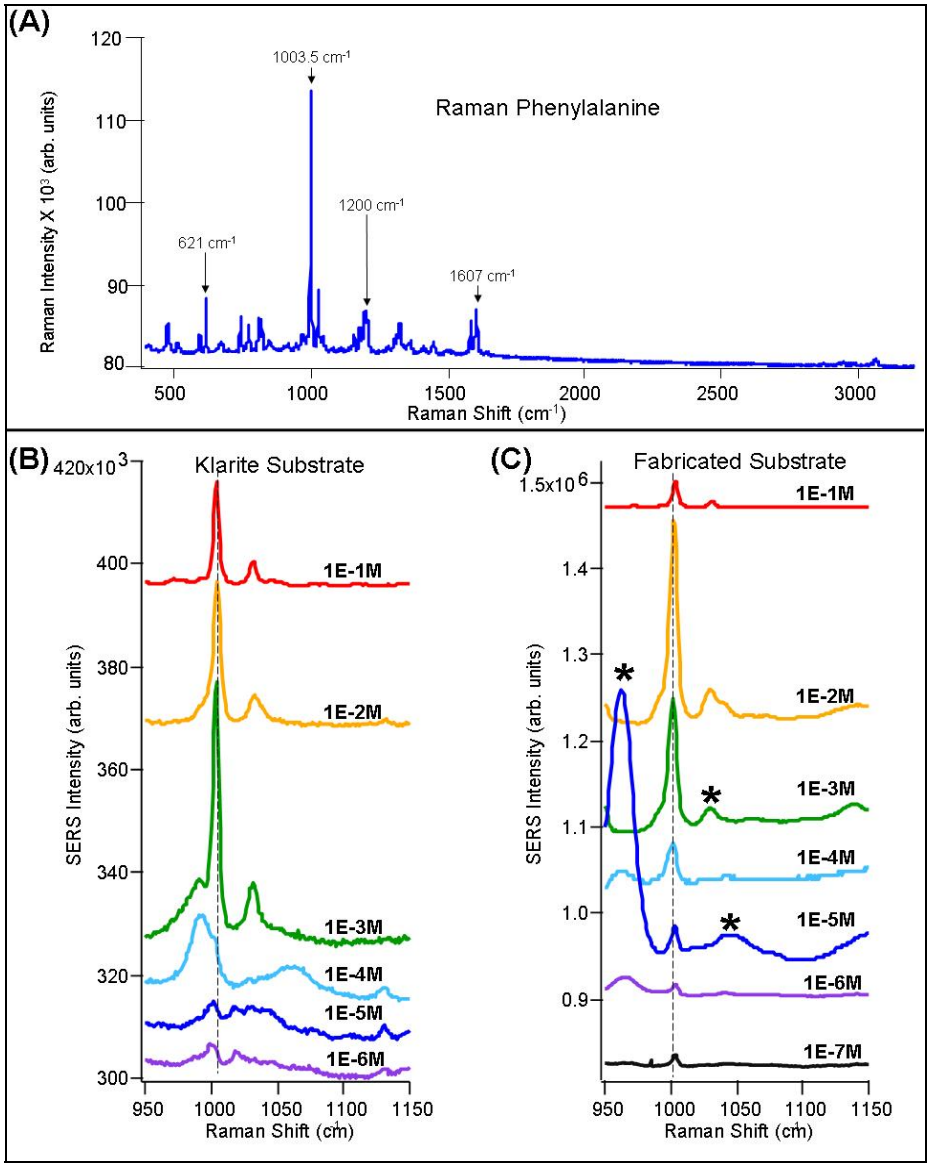

Figure 18. (a) Raman spectrum of PHE. Comparison of overall SERS signal from PHE demonstrated between (b) Klarite and (c) fabricated substrate as measured on Renishaw system. The stars (*) indicate areas on the fabricated substrate where varying background is observed.

To determine spot-to-spot reproducibility, signal-to-noise measurements across both fabricated and Klarite substrates were performed by selecting five separate locations on the substrate surface using a 0.001M concentration of PHE. Table 2 summarizes these results for the fabricated substrates, for three slides. From these results and other analysis within the sets, we

determined that typical %RSD across a single substrate typically ranges from 10–35% (see table 2). Analysis of slide-to-slide results within the same set at different concentrations (data analysis not shown) indicates that a %RSD range of 15-55% can be observed.

Table 2. Fabricated slide signal-to-noise (S/N) ratios from 0.001 M PHE.

	S/N Ratio Slide 1	S/N Ratio Slide 2	S/N Ratio Slide 3
Fabricated Slide PHE 0.001 M	230.1	179.2	252.6
	212.6	231.2	232.8
	228.7	111.2	190.2
	243.4	200.1	188.4
	204.5	206.6	219.2
Average S/N Ratio	223.9	185.7	216.6
Standard Deviation	15.4	45.5	27.7
% RSD	6.9	24.5	12.8

For comparison, the same measurements and experimental conditions were used to determine spot-to-spot and slide-to-slide reproducibility for the Klarite substrates. In general, these data exhibited better reproducibility. Analysis of slide-to-slide results within the same set at different concentrations indicates that a %RSD range of <15% is common. However, the % RSD was found to be as high as 25% in some cases. In other words, within a given substrate, the reproducibility is very good, but slide-to-slide variance can still be large.

To determine the lowest concentration visually identifiable for the various substrates, data from the PHE concentration curve was analyzed. From the data in figure 18b, it is clear that fabricated slides with PHE were detected as low as 1×10^{-7} M, and Klarite slides were detected as low as 1×10^{-3} M (figure 18c). From these results it is shown that there are at least four orders of magnitude difference in sensitivity between these substrates. Additionally, the overall enhancement for the substrates is also demonstrated. By comparing the overall signal from the 1×10^{-3} M PHE between the two substrates (with background subtraction), the fabricated substrates demonstrate a greater than 4X overall signal, as compared to the Klarite substrate.

To compare the overall detection capabilities between the Renishaw and portable system, PHE was measured over a range of concentrations using both FON and Klarite SERS substrates with the B&WTek system (see figure 19). In these experiments, three substrates were measured per concentration, and five measurements were collected per substrate. Similar instrumentation parameters were used between the two instruments to obtain comparable data results, as shown in table 3.

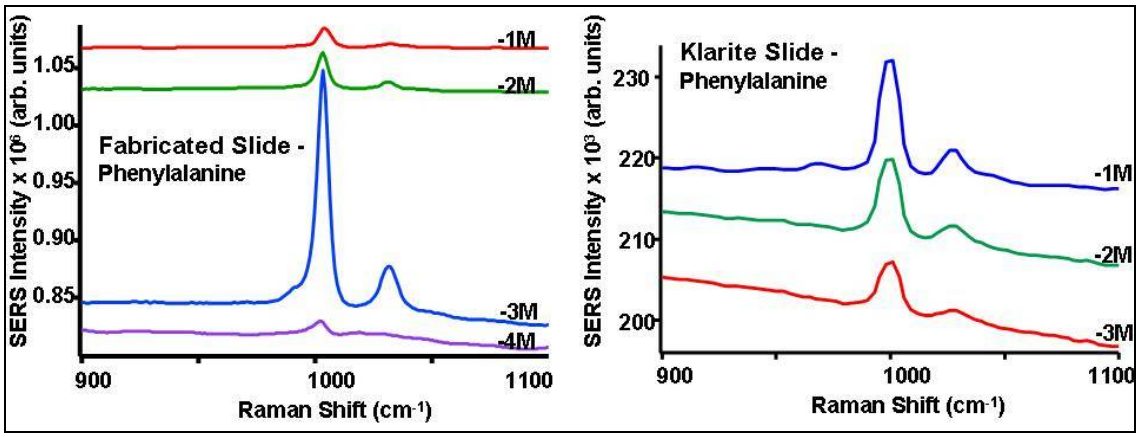

Figure 19. (a) Several concentration of PHE measured on fabricated substrate, data collected with B&WTek system. (b) Several concentrations of PHE measured on Klarite substrate, data collected with B&WTek system.

Table 3. Average S/N ratio comparison between Klarite and fabricated SERS substrates using a range of PHE concentrations and measured using the B&WTek Raman system.

PHE Concentration (M)	Substrate	Average S/N	Std. dev	%RSD
0.1	Klarite	26.9	1.0	3.8
	Fabricated	84.4	21.1	25.0
0.01	Klarite	13.0	1.0	7.8
	Fabricated	64.3	14.1	21.9
0.001	Klarite	7.9	1.0	12.9
	Fabricated	210.2	33.6	16.0
0.0001	Klarite	NA	NA	NA
	Fabricated	24.8	6	24.2

Using the B&WTek system, concentrations below 1 x 10^{-4} M PHE were not able to be detected. Comparing the detection limit results between the two systems demonstrates that the Renishaw system is capable of detecting almost three orders of magnitude lower than the B&WTek system. The detection capabilities of the B&WTek system are thus limited to very high concentrations of analyte (see figure 19).

From these results it is possible to draw some conclusions comparing the FON and Klarite substrates, as well as between the utility of the Renishaw and B&WTek Raman systems. The FON substrates demonstrate increased sensitivity but very poor reproducibility. These substrates may perform better with more optimization. The Klarite substrates demonstrate decreased background, high reproducibility in SERS signal enhancement but decreased sensitivity. Modification of the surface of these substrates may make them more application sensitive. Comparing the detection capabilities between the Renishaw and B&WTek system, the Renishaw, as expected, demonstrates much higher sensitivity. In conclusion, continued optimization of these systems for COTS Army application is still needed.

3.4 Explosives

To investigate the utility of the FON and Klarite SERS substrates for applications to other hazard sensing, explosive detection capabilities were evaluated. These results were then compared with data collected using the silver colloid solution. The explosives considered included TNT and RDX, as they represent commonly used explosives in most military explosive preparations, and can be found in the soil in locations where detonations have occurred or in the presence of unexploded ordinance (*70–73*).

TNT is a nitroaromatic, with common Raman bands located at 788 cm^{-1}, 820 cm^{-1}, 1031 cm^{-1}, 1308 cm^{-1}, 1350 cm^{-1}, 1370 cm^{-1}, 1419 cm^{-1}, and 1600 cm^{-1} (*72–76*). The SERS signal from concentrations of TNT ranging from 1000 ug/mL to 15 ug/mL were measured with the FON, silver colloids, and Klarite slides, using both the Renishaw and B&WTek Raman systems (see figure 20). The parameters employed for data collection with the Renishaw system were use of the 785 nm laser, 1% power, 10 s accumulation, three accumulations each data point, pinhole out, and 50X microscope objective. Three substrates were analyzed each set, and five data points were collected randomly from across the substrate surface. For data analysis of S/N ratios and lowest detectable concentration determination, the TNT SERS bands located at 788 cm^{-1} and 821 cm^{-1} were used.

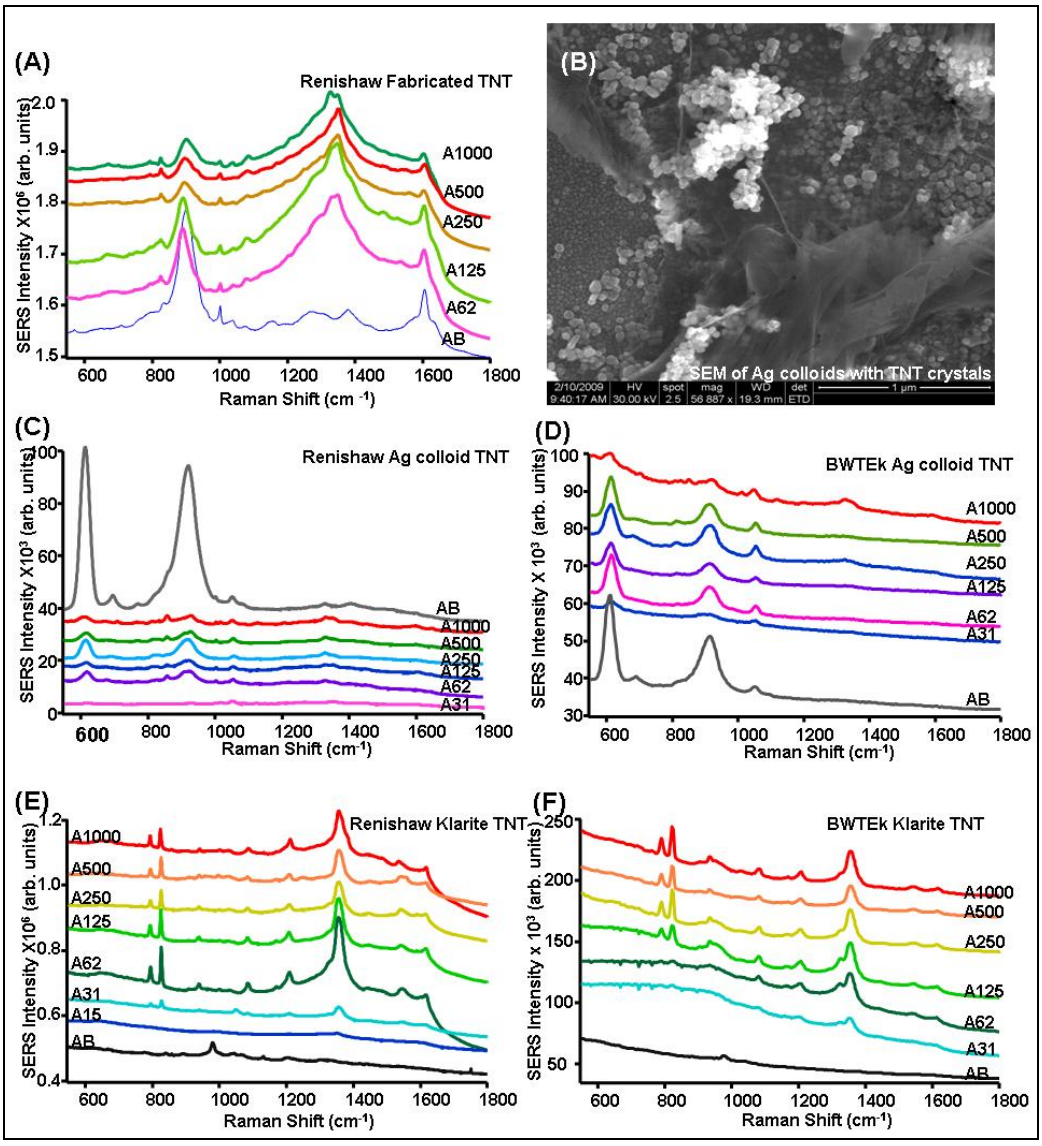

Figure 20. Average SERS spectra of TNT as measured with fabricated slide on Renishaw (a), SEM of silver colloids with TNT crystals (b), silver colloid measured with Renishaw (c) and B&WTek (d), Klarite substrate collected using the B&WTek (e) and Renishaw system (f). TNT concentration ranges from 1000 ug/mL to 15 ug/mL. Spectrum of solvent acetonitrile on blank substrate is also shown (AB). The average concentrations are marked as A###, where the # represents ug/mL.

In figure 20, an example of data collected with the fabricated FON slides, silver colloid, and the Klarite substrates, using both the B&WTek system and Renishaw system, is shown. Data from the fabricated slides measured with B&WTek system is not shown, as it was not possible to elucidate the TNT bands from the background bands. In figure 20a, the TNT 821 cm^{-1} band is visible next to the large background band located at 894 cm^{-1}. From figure 20c and d, it can be seen that no visible TNT bands are identifiable, which is due to a large background observed at 608 cm^{-1} and 900 cm^{-1}. However, when using the Klarite substrates, it was possible to clearly

determine TNT bands and see an increase in band intensity with a change in TNT concentration (see figure 20e). A summary of average S/N ratios for the data set shown in figure 14e, is shown in table 4. From these Renishaw measurements it was determined that the TNT can be measured for the fabricated slides as low as 62 ug/mL, and detected as low as 31 ug/mL using the Klarite substrates.

Table 4. Clearly demonstrates S/N ratios for average set of TNT SERS signal measured using Klarite substrate and Renishaw.

Concentration TNT (ug/mL or ppm)	**S/N**	**Std. Dev.**	**%RSD**
1000	55.9	3.6	6.4
500	62.3	2.4	3.9
250	60.2	7.1	11.8
125	40.7	5.0	12.3
62	22.3	7.0	31.4
31	30.7	4.5	14.7

A similar analysis was repeated for dinitrotoluene (DNT) and RDX, using the same parameters as for the TNT experiments. RDX is a nitramine that exhibits main Raman bands located at 876 cm^{-1}, 1031 cm^{-1}, 1310 cm^{-1}, 1570 cm^{-1}, and 1597 cm^{-1} (*70*). In figure 21a, the Raman spectrum of a crystal of RDX is shown. RDX was measured on fabricated multilayer, silver colloid, and Klarite substrates. The spectral signature of RDX was not able to be measured using any of the substrates with either the Renishaw or B&WTek system (see figure 21b). The dotted line located at 1040 cm^{-1} appears in the blank as well as the sample spectra, and is, therefore, not a Raman active RDX band. From analysis of this sample and DNT data collected (not shown), it was determined that explosive samples are challenging to measure, as they can have fluorescent backgrounds that prohibit distinguishing SERS bands. Additionally, due to the background signatures measured on several of the substrates, differentiating background bands from analyte bands with a low Raman cross-section remains challenging.

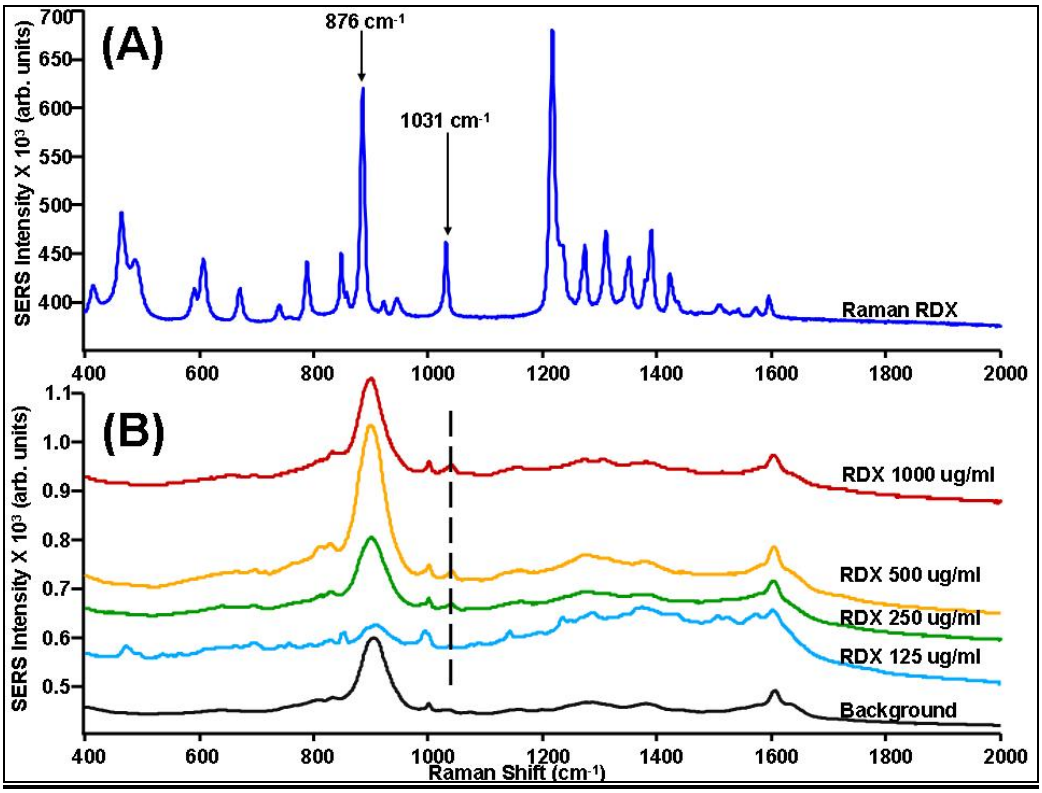

Figure 21. (a) Raman spectrum of RDX collected using Renishaw system. (b) RDX on fabricated slide showing no similar RDX bands.

3.5 Chemical Simulants

There is a great interest in the timely and accurate identification of hazardous chemicals and agents. Film over nanospheres and Klarite substrates were evaluated in both a benchtop Renishaw Raman microscope as well as a portable Raman system with chemical agent simulants to determine if there was an Army relevant application in using these sensing technologies.

Chemical agents are classified as organophosphates and include nerve agents, blister agents, choking agents, and blood agents (*3, 6, 31–33, 60, 77*). As nerve agents are becoming more commonly used by terrorist groups, there has been a focus on the detection of nerve agents like Sarin (1,2,2-trimethylpropyl ester; GB) and Soman (methylphosphoroflouridic acid) and their degradation products like DMMP and DIMP (*6*). The compounds DMMP and DIMP were also partially chosen because they do not require any special safety handling techniques to be employed (*6*). Typically for SERS measurements, vapors of these compounds are adsorbed onto a SERS active substrate and then measured (*77*). These simulants have been characterized as having very low Raman cross-sections on the order of 6×10^{-30} to 10×10^{-30} cm^2 sr^{-1} $molecule^{-1}$ with 514.5 nm excitation (*77*). DIMP is reported to have observable SERS bands located at 710 cm^{-1}, 830 cm^{-1}, 2846 cm^{-1}, 2877 cm^{-1}, and 2925 cm^{-1} (*77*). DMMP has observable SERS bands located at 712 cm^{-1}, 1260 cm^{-1}, 2855 cm^{-1}, 2930 cm^{-1}, 2960 cm^{-1} and 3000 cm^{-1} (*77*).

In these experiments, DMMP and DIMP were used as received at concentrations ranging from 50%, 25%, 12.5%, 6%, 3%, 1.5%, 0.8% and finally 0.4% in acetonitrile. For these experiments, a 2 uL aliquot of solution was applied to three substrates per concentration, and allowed to drop and dry on the SERS active surface. The solution dried for 2 min, and the resulting SERS spectra were immediately collected using the Renishaw and B&WTek system. Data was collected from five different random spots per substrate. This procedure was repeated for the fabricated slides and the Klarite substrates. Instrumentation parameters employed on the Renishaw were: 785 nm laser, 5% power, a 10 s exposure, and 3 accumulations per exposure. For the B&WTek system the 785 nm laser, 100% power, 1 accumulation/measurement, and a 6 s exposure. Data shown has not been background subtracted.

For data analysis, the SERS signals from the 718 cm^{-1}, 719 cm^{-1} (P-C stretch)[6], and 883 cm^{-1} bands were used for both the DIMP and DMMP simulants. SERS measurements were done with the fabricated and Klarite substrates. From the fabricated slides, it was not possible to distinguish Raman bands from simulants from the substrate background. With more optimization of these substrates—specifically, background elimination—it may have been possible to detect simulants. The Klarite substrates were able to be used for simulant measurements, as they did not have any large interfering background bands. From the results in figure 22, it is clear that under these testing conditions, the lowest concentration detectable is 6% for DMMP and 3% for DIMP in acetonitrile solution with a Klarite substrate and the Renishaw system.

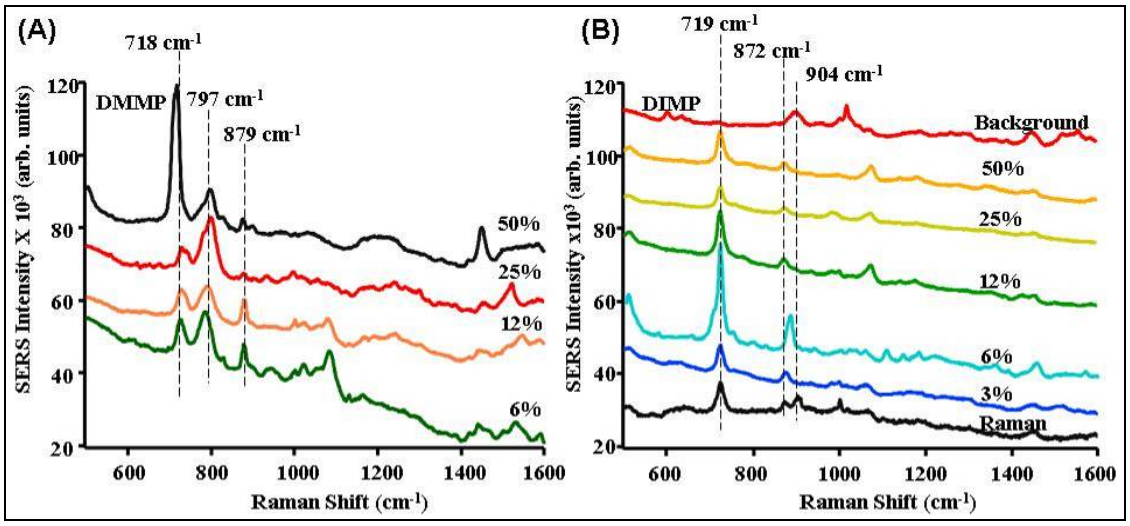

Figure 22. SERS spectra (a) DMMP and (b) DIMP on Klarite substrates. Data collected using Renishaw system.

Next, measurements were collected using the portable Raman B&WTek system (figure 23). For these measurements, a dilution series was made of the analyte in acetonitrile, and a 2 uL aliquot of analyte was applied to 3 substrates per set. Data was collected from five different random spots per substrate from both fabricated and Klarite substrates. For data analysis, the signals

from the DMMP 722cm^{-1} and DIMP 722 cm^{-1} bands were used. Under experimental conditions used, it is clear that the lowest concentration detectable is 6% DMMP and 1% DIMP in acetonitrile solution. When we used the fabricated substrates, it was not possible to detect the DIMP, as the background from the substrates interfered with band distinction.

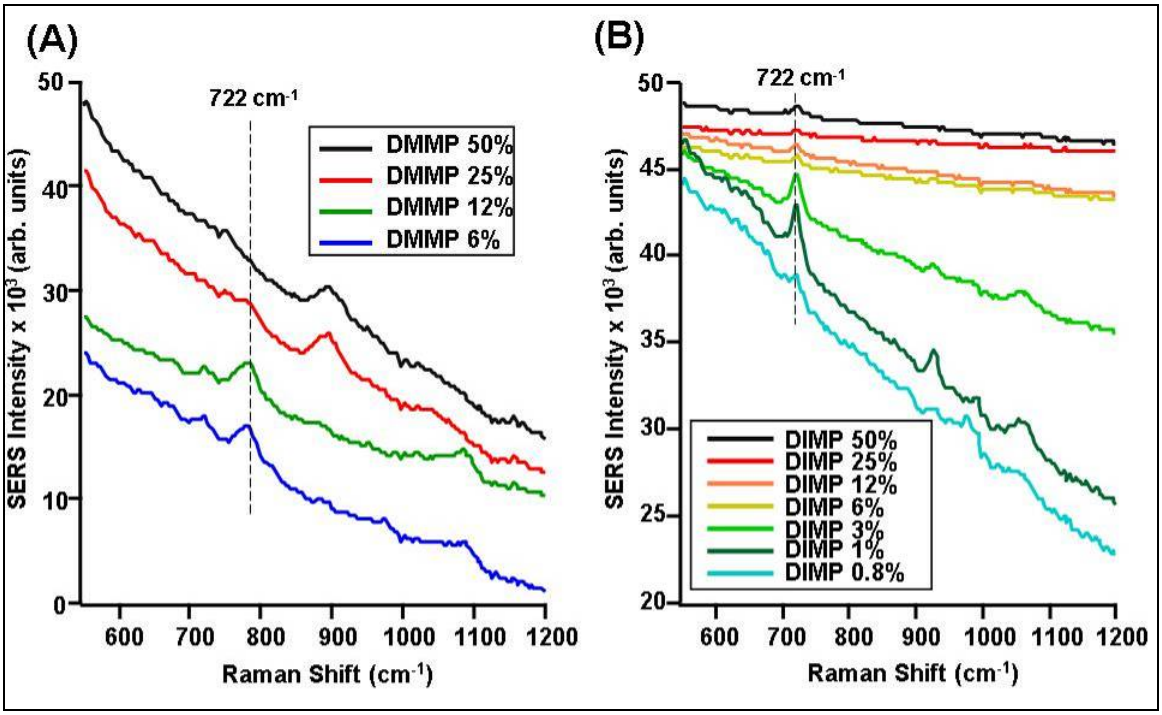

Figure 23. Data collected with B&WTek system and Klarite substrate, (a) DMMP and (b) DIMP.

4. Conclusions/Recommendations

4.1 Substrates

One of the goals of our work was to evaluate limits of detection, reproducibility, and real-world applicability of commercially available Klarite substrates and fabricated SERS substrates. These two different SERS substrates were selected because they require little to no sample preparation prior to use, and are easily obtained and fabricated. Comparing the chemical detection/explosive results between the multilayered fabricated and Klarite substrates, it has been shown that the fabricated substrates demonstrate greater sensitivity (roughly two orders of magnitude), but have a less reproducible SERS signal enhancement (10% RSD difference) and a larger background signature. Both SERS architectures also demonstrate a response curve that suggests a high degree of non-linearity. This type of response could severely impact any ability to apply quantification unless alternate measurements are used as external or internal calibration procedures.

In the literature, it has been suggested that the fabricated multilayer substrates demonstrate spot-to-spot reproducibility of >10%, and substrate-to-substrate reproducibility of ~15% (*54, 56, 68*). With further optimization of the fabricated substrates (improving fabrication skills, lessening the background signature, and decreasing the % RSDs), these substrates may be viable for application to biological sensing solely based on their superior sensitivity, but could require extensive studies focused on reducing the severe background by changing underlayer components. The Klarite commercial SERS substrates may have preferential application for complex analytes (biologicals) because of their low background and reproducible SERS signal; however, these substrates will require analogous studies to increase their sensitivity before they gain needed advantages to enable widespread use.

As there were advantages and disadvantages to the use of the fabricated multilayer substrate and commercial Klarite substrate, efforts to obtain spore signatures were made using silver colloids. It should be noted that colloid solutions are often fundamentally limited, as they require sample preparation prior to use (mixing with sample) and often are difficult to use in quantitative studies. However, towards the efforts of evaluating substrates, these colloid solutions have been previously shown in literature for successfully collecting spore signatures (*19*). Using the silver colloids, it was possible to obtain spore signatures. When we compared signatures obtained from the same sample with the literature, however, we still observed spectral differences. Also, as we compared the spore signatures obtained between the Klarite and colloid data, we found that for the same spore there were very different SERS bands that are observed, suggesting chemical selection rules might be preferentially increasing/decreasing/ shifting bands. This observation raises other concerns regarding the broad use of SERS substrates and how spatial relationship of the fields and the chemical moieties within these fields affect the spectrum of identical analytes.

4.2 Instruments

Comparing the detection systems, the Renishaw demonstrates significantly greater sensitivity than the portable B&WTek system—up to three orders of magnitude in some cases. Complete analysis of the systemic differences is difficult to obtain, given the aforementioned non-linear response from the substrates studied, but trends suggest that the Renishaw system outperforms the B&WTek system by a significant margin. For a portable SERS system to be a viable alternative to a benchtop Raman/SERS system, it would need to demonstrate better detector capabilities, filtering, and lower background noise. Many of these attributes could be traced back to engineering decisions to dramatically increase the laser power for increased signal strength and rely on inexpensive detector choices. Although wise from a business standpoint, this combination could prove to be an ineffective combination for usage with SERS active material. As a footnote, it should be mentioned that it may be a suspect choice for standard Raman measurements, also, due to the possibility of ignition of flammable materials directly stemming from high laser powers used. Further laboratory studies need to be conducted to fully determine exact parameter settings required for a portable system that is to be used in combination with SERS active material.

4.3 SERS Sensing Application

SERS applications for detecting and identifying chemicals have been widely shown in the literature. For pure samples, SERS can, in some cases, be used for quantitative work. However, there are still chemical effects that occur between the substrate and the analyte that can make assignment of observed SERS bands challenging. As demonstrated in this study, blanket increase in Raman scattering over wide ranges of chemicals is not consistent, and, furthermore, even substrates presenting the same coinage metals produce different spectral signatures. This type of response does not prohibit their use as a sensor technology, but it makes pure systematic and general studies much more complex. Finally, biological samples contain very complex mixtures of analytes, are inherently variable/dynamic (growth stage of cell), and may require sample preparation to limit matrix effects. Compounding this complexity further, the Raman scattering from these materials is empirically weaker, and the interaction of the SERS substrates with the biological components from a spatial standpoint is unclear. This suggestion of combining SERS active material and with a portable detection system to enable a new biosensor platform was ambitious, but somewhat short-sighted. Reproducibility of the commercial substrates alleviated one concern that was suggested to be a roadblock to usage and sacrificed a fundamental necessity of sensitivity, which is ultimately a property that cannot be dismissed given the targets of interest. It is clear from this and other investigation that SERS of biologicals is still challenging, and other analytical techniques must still be used for identification and quantification of analytes.

We firmly believe that this study has not brought closure to the investigations of SERS for chemical and biological detection, but has highlighted and reaffirmed recent observations as to its limitations. Continued and focused collaborative effort will be needed from both ECBC and ARL to unravel the fundamental phenomenology behind the empirical observations being made. One thing that is clear from these investigations is that it will require the concerted effort of all involved to mature this technology. But given its potentially wide applicability, as demonstrated within this report, it is well worth the risks involved.

5. References

1. Harris, W. A.; Reilly, P.T.A.; Whitten, W. B. *Anal. Chem.* **2007**, *79*, 2354–2358.
2. Wang, J.; Pumera, M.; Chatrathi, M. P.; Escarpa, A.; Musameh, M.; Collins, G.; Mulchandani, A.; Lin, Y.; Olsen, K. *Anal. Chem.* **2002**, *74*, 1187–1191.
3. Inscore, F.; Gift, A.; Maksymiuk, R.; Farquharson, S. *SPIE* **2004**, *5585*, 46–52.
4. McBride, M. T.; Gammon, S.; Pitesky, M.; O'Brien, T. W.; Smith, T.; Aldrich, J.; Langlois, R. G.; Colston, B.; Venkateswaran, K. S. *Anal. Chem.* **2003**, *75*, 1924–1930.
5. Hindson, B. J.; Brown, S. B.; Marshall, G. D.; McBride, M. T.; Makarewicz, A. J.; Gutierrez, D. M.; Wolcott, D. K.; Metz, T. R.; Madabhushi, R. S.; Dzenitis, J. M.; Colston, B. W. *Anal. Chem.* **2004**, *76*, 3492–3497.
6. Christesen, S. D. *Applied Spectroscopy* **1988**, *42*, 318–321.
7. Kalasinsky, K. S.; Hadfield, T.; Shea, A. A.; Kalasinsky, V. D.; Nelson, M. P.; Neiss, J.; Drauch, A. J.; Vanni, G. S.; Treado, P. J. *Anal. Chem.* **2007**, *79*, 2658–2673.
8. Wei, F.; Zhang, D.; Halas, N. J.; Hartgerink, J. D. *J. Phys. Chem. B* **2008**, *112*, 9158–9164.
9. Stiles, P. L.; Dieringer, J. A.; Shah, N. C.; Duyne, R. P. V. *Annu. Rev. Anal. Chem.* **2008**, *1*, 601–626.
10. Kneipp, K.; Kneipp, H. *Appl. Spectros.* **2006**, *60*, 322A.
11. Kneipp, K.; Kneipp, H.; Kartha, V. B.; Manoharan, R.; Deinum, G.; Itzkan, I.; Dasari, R. R.; Feld, M. S. *Physical Review E* **1998**, *57*, R6281–R6284.
12. Kneipp, K.; Kneipp, H.; Manoharan, R.; Itzkan, I.; Dasari, R. R.; Feld, M. S. *Journal of Raman Spectroscopy* **1998**, *29*, 743–747.
13. Kneipp, K.; Kneipp, H.; Itzkan, I.; Dasari, R. R.; Feld, M. S. *Chemical Physics* **1999**, *247*, 155–162.
14. Kneipp, K.; Kneipp, H.; Abdali, S.; Berg, R. W.; Bohr, H. *Spectroscopy-an International Journal* **2004**, *18*, 433–440.
15. Aroca, R. F.; Alvarez-Puebla, R. A.; Pieczonka, N.; Sanchez-Cortez, S.; Garcia-Ramos, J. V. *Advances in Colloid and Interface Science* **2005**, *116*, 45–61.
16. Kenipp, K.; Kneipp, H.; Bohr, H. G. In *Topics in Applied Physics*; Springer Berlin: Heidelberg, 2006; Vol. 103/2006, pp 261–277.

17. Lombardi, J. R.; L.Birke, R. *J. Phys. Chem. B* **2008**, *112*, 5605–5617.

18. Schwartzberg, A. M.; Zhang, J. Z. *J. Phys. Chem. C* **2008**, *112*, 10323–10337.

19. Guicheteau, J.; Argue, L.; Emge, D.; Hyre, A.; Jacobson, M.; Christesen, S. *Applied Spectroscopy* **2008**, *62*, 267–272.

20. Kahraman, M.; Yazici, M. M.; Sahin, F.; Culha, M. *Journal of Biomedical Optics* **2007**, *12*, 0540151–0540156.

21. Efrima, S.; Bronk, B. V.; Czege, J. *SPIE* **1999**, *3602*, 164–171.

22. Jarvis, R. M.; Law, N.; Shadi, I. T.; O'Brian, P.; Lloyd, J. R.; Goodacre, R. *Anal. Chem.* **2008**, *80*, 6741–6746.

23. Alexander, T. A.; Le, D. M. *Appl. Opt.* **2007**, *46*.

24. Sengupta, A.; Mujacic, M.; Davis, E. J. *Anal. Bioanal. Chem.* **2006**, *386*, 1379–1386.

25. Jarvis, R. M.; Goodacre, R. *Anal. Chem.* **2004**, *76*, 40–47.

26. Premasiri, W. R.; Moir, D. T.; Klempner, M. S.; Krieger, N.; Jones, G.; Ziegler, D. *J. Phys. Chem. B* **2005**, *109*, 312–320.

27. Jones, J. P.; Fell, N. F.; Alexander, T.; Fountain, A. W. *SPIE* **2004**, *5416*, 94–104.

28. Fountain, A. W.; Pearman, W. F. *SPIE* **2005**, *5994*, 59940P59941–59940P59914.

29. Guzelian, A. A.; Sylvia, J. M.; Janii, J. A.; Clauson, S. L.; Spencer, K. M. *SPIE* **2002**, *4577*, 182–192.

30. Alexander, T. A.; Pellegrino, P. M.; Gillespie, J. B. *Applied Spectroscopy* **2003**, *57*, 1340–1345.

31. Stuart, D. A.; Biggs, K. B.; VanDuyne, R. P. *Analyst* **2006**, *131*, 568–572.

32. Alak, A. M.; Vo-Dinh, T. *Anal. Chem.* **1987**, *59*, 2149–2153.

33. Yan, F.; Wabuyele, M. B.; Griffin, G. D.; Vass, A. A.; Vo-Dinh, T. *IEEE Sens. J.* **2005**, *5*.

34. Yan, F.; Vo-Dinh, T. *Sensors and Actuators B* **2006**, *121*, 61–66.

35. Taranenko, N.; Alarie, J.-P.; Stokes, D. L.; Vo-Dinh, T. *Journal of Raman Spectroscopy* **1995**, *21*, 379–384.

36. Kuncicky, D. M.; Christesen, S. D.; Velev, O. D. *Applied Spectroscopy* **2005**, *59*, 401–409.

37. Schueler, P. A.; Ives, J. T.; DeLaCroix, F.; Lacy, W. B.; Becker, P. A.; Li, J.; Caldwell, K. D.; Drake, B.; Harris, J. M. *Anal. Chem.* **1993**, *65*, 3177–3186.

38. Odom, T. W.; Nehl, C. L. *ACS Nano* **2008**, *2*, 612–616.

39. Tiwari, V. S.; Oleg, T.; Darbha, G. K.; Hardy, W.; Singh, J. P.; Ray, R. C. *Chemical Physics Letters* **2007**, *446*, 77–82.

40. Kuncicky, D. M.; Prevo, B. G.; Velev, O. D. *J. Mater. Chem.* **2006**, *16*, 1207–1211.

41. Vo-Dinh, T.; Stokes, D. L.; Griffin, G. D.; Volkan, M.; Kim, U. J.; Simon, M. I. *Journal of Raman Spectroscopy* **1999**, *30*, 785–793.

42. Tao, A.; Kim, F.; Hess, C.; Goldberger, J.; He, R.; Sun, Y.; Xia, Y.; Yang, O. *Nano Letters* **2003**, *3*, 1229–1233.

43. Braun, G.; Pavel, I.; Morrill, A. R.; Seferos, D. S.; Bazan, G. C.; Reich, N. O.; Moskovits, M. *J. Am. Chem. Soc.* **2007**, *129*, 7760–7761.

44. Schider, G.; Krenn, J. R.; Hohenau, A.; Diltbacher, H.; Leitner, A.; Aussenegg, F. R.; Schaich, W. L.; Puscasu, I.; Monacelli, B.; Boreman, G. *Physical Review B* **2003**, *68*, 1554271–1554244.

45. Bantz, K. C.; Haynes, C. L. *Langmuir* **2008**, *24*, 5862-5867.

46. Li, K.; Clime, L.; Tay, L.; Cui, B.; Geissler, M.; Veres, T. *Anal. Chem.* **2008**, *80*, 4945–4950.

47. Alexander, T. A. *SPIE* **2005**, *6007*, 600703.

48. Alexander, T. A. *Anal. Chem.* **2008**, *80*, 2817–2825.

49. Beljebbar, A.; Sockalingum, G. D.; Morjani, H.; Angiboust, J. F.; Manfait, M. *Spectrochimica Acta Part A: Molecular and Biomolecular Spectroscopy* **1997**, *53*, 123–128.

50. Doering, W. E.; Piotti, M. E.; Natan, M. J.; Freeman, R. G. *Adv. Mater.* **2007**, *19*, 3100.

51. Fabris, L.; Dante, M.; Nguyen, T. Q.; Tok, J.B.H.; Bazan, G. C. *Advanced Functional Materials* **2008**, *18*, 2518–2525.

52. Fang, C.; Agarwal, A.; Buddharaju, K. D.; Khalid, N. M.; Salim, S. M.; Widjaja, E.; Garland, M. V.; Balasubramanian, N.; Kwong, D. L. *Biosens. Bioelectron.* **2008**, *24*, 216.

53. Hankus, M. E.; Gibson, G. J.; Cullum, B. M. *Proceedings of the SPIE - The International Society for Optical Engineering* **2005**, 600704-600701-600711.

54. Li, H.; Baum, C. E.; Sun, J.; Cullum, B. M. *SPIE* **2006**, *6218*, 621804.

55. Xie, J. P.; Zhang, Q. B.; Lee, J. Y.; Wang, D.I.C. *ACS Nano* **2008**, *2*, 2473–2480.

56. Li, H.; Patel, P. H.; Cullum, B. M. *SPIE* **2004**, *5588*.

57. Netti, M. C.; Zoorob, M. E.; Charlton, M.C.B.; Ayliffe, P.; Mahnkopf, S.; Stopford, P.; Todd, K.; Lincoln, J. R.; Perney, N.M.B.; Baumberg, J. J. *SPIE* **2006**, *6093*.

58. Szeghalmi, A.; Kaminskjy, S.; Rosch, P.; Popp, J.; Gough, K. M. *J. Phys. Chem. B* **2007**, *111*, 12916–12924.

59. Flaukenrath, R. A.; Newman, R. D.; Thayer, B. A. *Americas' Achilles Heel: Nuclear, Biological and Chemical Terrorism and Covert Attack*; MIT Press: Cambridge, 1998.

60. Pearman, W. F.; Fountain, A. W. *Appl. Spectros.* **2006**, *60*.

61. Schatz, G. C.; Young, M. A.; Van Duyne, R. P. *Topics in Applied Physics* **2006**, *103*, 19–46.

62. Haynes, C. L.; McFarland, A. D.; Van Duyne, R. P. *Analytical Chemistry* **2005**, *77*, 338A–346A.

63. Fleischmann, M.; Handra, P. J.; McQuillan, A. J. *Chemical Physics Letters* **1974**, *26*, 163.

64. Jeanmaire, D. L.; Duyne, R.P.V. *Journal of Electroanalytical Chemistry* **1977**, *84*, 1.

65. Kneipp, J.; Kneipp, H.; McLaughlin, M.; Brown, D.; Kneipp, K. *Nanoletters* **2006**, *6*, 2225–2231.

66. Moskovits, M.; Tay, L.-L.; Yang, J.; Haslett, T. *Topics in Applied Physics* **2002**, *82*, 215–226.

67. Jensen, T. R.; Duyne, R. P. V.; Johnson, S. A.; Maroni, V. A. *Applied Spectroscopy* **2000**, *54*, 371–377.

68. Li, H.; Baum, C. E.; Cullum, B. M. *SPIE* **2006**, *6380*.

69. Ravikumar, B.; Rajaram, R. K.; Ramakrishnan, V. *Journal of Raman Spectroscopy* **2006**, *37*, 597–605.

70. Torres, P.; Mercado, L.; Mortimer, L.; Mina, N.; Hernandez, S.; Larau, R.; Chamberlain, R. T.; Castro-Rosario, M. E. *SPIE* **2003**, *5089*, 1054–1064.

71. McNesby, K. L.; Fell, N. F.; Vanderhoff, J. A. *SPIE* **1997**, *3082*, 121–135.

72. Rozo, J.I.J.; Balaguara, M.D.R.; Cabanzo, A.; Montoya, E.D.L.C.; Hernadez-Rivera, S. P. *SPIE* **2006**, *6201*, 62012G62011–62012G62018.

73. Santillan, J. D.; Brown, C. D.; Jalenak, W. *SPIE* **2007**, *6540*, 65400P65401–65400P65408.

74. Docherty, F. T.; Monaghan, P. B.; McHugh, C. J.; Graham, D.; Smith, W. E.; Cooper, J. M. *IEEE Sensors Journal* **2005**, *5*, 632–640.

75. Lewis, I. R.; Daniel, N. W.; Griffiths, P. R. *Applied Spectroscopy* **1997**, *51*, 1854–1867.

76. Kneipp, K.; Wang, Y.; Dasari, R. R.; Feld, M. S.; Gilbert, B. D.; Janni, J.; Steinfeld, J. I. *Spectrochimica Acta Part a-Molecular and Biomolecular Spectroscopy* **1995**, *51*, 2171–2175.

77. Taranenko, N.; Alarie, J. P.; Stokes, D. L.; VoDinh, T. *Journal of Raman Spectroscopy* **1996**, *27*, 379–384.

Appendix A. FON Optimization Supplemental

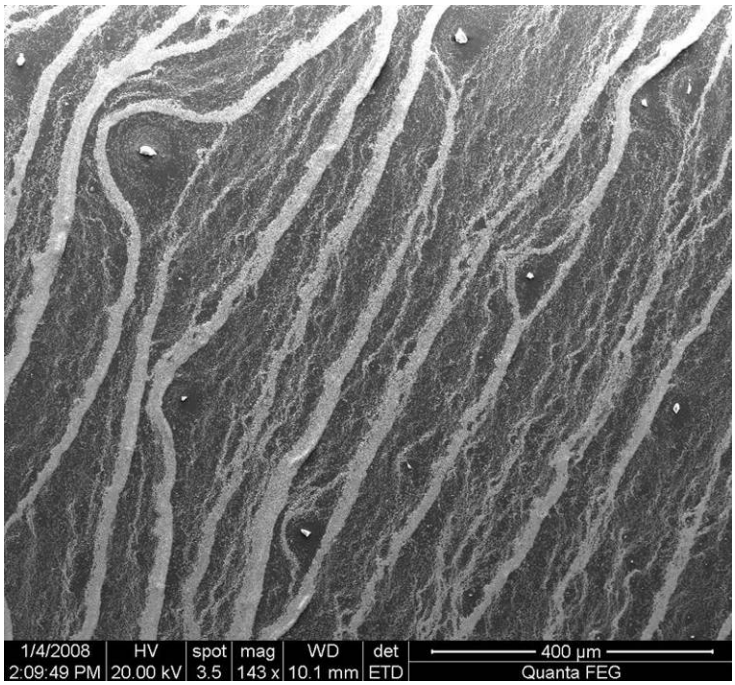

Figure A-1. SEM image of 1%w/v sphere to EtOH/acetone solution.

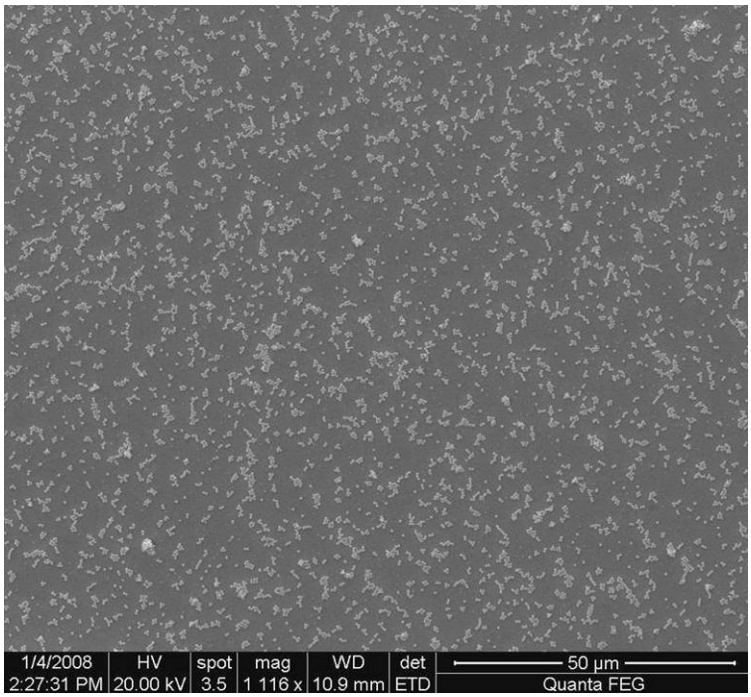

Figure A-2. SEM image of 2%w/v sphere to EtOH/acetone solution.

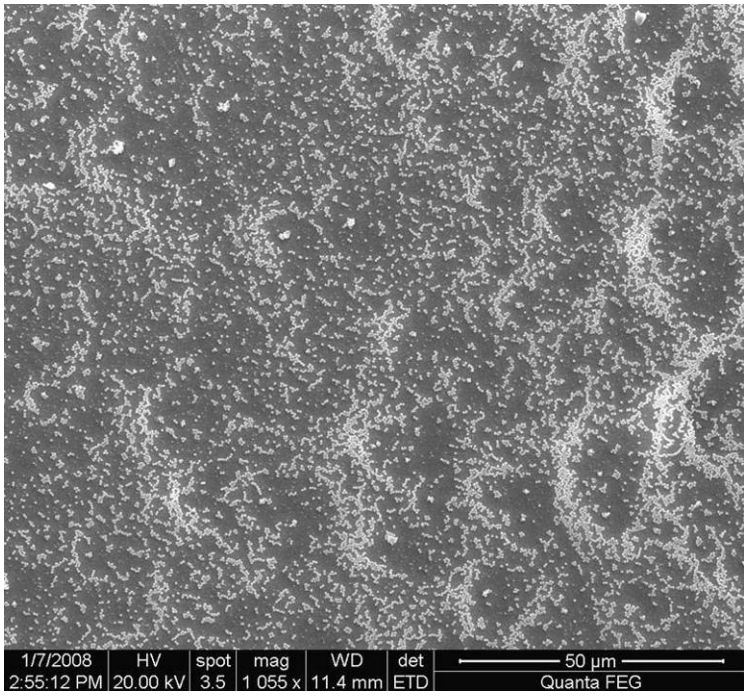

Figure A-3. SEM image of 3%w/v sphere to EtOH/acetone solution.

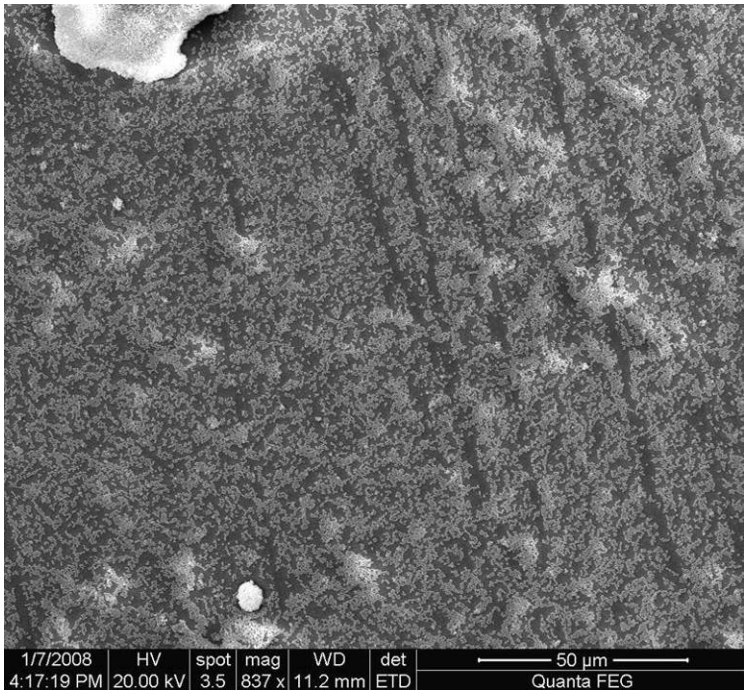

Figure A-4. SEM image of 4%w/v sphere to EtOH/acetone solution.

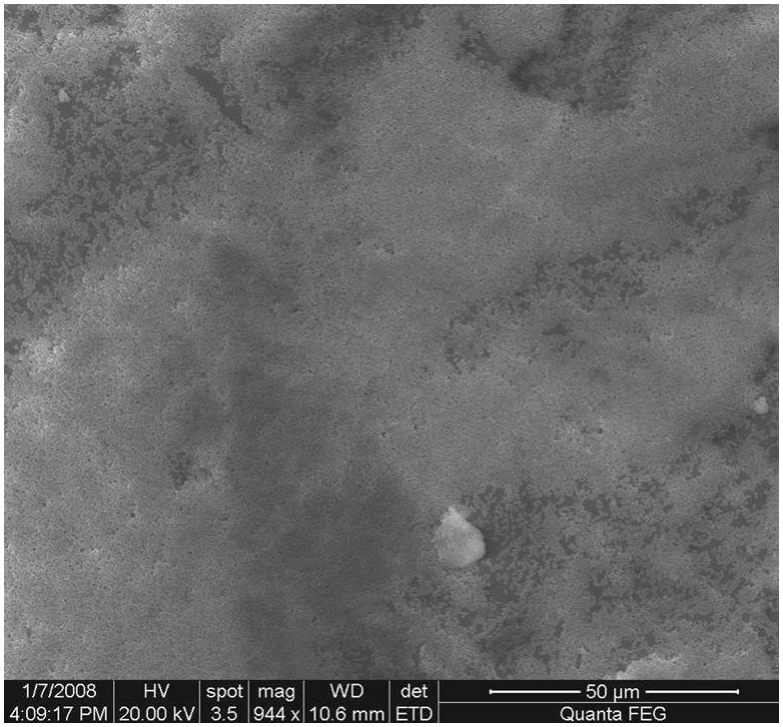

Figure A-5. SEM image of 5%w/v sphere to EtOH/acetone solution.

INTENTIONALLY LEFT BLANK.

Appendix B. Endospore Supplemental

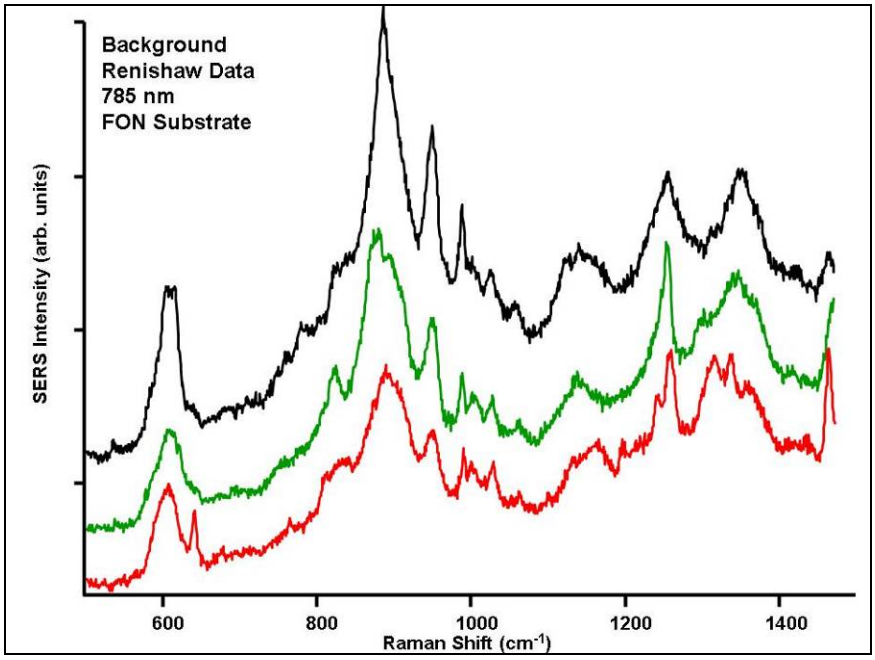

Figure B-1. Example SERS spectra of FON background collected using Renishaw system and 785 nm laser.

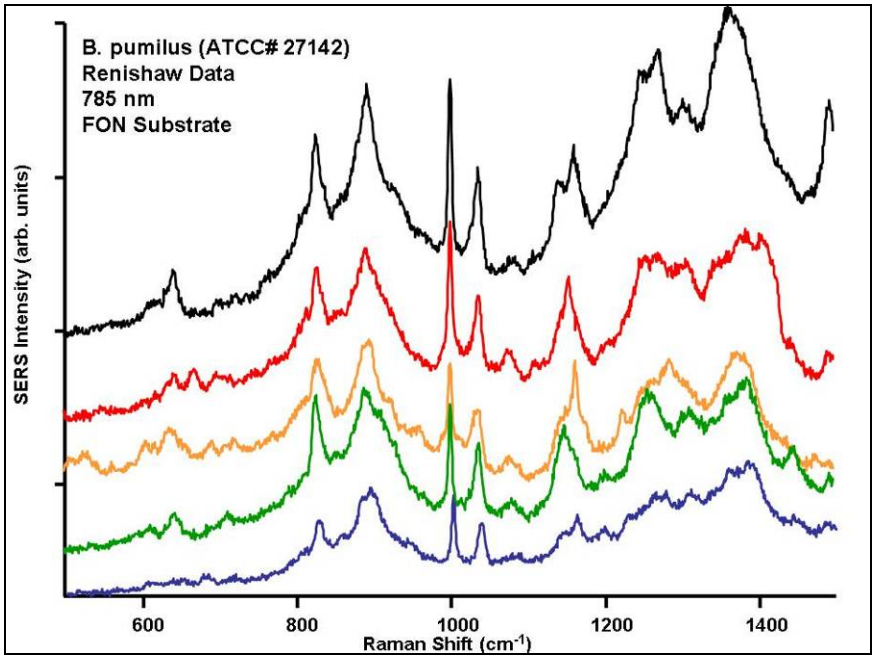

Figure B-2. Example SERS spectra of *B. pumilus* collected on FON using Renishaw system and 785 nm laser.

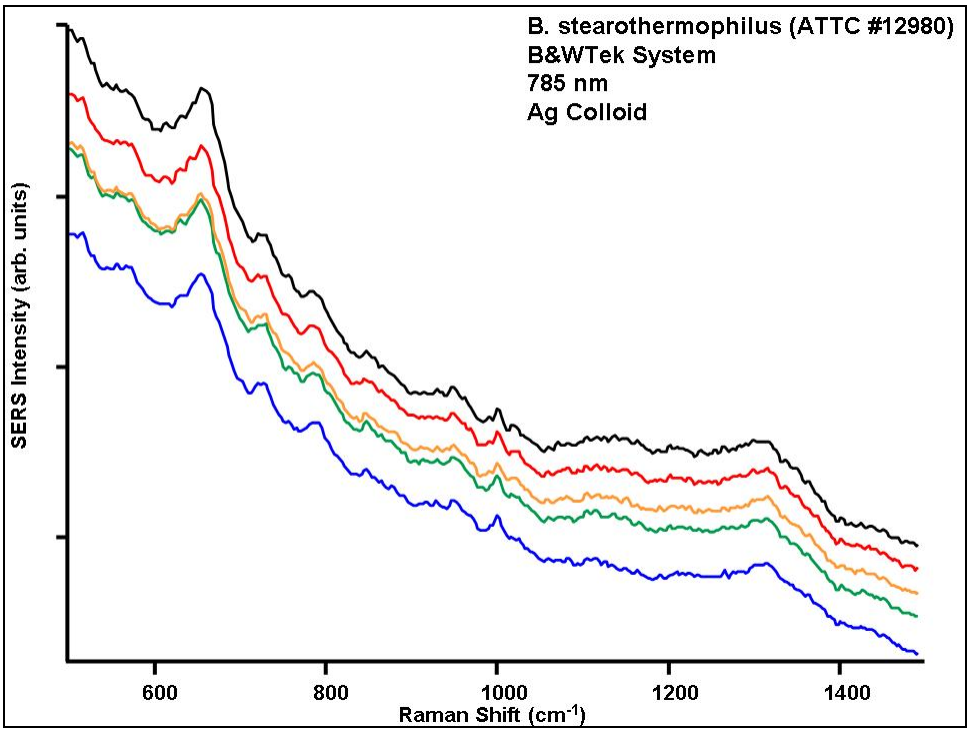

Figure B-3. Example SERS spectra of *B. stearothermophilus* collected on FON using Renishaw system and 785 nm laser.

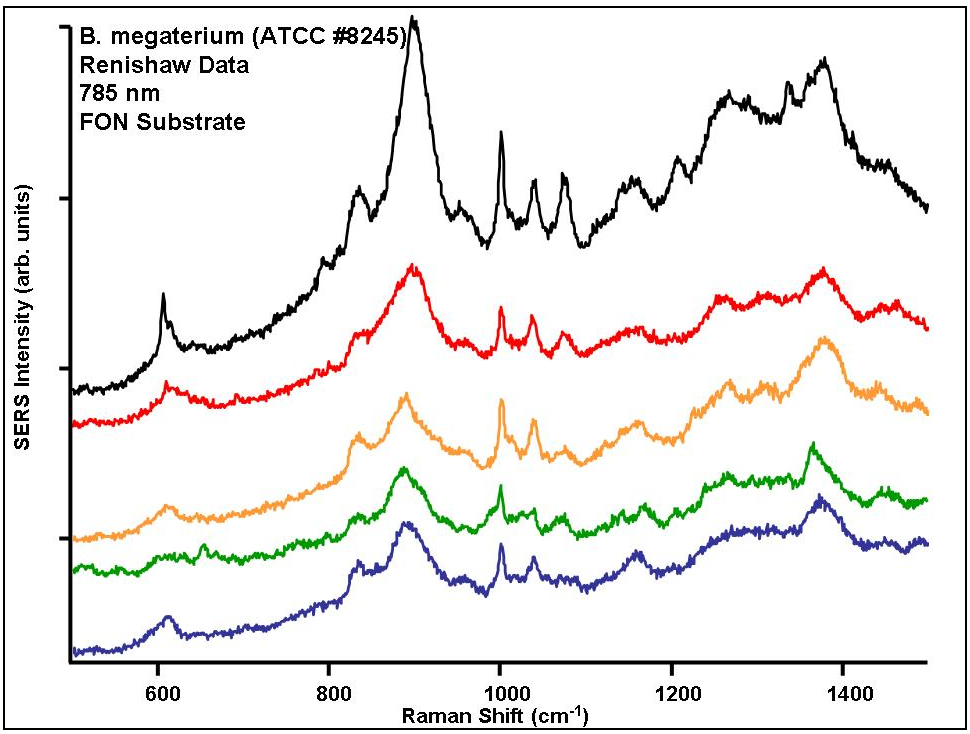

Figure B-4. Example SERS spectra of *B. megaterium* collected on FON using Renishaw system and 785 nm laser.

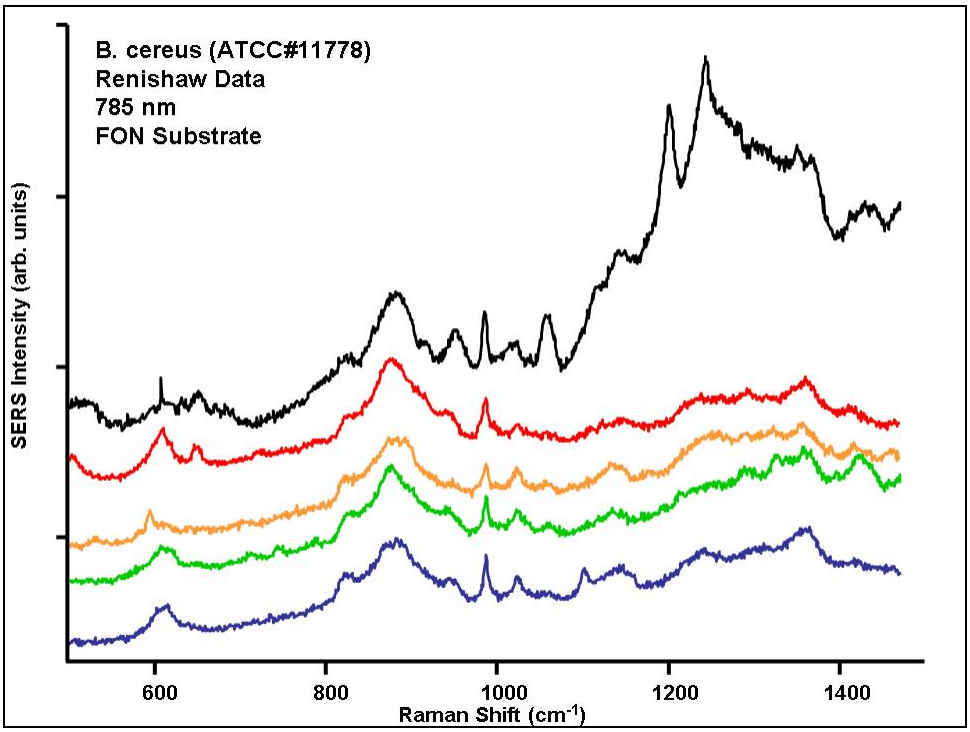

Figure B-5. Example SERS spectra of *B. cereus* collected on FON using Renishaw system and 785 nm laser.

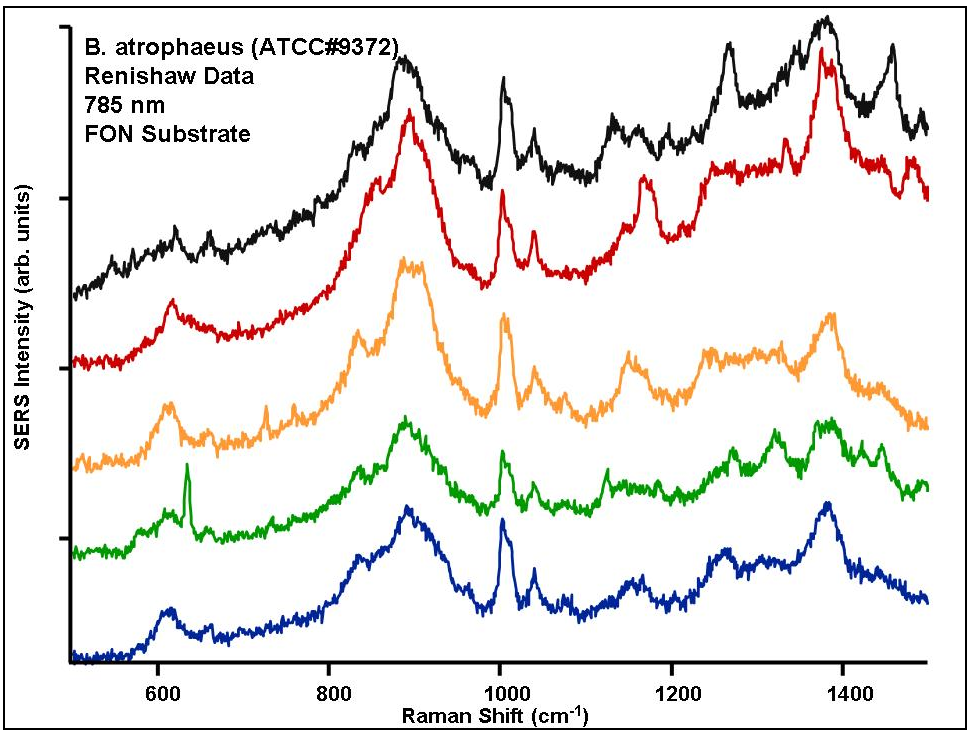

Figure B-6. Example SERS spectra of *B. atrophaeus* collected on FON using Renishaw system and 785 nm laser.

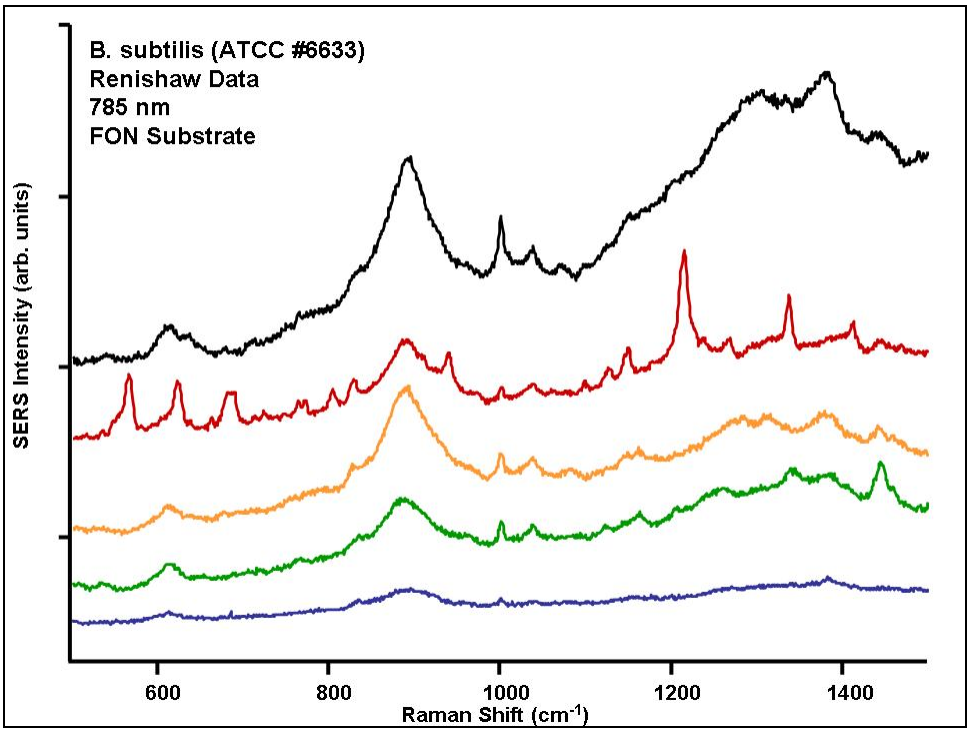

Figure B-7. Example SERS spectra of *B. subtilis* collected on FON using Renishaw system and 785 nm laser.

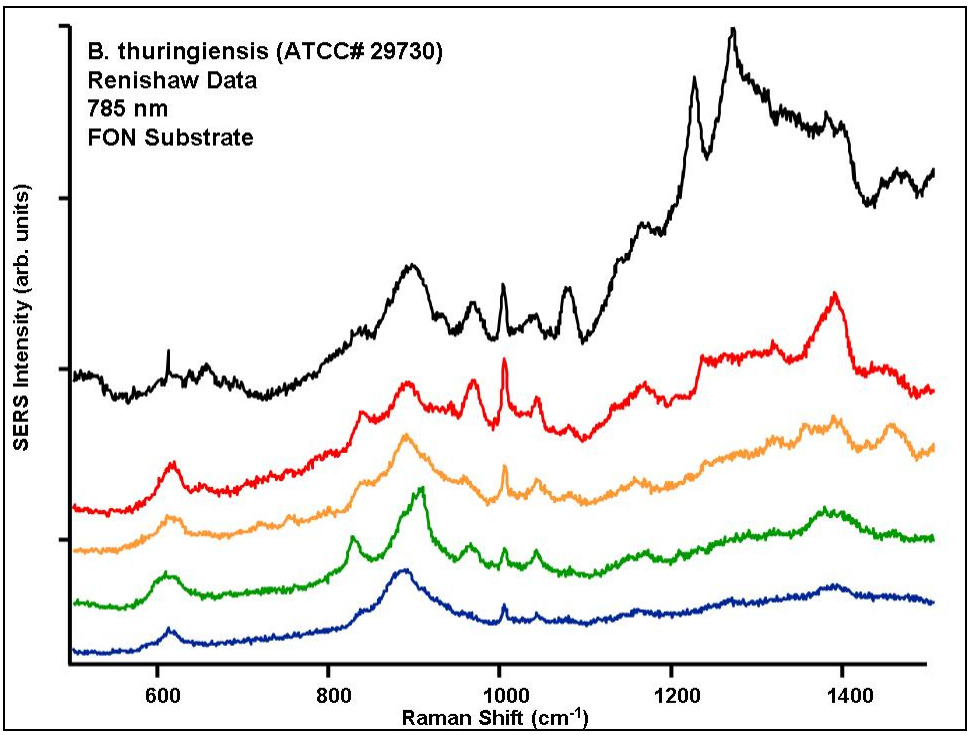

Figure B-8. Example SERS spectra of *B. thuringiensis* collected on FON using Renishaw system and 785 nm laser.

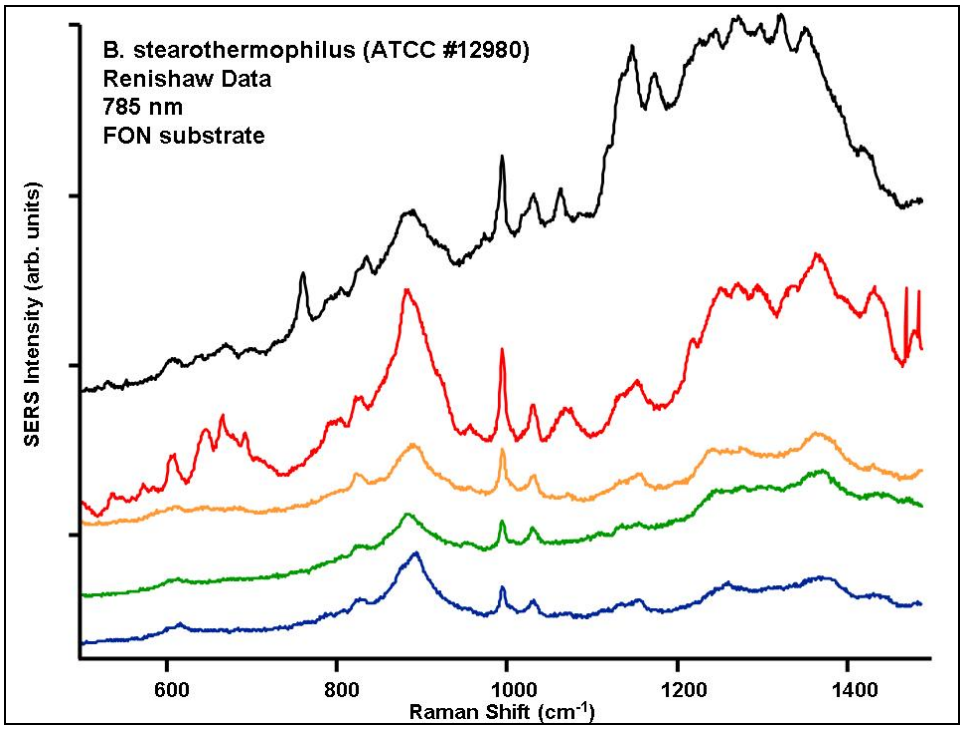

Figure B-9. Example SERS spectra of *B. stearothermophilus* collected on FON using Renishaw system and 785 nm laser.

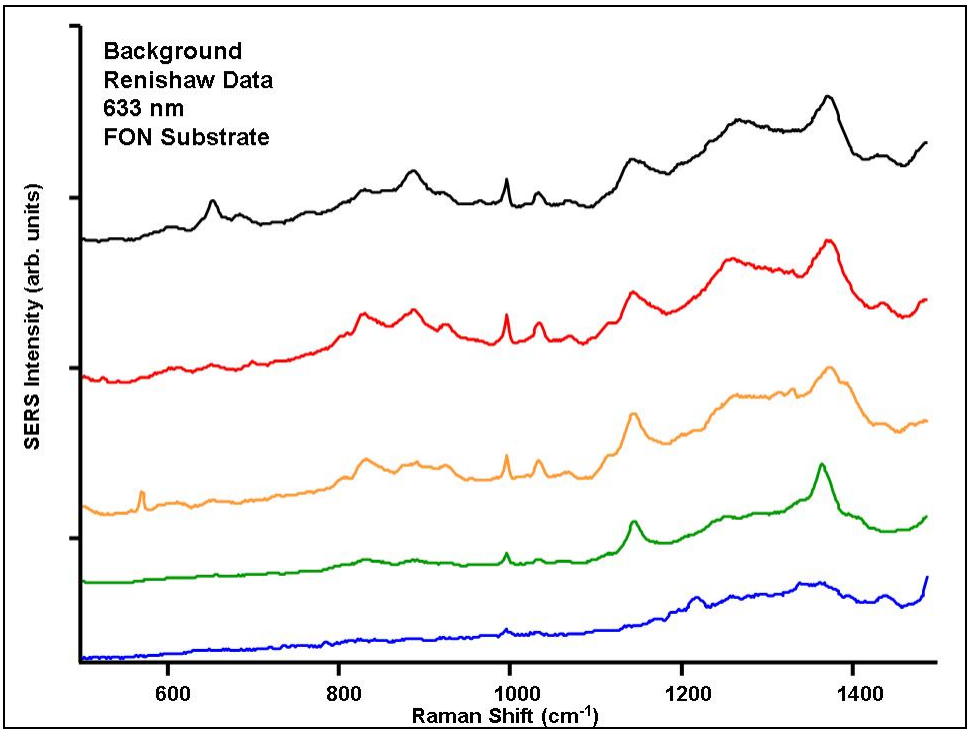

Figure B-10. Example SERS spectra of background FON collected using Renishaw system and 633 nm laser.

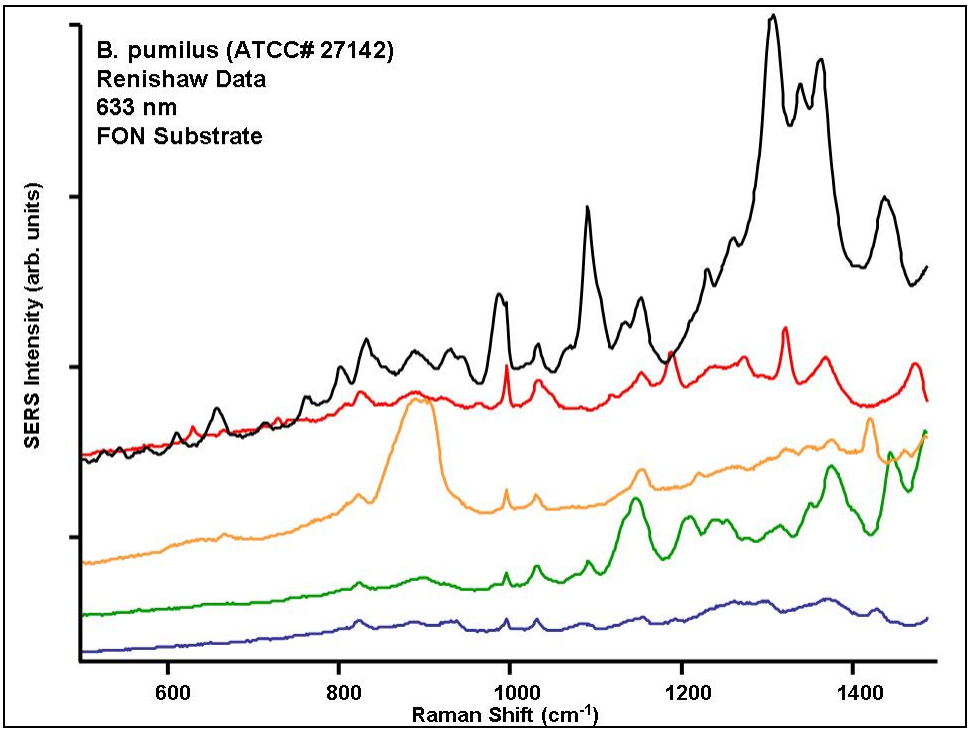

Figure B-11. Example SERS spectra of *B. pumilus* collected on FON using Renishaw system and 633 nm laser.

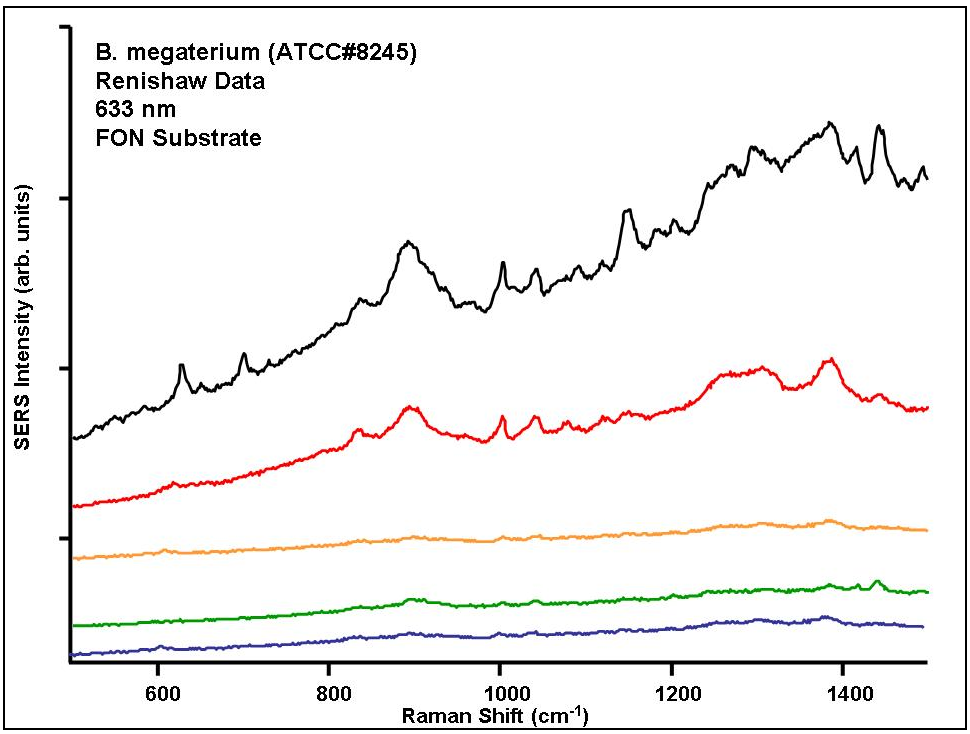

Figure B-12. Example SERS spectra of *B. megaterium* collected on FON using Renishaw system and 633 nm laser.

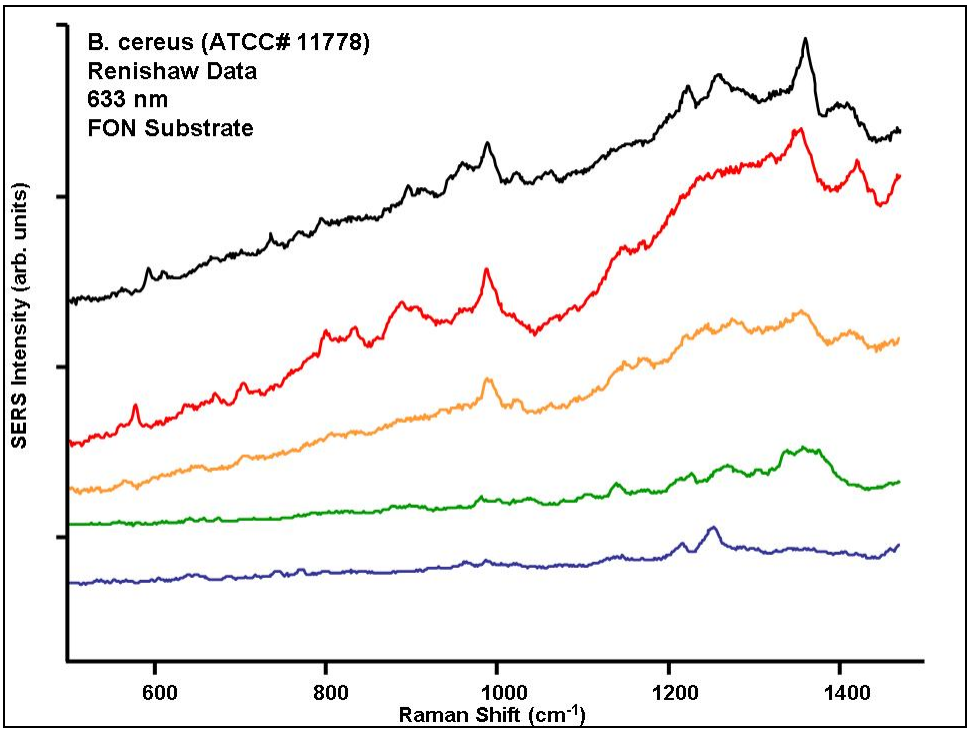

Figure B-13. Example SERS spectra of *B. cereus* collected on FON using Renishaw system and 633 nm laser.

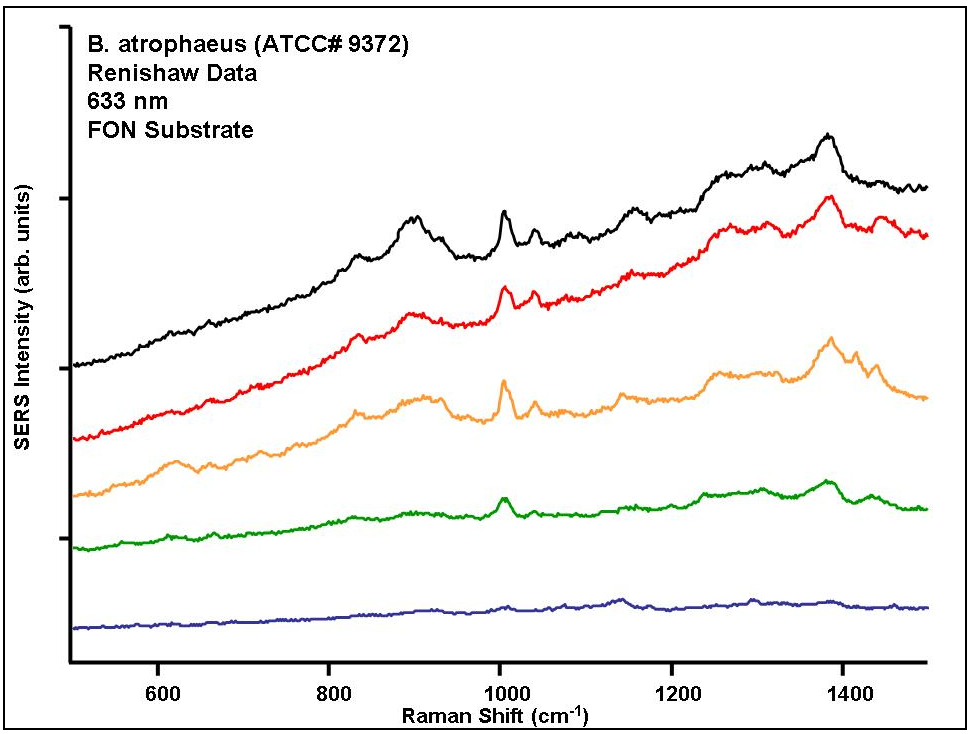

Figure B-14. Example SERS spectra of *B. atrophaeus* collected on FON using Renishaw system and 633 nm laser.

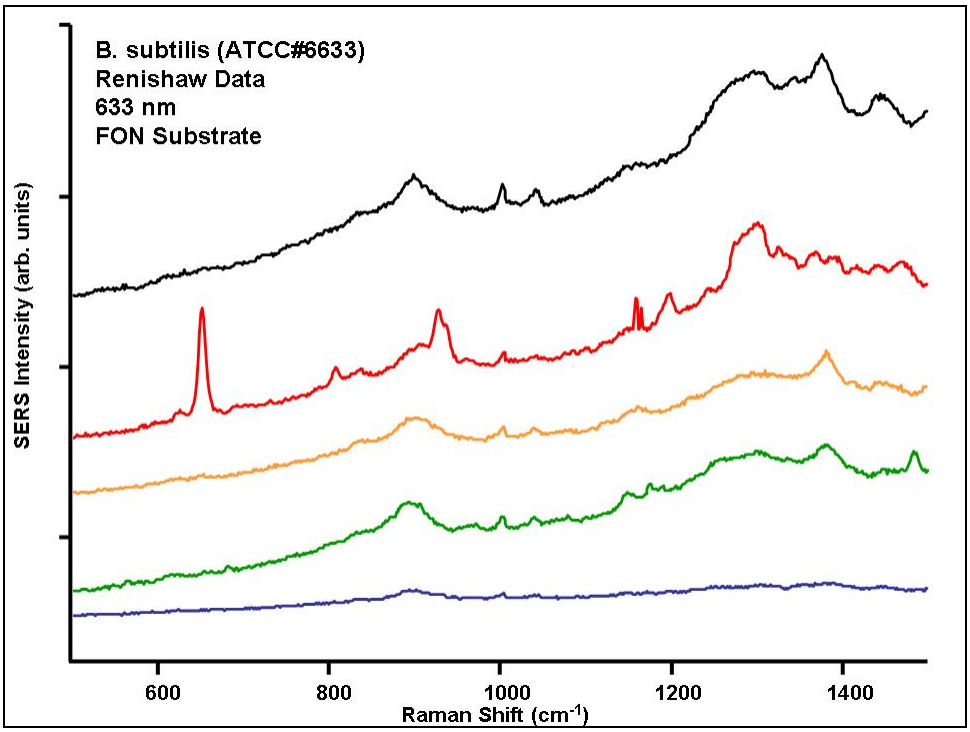

Figure B-15. Example SERS spectra of *B. subtilis* collected on FON using Renishaw system and 633 nm laser.

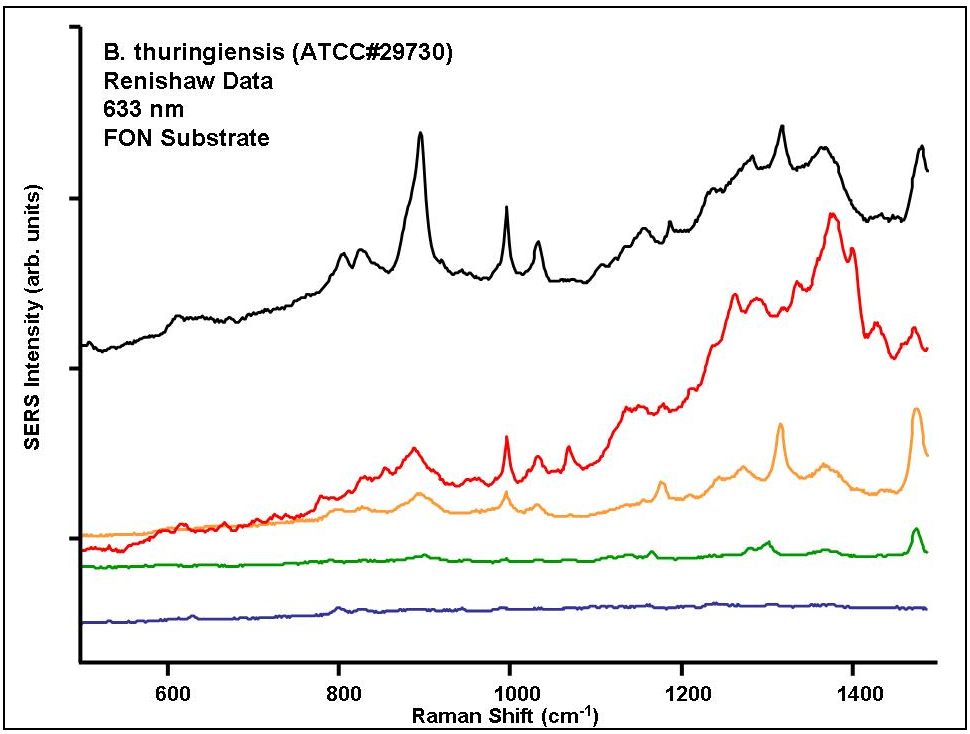

Figure B-16. Example SERS spectra of *B. thuringiensis* collected on FON using Renishaw system and 633 nm laser.

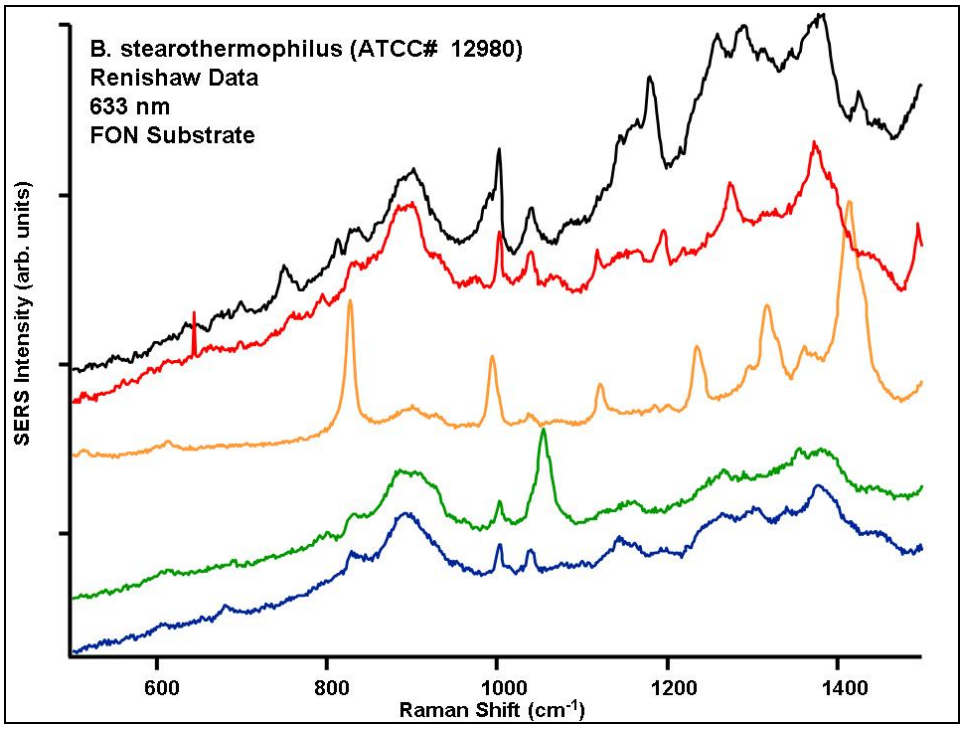

Figure B-17. Example SERS spectra of *B. stearothermophilus* collected on FON using Renishaw system and 633 nm laser.

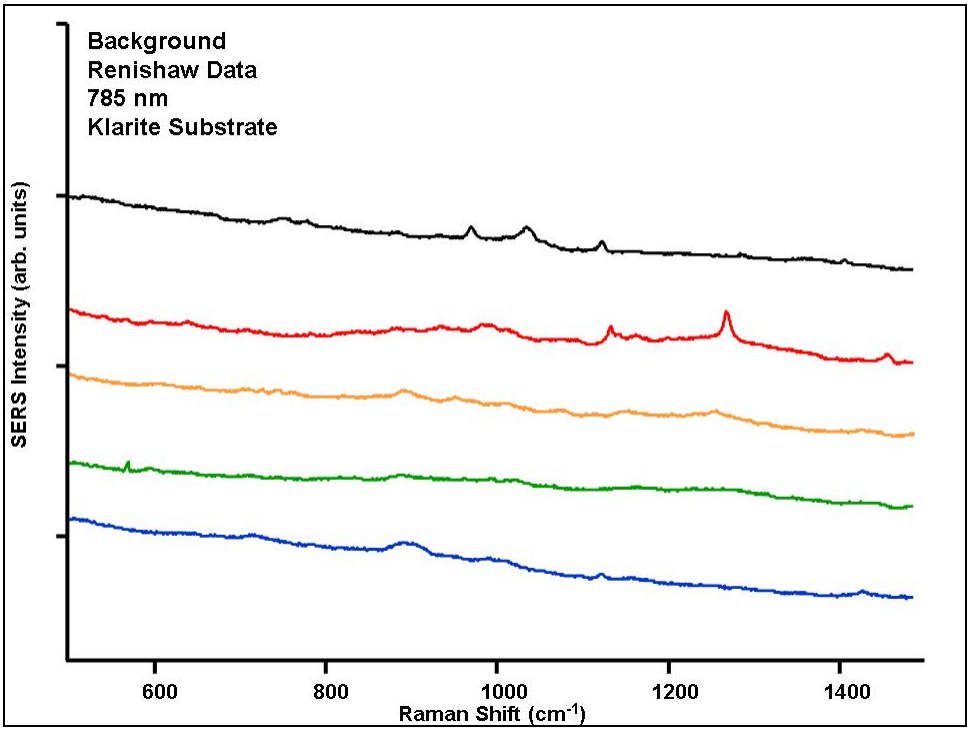

Figure B-18. Example SERS spectra of Klarite Background collected using Renishaw system and 785 nm laser.

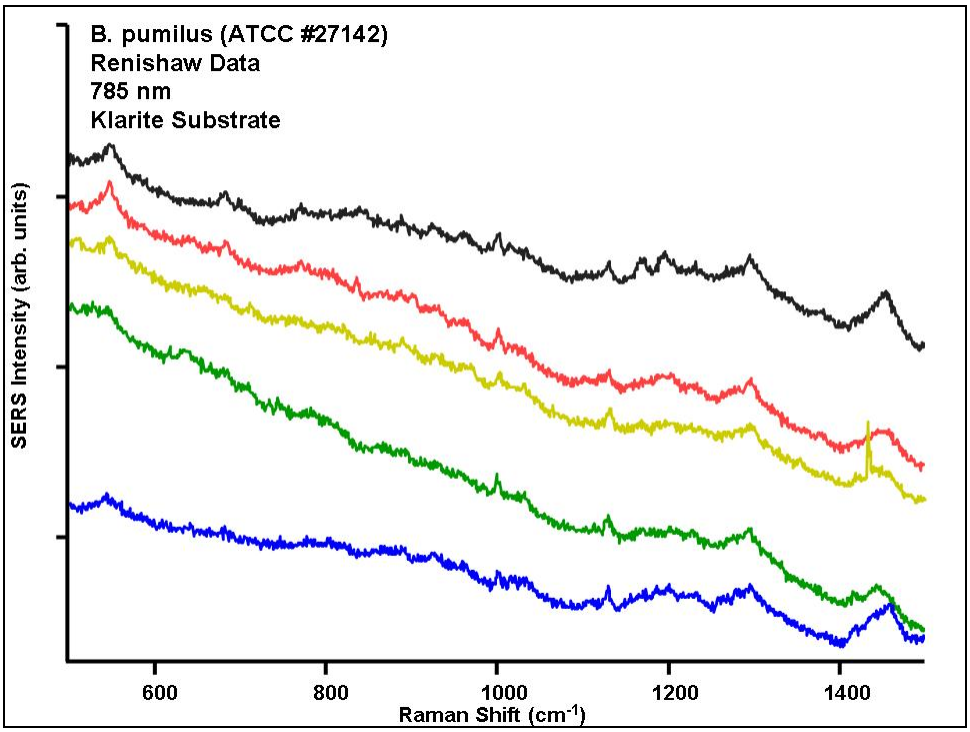

Figure B-19. Example SERS spectra of *B. pumilus* collected on Klarite using Renishaw system and 785 nm laser.

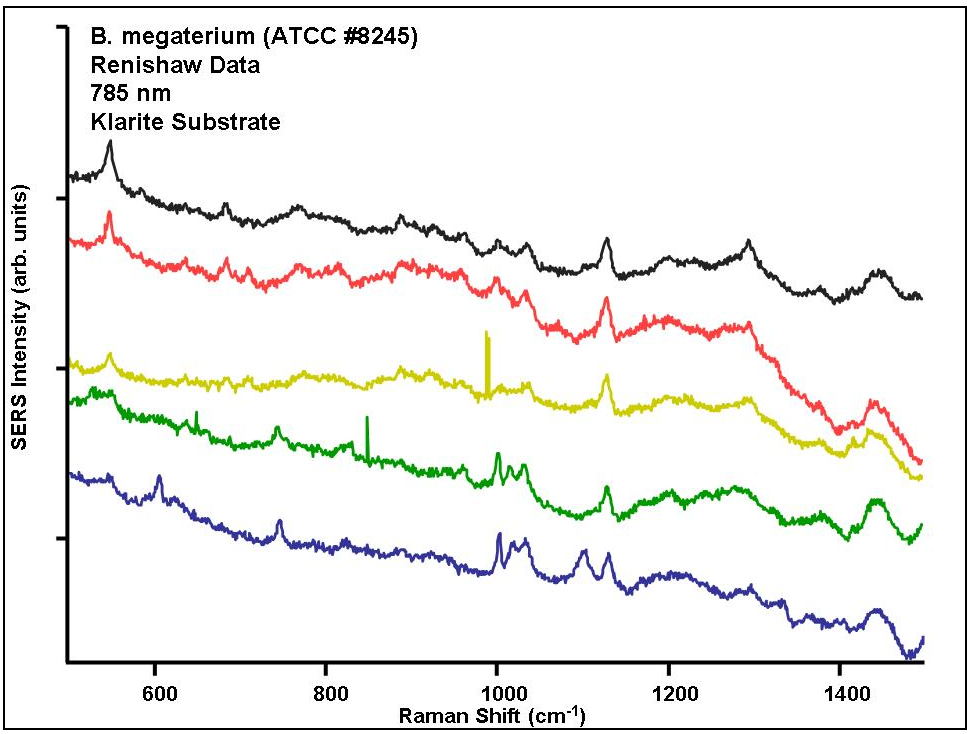

Figure B-20. Example SERS spectra of *B. megaterium* collected on Klarite using Renishaw system and 785 nm laser.

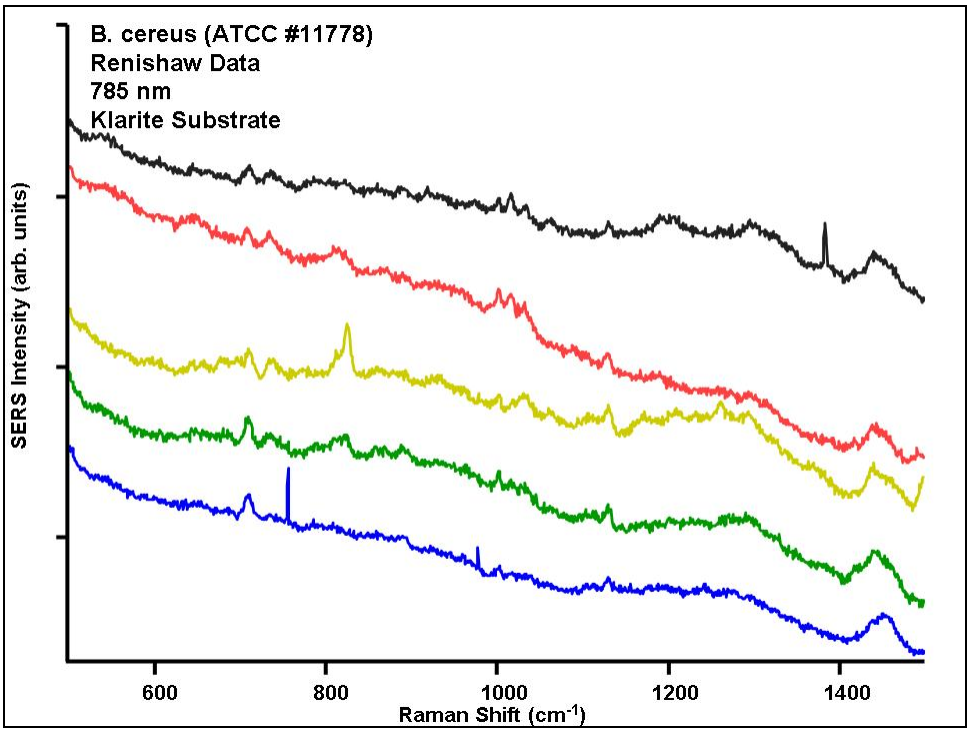

Figure B-21. Example SERS spectra of *B. cereus* collected on Klarite using Renishaw system and 785 nm laser.

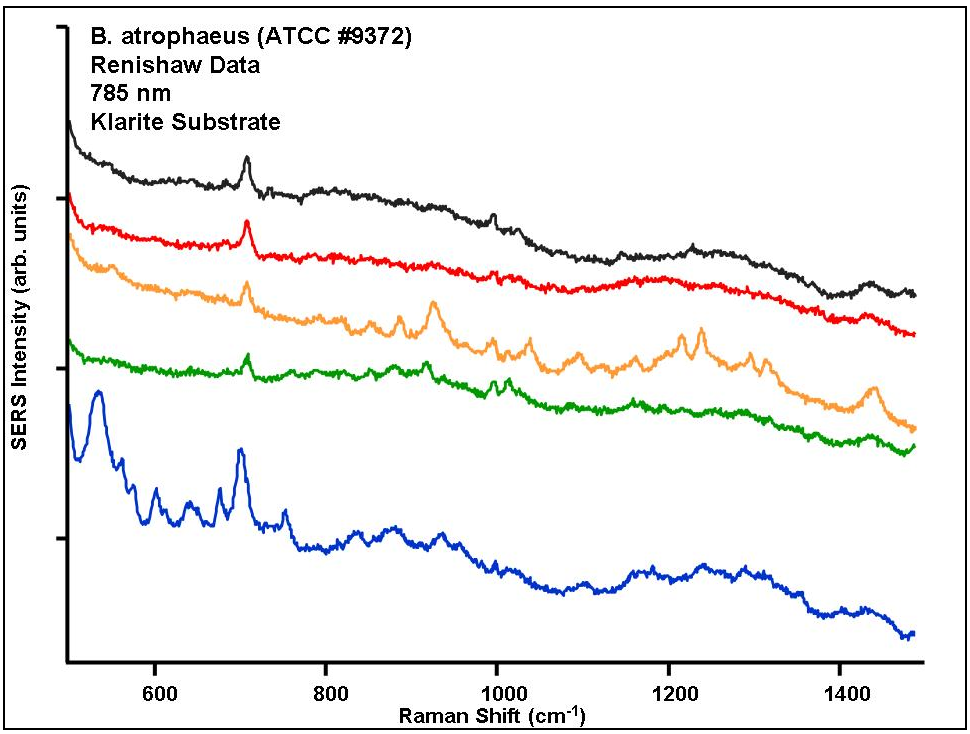

Figure B-22. Example SERS spectra of *B. atrophaeus* collected on Klarite using Renishaw system and 785 nm laser.

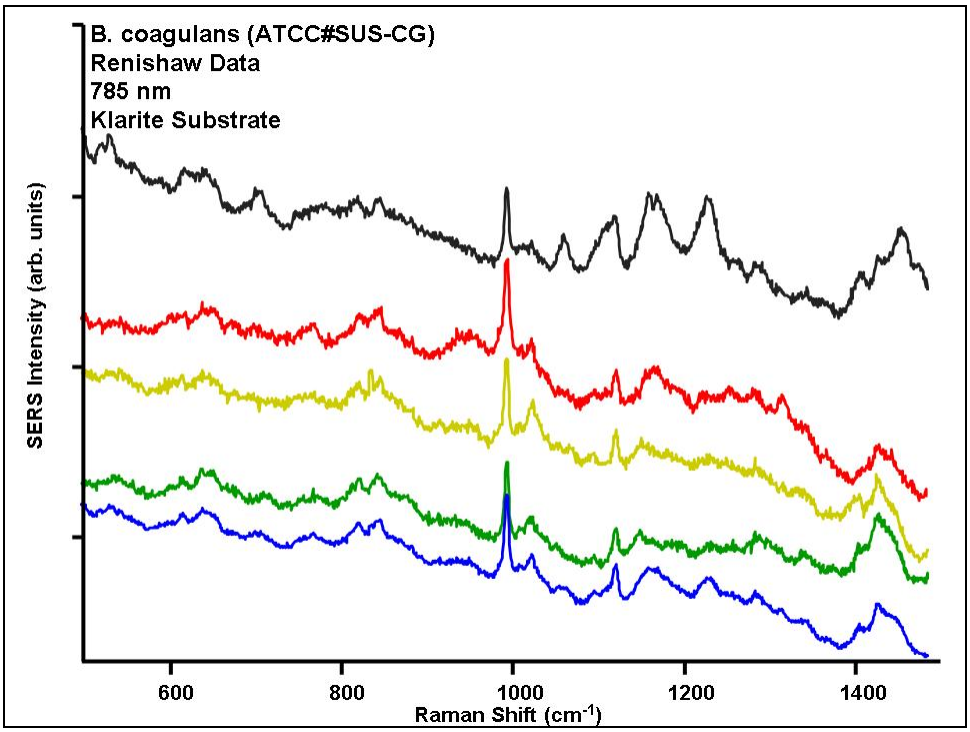

Figure B-23. Example SERS spectra of *B. coagulans* collected on Klarite using Renishaw system and 785 nm laser.

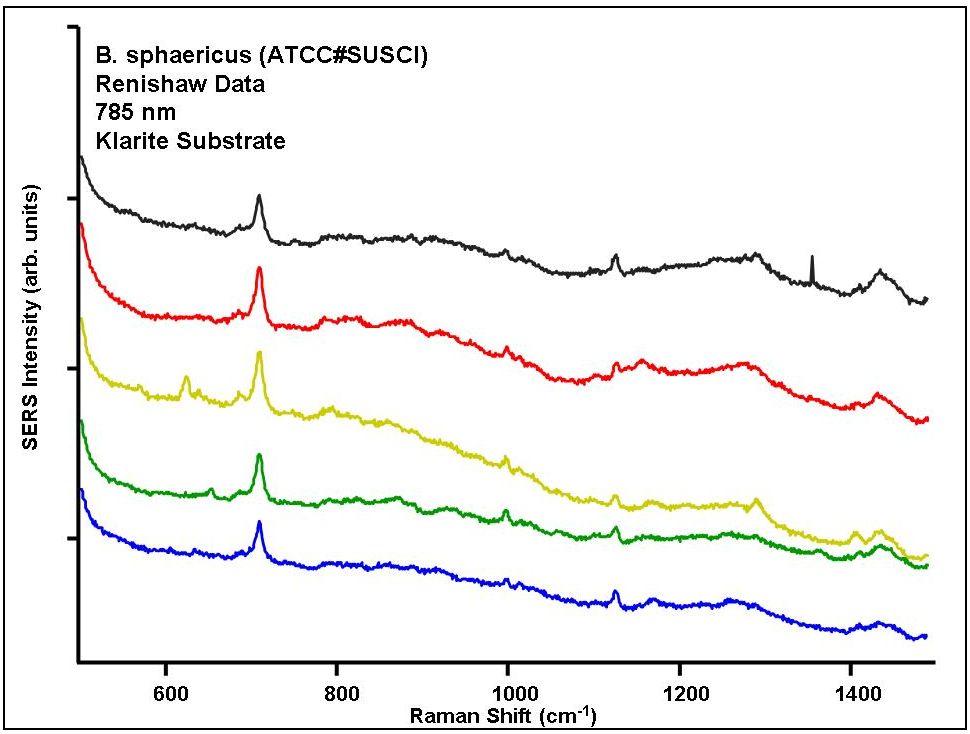

Figure B-24. Example SERS spectra of *B. sphaericus* collected on Klarite using Renishaw system and 785 nm laser.

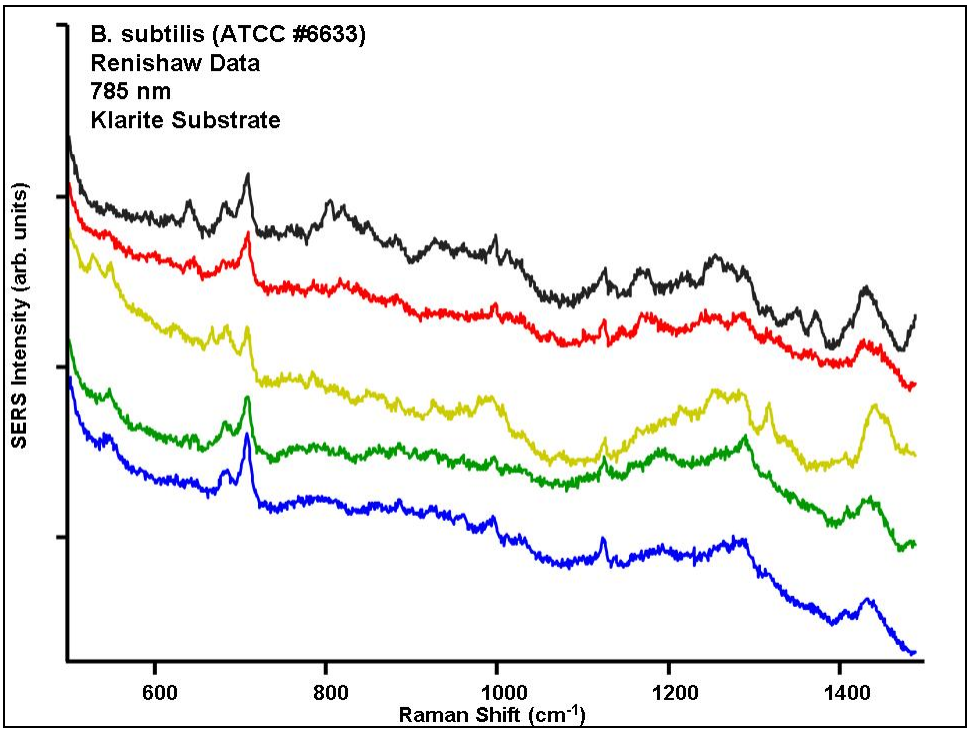

Figure B-25. Example SERS spectra of *B. subtilis* collected on Klarite using Renishaw system and 785 nm laser.

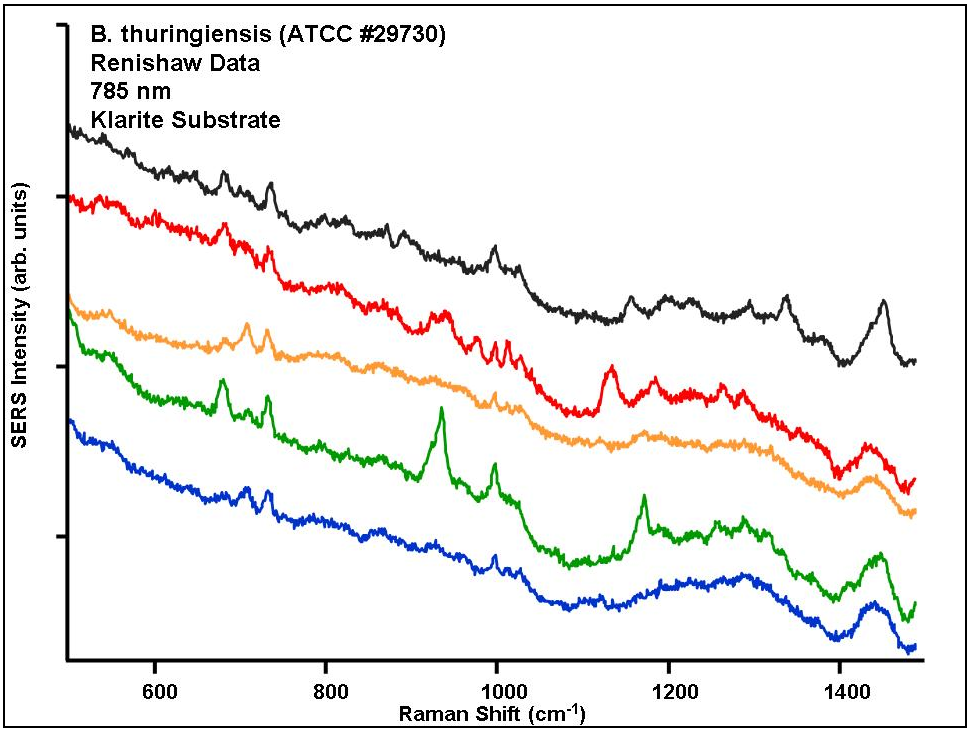

Figure B-26. Example SERS spectra of *B. thuringiensis* collected on Klarite using Renishaw system and 785 nm laser.

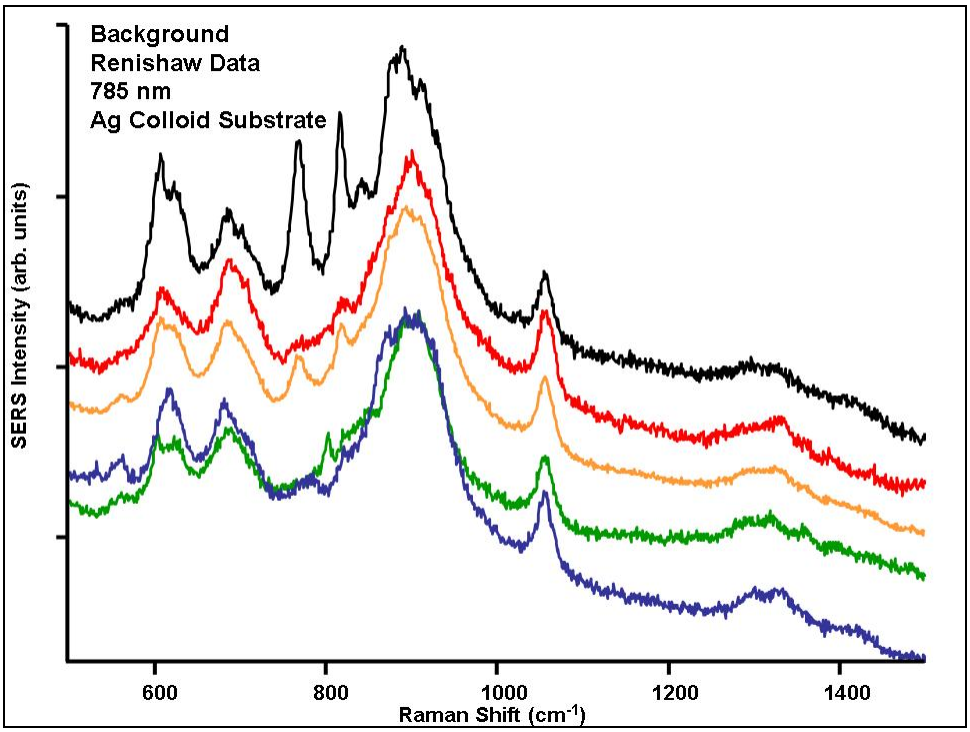

Figure B-27. Example SERS spectra Ag colloid background collected on Renishaw system and 785 nm laser.

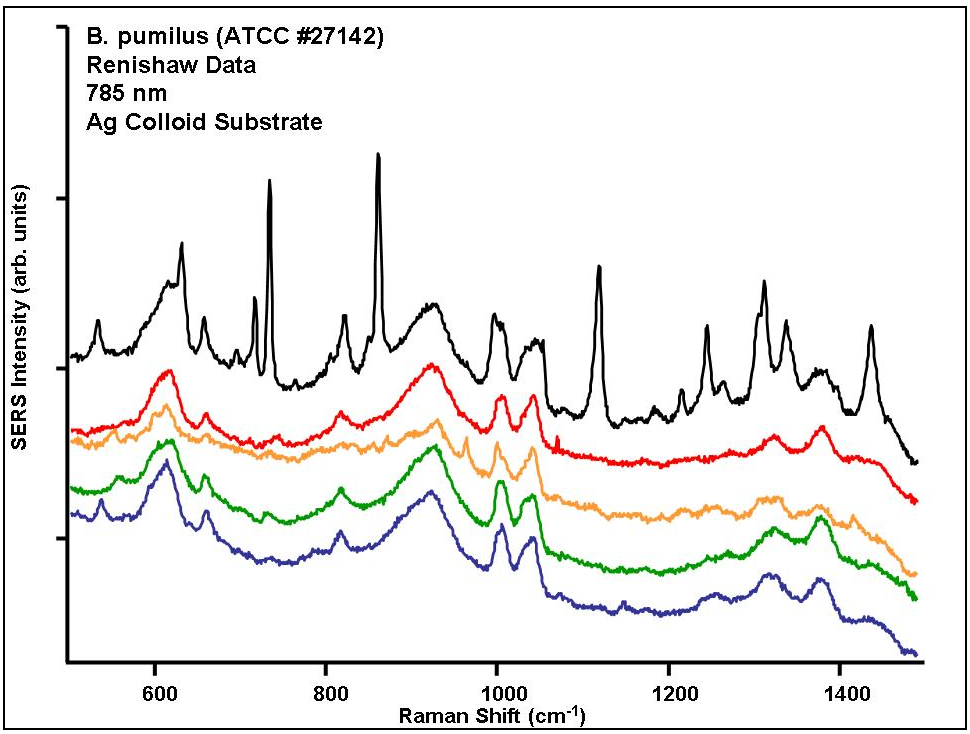

Figure B-28. Example SERS spectra of *B. pumilus* collected using Ag colloids on Renishaw system using 785 nm laser.

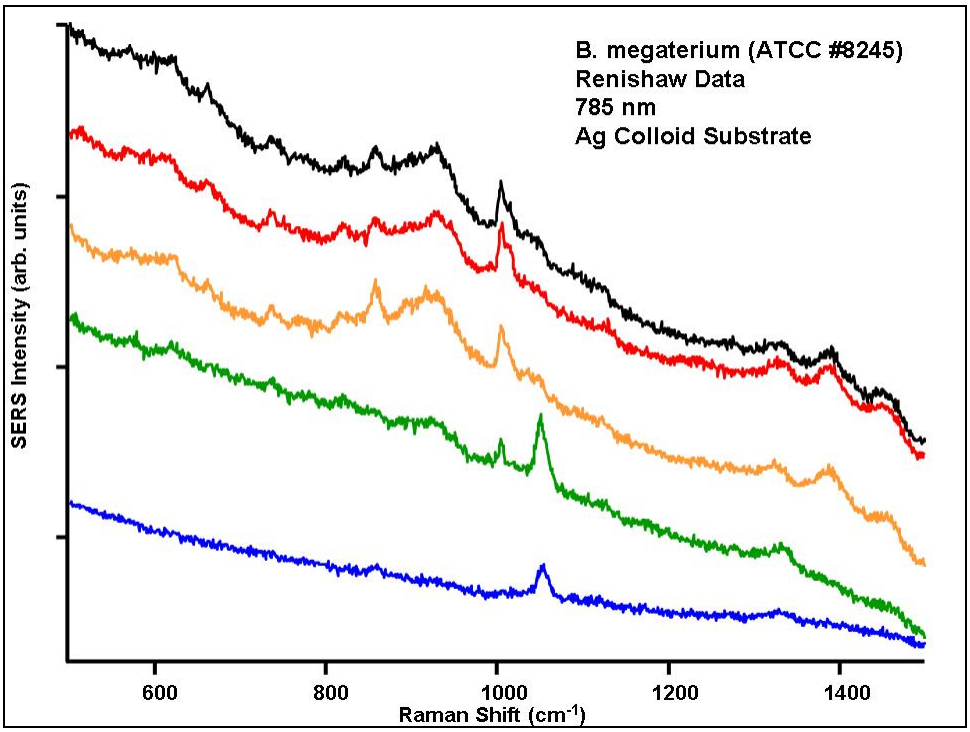

Figure B-29. Example SERS spectra of *B. megaterium* collected using Ag colloids on Renishaw system using 785 nm laser.

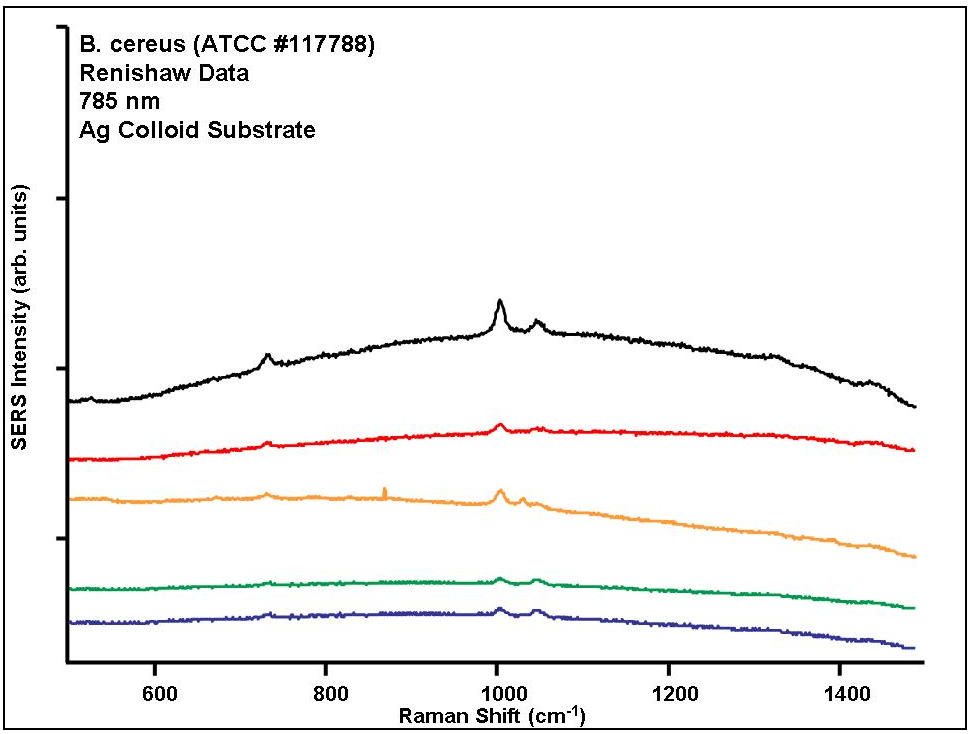

Figure B-30. Example SERS spectra of *B. cereus* collected using Ag colloids on Renishaw system using 785 nm laser.

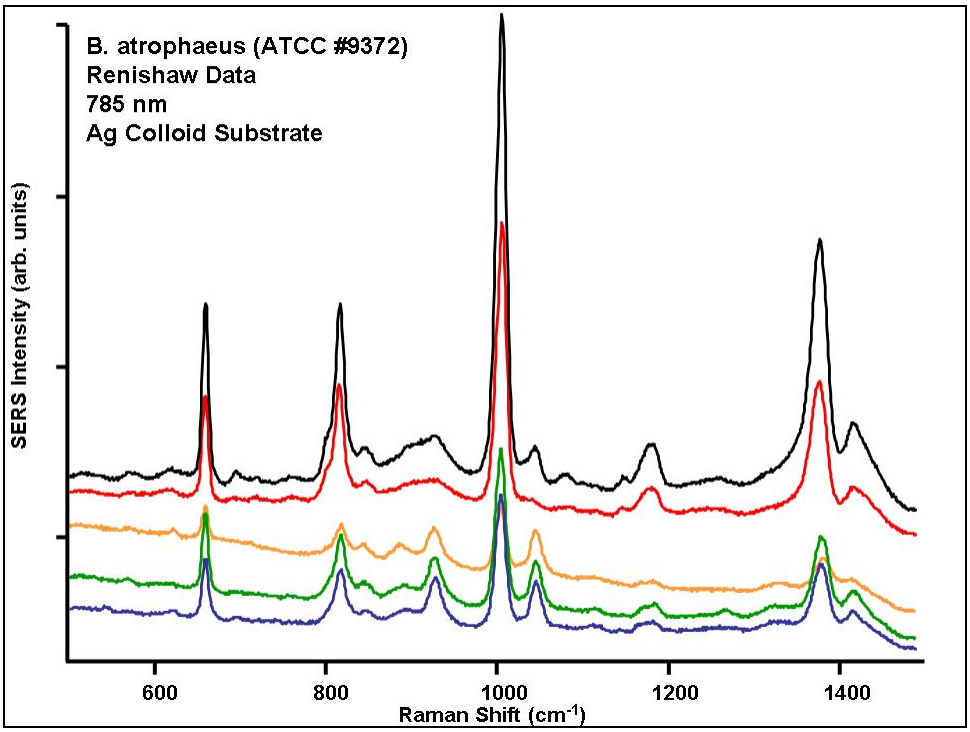

Figure B-31. Example SERS spectra of *B. atrophaeus* collected using Ag colloids on Renishaw system using 785 nm laser.

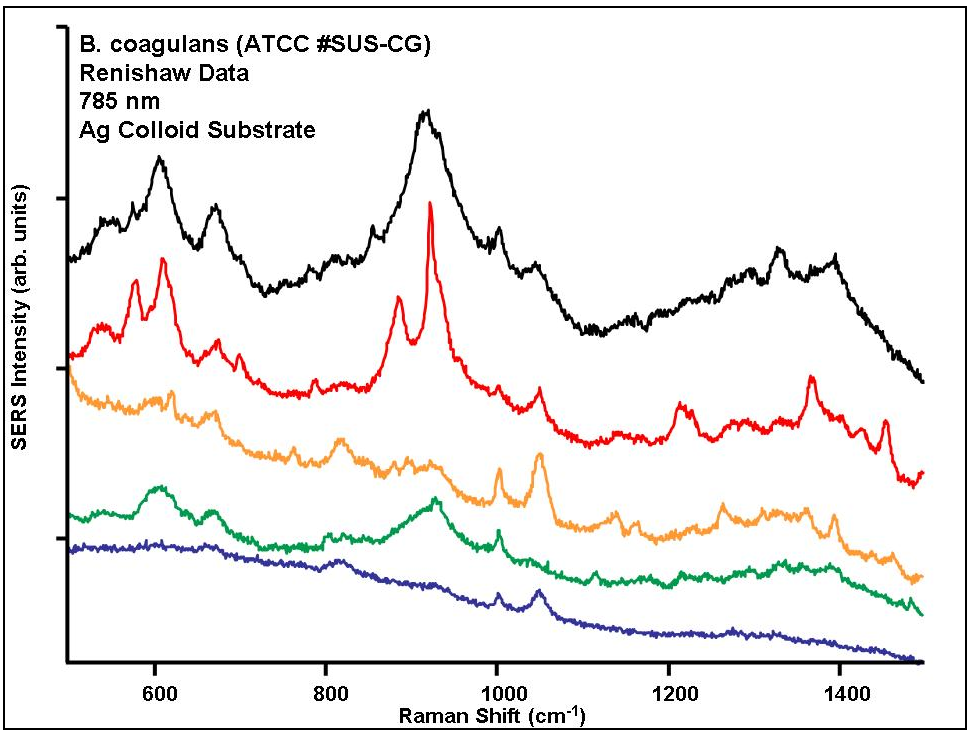

Figure B-32. Example SERS spectra of *B. coagulans* collected using Ag colloids on Renishaw system using 785 nm laser.

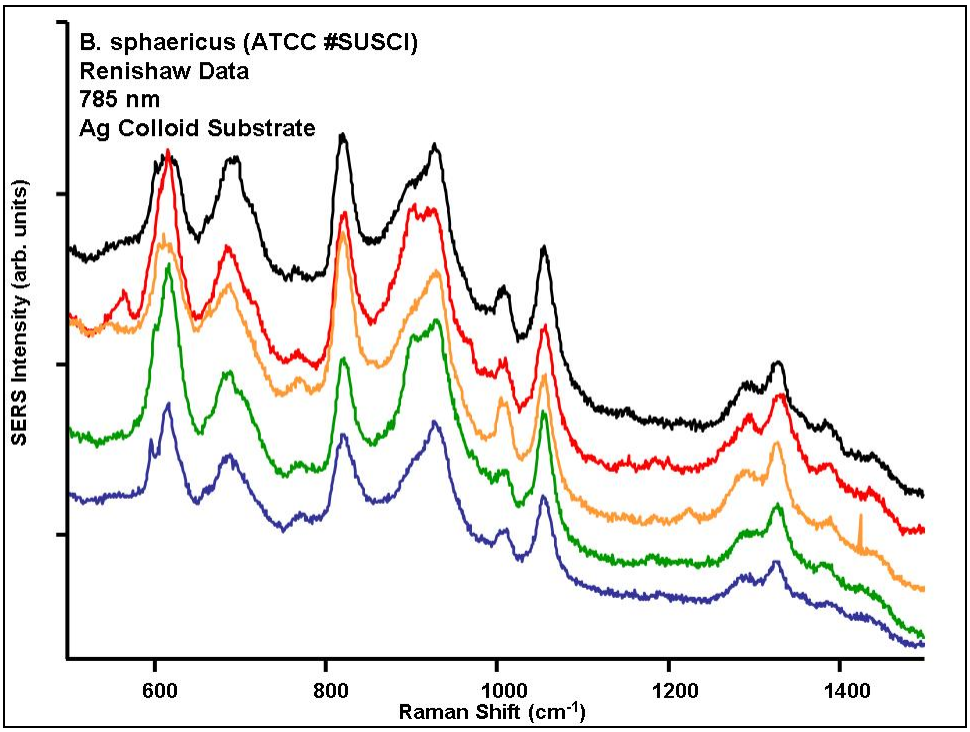

Figure B-33. Example SERS spectra of *B. sphaericus* collected using Ag colloids on Renishaw system using 785 nm laser.

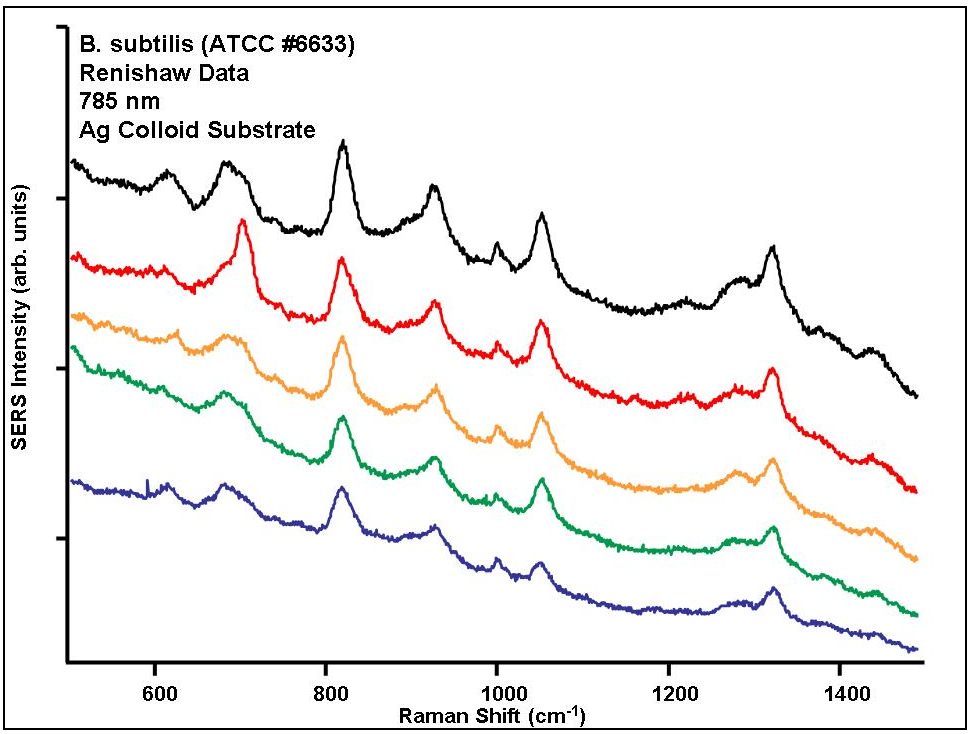

Figure B-34. Example SERS spectra of *B. subtilis* collected using Ag colloids on Renishaw system using 785 nm laser.

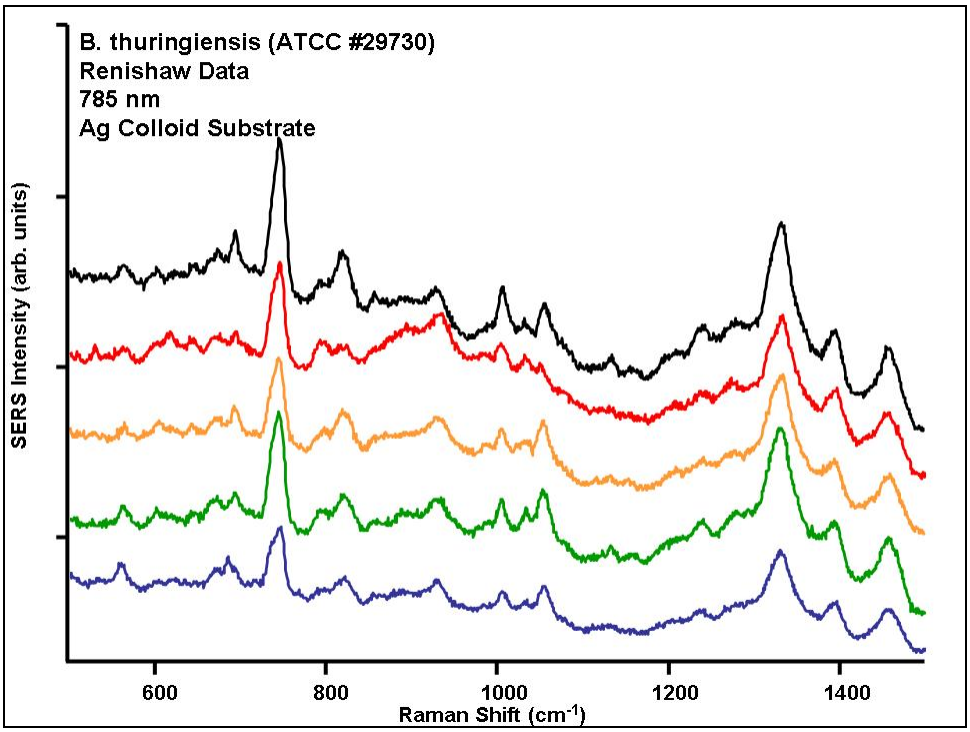

Figure B-35. Example SERS spectra of *B. thuringiensis* collected using Ag colloids on Renishaw system using 785 nm laser.

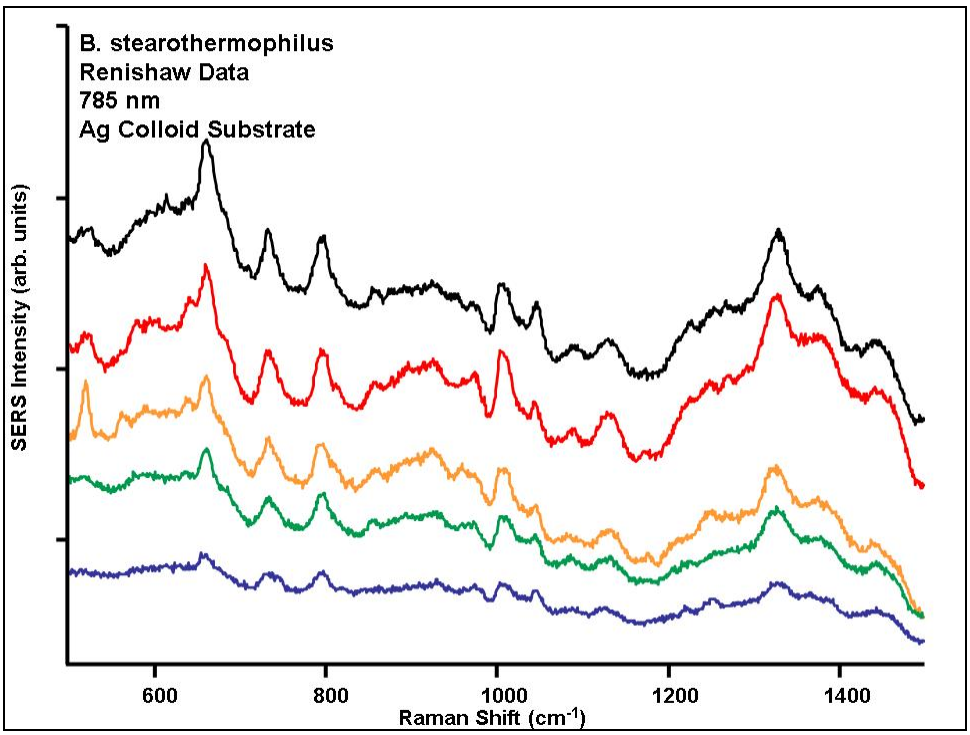

Figure B-36. Example SERS spectra of *B. stearothermophilus* collected using Ag colloids on Renishaw system using 785 nm laser.

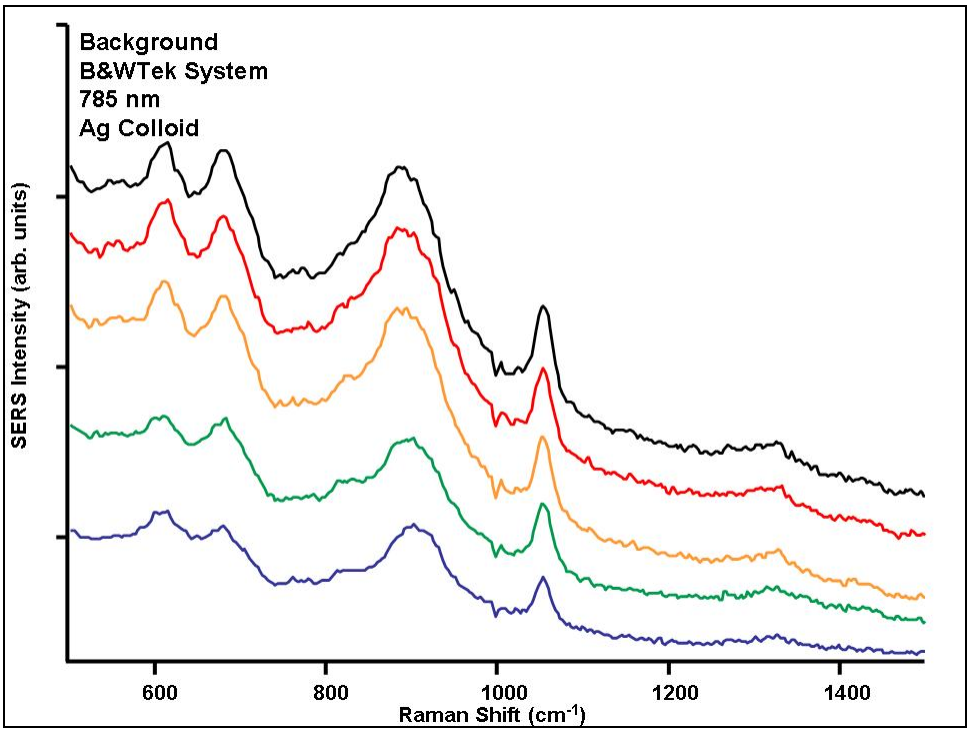

Figure B-37. Example SERS spectra of Ag colloid background collected on B&WTek system using 785 nm laser.

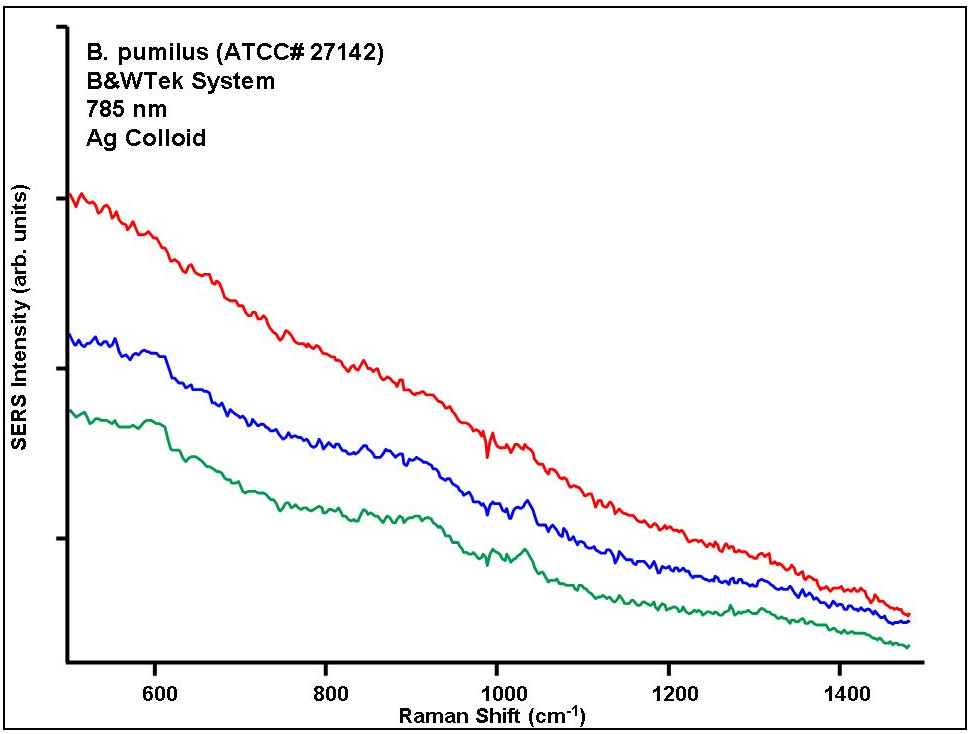

Figure B-38. Example SERS spectra of *B. pumilus* collected with Ag colloid on B&WTek system using 785 nm laser.

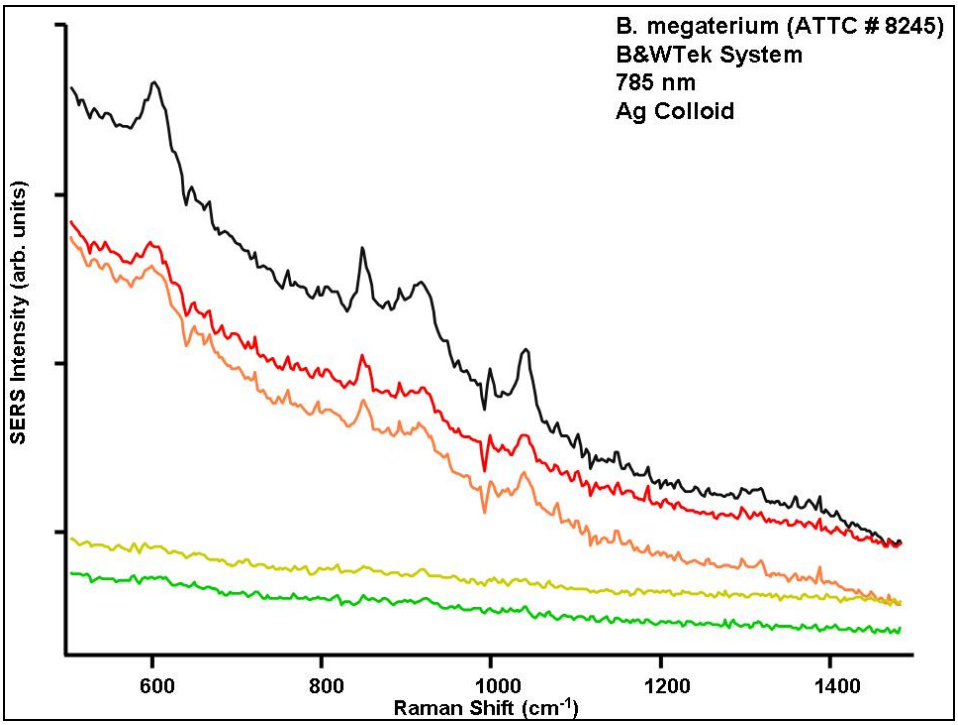

Figure B-39. Example SERS spectra of *B. megaterium* collected with Ag colloid on B&WTek system using 785 nm laser.

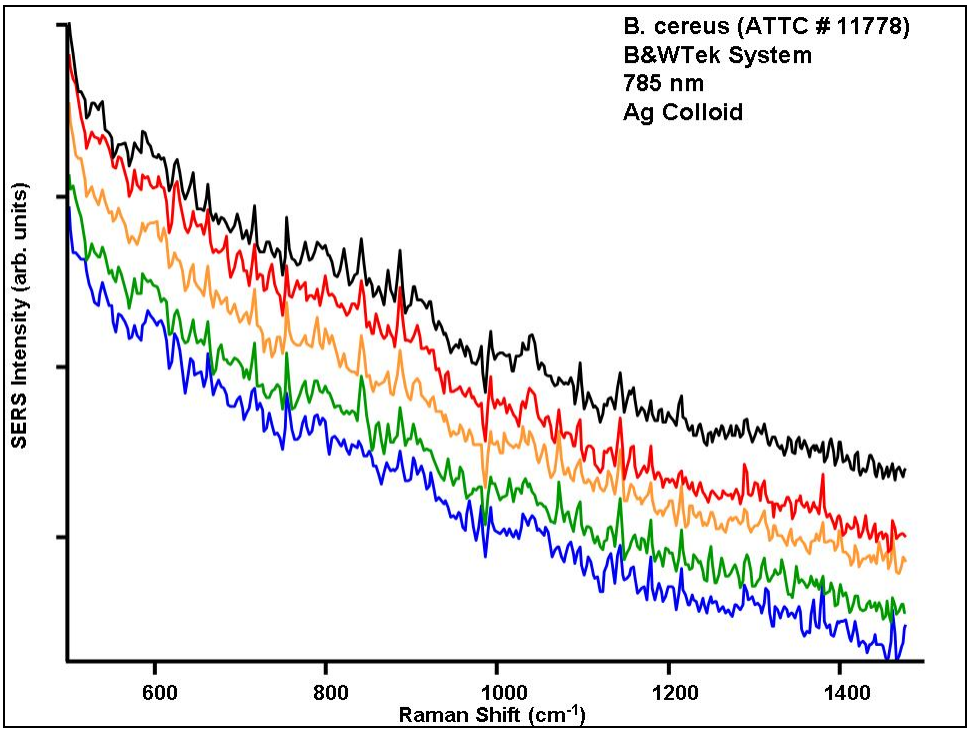

Figure B-40. Example SERS spectra of *B. cereus* collected with Ag colloid on B&WTek system using 785 nm laser.

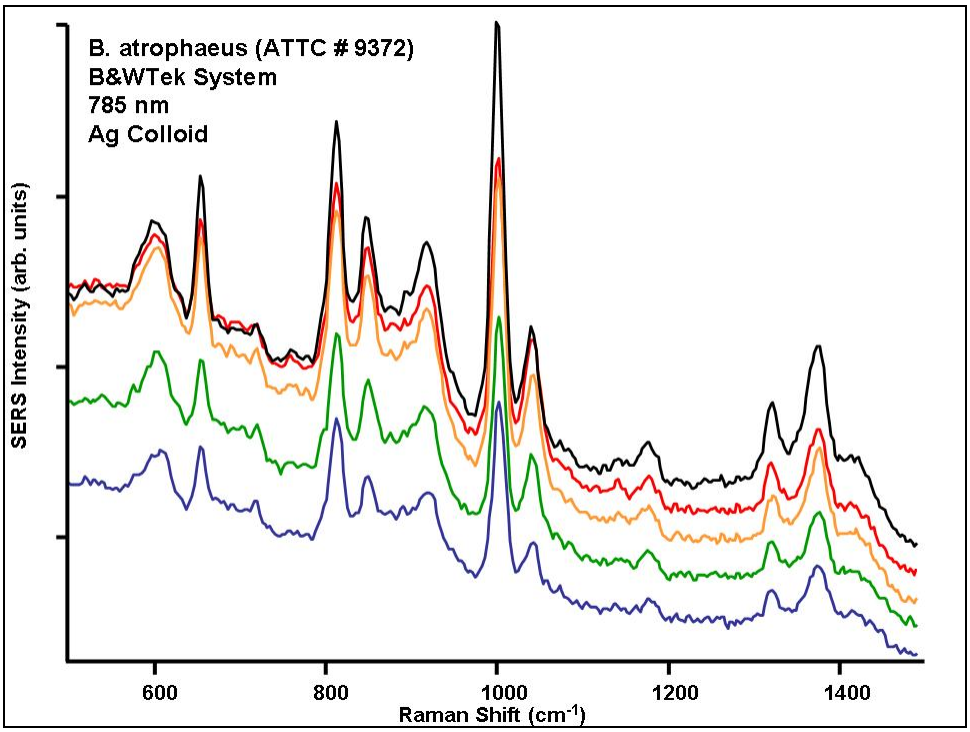

Figure B-41. Example SERS spectra of *B. atrophaeus* collected with Ag colloid on B&WTek system using 785 nm laser.

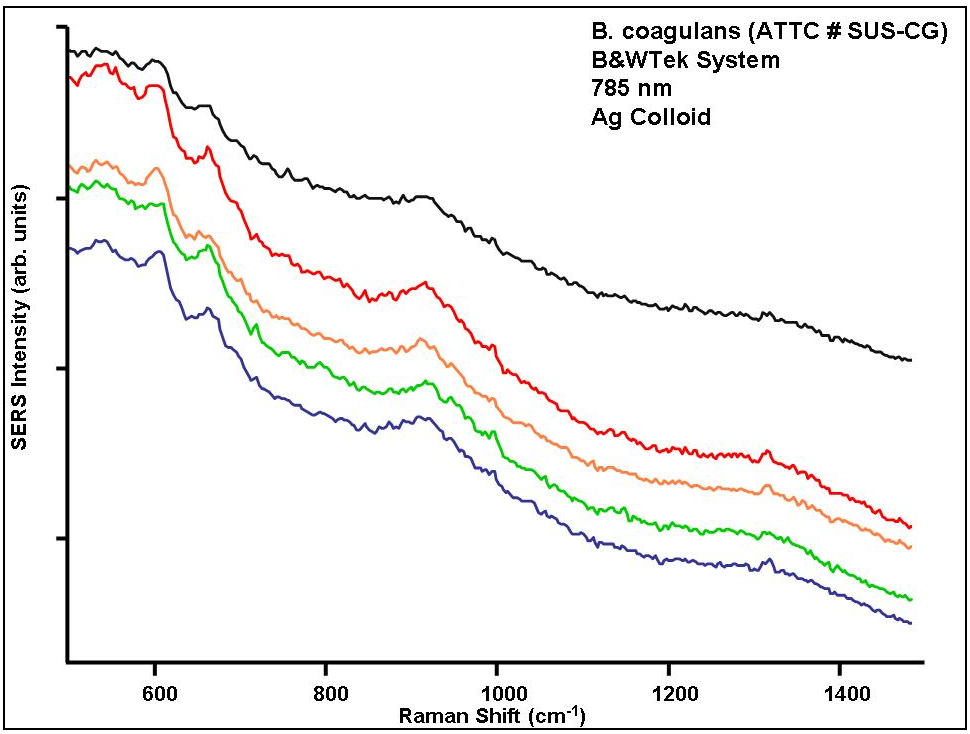

Figure B-42. Example SERS spectra of *B. coagulans* collected with Ag colloid on B&WTek system using 785 nm laser.

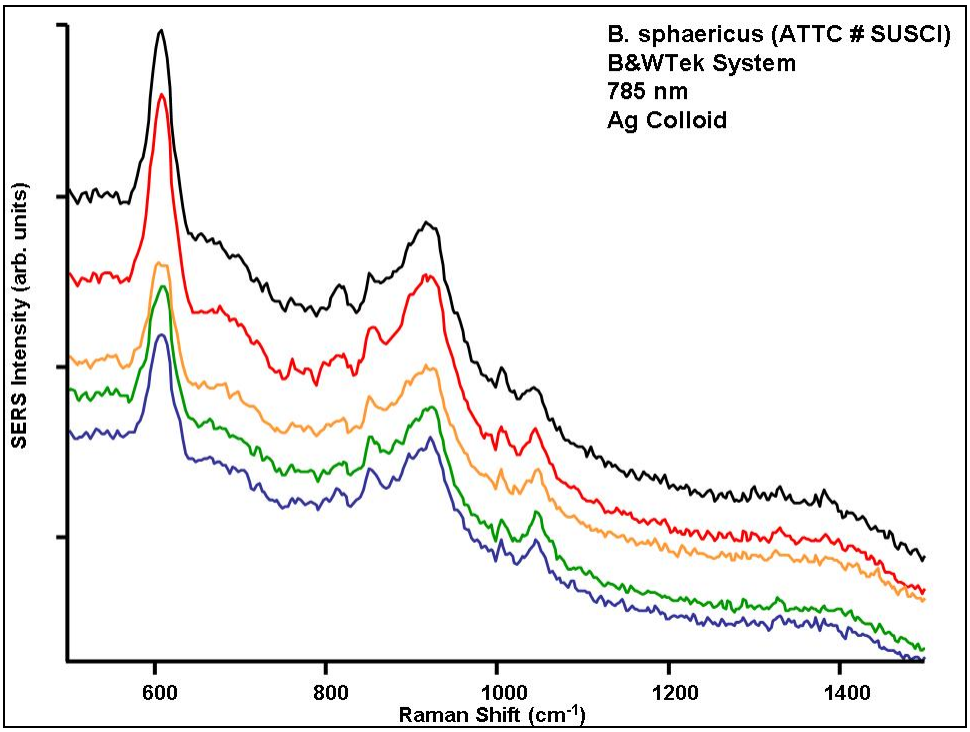

Figure B-43. Example SERS spectra of *B. sphaericus* collected with Ag colloid on B&WTek system using 785 nm laser.

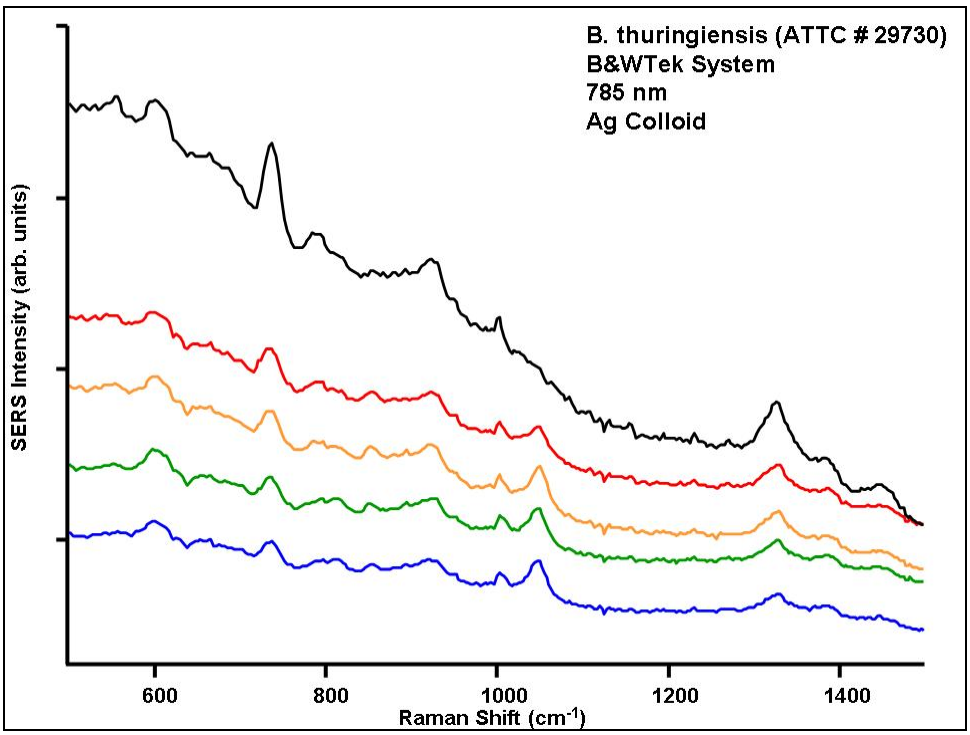

Figure B-44. Example SERS spectra of *B. thuringiensis* collected with Ag colloid on B&WTek system using 785 nm laser.

Appendix C. Chemical Supplemental

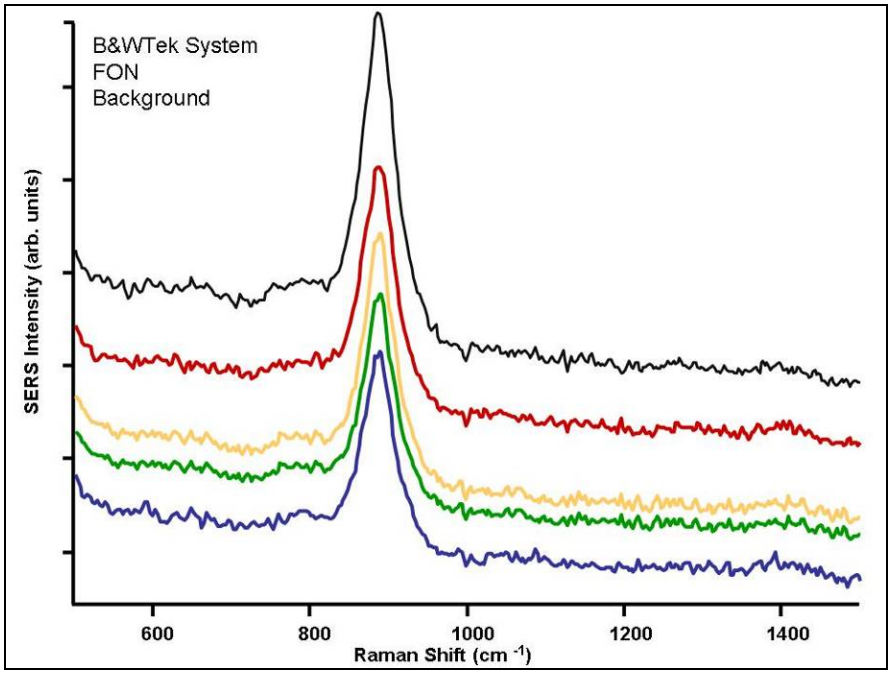

Figure C-1. SERS background of FON substrate as measured with the B&WTek system.

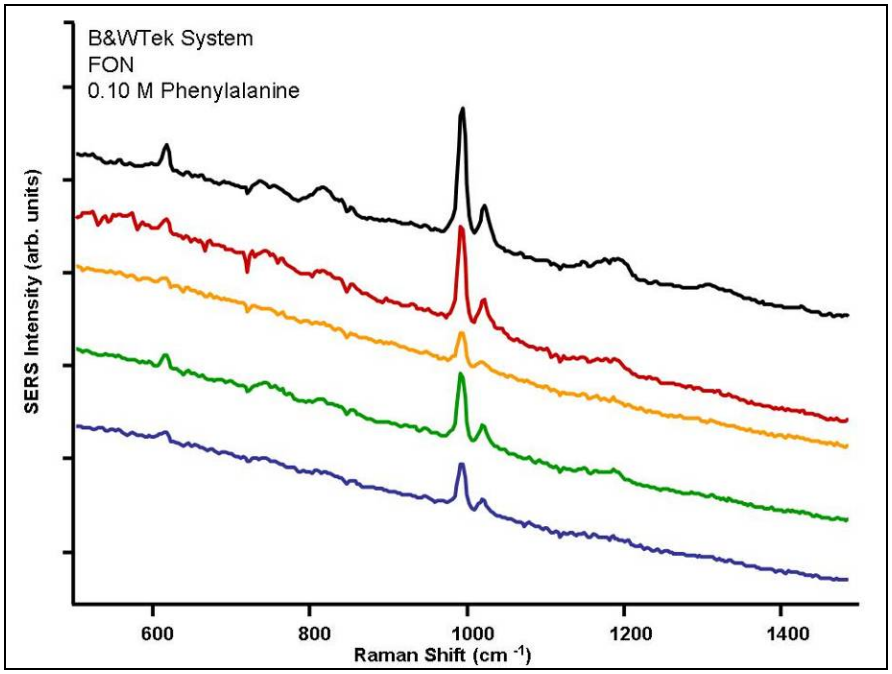

Figure C-2. SERS of 0.10 M PHE measured on FON substrate with the B&WTek system.

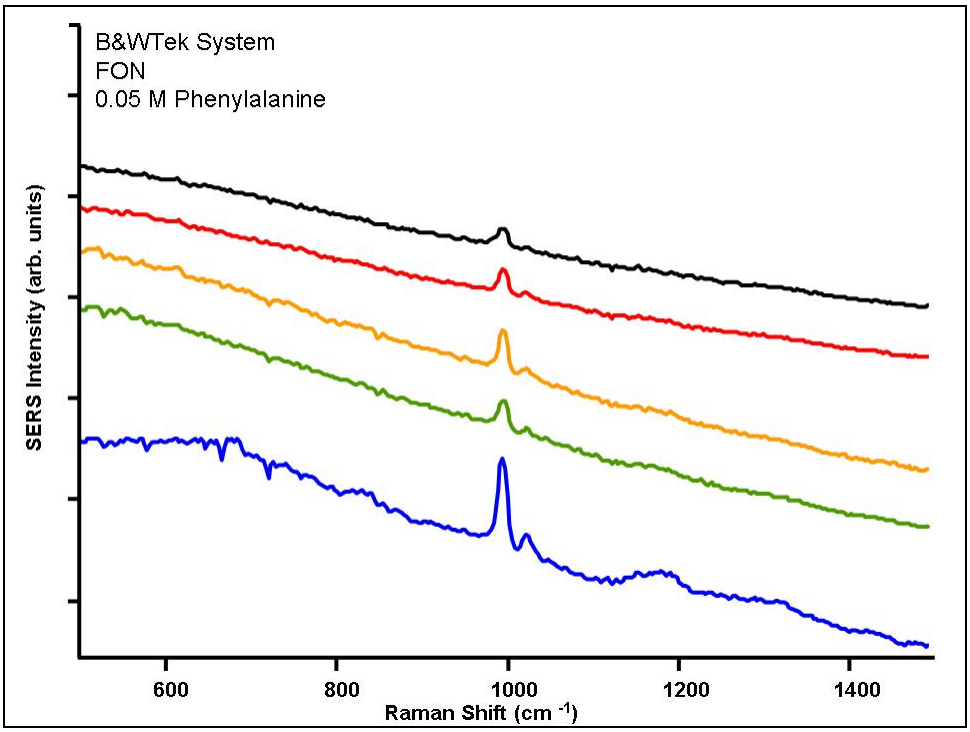

Figure C-3. SERS of 0.05 M PHE measured on FON substrate with the B&WTek system.

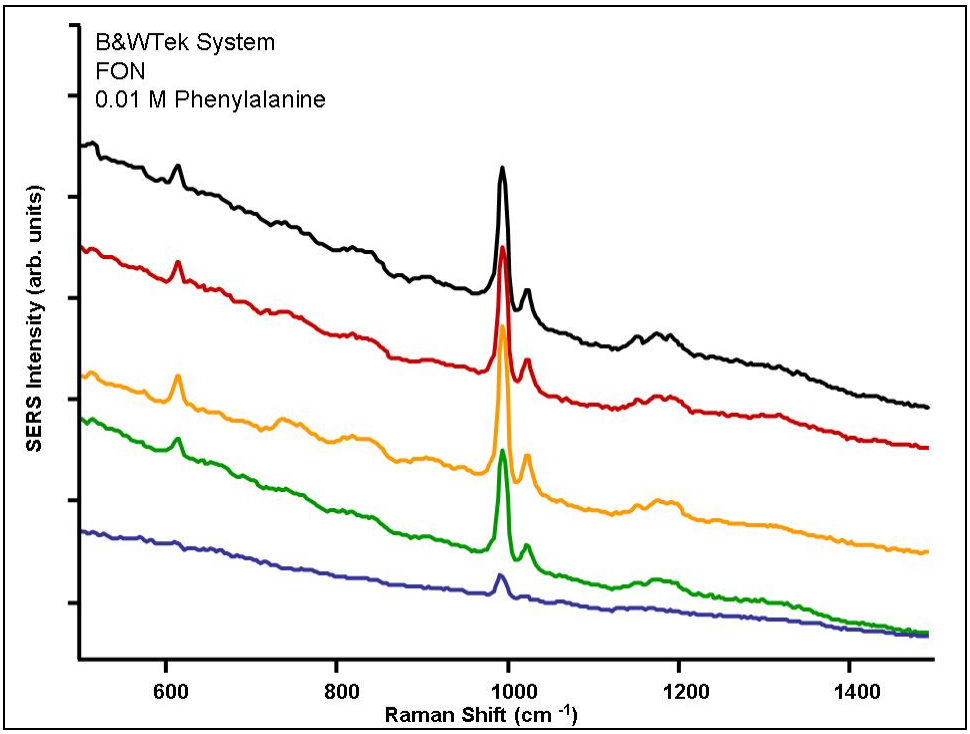

Figure C-4. SERS of 0.01 M PHE measured on FON substrate with the B&WTek system.

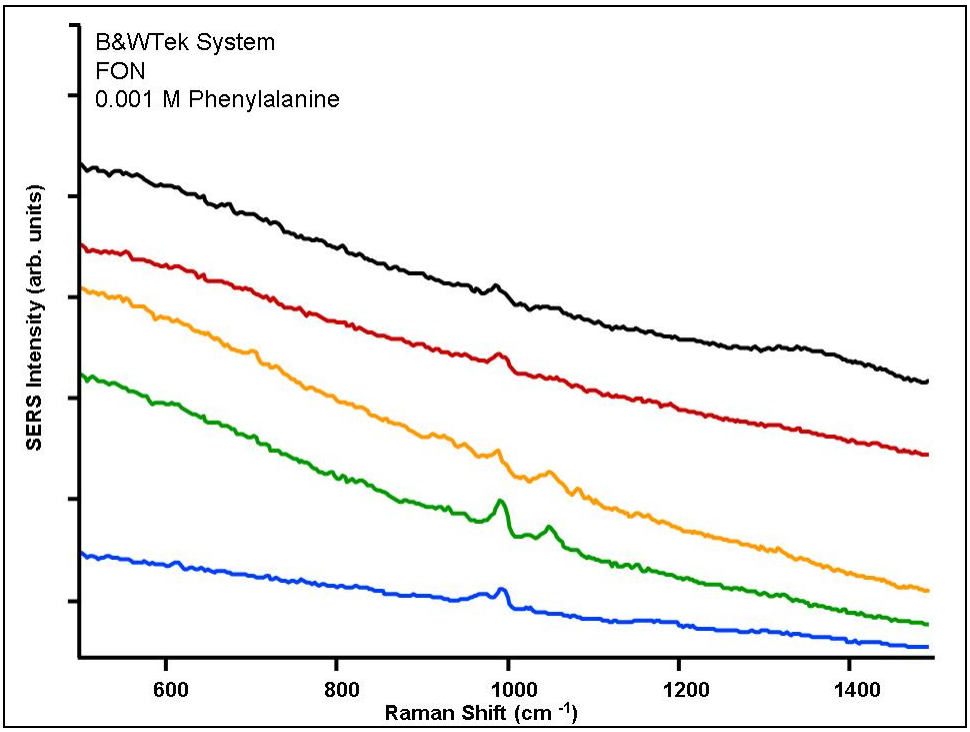

Figure C-5. SERS of 0.001 M PHE measured on FON substrate with the B&WTek system.

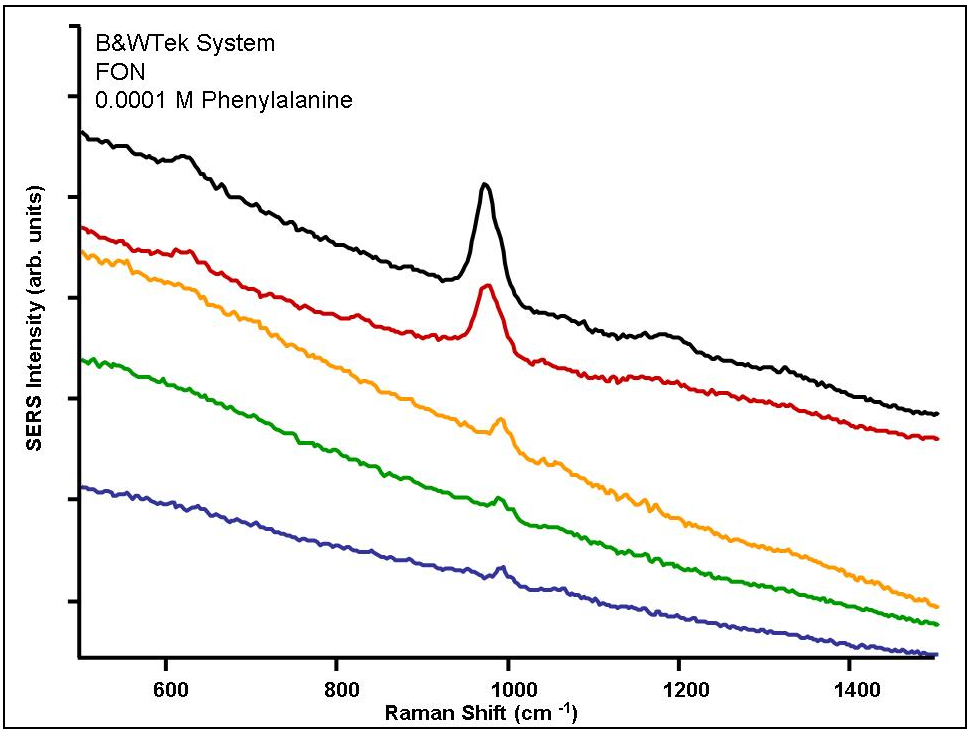

Figure C-6. SERS of 0.0001 M PHE measured on FON substrate with the B&WTek system.

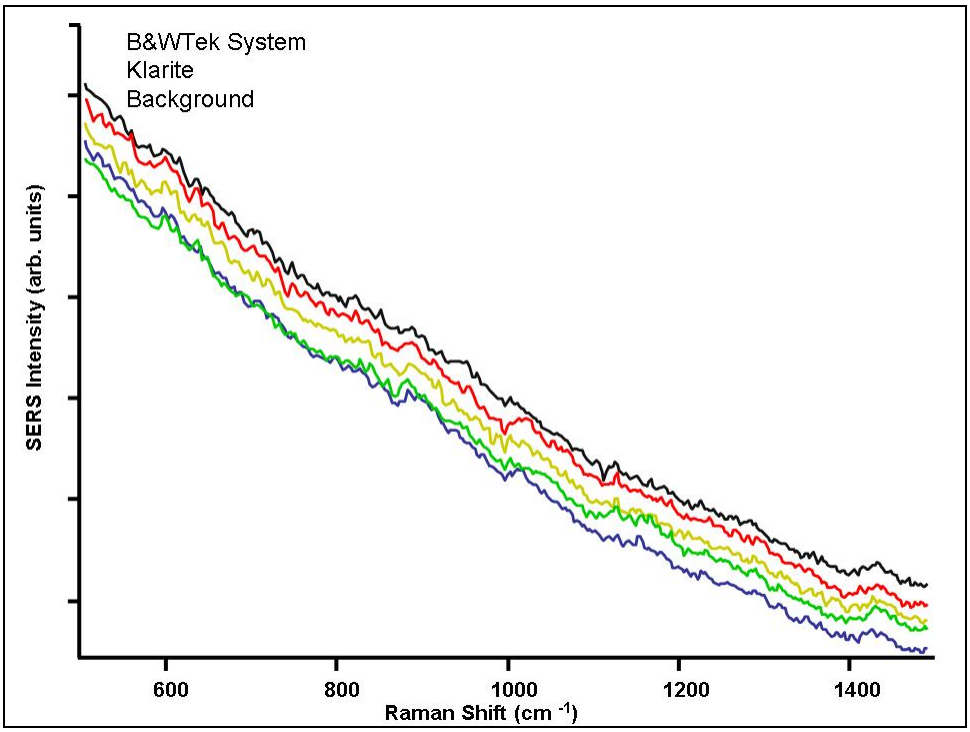

Figure C-7. SERS background of Klarite substrate measured with the B&WTek system.

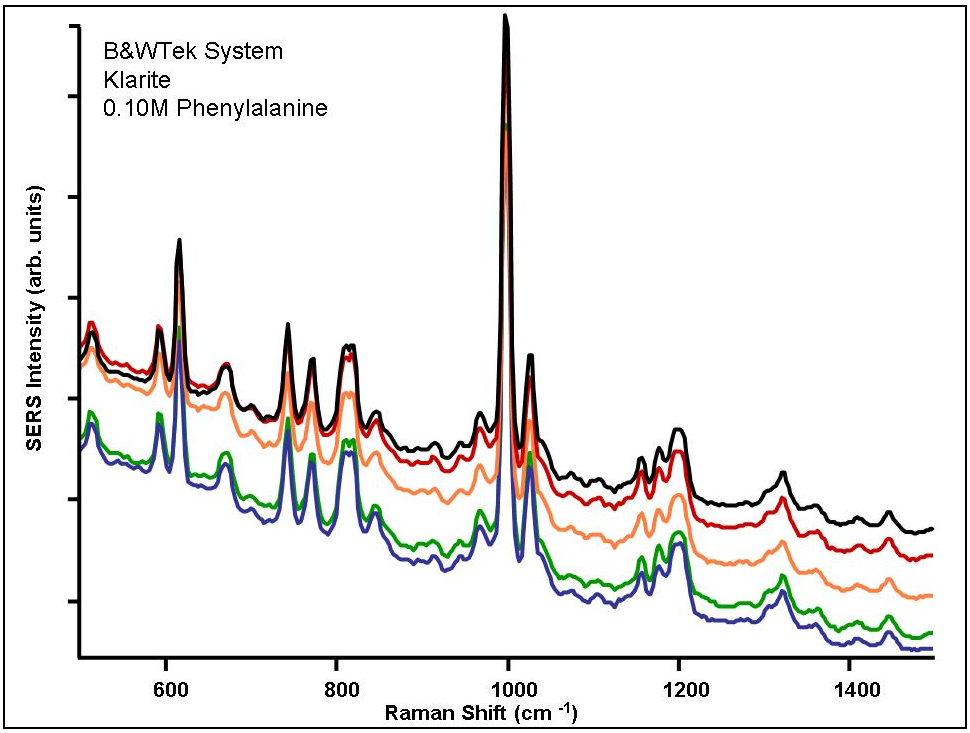

Figure C-8. SERS of 0.10 M PHE as measured with Klarite substrate with the B&WTek system.

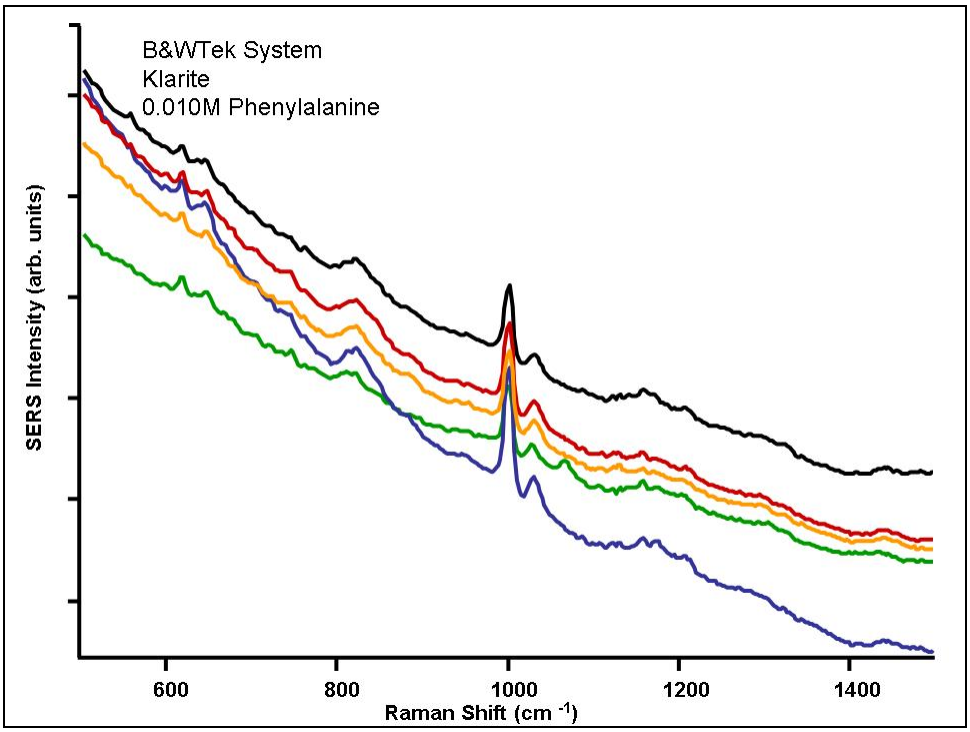

Figure C-9. SERS of 0.010 M PHE as measured with Klarite substrate with the B&WTek system.

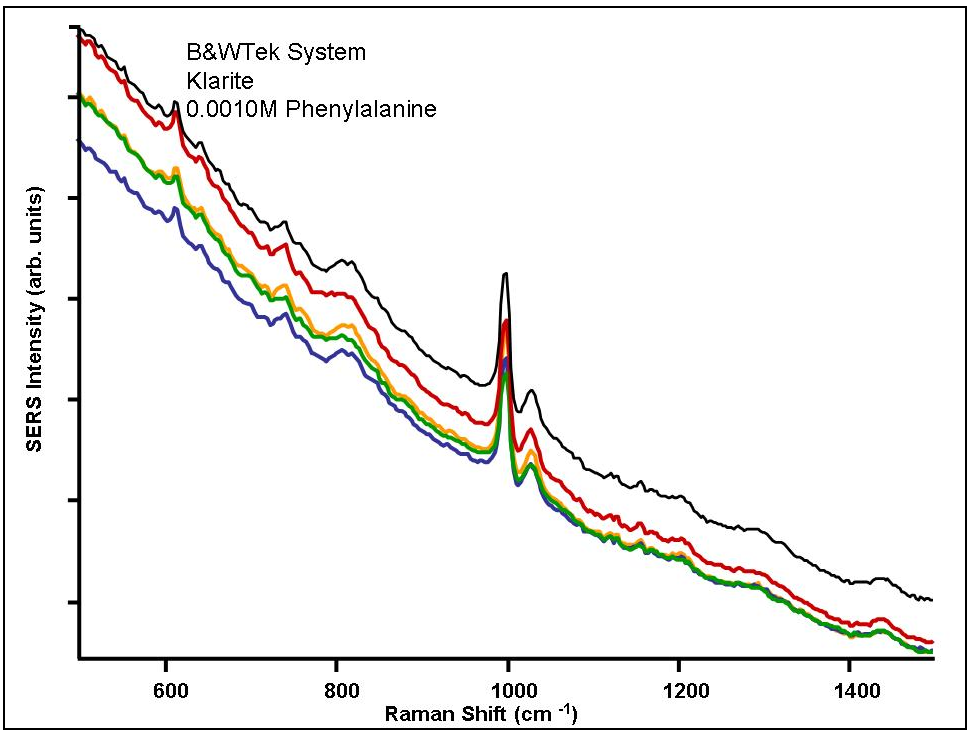

Figure C-10. SERS of 0.001 M PHE as measured with Klarite substrate with the B &WTek system.

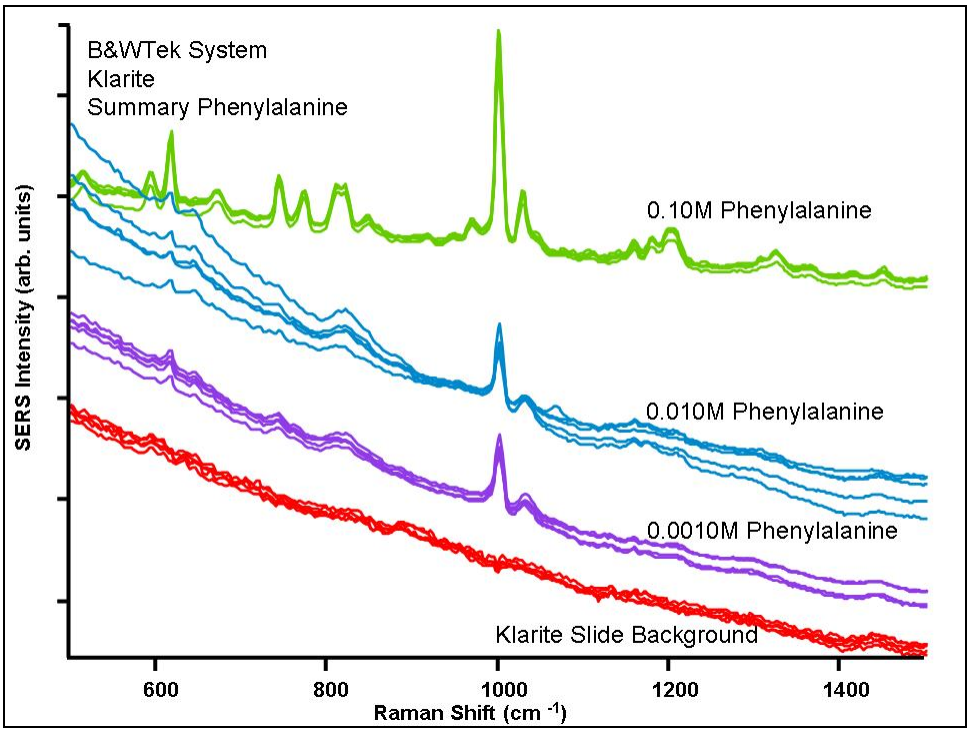

Figure C-11. SERS summary of PHE as measured with Klarite substrate with the B&WTek system.

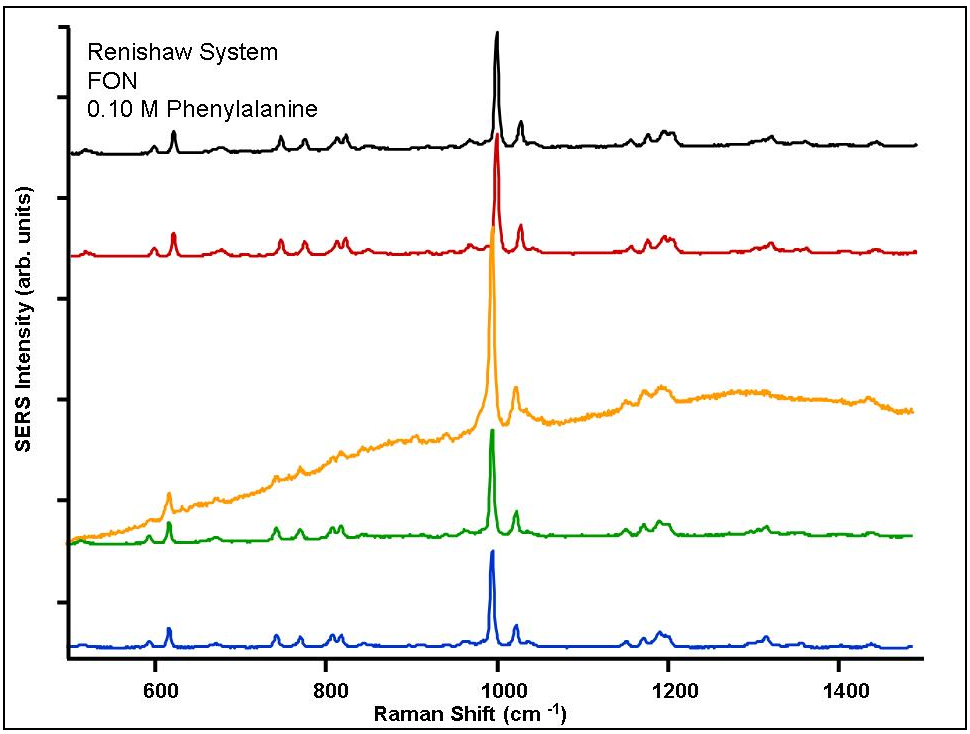

Figure C-12. SERS of 0.10 M PHE as measured with FON substrate with the Renishaw system.

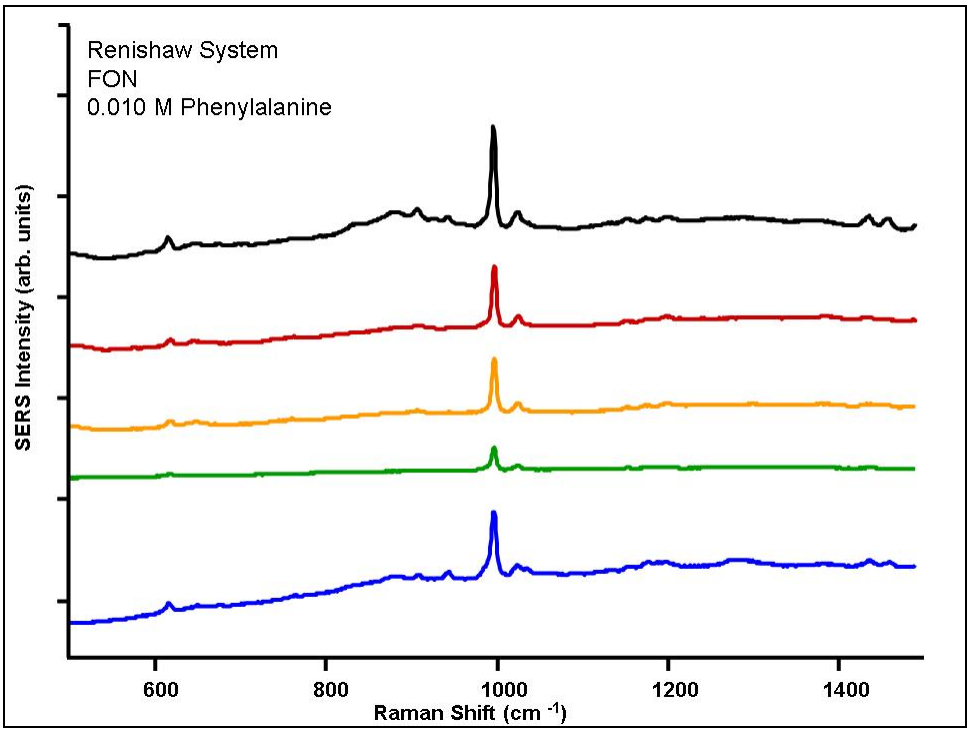

Figure C-13. SERS of 0.010 M PHE as measured with FON substrate with the Renishaw system.

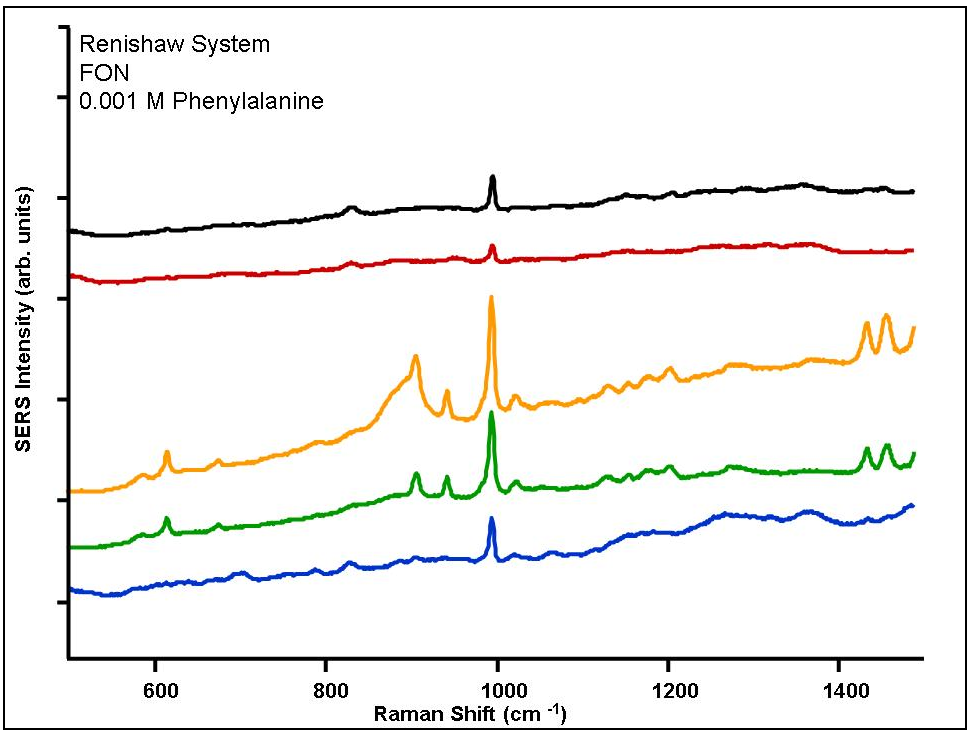

Figure C-14. SERS of 0.001 M PHE as measured with FON substrate with the Renishaw system.

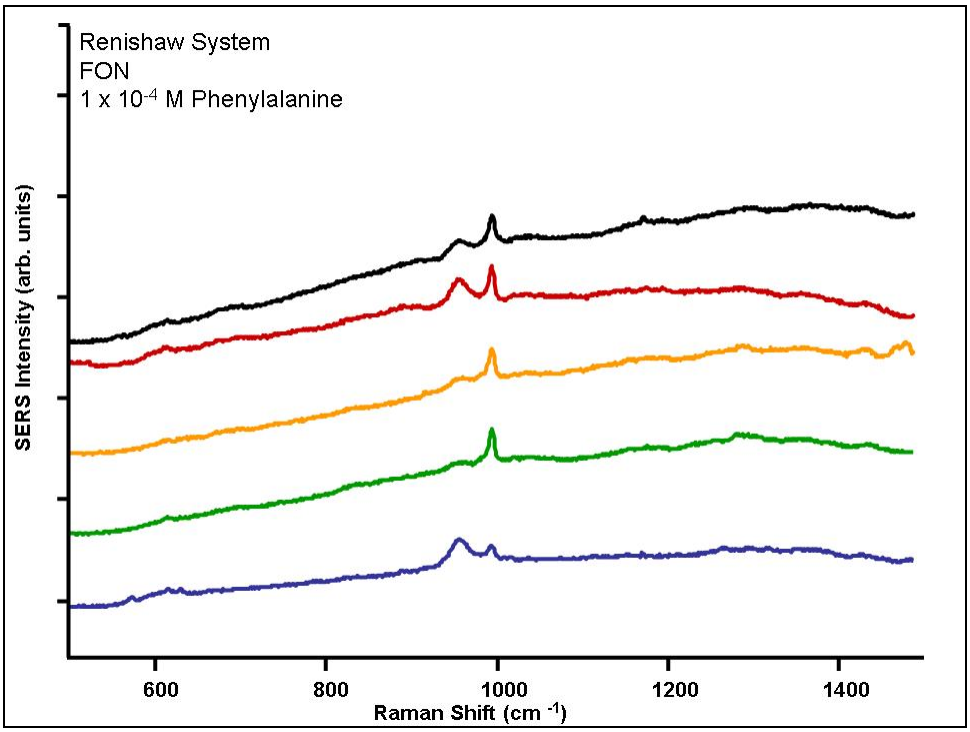

Figure C-15. SERS of 0.0001 M PHE as measured with FON substrate with the Renishaw system.

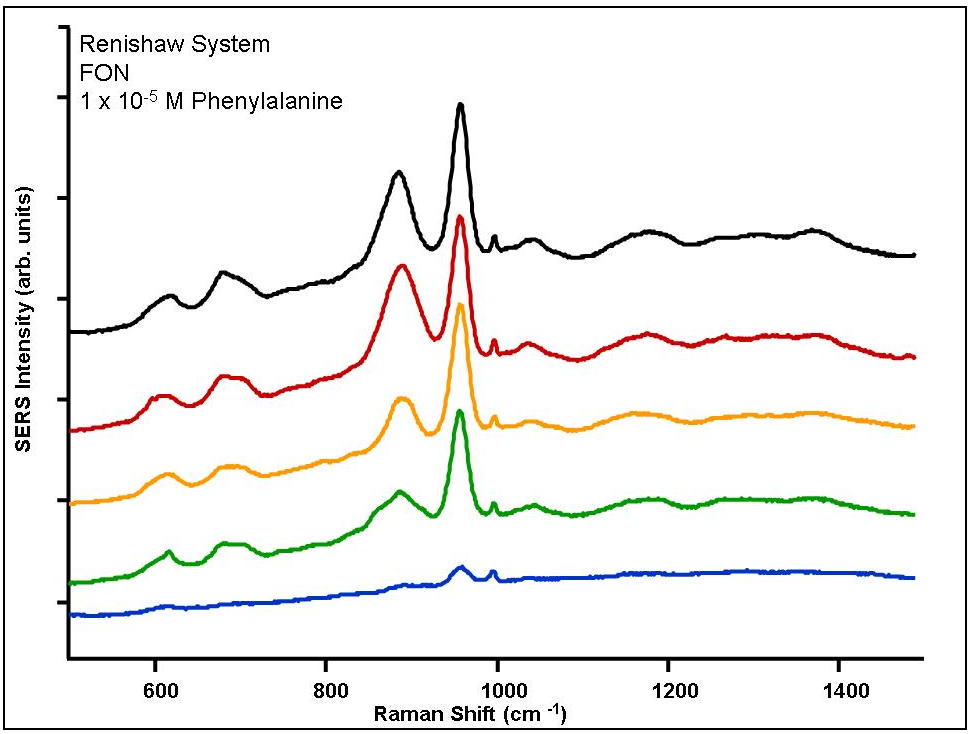

Figure C-16. SERS of 1 x 10^{-5} M PHE as measured with FON substrate with the Renishaw system.

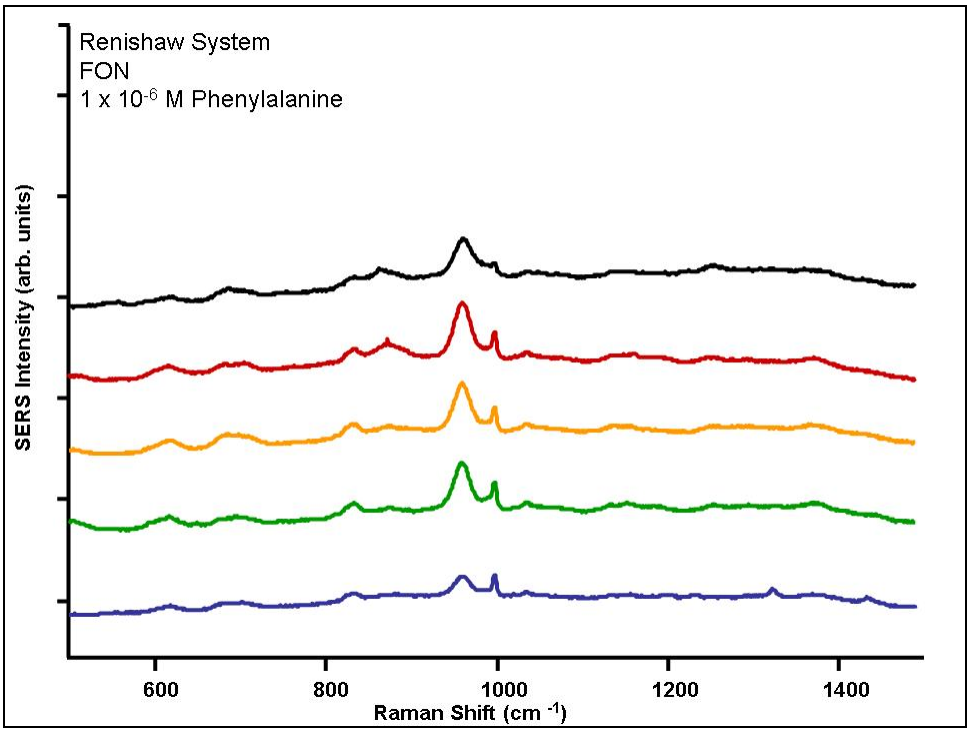

Figure C-17. SERS of 1 x 10^{-6} M PHE as measured with FON substrate with the Renishaw system.

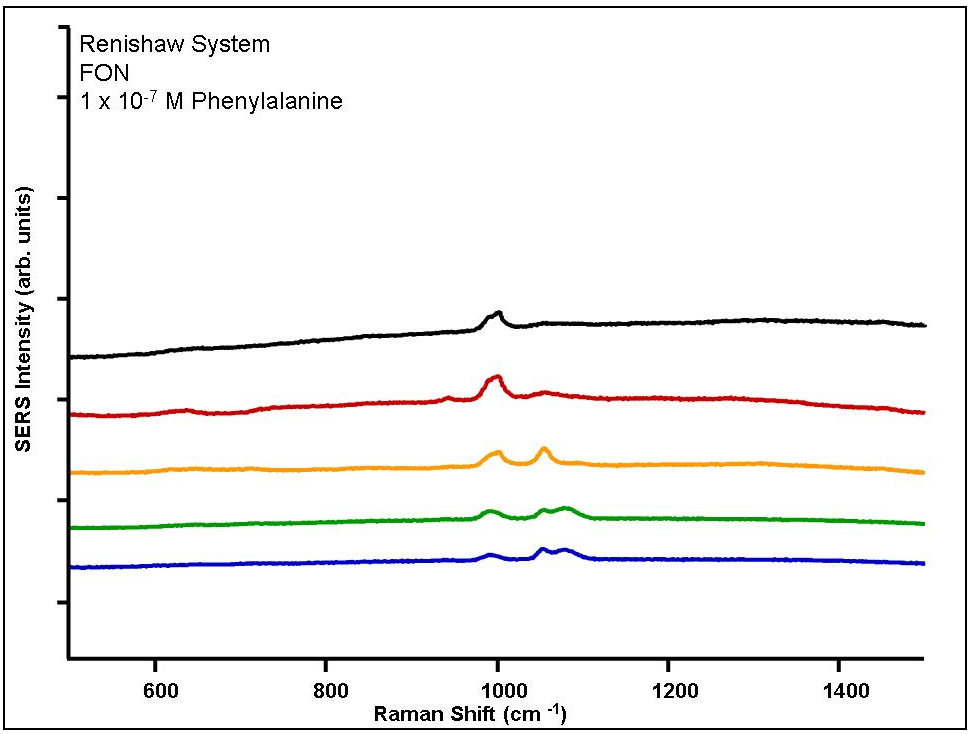

Figure C-18. SERS of 1 x 10^{-7} M PHE as measured with FON substrate with the Renishaw system.

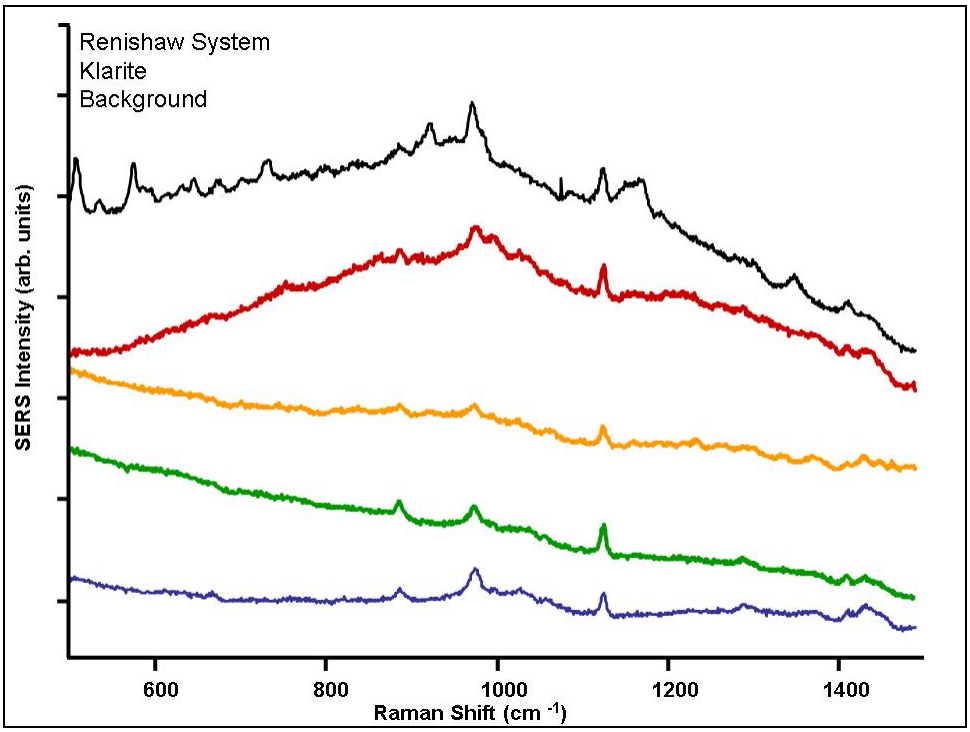

Figure C-19. SERS of Klarite background as measured with the Renishaw system.

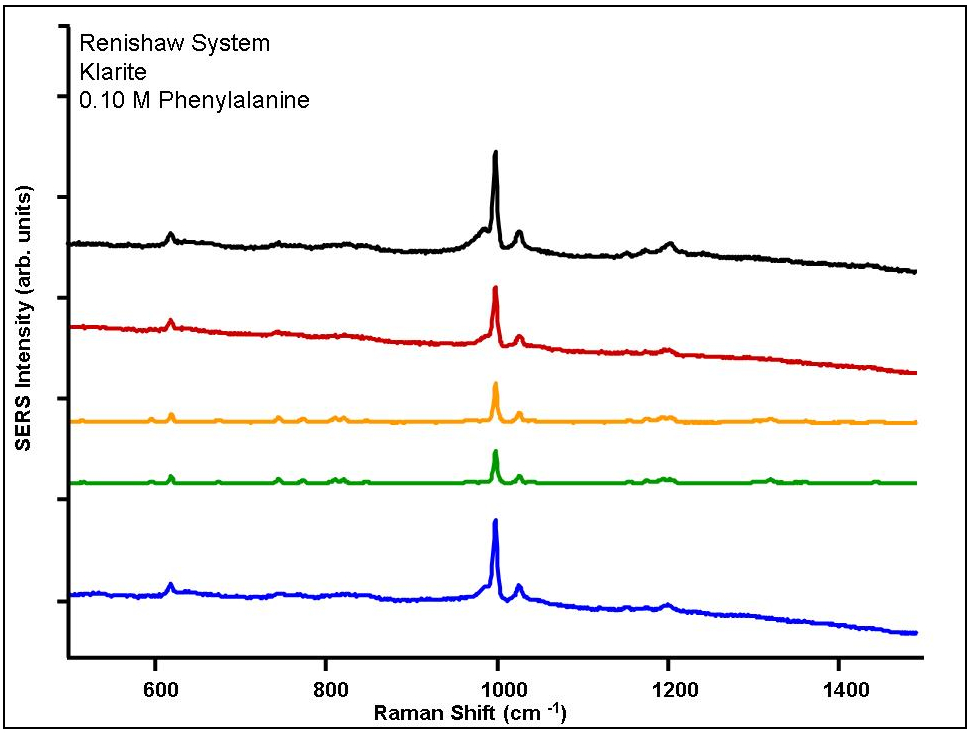

Figure C-20. SERS of 0.10 M PHE as measured on Klarite substrate with the Renishaw system.

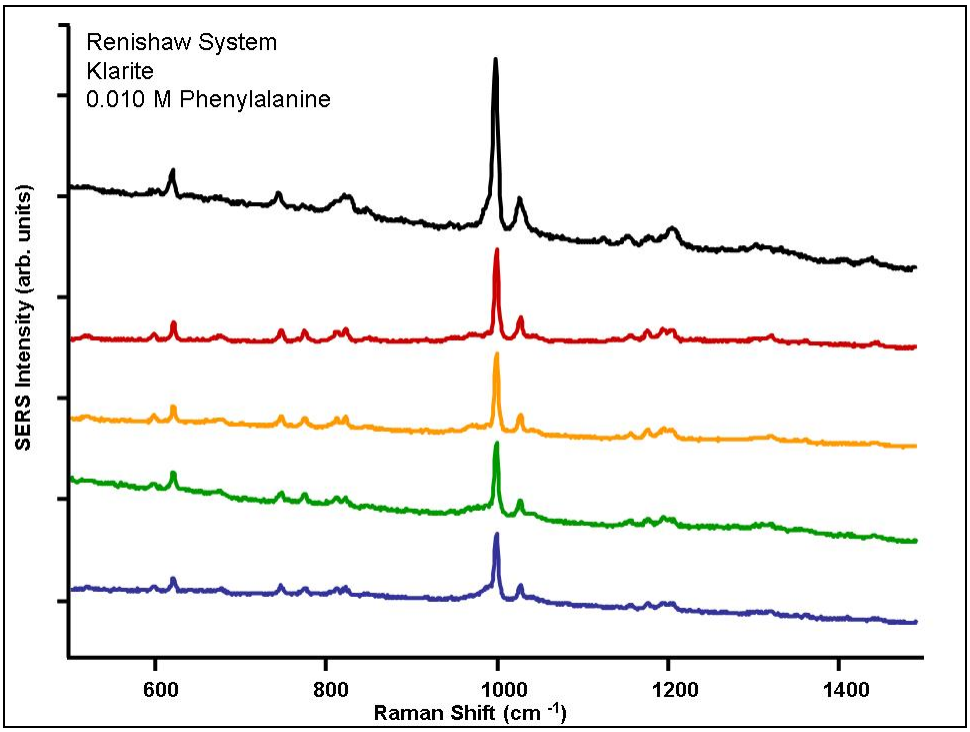

Figure C-21. SERS of 0.01 M PHE as measured on Klarite substrate with the Renishaw system.

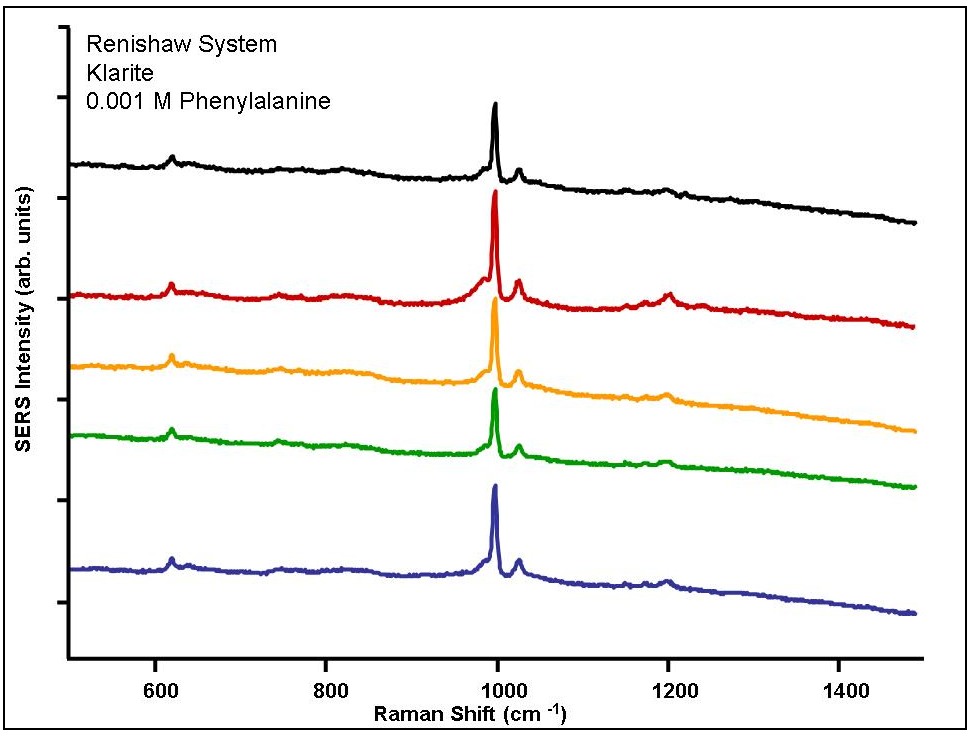

Figure C-22. SERS of 0.001 M PHE as measured on Klarite substrate with the Renishaw system.

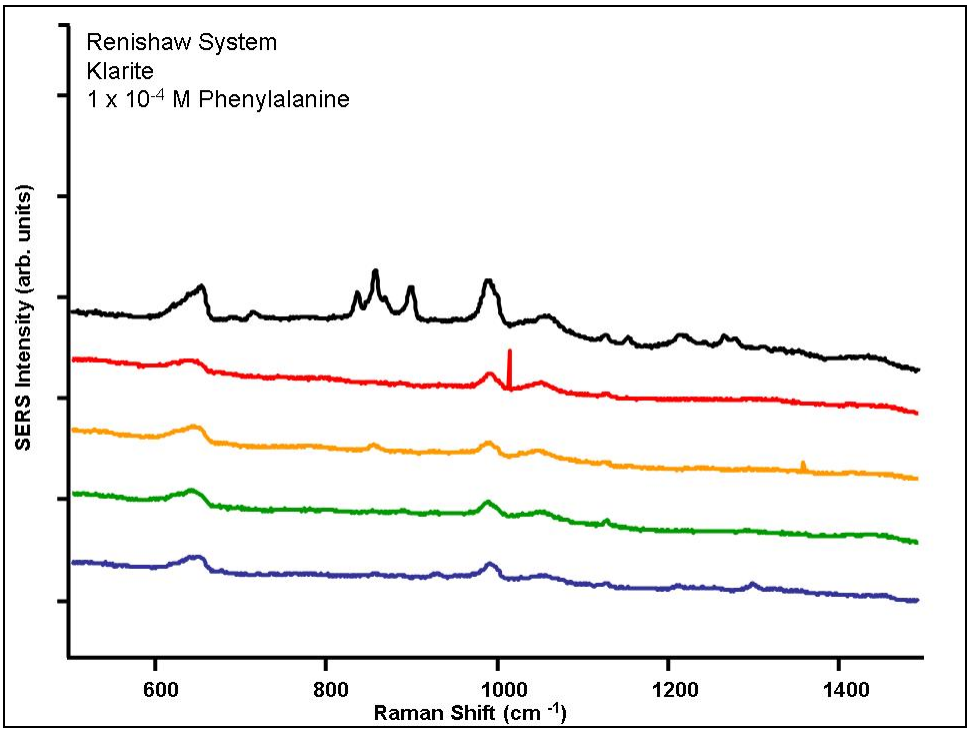

Figure C-23. SERS of 1 x 10^{-4} M PHE as measured on Klarite substrate with the Renishaw system.

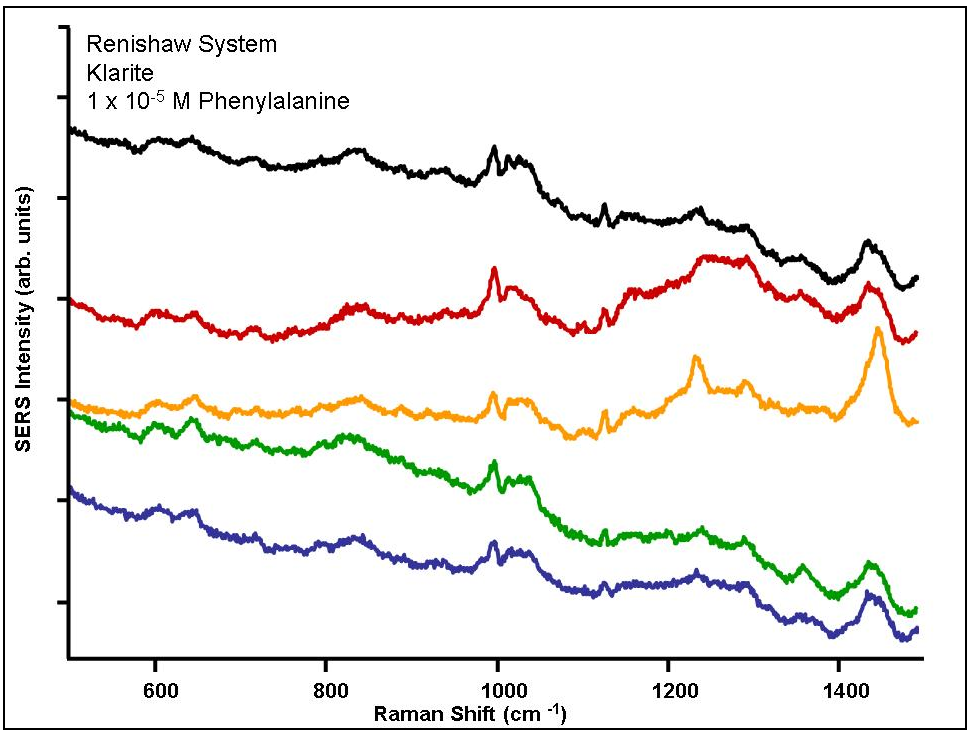

Figure C-24. SERS of 1 x 10^{-5} M PHE as measured on Klarite substrate with the Renishaw system.

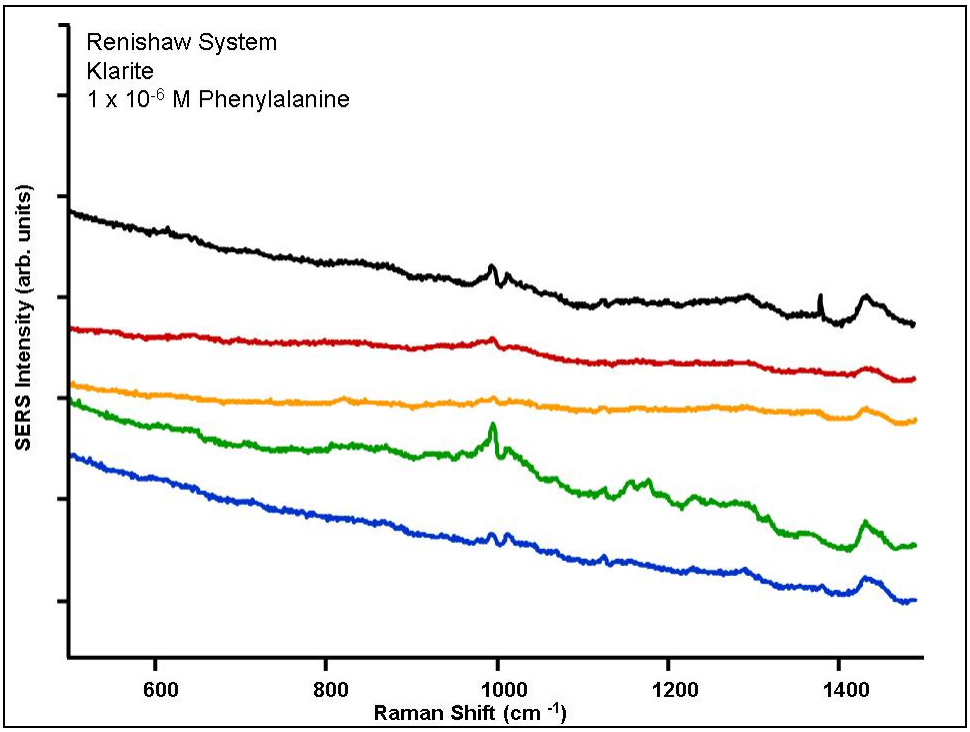

Figure C-25. SERS of 1 x 10^{-6} M PHE as measured on Klarite substrate with the Renishaw system.

INTENTIONALLY LEFT BLANK.

Appendic D. Explosives Supplemental

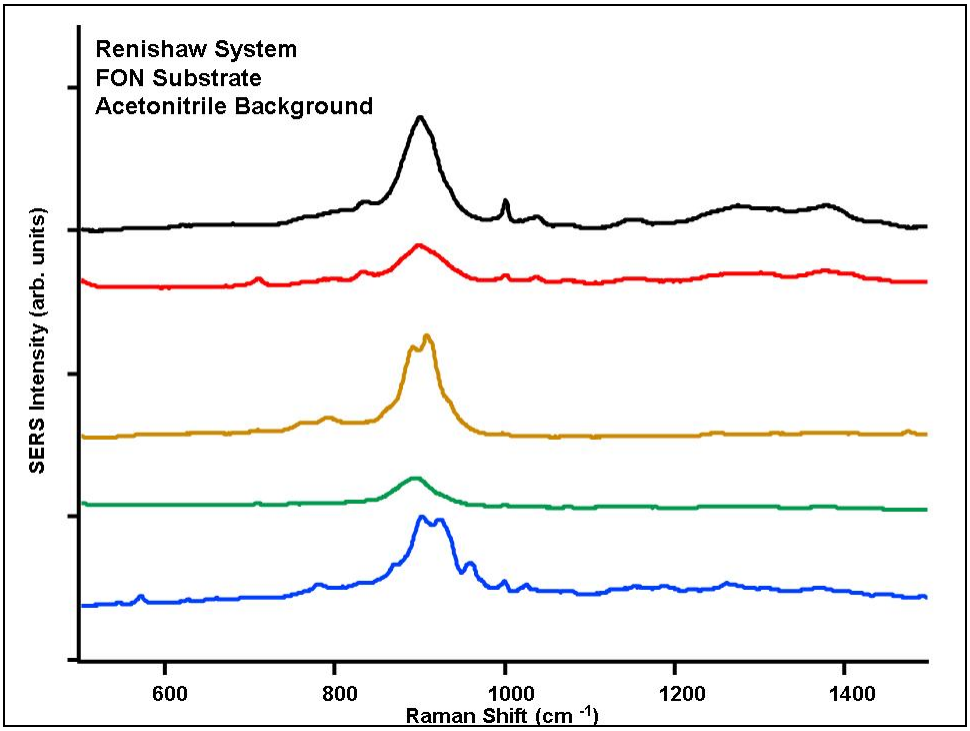

Figure D-1. SERS background of FON substrate and acetonitrile as measured with the Renishaw system.

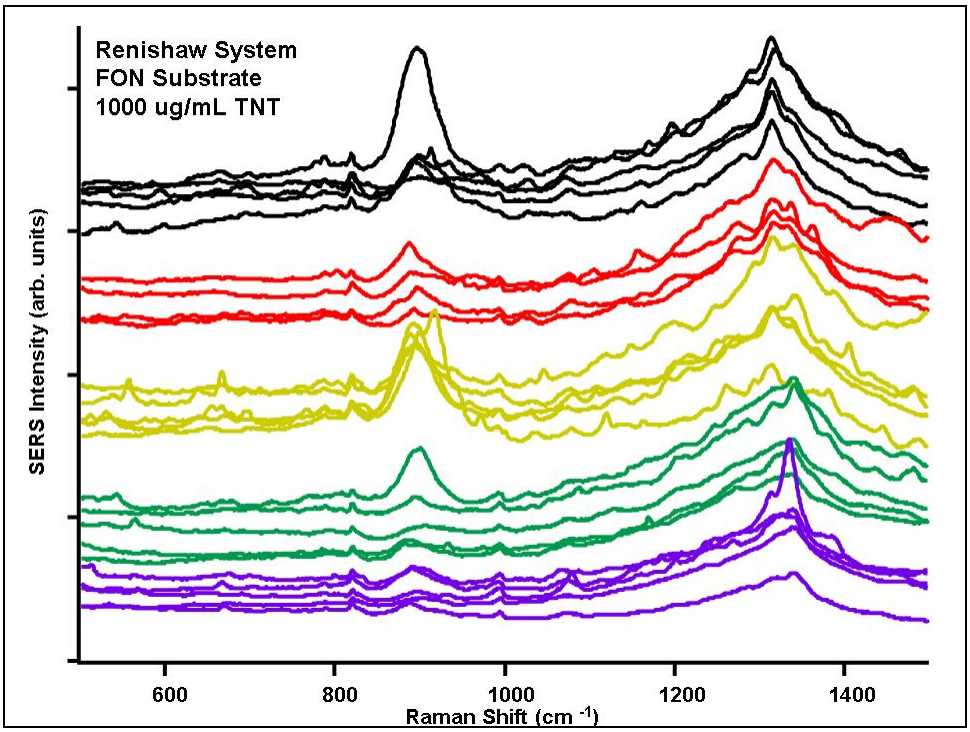

Figure D-2. SERS of 1000 ug/mL TNT measured on FON substrate with the Renishaw system.

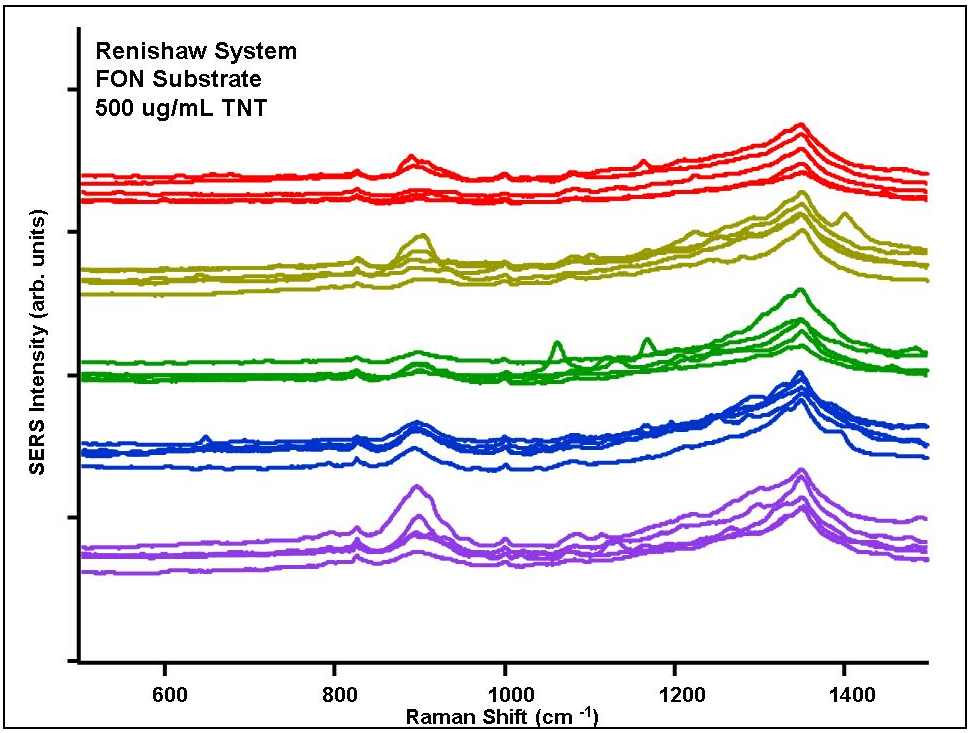

Figure D-3. SERS of 500 ug/mL TNT measured on FON substrate with the Renishaw system.

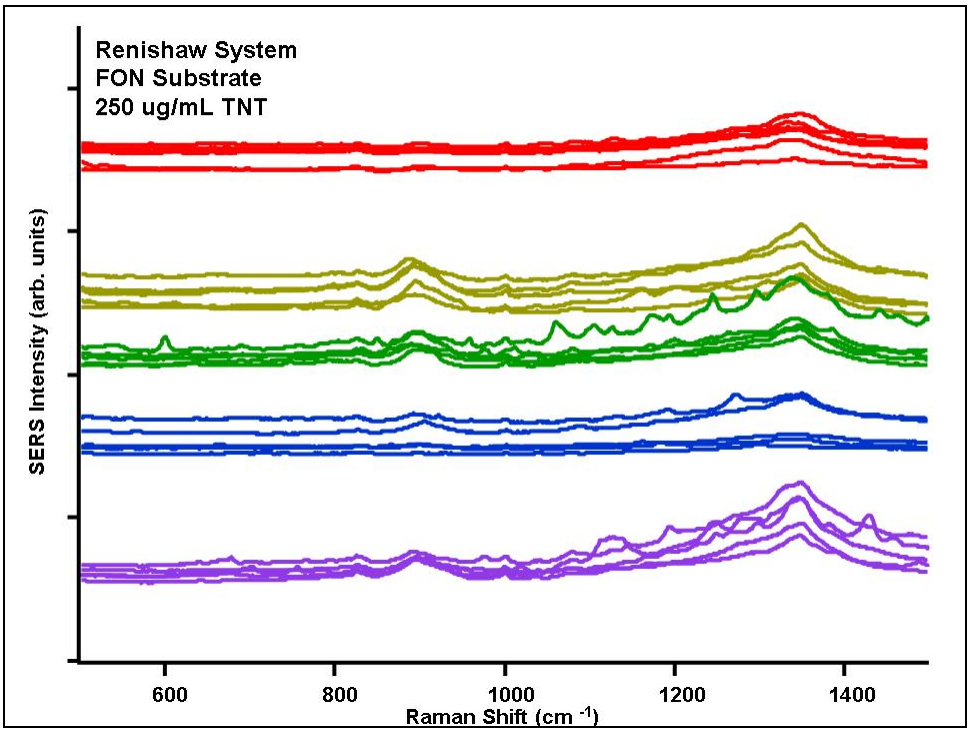

Figure D-4. SERS of 250 ug/mL TNT measured on FON substrate with the Renishaw system.

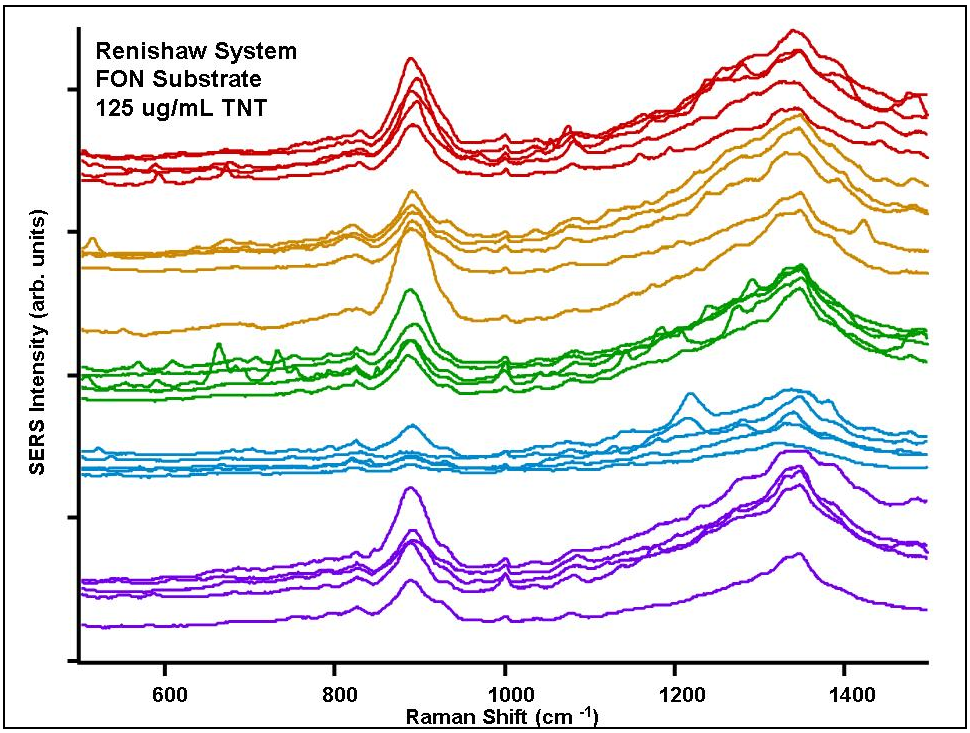

Figure D-5. SERS of 125 ug/mL TNT measured on FON substrate with the Renishaw system.

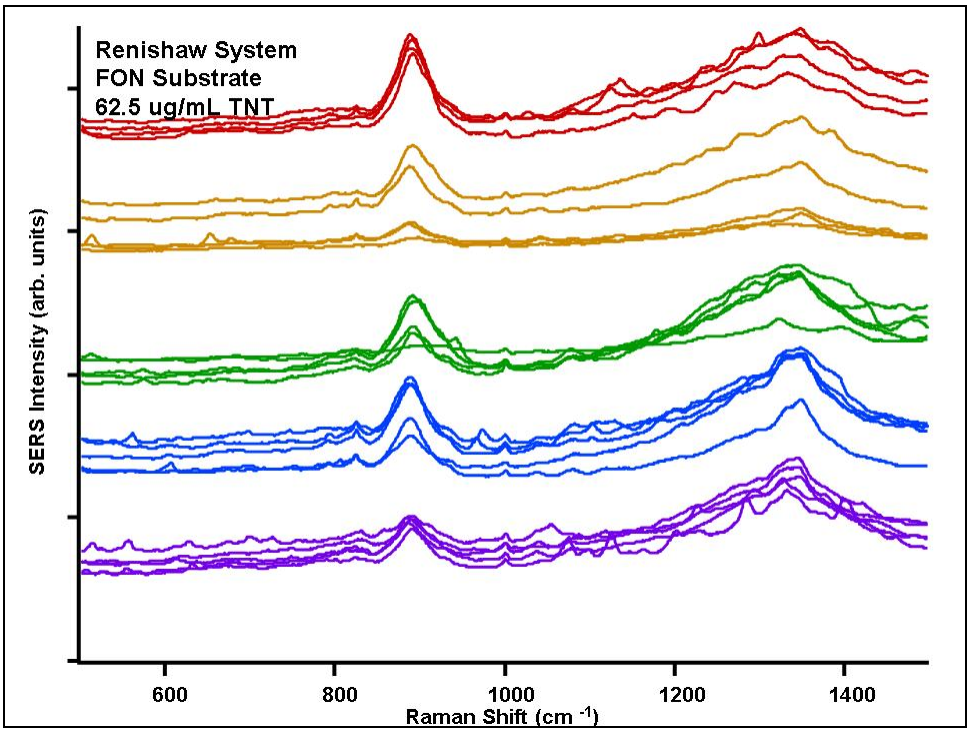

Figure D-6. SERS of 62.5 ug/mL TNT measured on FON substrate with the Renishaw system.

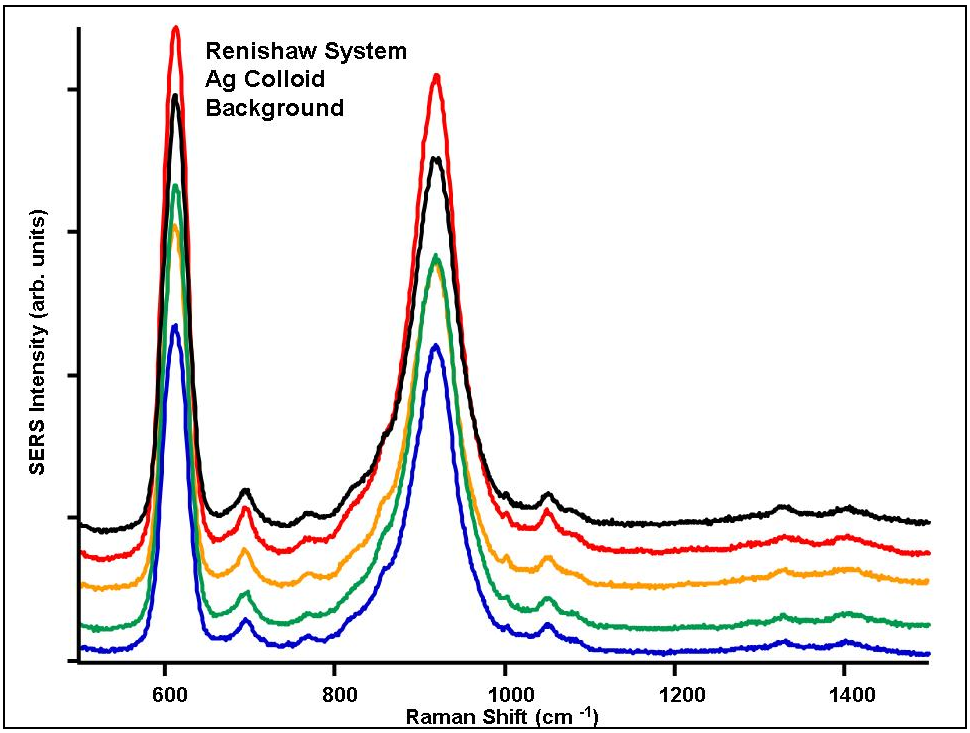

Figure D-7. SERS of Ag colloid substrate background as measured using the Renishaw system.

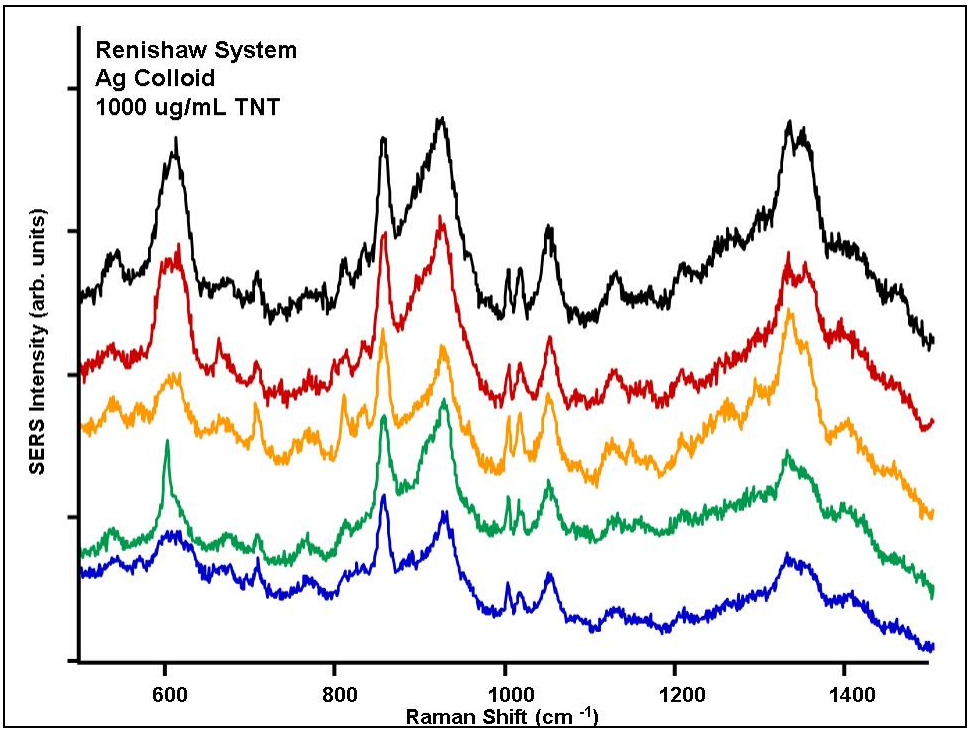

Figure D-8. SERS of 1000 ug/mL TNT as measured with Ag colloid substrate using the Renishaw system.

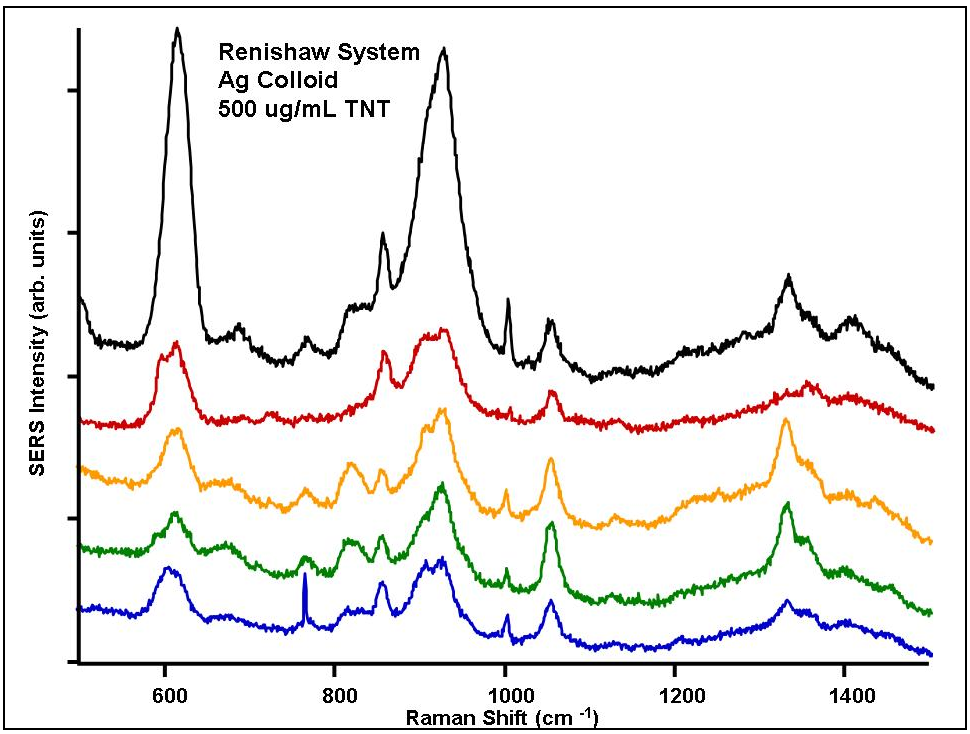

Figure D-9. SERS of 500 ug/mL TNT as measured with Ag colloid substrate using the Renishaw system.

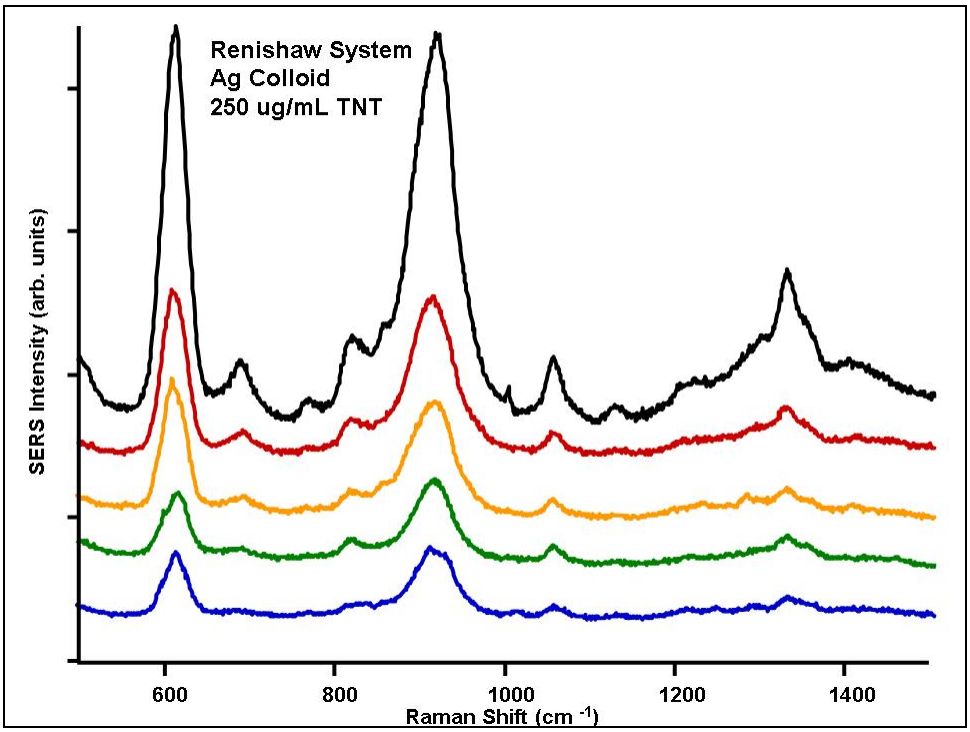

Figure D-10. SERS of 250 ug/mL TNT as measured with Ag colloid substrate using the Renishaw system.

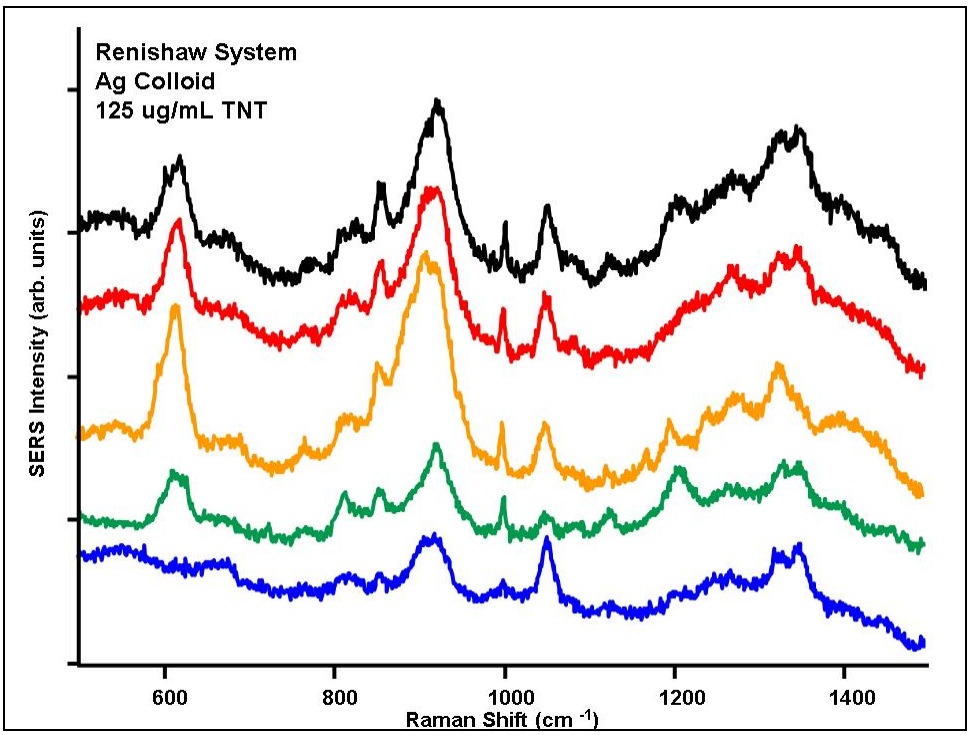

Figure D-11. SERS of 125 ug/mL TNT as measured with Ag colloid substrate using the Renishaw system.

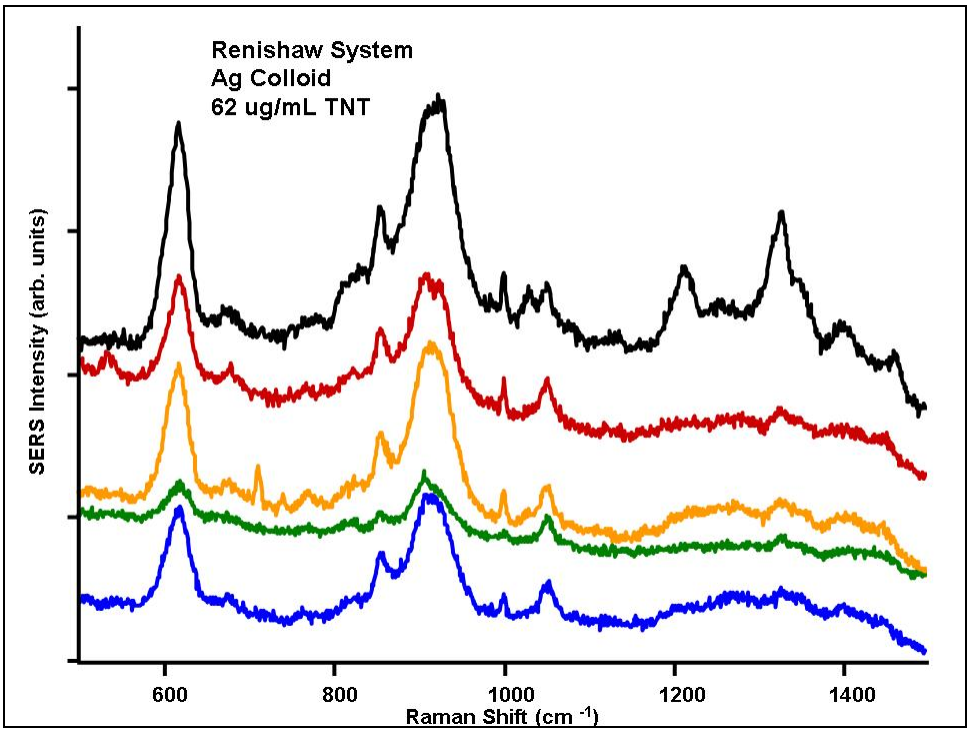

Figure D-12. SERS of 62 ug/mL TNT as measured with Ag colloid substrate using the Renishaw system.

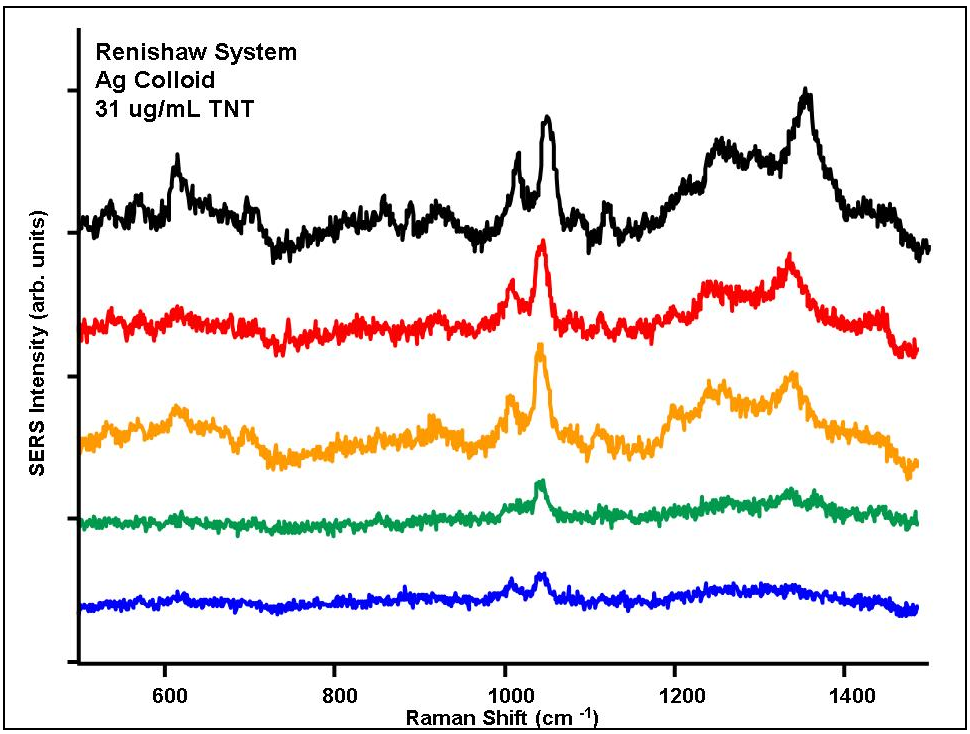

Figure D-13. SERS of 31 ug/mL TNT as measured with Ag colloid substrate using the Renishaw system.

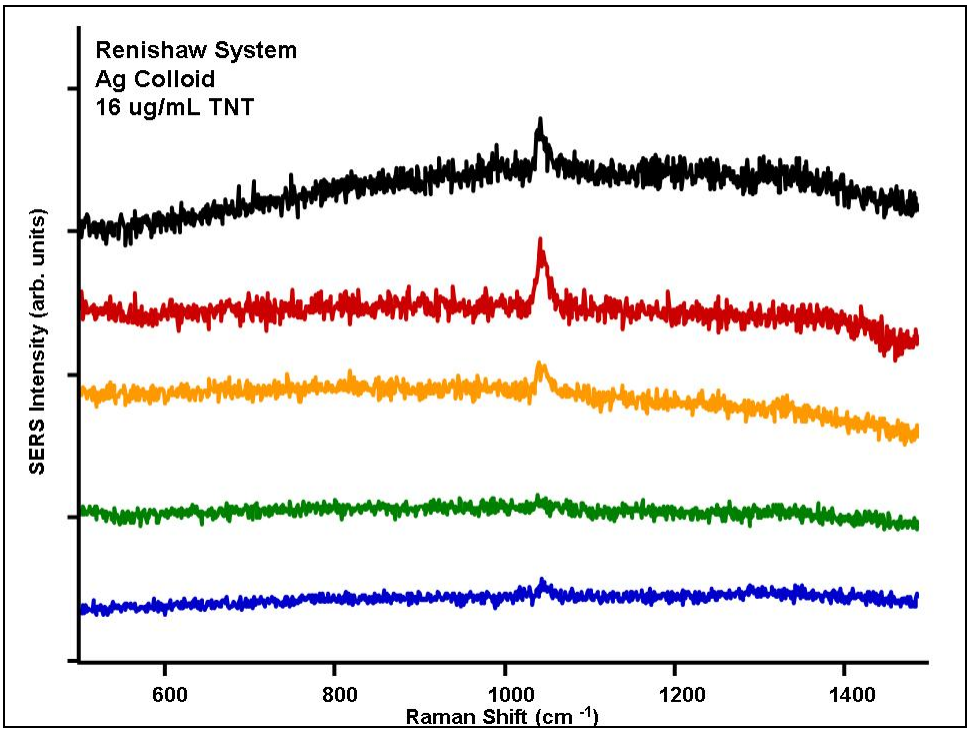

Figure D-14. SERS of 16 ug/mL TNT as measured with Ag colloid substrate using the Renishaw system.

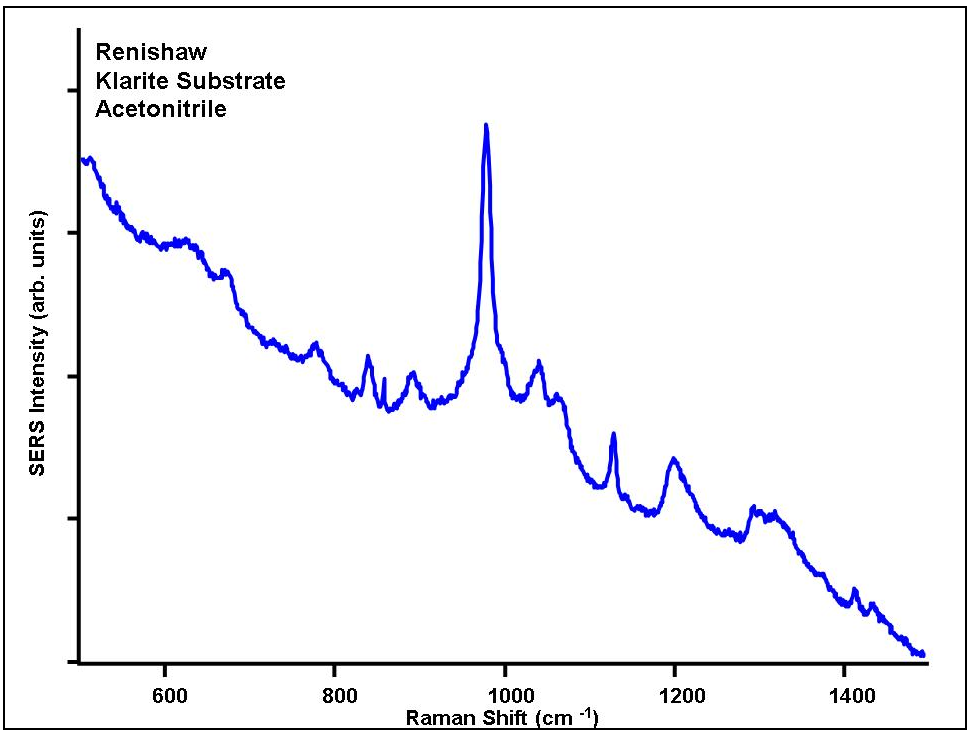

Figure D-15. SERS of Klarite substrate and acetonitrile measured using the Renishaw system.

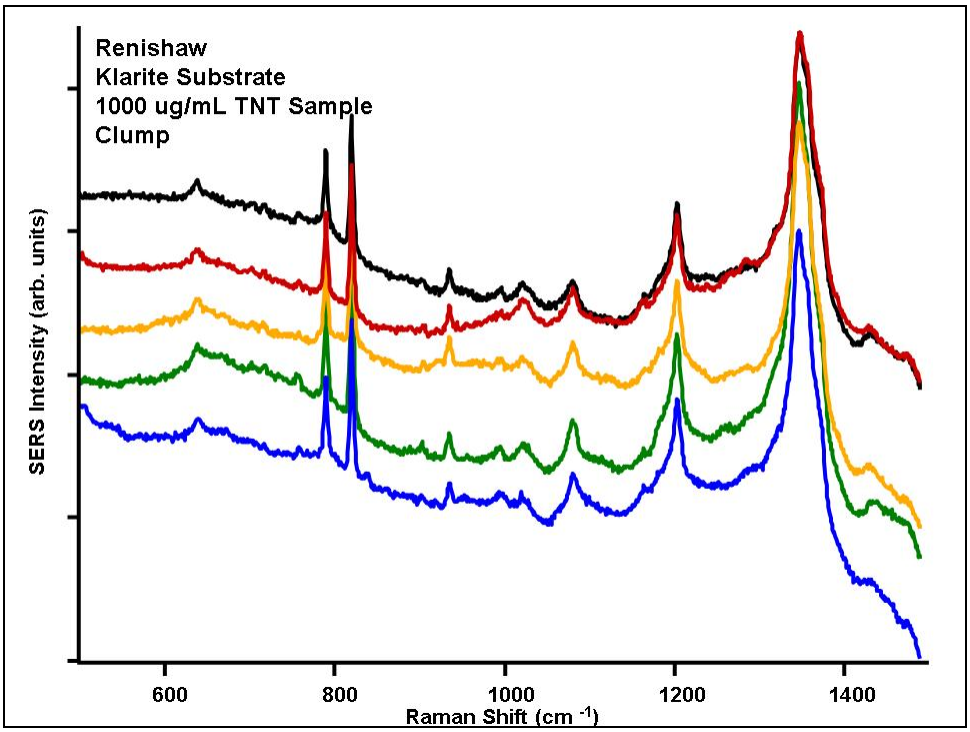

Figure D-16. SERS of 1000 ug/mL TNT measured on Klarite substrate using the Renishaw system.

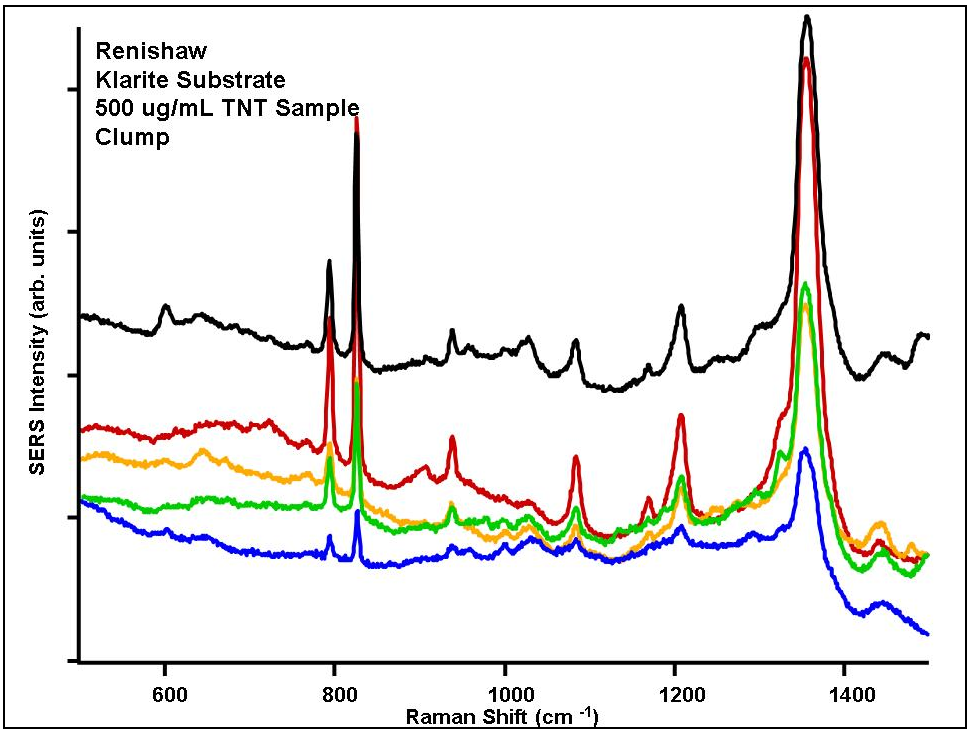

Figure D-17. SERS of 500 ug/mL TNT measured on Klarite substrate using the Renishaw system.

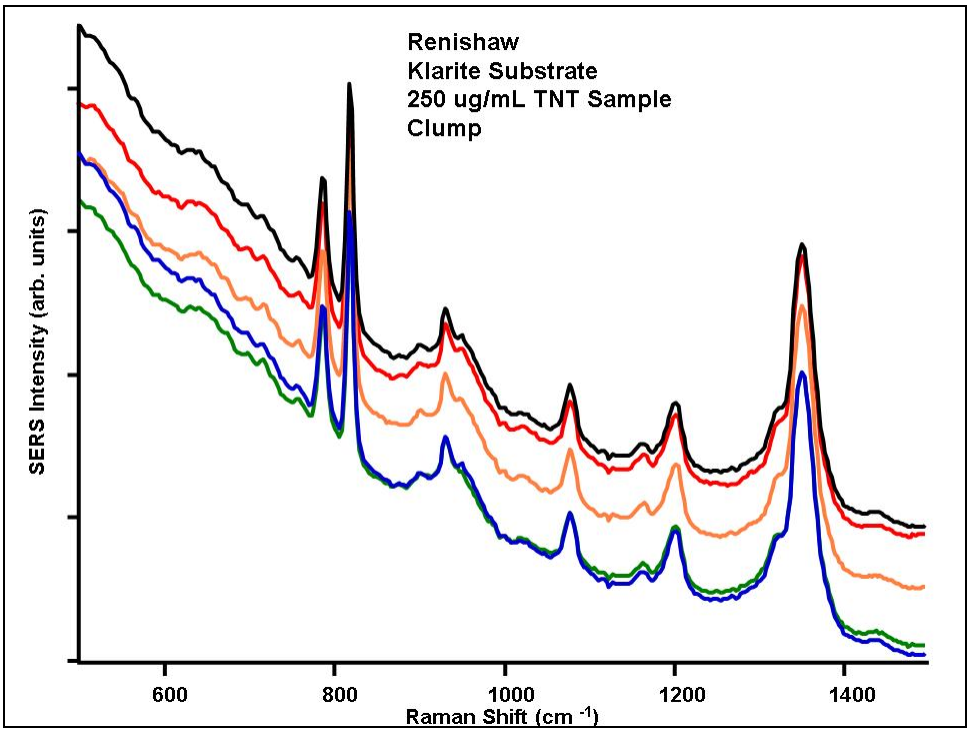

Figure D-18. SERS of 250 ug/mL TNT measured on Klarite substrate using the Renishaw system.

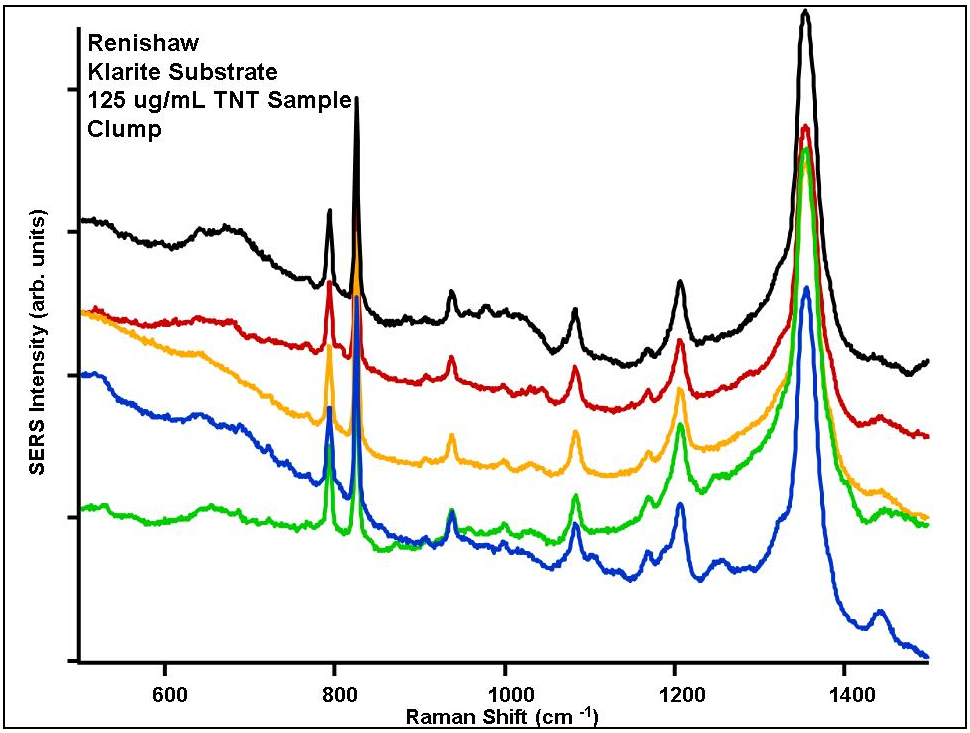

Figure D-19. SERS of 125 ug/mL TNT measured on Klarite substrate using the Renishaw system.

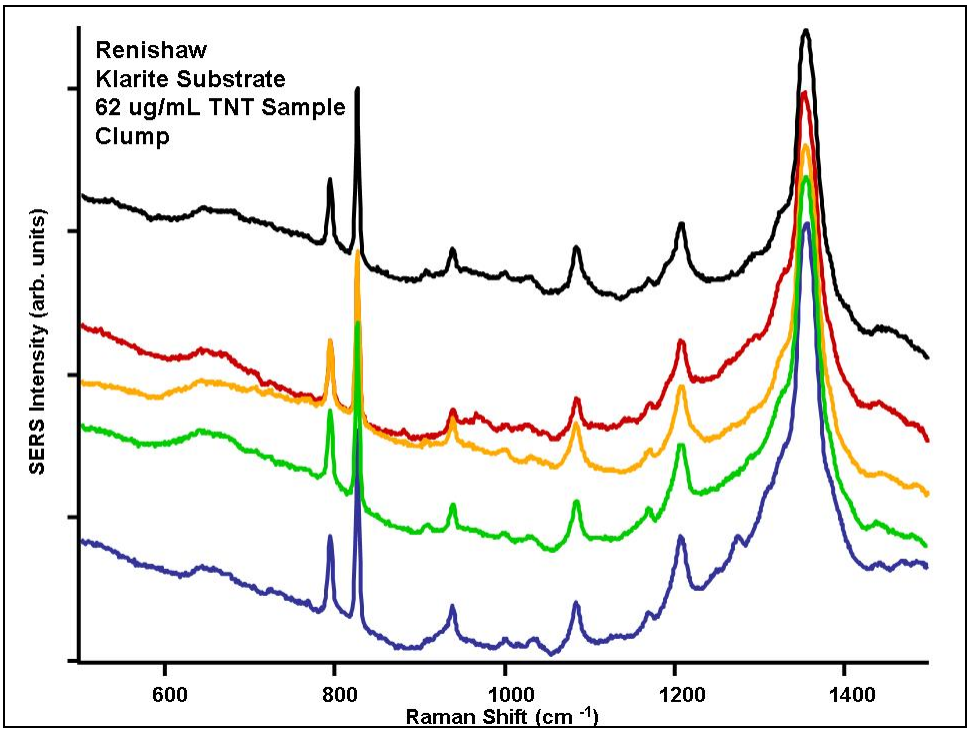

Figure D-20. SERS of 62 ug/mL TNT measured on Klarite substrate using the Renishaw system.

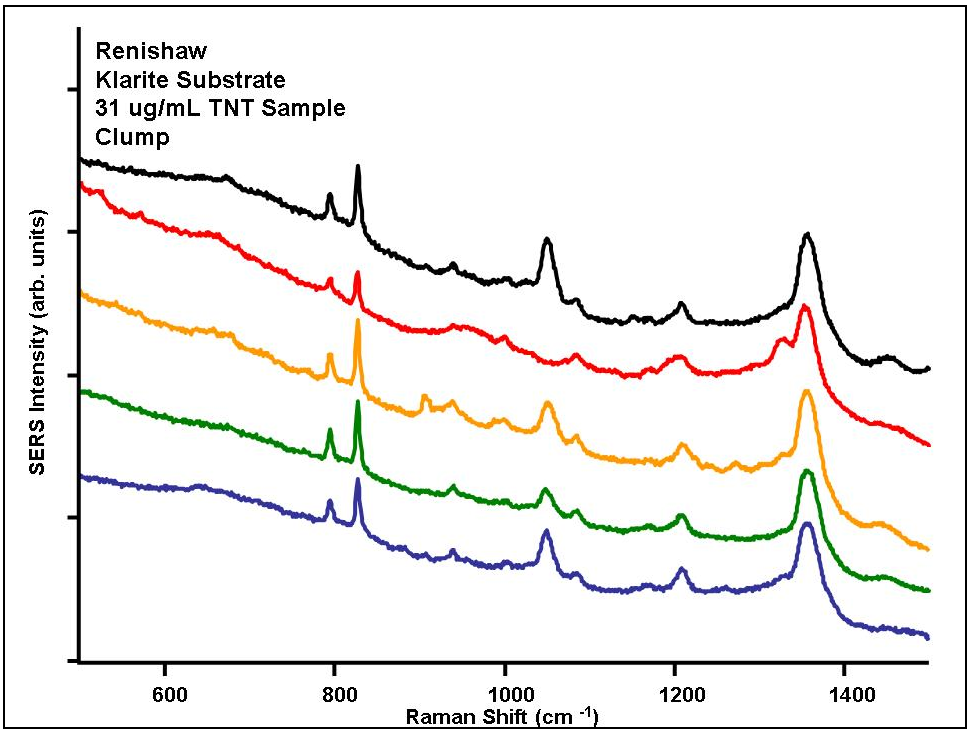

Figure D-21. SERS of 31 ug/mL TNT measured on Klarite substrate using the Renishaw system.

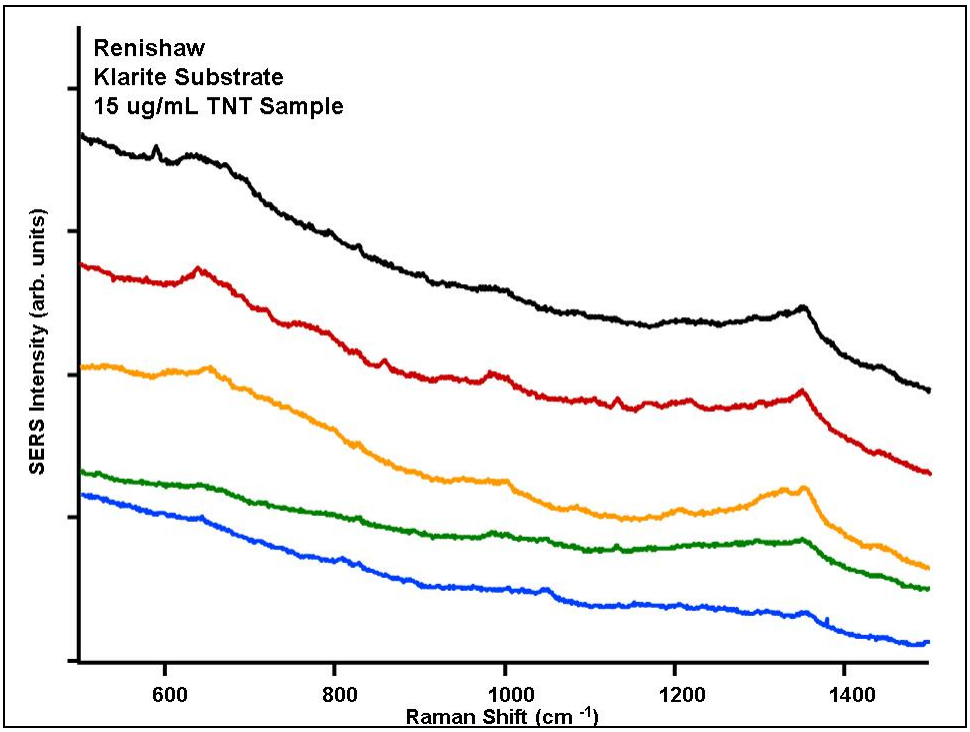

Figure D-22. SERS of 15 ug/mL TNT measured on Klarite substrate using the Renishaw system.

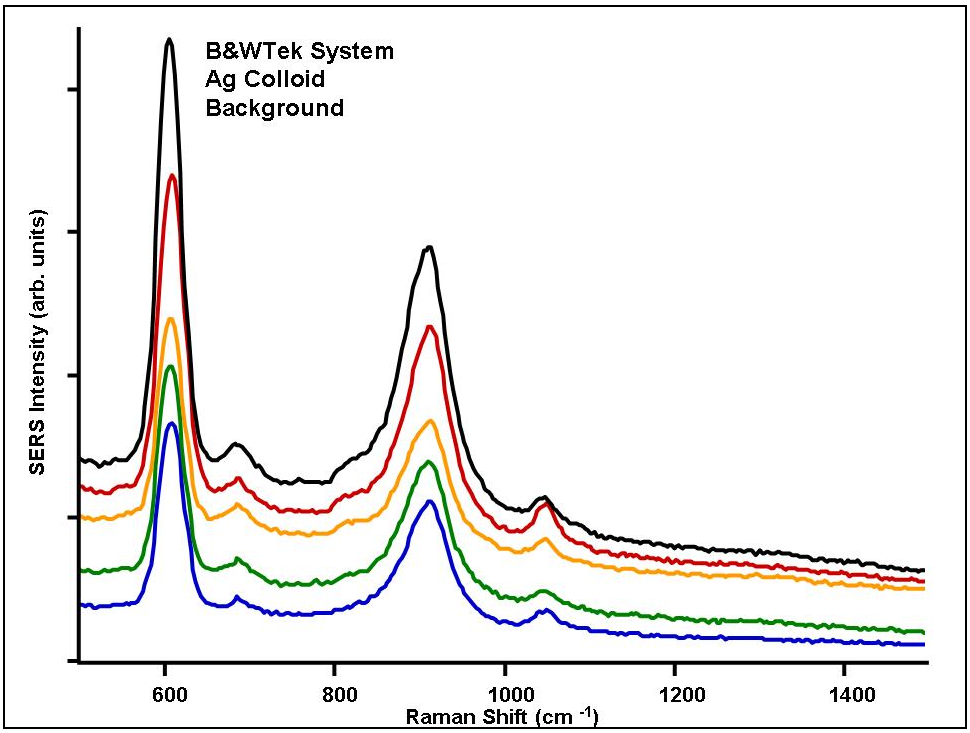

Figure D-23. SERS background measured with Ag colloid using the B&WTek system.

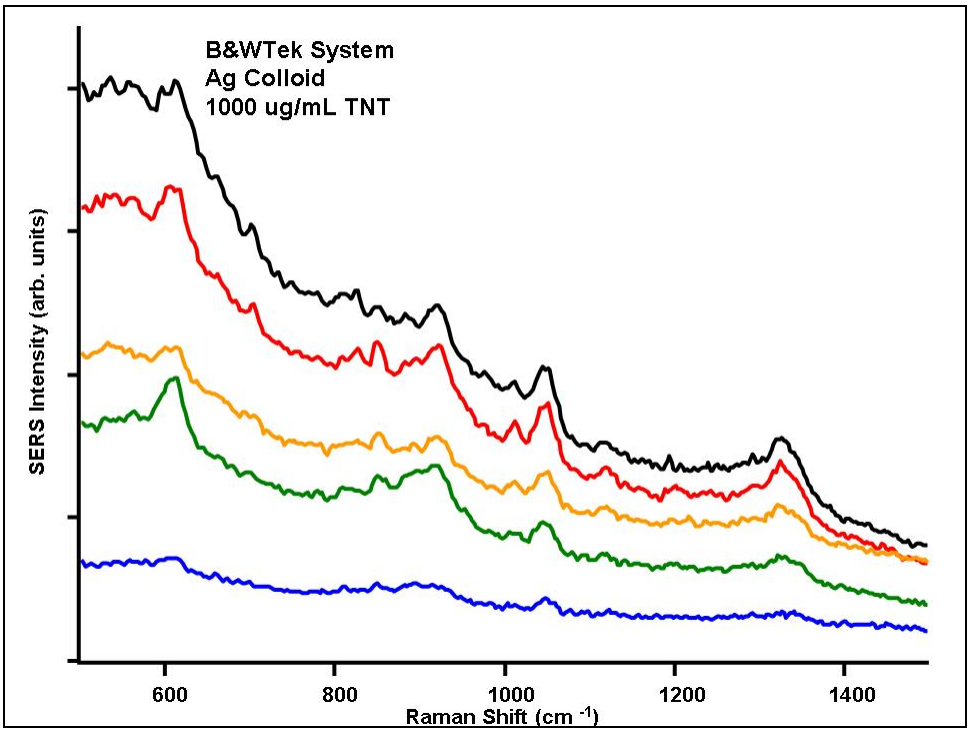

Figure D-24. SERS of 1000 ug/mL TNT as measured with Ag colloid using the B&WTek system.

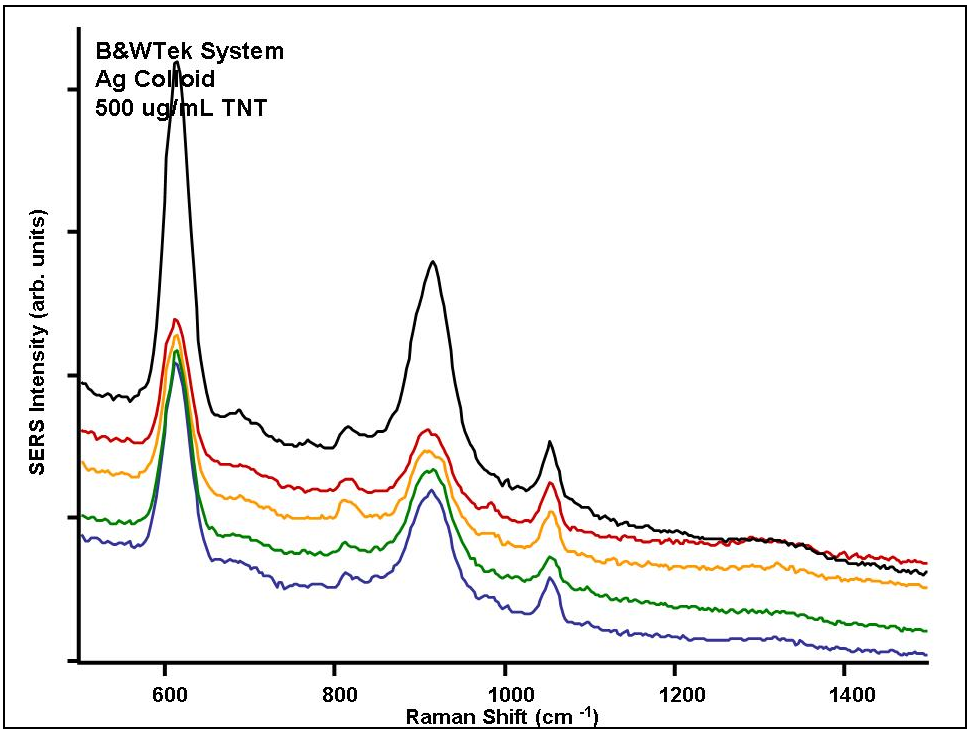

Figure D-25. SERS of 500 ug/mL TNT as measured with Ag colloid using the B&WTek system.

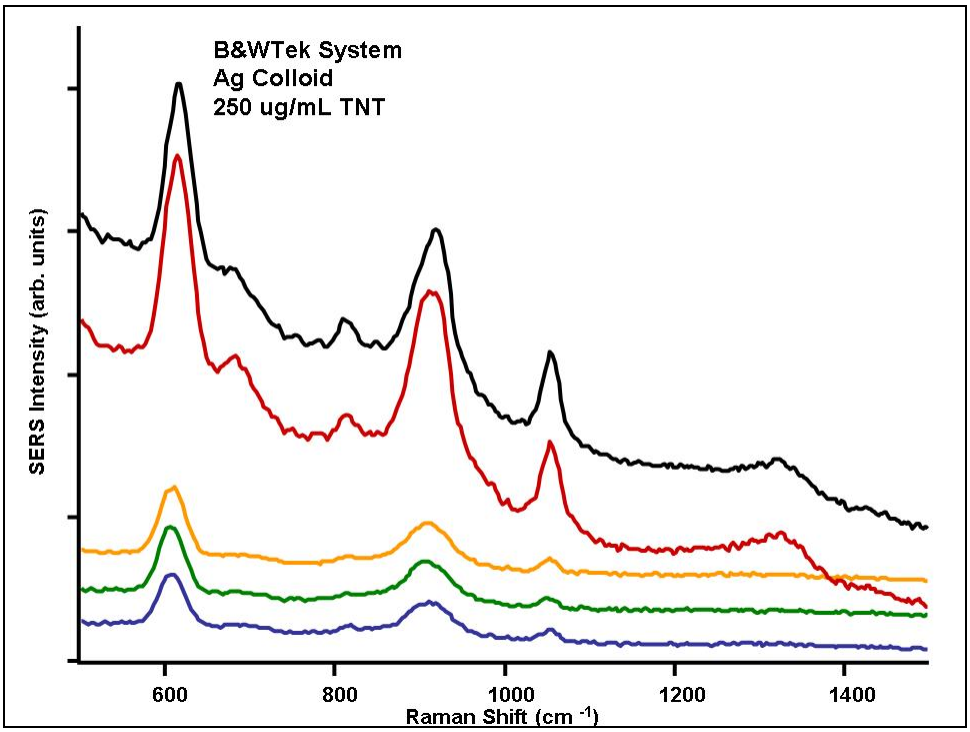

Figure D- 26. SERS of 250 ug/mL TNT as measured with Ag colloid using the B&WTek system.

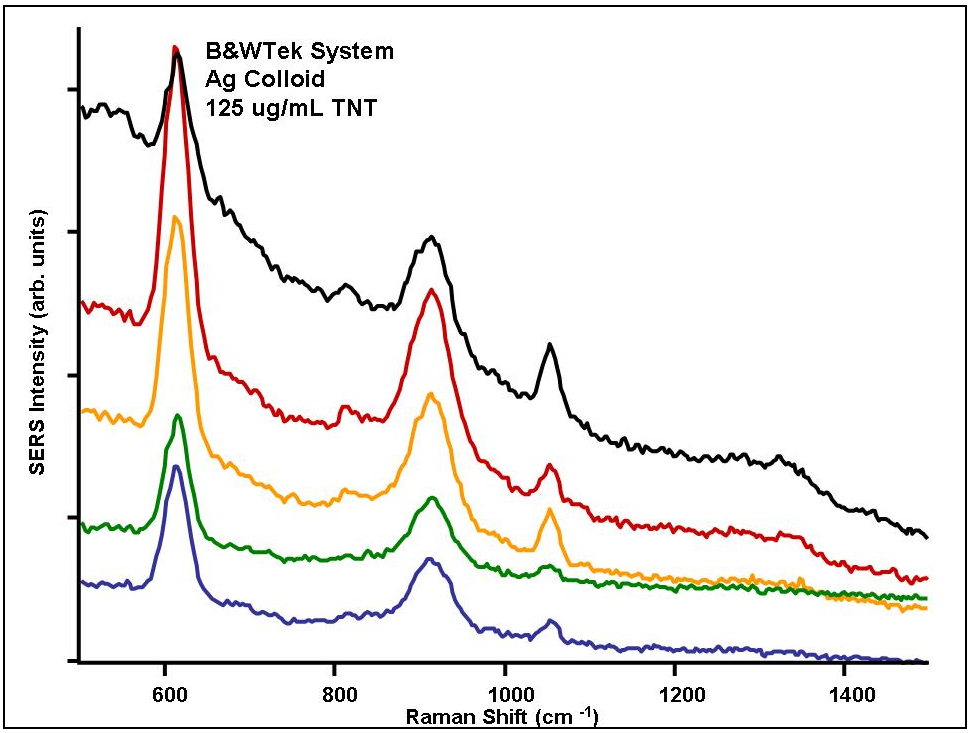

Figure D-27. SERS of 125 ug/mL TNT as measured with Ag colloid using the B&WTek system.

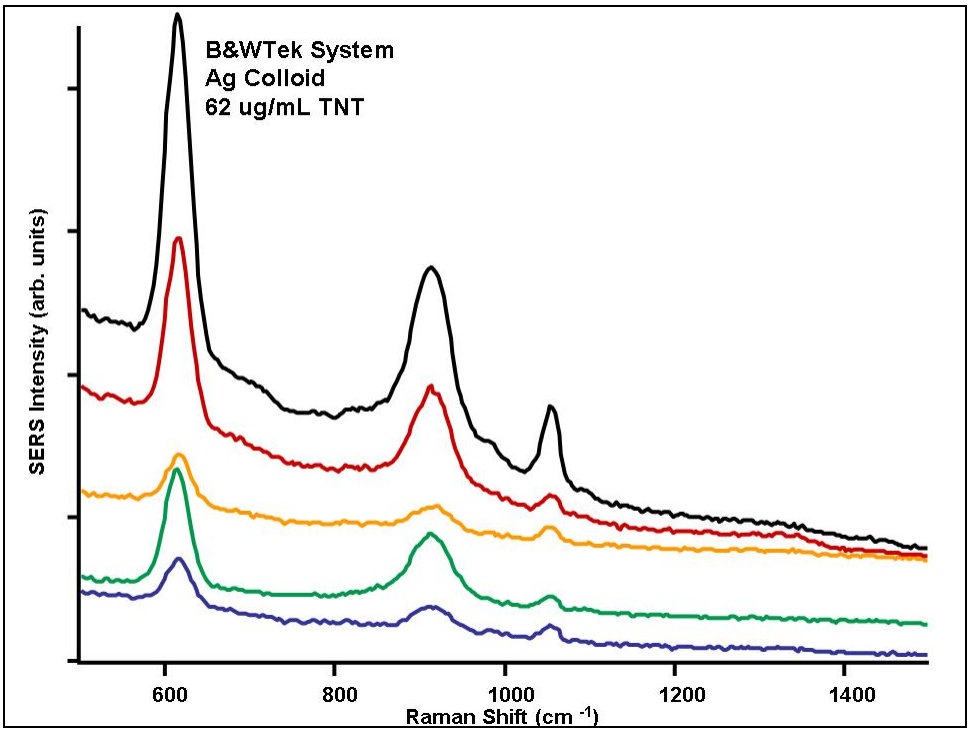

Figure D-28. SERS of 62 ug/mL TNT as measured with Ag colloid using the B&WTek system.

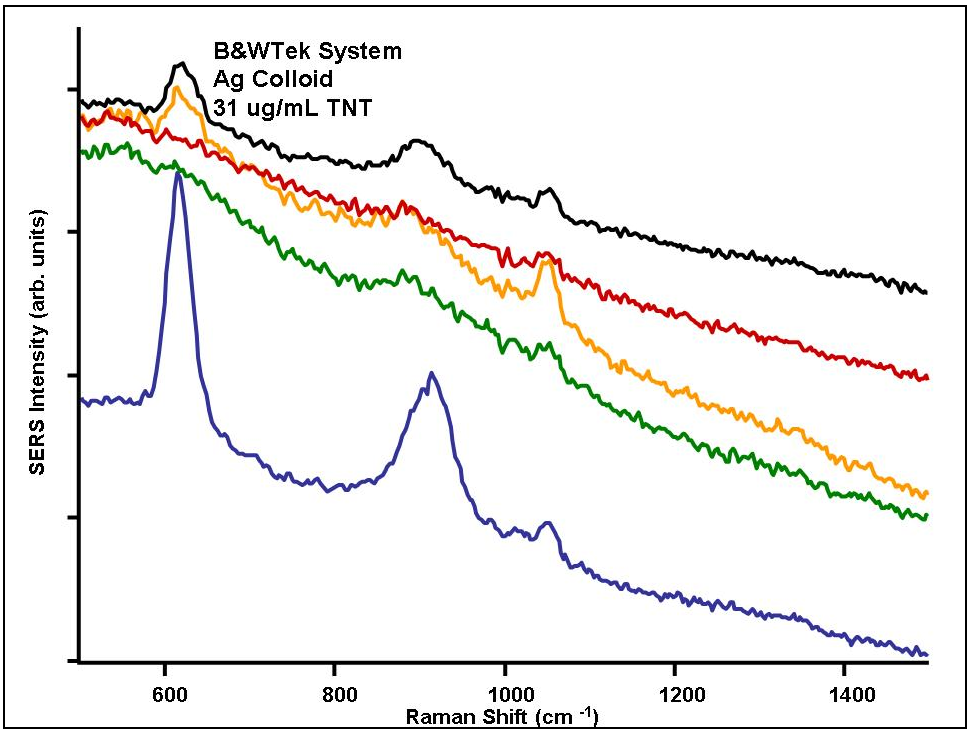

Figure D-29. SERS of 31 ug/mL TNT as measured with Ag colloid using the B&WTek system.

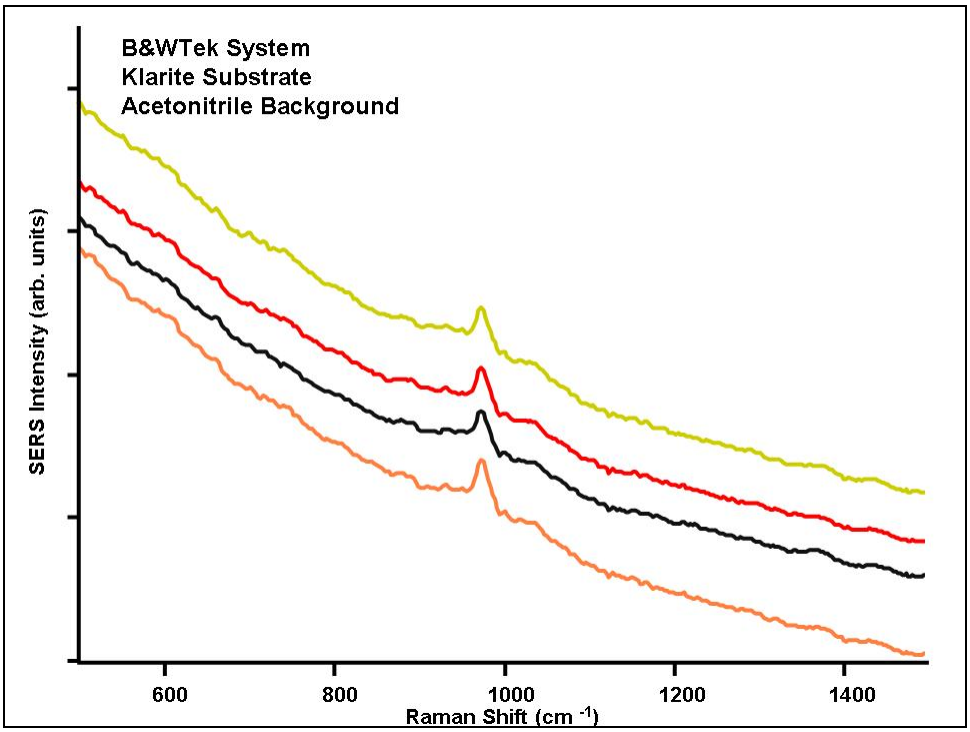

Figure D-30. SERS background of acetonitrile on a Klarite substrate as measured using the B&WTek system.

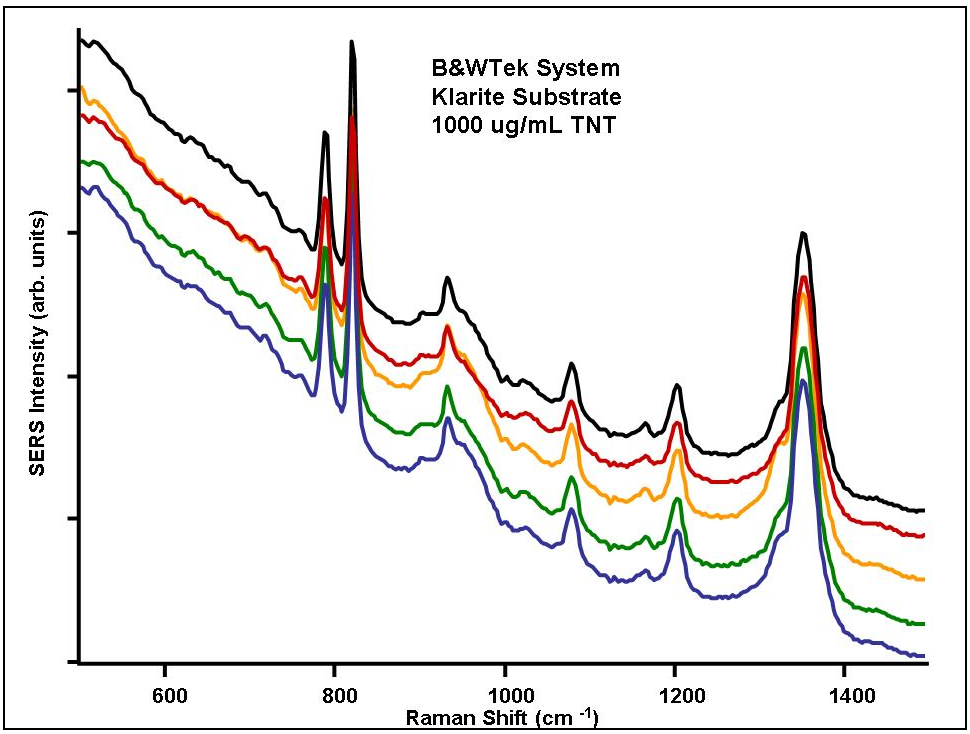

Figure D-31. SERS of 1000 ug/mL TNT measured on Klarite substrate using the B&WTek system.

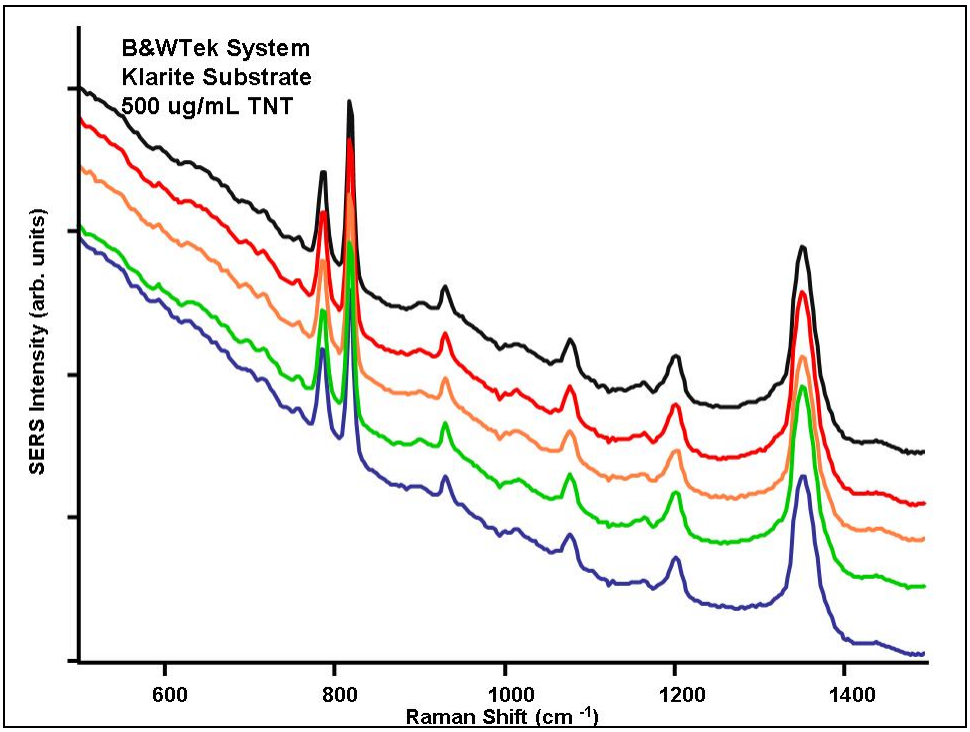

Figure D-32. SERS of 500 ug/mL TNT measured on Klarite substrate using the B&WTek system.

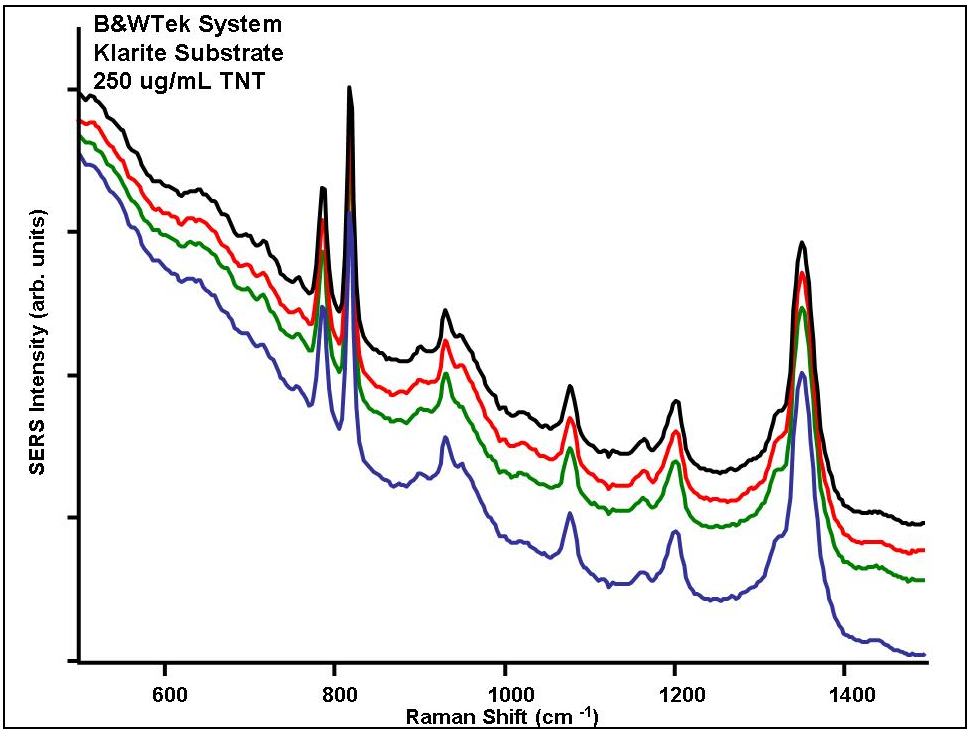

Figure D-33. SERS of 250 ug/mL TNT measured on Klarite substrate using the B&WTek system.

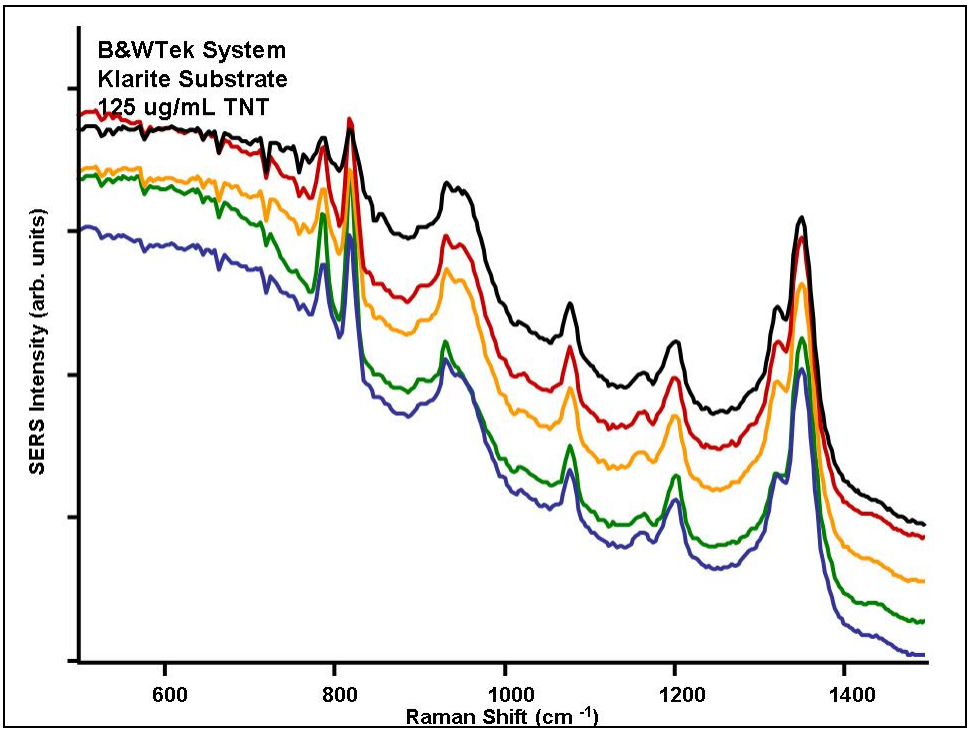

Figure D-34. SERS of 125 ug/mL TNT measured on Klarite substrate using the B&WTek system.

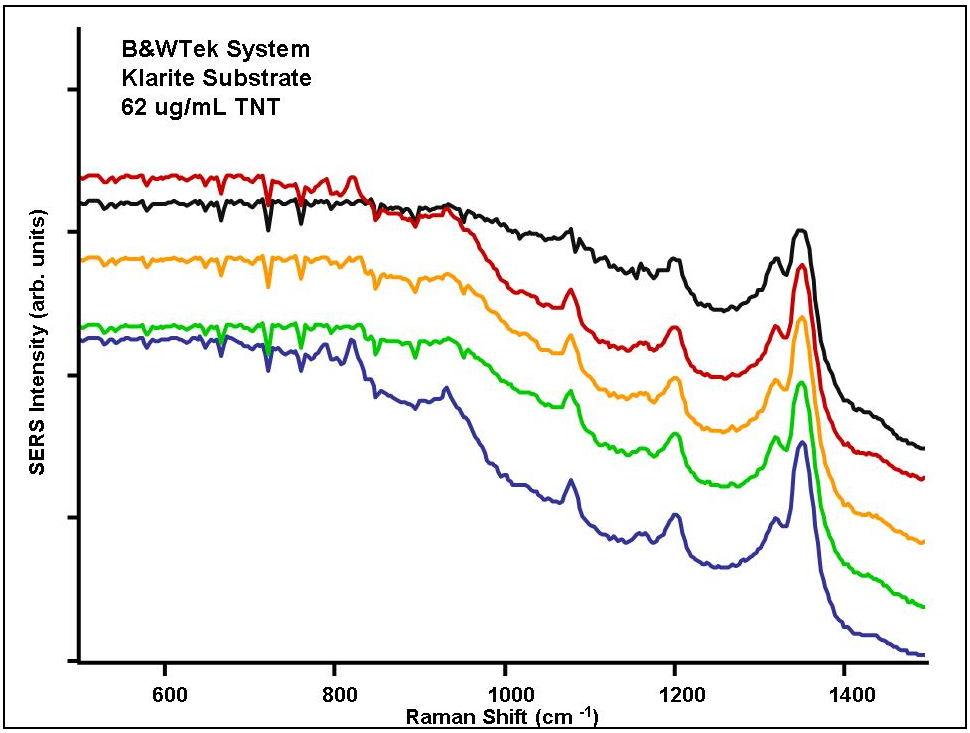

Figure D-35. SERS of 62 ug/mL TNT measured on Klarite substrate using the B&WTek system.

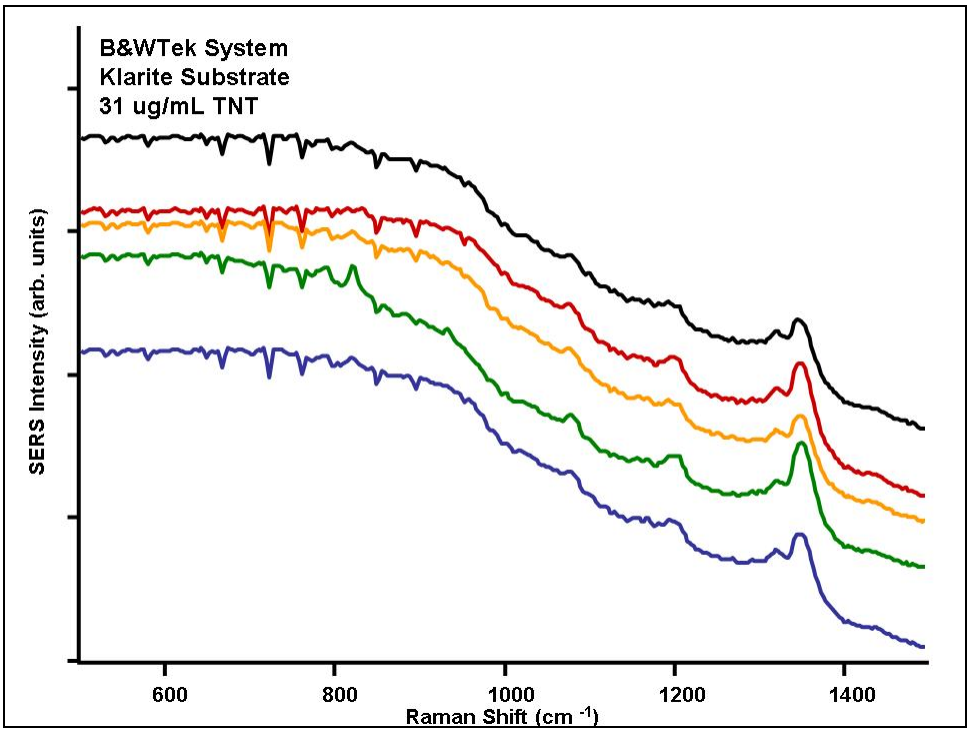

Figure D-36. SERS of 31 ug/mL TNT measured on Klarite substrate using the B&WTek system.

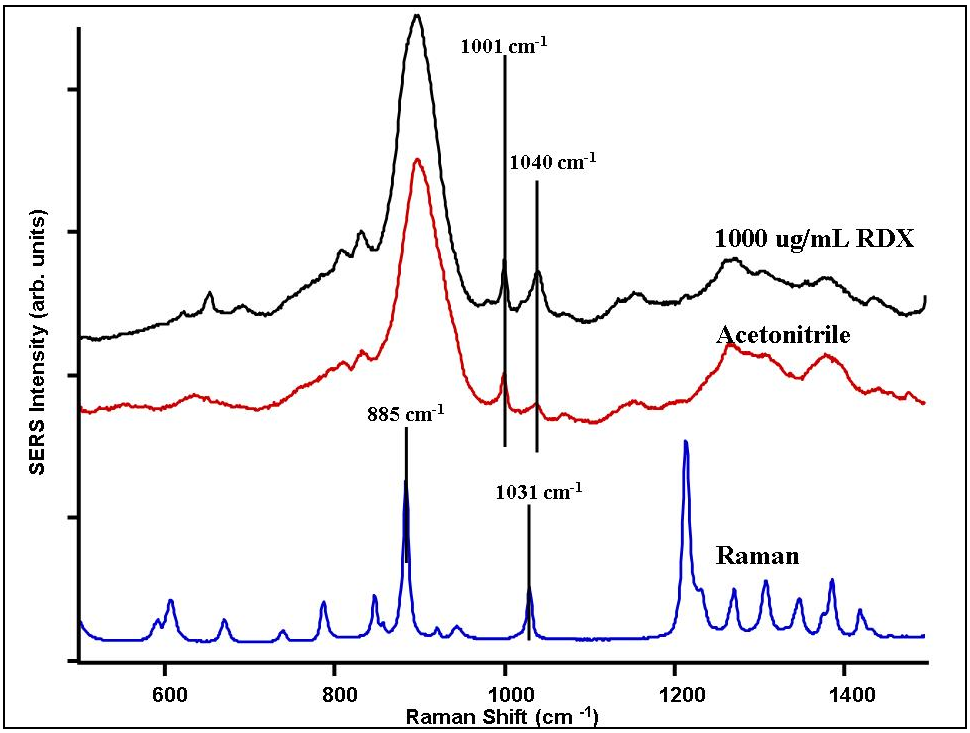

Figure D-37. SERS 1000 ug/mL RDX, acetonitrile and Raman of RDX as measured on a FON substrate using the Renishaw system. Raman RDX bands do not correspond to any SERS bands observed in the 1000 ug/mL RDX sample. The 1000 ug/mL RDX sample looks very similar to the acetonitrile spectrum.

INTENTIONALLY LEFT BLANK.

Appendix E. Simulants Supplemental

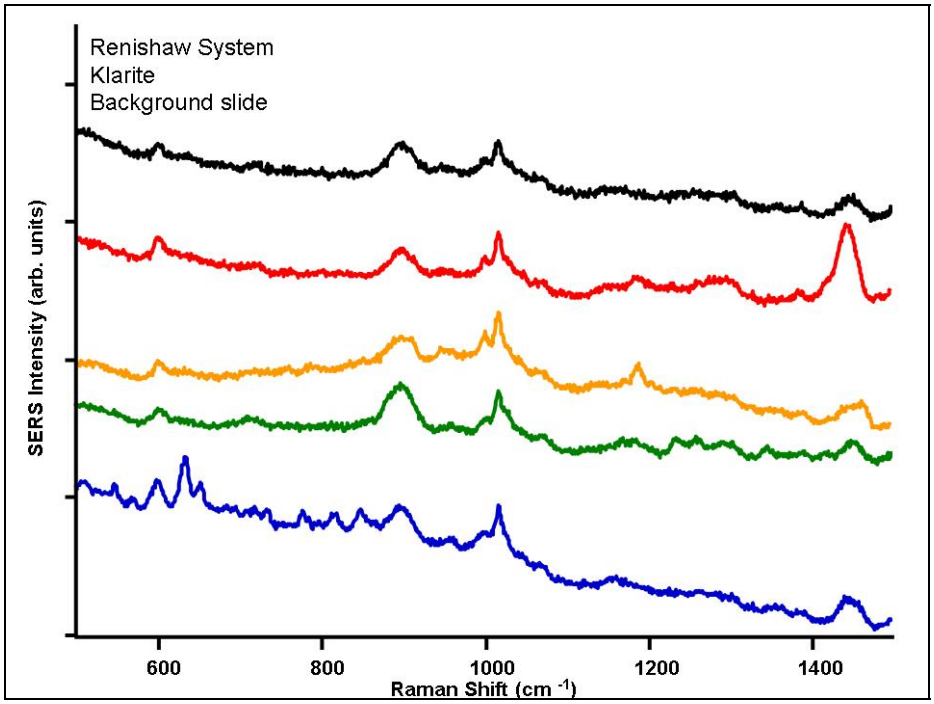

Figure E-1. SERS of Klarite background as measured with Renishaw system.

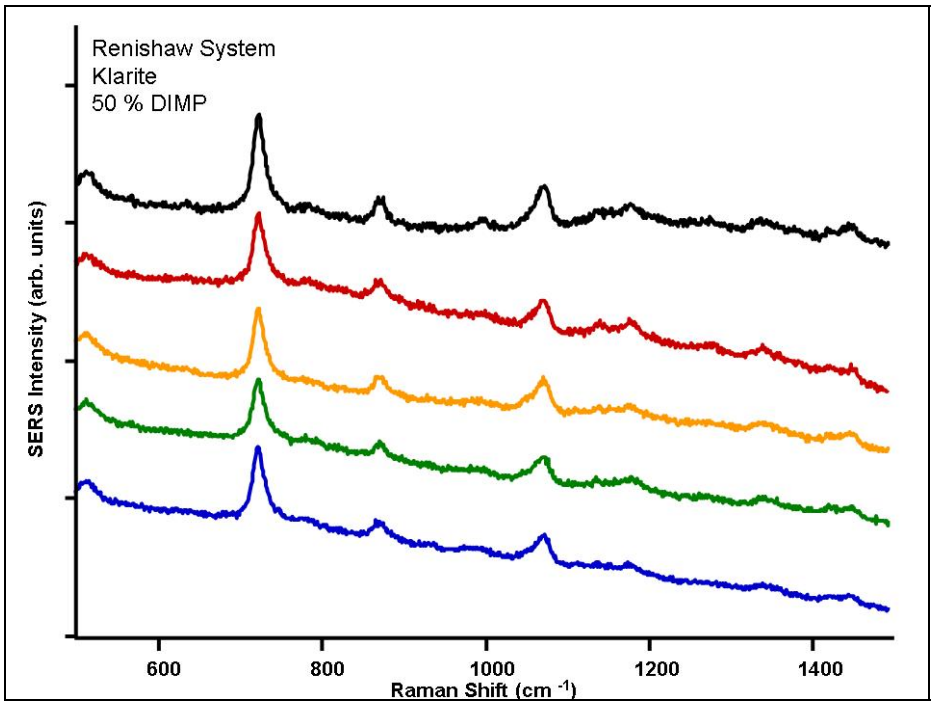

Figure E-2. SERS of 50% DIMP on Klarite substrate as measured with Renishaw system.

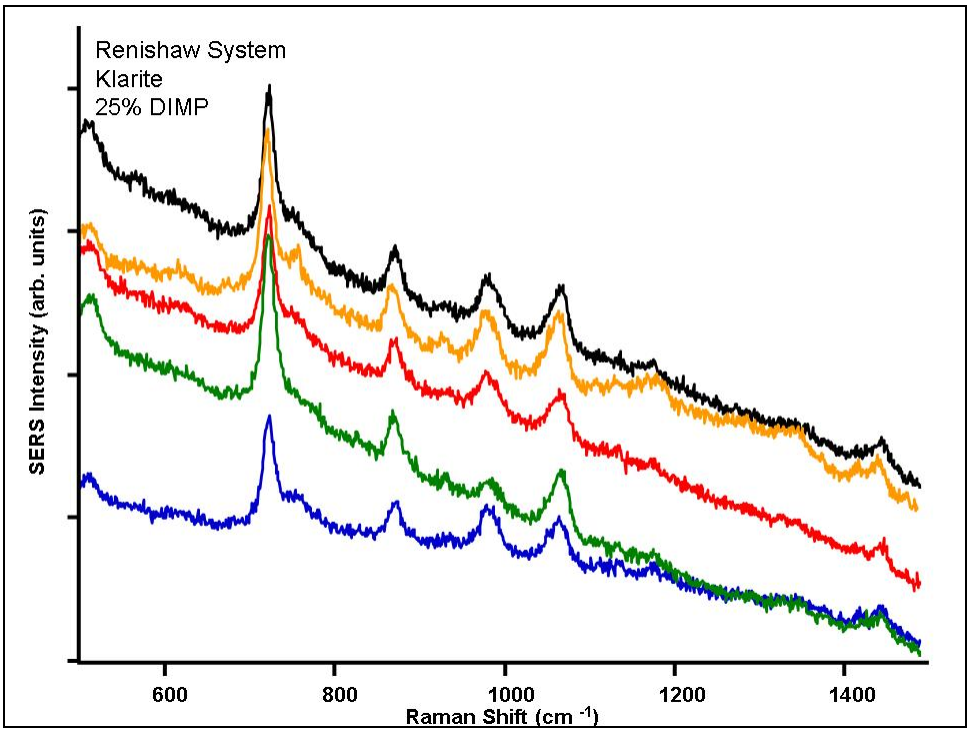

Figure E-3. SERS of 25% DIMP on Klarite substrate as measured with Renishaw system.

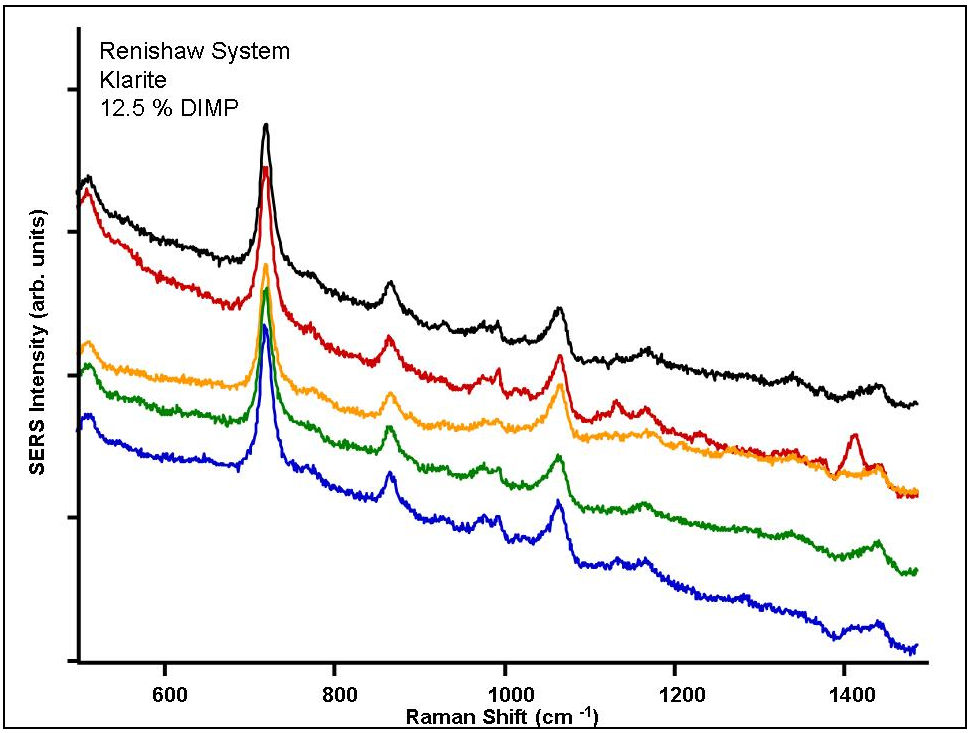

Figure E-4. SERS of 12.5% DIMP on Klarite substrate as measured with Renishaw system.

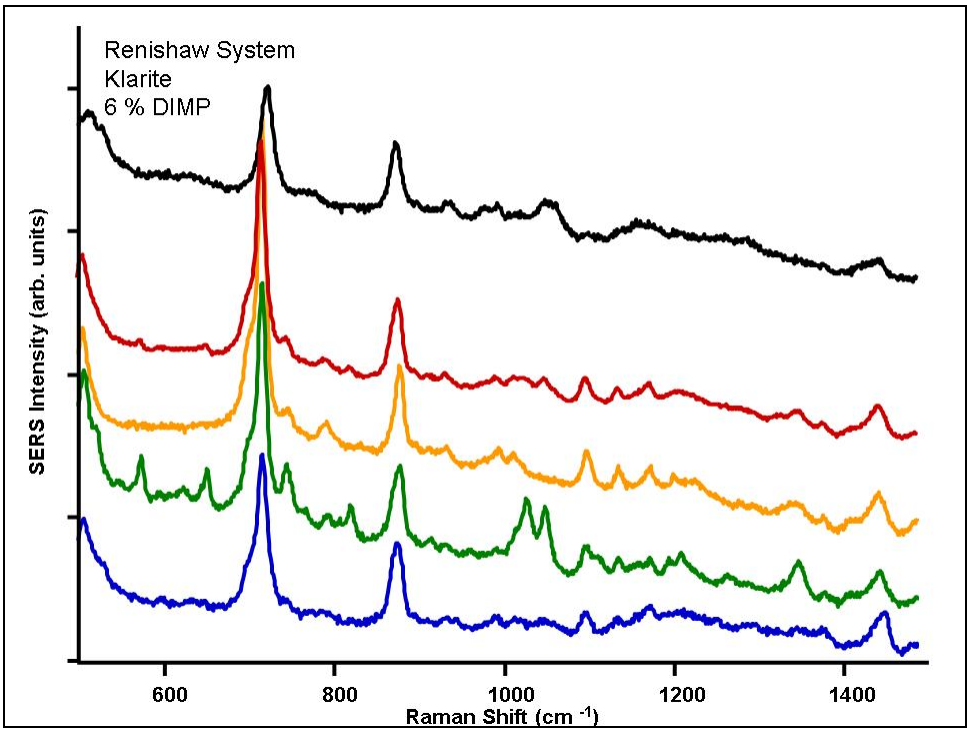

Figure E-5. SERS of 6% DIMP on Klarite substrate as measured with Renishaw system.

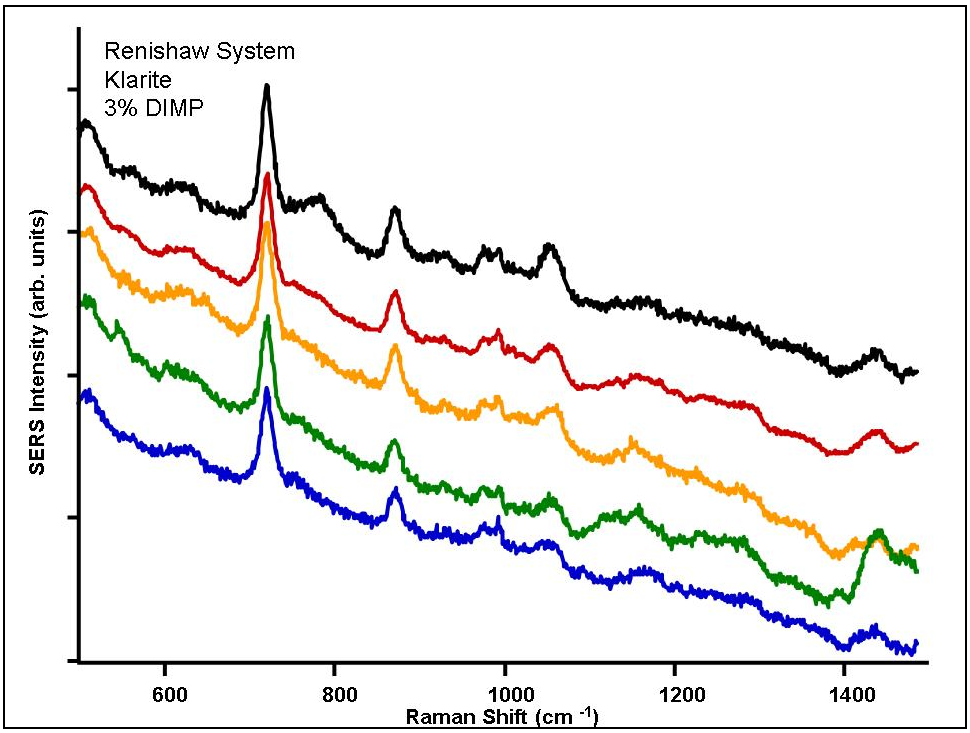

Figure E-6. SERS of 3% DIMP on Klarite substrate as measured with Renishaw system.

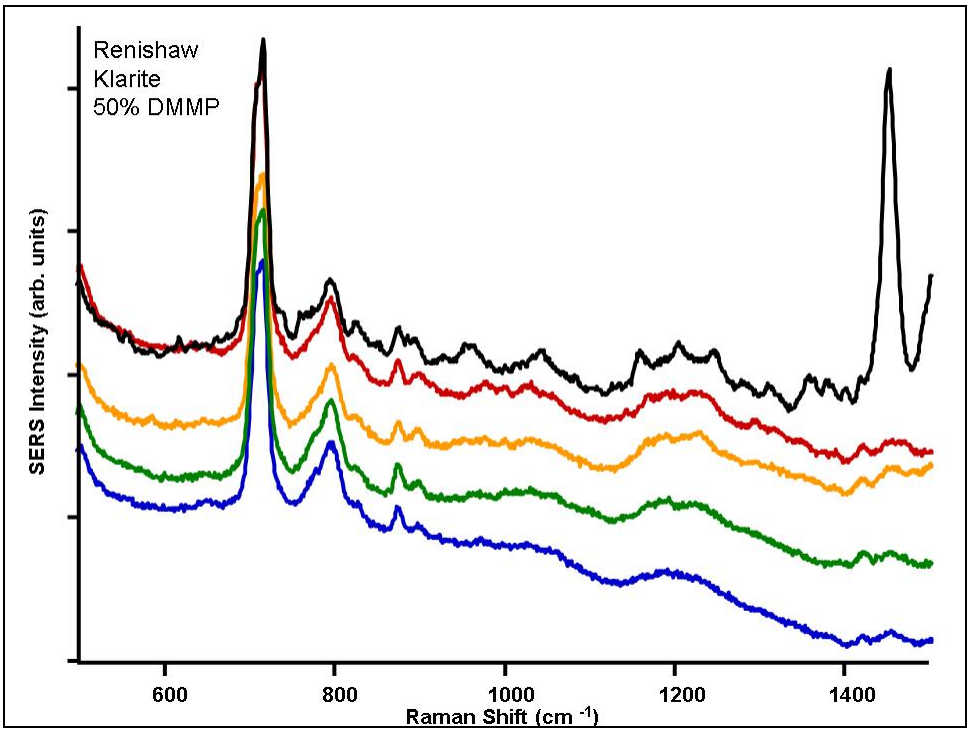

Figure E-7. SERS of 50% DMMP on Klarite substrate as measured with Renishaw system.

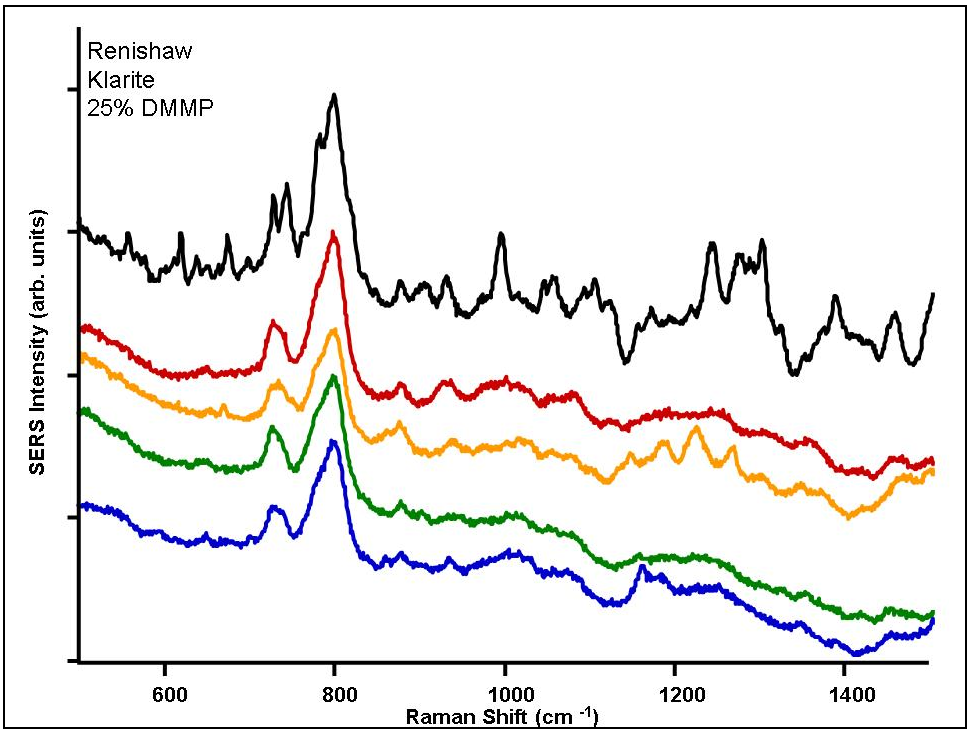

Figure E-8. SERS of 25% DMMP on Klarite substrate as measured with Renishaw system.

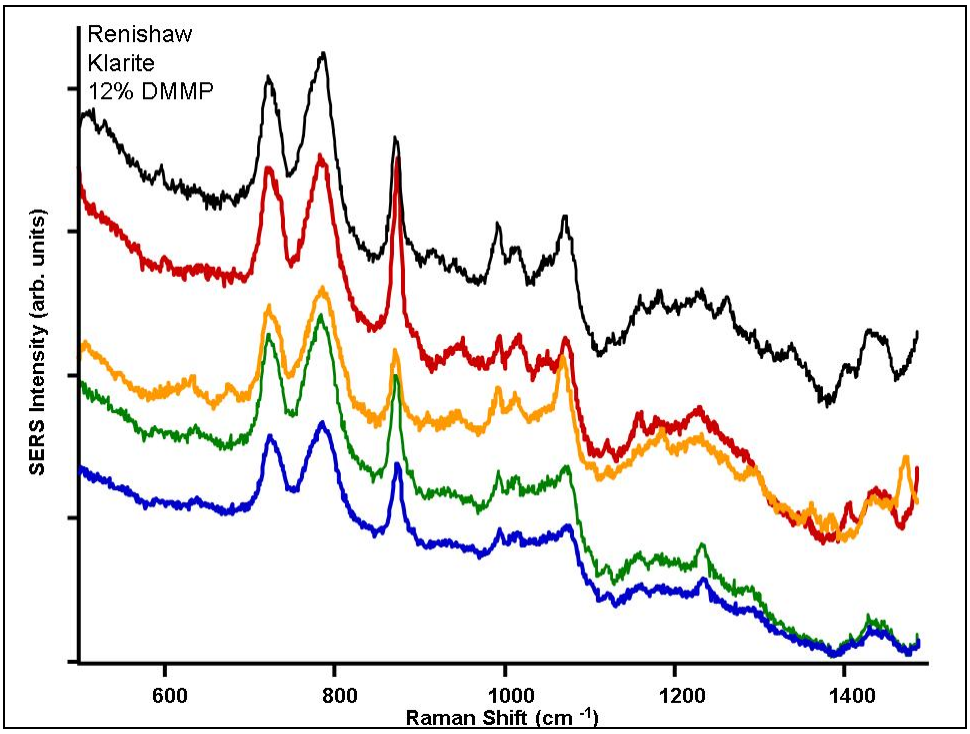

Figure E-9. SERS of 12% DMMP on Klarite substrate as measured with Renishaw system.

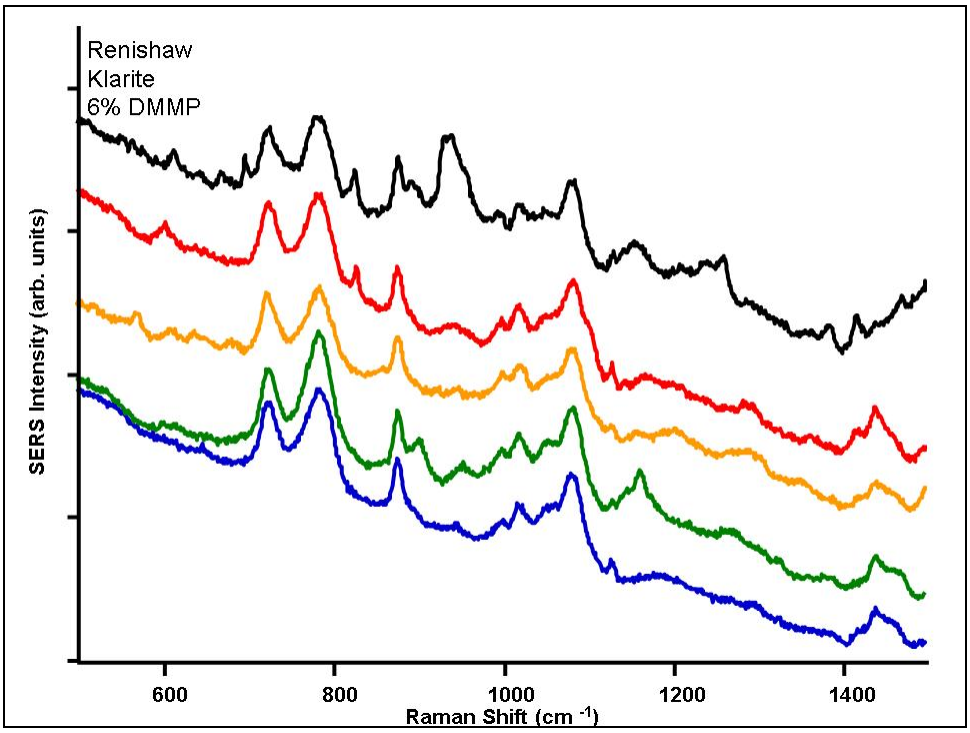

Figure E-10. SERS of 6% DMMP on Klarite substrate as measured with Renishaw system.

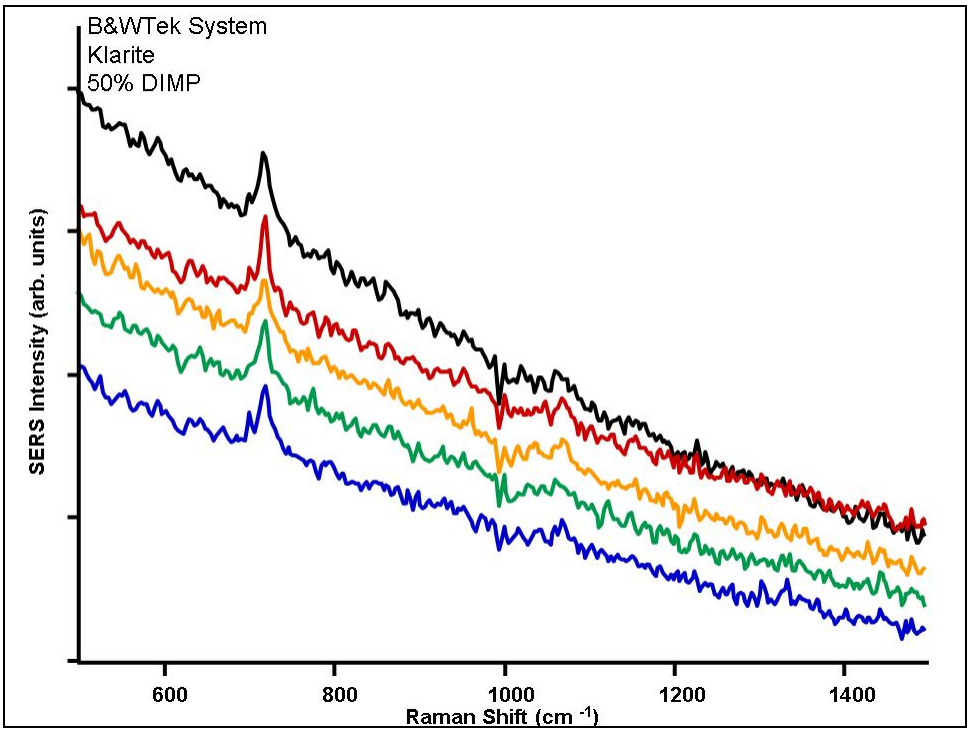

Figure E-11. SERS of 50% DIMP on Klarite substrate as measured with B&WTek system.

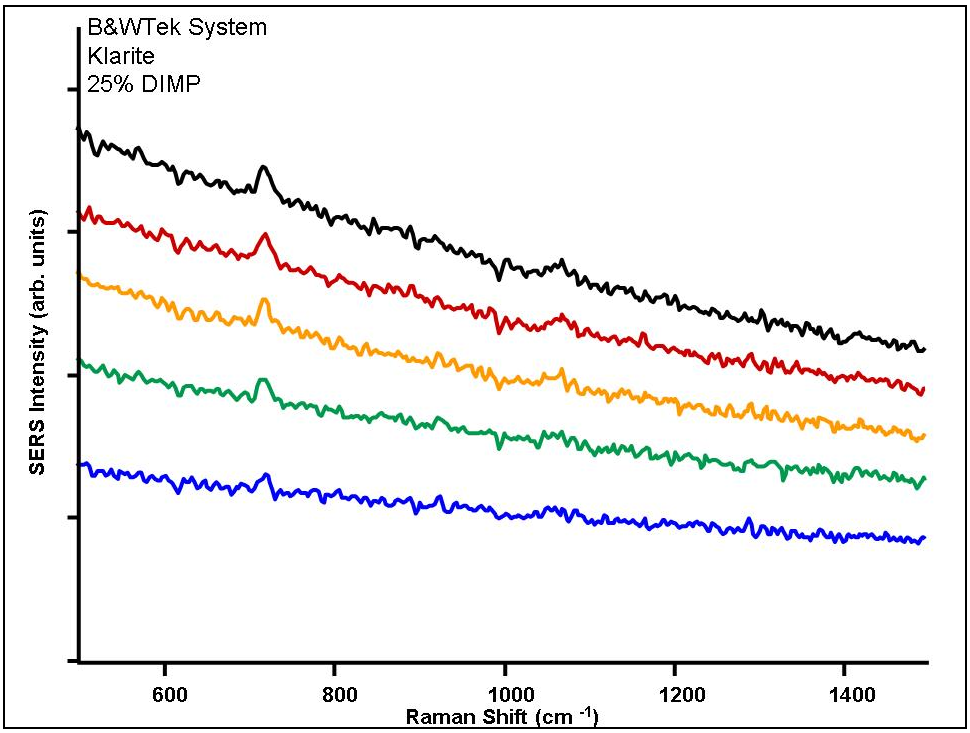

Figure E-12. SERS of 25% DIMP on Klarite substrate as measured with B&WTek system.

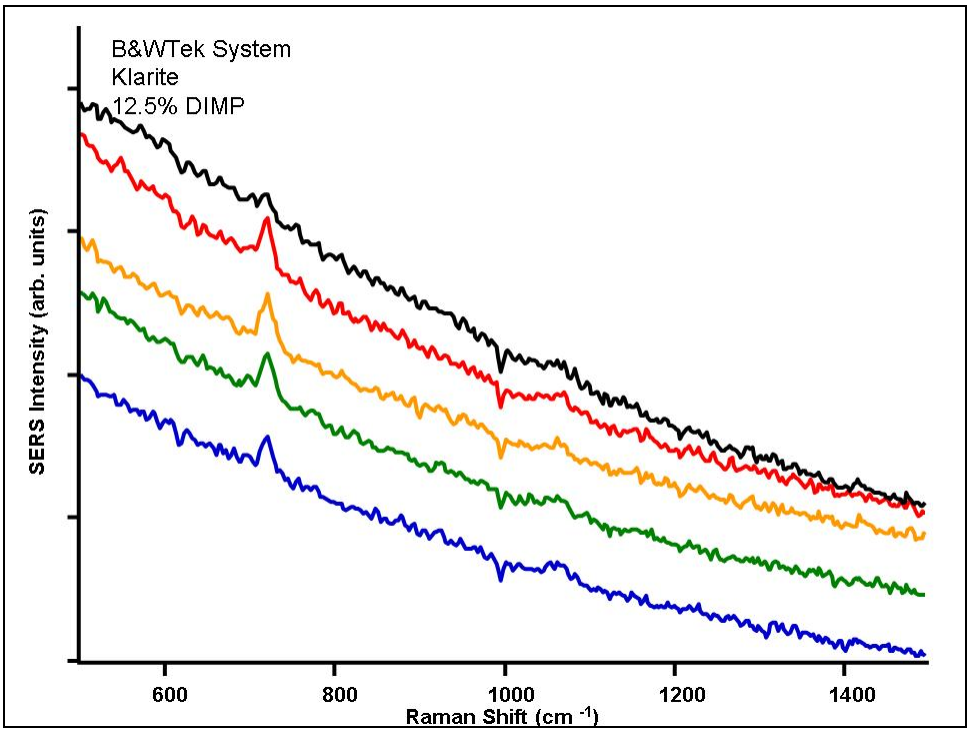

Figure E-13. SERS of 12.5% DIMP on Klarite substrate as measured with B&WTek system.

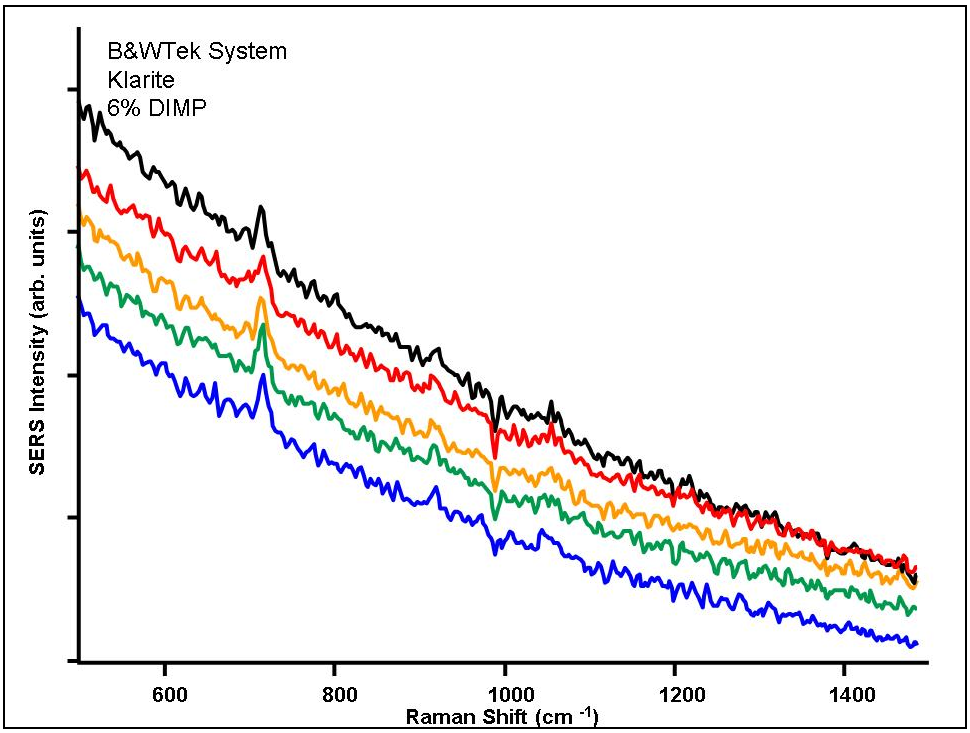

Figure E-14. SERS of 6% DIMP on Klarite substrate as measured with B&WTek system.

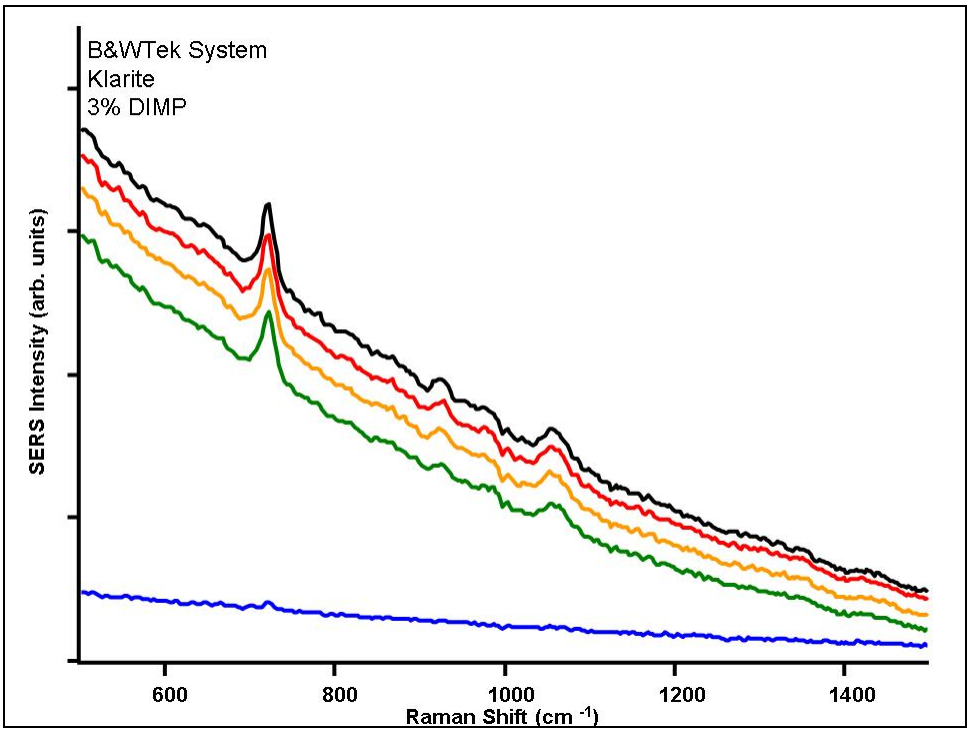

Figure E-15. SERS of 3% DIMP on Klarite substrate as measured with B&WTek system.

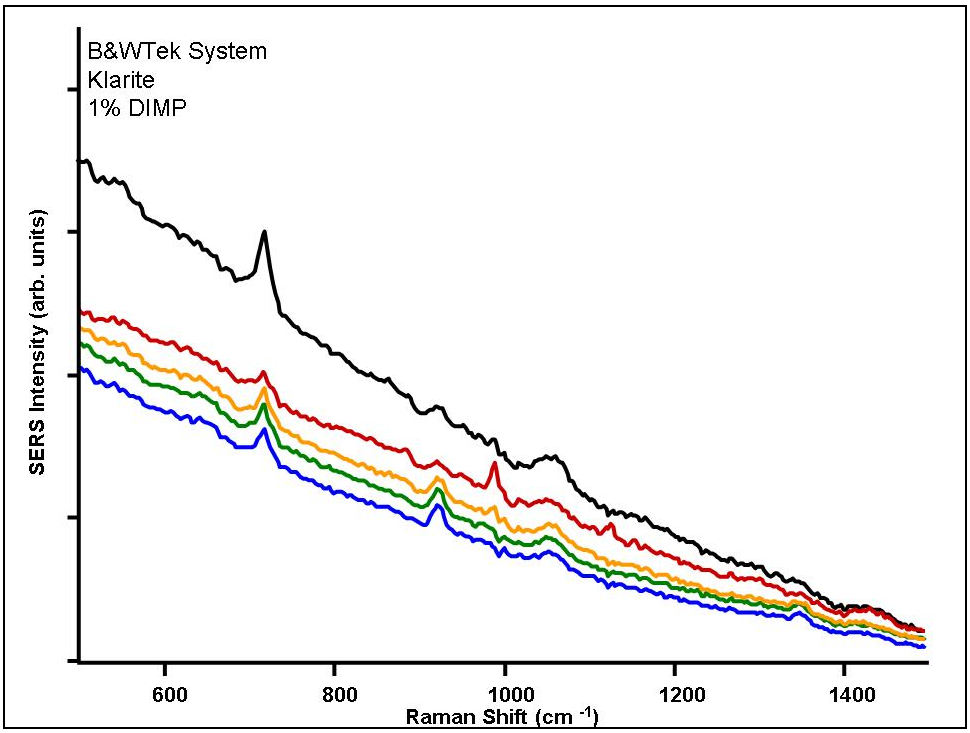

Figure E-16. SERS of 1% DIMP on Klarite substrate as measured with B&WTek system.

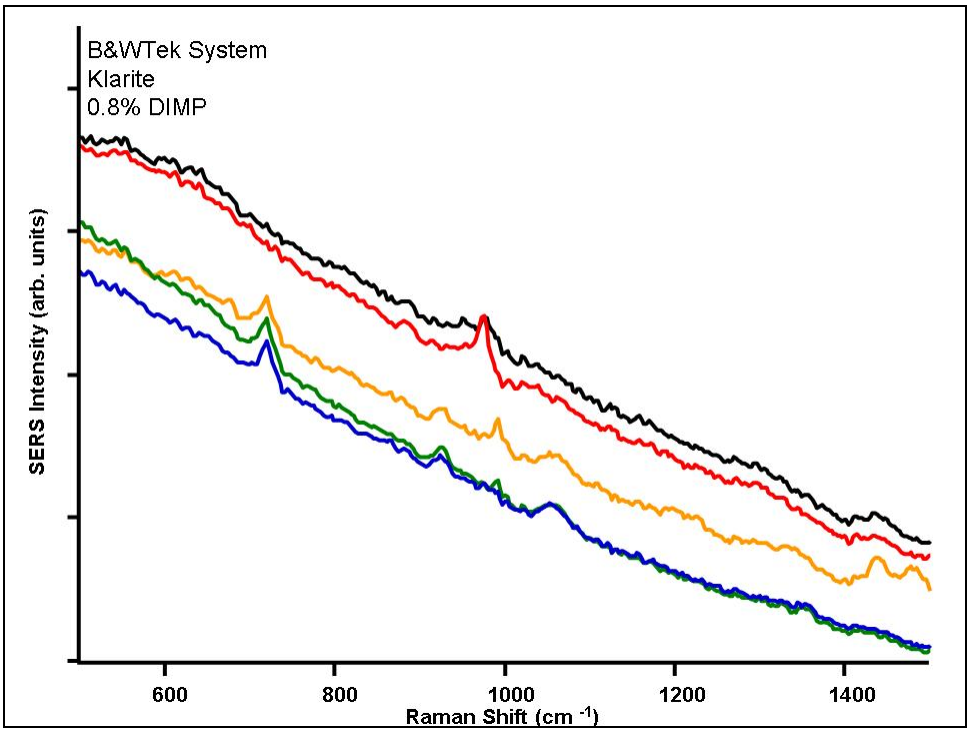

Figure E-17. SERS of 0.8% DIMP on Klarite substrate as measured with B&WTek system.

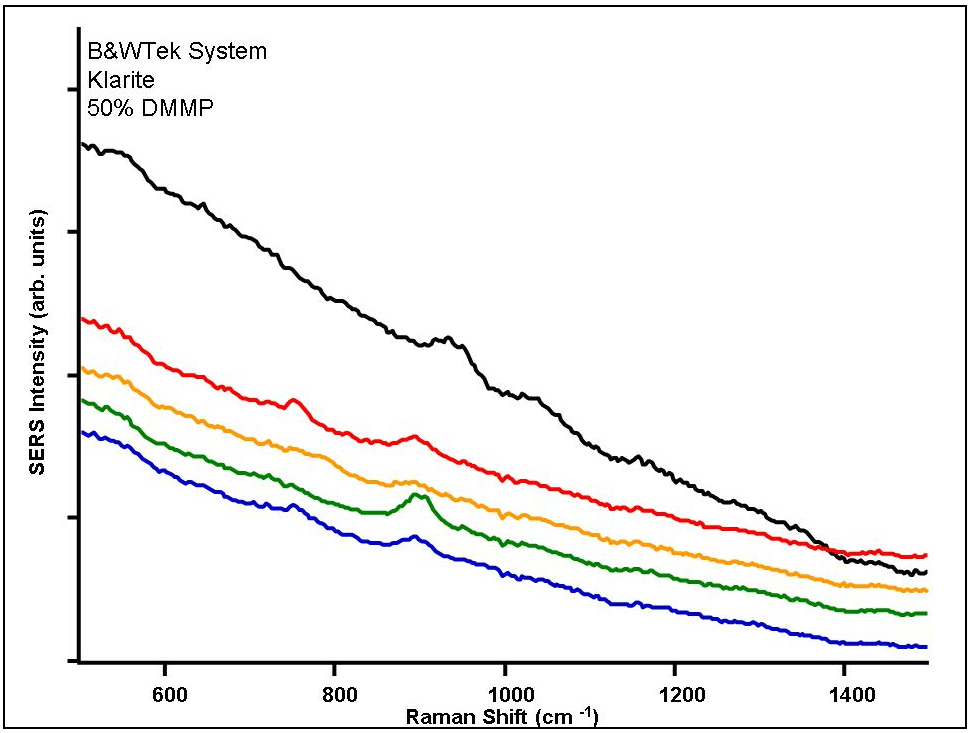

Figure E-18. SERS of 50% DMMP on Klarite substrate as measured with B&WTek system.

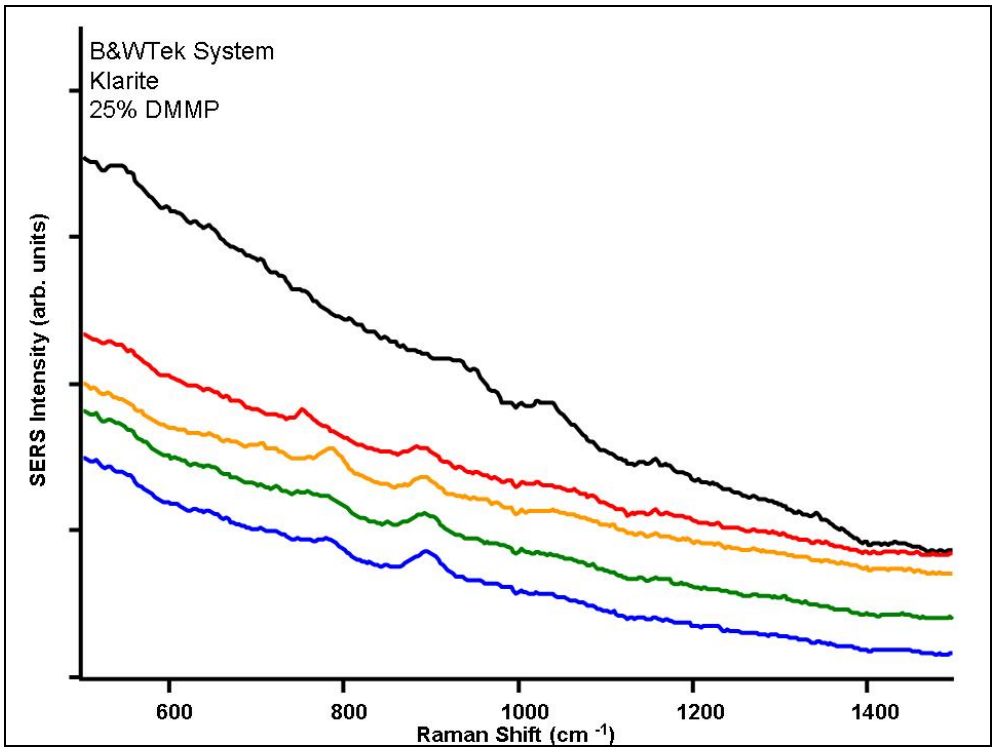

Figure E-19. SERS of 25% DMMP on Klarite substrate as measured with B&WTek system.

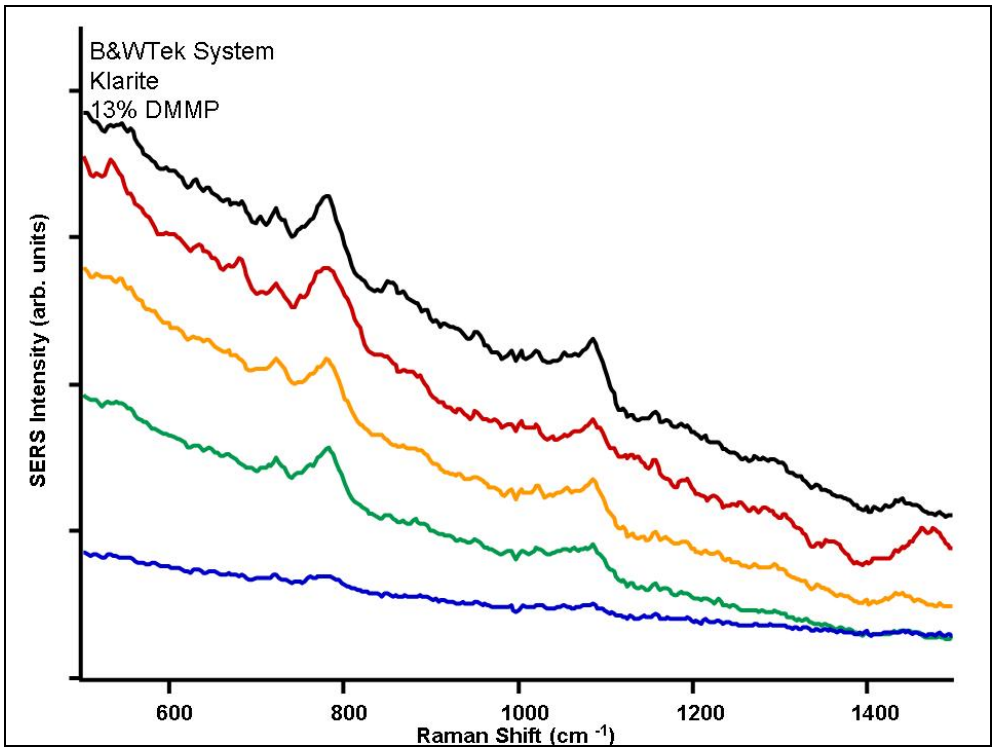

Figure E-20. SERS of 13% DMMP on Klarite substrate as measured with B&WTek system.

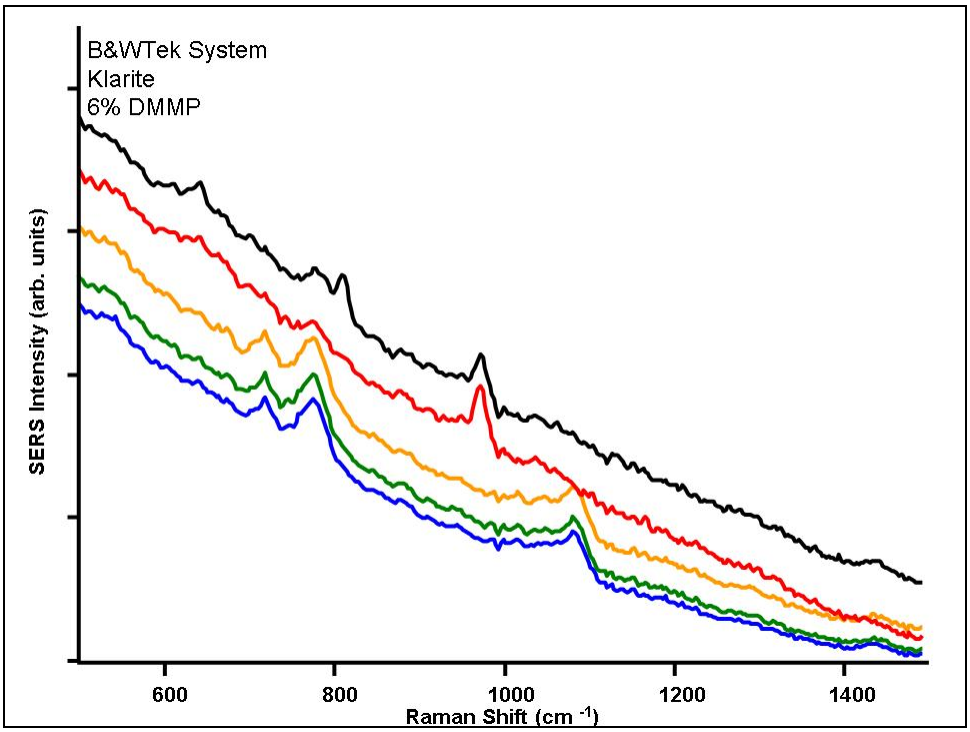

Figure E-21. SERS of 6% DMMP on Klarite substrate as measured with B&WTek system.

INTENTIONALLY LEFT BLANK.

List of Symbols, Abbreviations, and Acronyms

AFM	atomic force microscopy
BCB	brilliant cresyl blue
CBW	Chemical and biological warfare
CCD	charged coupled device
COTS	commercial-off-the-shelf
CT	charge transfer
DIMP	diisopropyl methylphosphonate
DMMP	dimethyl methylphosphonate
DNT	dinitrotoluene
ECBC	Edgewood Chemical Biological Center
FON	film over nanosphere
GC/MS	gas chromatography/ mass spectrometry
HNO_3	nitric acid
HPLC/MS	high performance liquid chromatography/mass spectrometry
IMS	ion mobility spectrometry
JSAWM	Joint Service Agent Water Monitoring program
KOH	potassium hydroxide
PHE	phenylalanine
RDX	cyclotrimethylenetrinitramine
RSD	relative standard deviation
S/N	signal-to-noise
SEM	Scanning electron microscope
SERS	Surface Enhanced Raman Scattering
SUS-CG	*B. coagulans*

SUSCI	*B. sphericus*
TE	thermoelectric
TNT	2,4,6-trinitrotoluene
UMBC	University of Maryland Baltimore County

NO. OF COPIES	ORGANIZATION
1 ELEC	ADMNSTR DEFNS TECHL INFO CTR ATTN DTIC OCP 8725 JOHN J KINGMAN RD STE 0944 FT BELVOIR VA 22060-6218
1	DARPA ATTN IXO S WELBY 3701 N FAIRFAX DR ARLINGTON VA 22203-1714
1 CD	OFC OF THE SECY OF DEFNS ATTN ODDRE (R&AT) THE PENTAGON WASHINGTON DC 20301-3080
1	US ARMY RSRCH DEV AND ENGRG CMND ARMAMENT RSRCH DEV AND ENGRG CTR ARMAMENT ENGRG AND TECHNLGY CTR ATTN AMSRD AAR AEF T J MATTS BLDG 305 ABERDEEN PROVING GROUND MD 21005-5001
1	EDGEWOOD CHEMICAL BIOLOGICAL CTR ATTN AMSRD ECB RT D S CHRISTESEN 5183 BLACKHAWK RD ABERDEEN PROVING GROUND MD 21010-5424
1	EDGEWOOD CHEMICAL BIOLOGICAL CTR SENIOR RSRCH SCIENTIST (ST) – CHEMISTRY ATTN AMSRD ECB RT D A FOUNTAIN 5183 BLACKHAWK RD ABERDEEN PROVING GROUND MD 21010-5424
1	PM TIMS, PROFILER (MMS-P) AN/TMQ-52 ATTN B GRIFFIES BUILDING 563 FT MONMOUTH NJ 07703

NO. OF COPIES	ORGANIZATION
1	US ARMY INFO SYS ENGRG CMND ATTN AMSEL IE TD A RIVERA FT HUACHUCA AZ 85613-5300
1	COMMANDER US ARMY RDECOM ATTN AMSRD AMR W C MCCORKLE 5400 FOWLER RD REDSTONE ARSENAL AL 35898-5000
1	US GOVERNMENT PRINT OFF DEPOSITORY RECEIVING SECTION ATTN MAIL STOP IDAD J TATE 732 NORTH CAPITOL ST NW WASHINGTON DC 20402
1	US ARMY RSRCH LAB ATTN RDRL CIM G T LANDFRIED BLDG 4600 ABERDEEN PROVING GROUND MD 21005-5066
16	US ARMY RSRCH LAB ATTN IMNE ALC HRR MAIL & RECORDS MGMT ATTN RDRL CIM L TECHL LIB ATTN RDRL CIM P TECHL PUB ATTN RDRL SEE O D STRATIS-CULLUM ATTN RDRL SEE O M HANKUS (10 COPIES) ATTN RDRL SEE O N FELL ATTN RDRL SEE O P PELLEGRINO ADELPHI MD 20783-1197

TOTAL: 27 (1 ELEC, 1 CD, 25 HCS)

INTENTIONALLY LEFT BLANK.